Molecular mechanism of HIV-1 integrase inhibition by Raltegravir proposed by using of molecular modeling approaches

Rohit Arora

ENSC - 2012n°394

THESE DE DOCTORAT

DE L'ECOLE NORMALE SUPERIEURE DE CACHAN

Présentée par

Monsieur Rohit ARORA

pour obtenir le grade de

DOCTEUR DE L'ECOLE NORMALE SUPERIERE DE CACHAN

Domaine :
Sciences de la Vie et de la Santé

Sujet de la thèse :

Molecular mechanism of HIV-1 integrase inhibition by Raltegravir proposed by using of molecular modeling approaches

Thèse présentée et soutenue à Cachan le 26 octobre 2012 devant le jury composé de :

Philippe CUNIASSE	Directeur de Recherche	Rapporteur/President
Florent BARBAULT	Maitre des Conférences	Rapporteur
Liliane MOUAWAD	Chargé de Recherche	Examinatrice
Luba TCHERTANOV	Directrice de Recherche	Directrice de thèse

Nom du Laboratoire : Laboratoire de Biologie et Pharmacologie Appliquée
ENS CACHAN/CNRS/UMR8113
61, avenue du Président Wilson, 94235 CACHAN CEDEX, France

Mots clefs: SIDA, Intégrase du VIH-1, ADN virale, inhibition des cibles, Raltegravir, modélisation, reconnaissance moléculaire, simulation de dynamique moléculaire, amarrage

Le résumé

L'intégrase (IN) rétrovirale est responsable de l'intégration de l'ADN viral du VIH-1dans l'ADN cellulaire, processus indispensable à la réplication virale. Ce processus se déroule en deux étapes indépendantes, le 3'-processing et le transfert de brins, catalysées par l'IN. La compréhension des interactions entre l'IN et l'ADN viral et de la cinétique de formation des complexes pré-intégratifs a permis l'identification du raltégravir (RAL) et de l'elvitégravir (ELV) qui se sont avérés être des inhibiteurs très efficaces de la réplication virale. Le RAL, auparavant désigné sous le code MK-0518, est un nouveau médicament anti-VIH qui a obtenu son autorisation de commercialisation aux Etats-Unis sous le nom de Isentress^{TM} le 12 octobre 2007. Le ELV est toujours en essais cliniques. Toutefois, comme on l'observe pour d'autres antirétroviraux, ces composés n'échappent cependant pas aux phénomènes de résistance. Des mutations de résistance spécifiques au RAL ont ainsi été identifiées chez des patients. À ce jour, aucune donnée expérimentale caractérisant la structure de l'IN du VIH-1, la structure au RAL et/ou les interactions du RAL avec sa cible n'a été rapporté.

Premièrement, nous avons caractérisé les propriétés structurales et conformationnelles du RAL dans des états différents, en phase gazeuse, en solution dans l'eau et à l'état solide. Une etude détaillée a permis de caracteriser la reconnaissance du RAL par des cibles virals, l'IN et l'ADN viral avant et après la réaction de 3'-processing. Nous avons trouvé que le RAL adopte un large spectre de conformations et configurations dans des états isolés et/ou liés avec le(s) cible(s). Les meilleures score et poses de docking confirment que le modèle représentant le complexe IN•vADN est la cible biologiquement pertinente du RAL. Ce résultat est cohérent avec le mécanisme d'inhibition du RAL communément admise. Nous avons suggéré que le processus d'inhibition peut comprendre dans un premier temps la reconnaissance du RAL par l'ADN viral clivé et lié à un état intermédiaire de l'IN. Le RAL couplé à l'ADN viral montre une orientation à l'extérieur de tous les atomes d'oxygène, d'excellents agents putatifs pour capturer de cations Mg^{2+}, ce qui pourrait faciliter l'insertion du RAL dans le site actif. La flexibilité conformationnelle du RAL permet l'adaptation de l'inhibiteur dans une poche relativement grande de du complexe IN•vADN, permettant la production de diverses conformations du RAL. Nous croyons que cette diversité des conformations du RAL contribue à la reconnaissance de résidus enzymatiques et peut influer sur le choix des voies alternatives de résistance au RAL observées cliniquement.

Nous avons étudié également la reconnaissance par l'IN des inhibiteurs du VIH appartenant à différents souches, B et CRF02_AG. Nous avons montré que la structure de l'IN des deux souches est quasi-identique. Le docking du RAL et de deux autres inhibiteurs de transfert de brins (ELV et L731_988) sur chaque modèle montre que leur reconnaissance par deux différentes souches cibles est identique.

Notre analyse des effets moléculaires et structuraux des mutations de résistance sur la structure de l'IN a montré que les structures de l'enzyme sauvage et mutante sont aussi quasi-identique. Par contre, les mutations modifient considérablement la spécificité de reconnaissance de l'ADN par l'IN.

Nous avons effectué la simulation de dynamique moléculaire (MD) de l'IN sauvage et mutant, avec une mutation ponctuelle R228A localisée dans le domaine C-terminale. Notre étude de la flexibilité de l'IN et du complexe IN•ADN par la dynamique moléculaire ouvre une voie très prometteuse non seulement sur le plan de la recherche fondamentale mais aussi pour l'application de nos concepts au développement de nouvelles générations d'inhibiteurs ciblant l'IN.

Keywords: AIDS, HIV-1 Integrase, viral DNA, targets inhibition, Raltegravir, modeling, molecular recognition, molecular dynamics simulation, docking

Summary

The HIV-1 integrase catalyzes the integration of HIV-1 viral DNA (vDNA) into the host cell chromosome in a process, which is essential for viral replication through two independent reactions, 3'-processing (3'-P) and strand transfer (ST), catalyzed by IN. Deciphering the structural determinants of the interaction between integrase and its substrates and the kinetics of this interaction sheds light on the importance of inhibitors targeting the pre-integration IN•vDNA complex. This approach led to the identification of raltegravir (RAL) and elvitegravir (ELV), which turned out to be highly efficient inhibitors of ST. RAL, formerly known under the code MK-0518, is a new anti-HIV drug that obtained clinical approval in the United States under the name Isentress^{TM} on October 12, 2007. ELV is still in clinical trials. However, these compounds nevertheless encounter resistance phenomenon. To date, no experimental data characterizing the RAL structure, structure of the HIV-1 IN and/or interactions of RAL with its targets, has been reported.

First, we characterized the structural and conformational properties of RAL in different states – the gas phase, in water solution and the solid state. Second, a detailed study allowed characterisation the RAL recognition by the viral targets – IN and the vDNA, before and after the 3'-P. We found that RAL shows a broad spectrum of conformations and configurations in isolated state and/or associated with the target(s). The best docking poses and scores confirmed that the model representing IN•vDNA complex is a biologically relevant target of RAL. This result is consistent with the commonly accepted mechanism of RAL inhibition.

Based on the docking results we suggested that the inhibition process may include, as a first step, the RAL recognition by the processed vDNA bound to a transient intermediate IN state. RAL coupled to vDNA shows an outside orientation of all oxygen atoms, excellent putative chelating agents of Mg^{2+} cations, which could facilitate the insertion of RAL into the active site. The conformational flexibility of RAL further allows the accommodation/adaptation of the inhibitor in a relatively large binding pocket of IN•vDNA pre-integration complex thus producing various RAL conformation. We believe that such variety of the RAL conformations contributing alternatively to the enzyme residue recognition may impact the selection of the clinically observed alternative resistance pathways to the drug.

We also studied the recognition of the HIV-1 IN inhibitors from two different strains, B and CRF02_AG. Our *in silico* study showed that the sequence variations between CRF02_AG and B strains did not lead to any notable difference in the structural features of the enzyme and did not impact the susceptibility to the IN inhibitors.

Our analysis of the resistance mutations effects showed that structure of the wild-type enzyme and mutants is almost identical. However, the resistance mutations significantly altered the specificity of the viral DNA recognition by IN.

We performed molecular dynamics simulations of the native and mutated IN with a point mutation R228A localized in the C-terminal domain. The study of targets flexibility opens a very promising way, not only in terms of fundamental research, but also for the application of our concepts to the development of new generations of inhibitors targeting IN.

Acknowledgements

Working on my Ph.D. has been a wonderful and often overwhelming experience. It is hard to say whether is has been grappling with the topic itself which has been the real learning experience, or grappling with how to write papers, give talks and work in a group. In any case, I am indebted to many people for making the time working on my Ph.D. an unforgettable experience.

I am grateful to Doctors Phillipe Cuniasse and Florent Barbault for accepting to be the reviewers of my thesis. Their comments and critique have been extremely helpful in improving my thesis and making it a rather learning experience. I sincerely thank Doctor Liliane Mouwad who accepted to examine my work.

Words cannot describe my gratitude to my thesis supervisor, Doctor Luba Tchertanov, for welcoming me to her team BiMoDyM at LBPA. She patiently guided me through my master's project – which was a relatively new field for me – and helped me prepare for my PhD thesis. We have had many fruitful discussions and brainstorming sessions over the last 4 years. Her outstanding ability, scientific and pedagogical, together with personal kindness and openness turned my work into truly one of a kind experience. Whatever she does, she does it with taste and elegance and I hope I was able to absorb at least a little bit of these qualities.

My sincere gratitude is reserved for all the current and former members of my group, for making it a memorable experience. Especially - Elodie Laine, Isaure Chauvot de Beauchene, Safwat Abdel-Azeim and Joseph Andre – who contributed in one way or the other to my research. This work would not have been possible without the great number collaborators. I am much obliged to Jean-Christophe Lambry (Ecole Polytechnique), Marina Gottikh (Moscow State University), the team of Jean-Francois Mouscadet (LBPA, ENS de Cachan) and clinicians from the Hospital Pitié-Salpetriere (Paris). A special mention to companies - Schrodinger, Tripos and CCDC - who helped in providing licenses and maintenance of some key softwares used in my research. A special thanks to Florent Langenfeld for his patience in correcting my oral and written French.

I am also indebted to the ENS Cachan for giving me an opportunity to conduct my PhD thesis at this prestigious institute. I am grateful to the Ecole Doctorale des Sciences Pratiques (EDSP) de Cachan and the French Ministry of Higher Education for providing and managing the financial support for my PhD research during a period of three years.

I am extremely grateful to Professor Isabelle Ledoux-Rak who introduced me to ENS Cachan and LBPA, and provided support at every step during my Master's program as well as during the application process of my PhD. I am also very thankful to all the professors of my Master's program for providing me with excellent guidance and education.

Finally, I thank my parents and my family without whom none of this would have been possible. I thank my dear friends – Hillary Kloeckner, Dhruv Shah and Karthik Aluru – who provided me with support and encouragement whenever I needed it the most. They have been my family away from home.

Content

ABBREVIATIONS

2D	In two dimensions
3D	In three dimensions
3'-P	3'-Processing Reaction
AIDS	Acquired Immuno-deficiency Syndrome
ARV	Anti-retroviral
CCD	Catalytic Core Domain
CTD	C-Terminal Domain
DNA	Deoxyribonucleic Acid
ELV	Elvitagravir
GLIDE	Grid-based Ligand Docking with Energetics
HIV	Human Immuno-deficiency Virus
INSTI	Integrase Strand Transfer Inhibitors
LEDGF	Lens epithelium-derived growth factor
MD	Molecular Dynamics
NMR	Nuclear Magnetic Resonance
NTD	N-Terminal Domain
PCA	Principal Component Analysis
PDB	Protein Data Bank
PFV	Primate Foamy Virus
PIC	Pre-Integration Complex
RAL	Raltegravir
RMSD	Root Mean Squared Distance
RMSF	Root Mean Squared Fluctuations
RNA	Ribonucleic Acid
ST	Strand Transfer Reaction
WT	Wild Type

Chapter 1. **INTRODUCTION**

I. HIV, AIDS and Antiretroviral Therapy

1. HIV Epidemiology and Polymorphism

In 1981, early cases of a new human epidemic began to emerge in the United States of America. In June 1981, the Centre for Disease Control and Prevention (CDC) published an article in *Morbidity and Mortality Weekly Report* which reported that 5 homosexual men were diagnosed with *Pneumocystis carinii* pneumonia in Los Angeles (Centers for Disease Control, 1981a). Soon after this report, another article published by CDC reported the cases of Kaposi's Sarcoma among 26 homosexual men in the United States of America - 20 in New York and 6 in Los Angeles (Centers for Disease Control, 1981b). These reports were the first official reporting of a disease that would later become known as the AIDS epidemic. The CDC published its first definition of AIDS in September 1982 as "a disease, at least moderately predictive of a defect in cell mediated immunity, occurring in a person with no known cause for diminished resistance to that disease"(Centers for Disease Control, 1982). It was characterized by diseases resulting from an impaired immune system.

In 1978, Robert C. Gallo's group reported the discovery of the first human retrovirus, Human T-cell Leukemia Virus Type 1 (HTLV-I) (Gallo et al., 1978). HTLV-I was the first of the only four retroviruses that infect human beings (the other three being HTLV-II, HIV-1 and HIV-2). HTLV-I is a retrovirus containing single-stranded RNA and causes cancers such as T-cell leukemia and T-cell lymphoma in adults. Gallo's team and his collaborators had also discovered the first cytokine called T-Cell Mitogenic factor, which was later named as Interleukine-2 (IL-2) in 1976 (Morgan, Ruscetti, & Gallo, 1976) which was the to be identified. IL-2 is a vital growth factor for the T-lymphocytes in the presence of which the

cells proliferate at significantly higher levels. This was one of the most important technological developments that helped isolation of HIV eventually.

Gallo suggested in 1982, that AIDS was possibly caused by a retrovirus similar to HTLV. Prior to that, James Curran of the CDC in Atlanta, USA, also proposed that AIDS was possibly caused by an infectious agent, most likely a new virus. In 1984, Gallo and his collaborators published a series of papers (Sarngadharan, Popovic, Bruch, Schupbach, & Gallo, 1984; Schupbach et al., 1984; Gallo et al., 1984; Popovic, Sarngadharan, Read, & Gallo, 1984) demonstrating that a retrovirus they had isolated, called HTLV-III in the belief that the virus was related to the leukemia viruses of Gallo's earlier work, was the cause of AIDS. In 1983, Luc Montagnier and his team at Pasteur Institute in Paris, France, had published a paper, describing a retrovirus they called LAV (lymphadenopathy associated virus, LAV), isolated from a patient at risk for AIDS (Barre-Sinoussi et al., 1983). The Nobel Prize for Physiology or Medicine in 2008 was awarded to Montagnier and Barré-Sinoussi for their co-discovery of the infectious agent, which came to be known as Human Immunodeficiency Virus (HIV).

Following the discovery of the HIV as the causative agent of AIDS, many advances were made in a short period of time. Some of the noteworthy advances include the understanding of the modes of transmission in 1984-85; the sequencing of the HIV-1 genome (Sanchez-Pescador et al., 1985; Ratner et al., 1985; Wain-Hobson, Sonigo, Danos, Cole, & Alizon, 1985); the main target cells CD4 T cells and macrophages were elucidated (Harper, Marselle, Gallo, & Wong-Staal, 1986; Shaw et al., 1984); production of key reagents; the genomic heterogeneity of HIV ('84) – including the innumerable micro-variants within a single patient (Saag et al., 1988; Hahn et al., 1986); the epidemic was closely monitored for the first time; the SIV-monkey model (Chalifoux et al., 1987; Chakrabarti et al., 1987); and the understanding of pathogenesis began (Lane & Fauci, 1985).

The spread of AIDS was rapid, soon after first reported in 1981 in the USA; fourteen countries reported cases of AIDS in 1982, and 33 already in 1983. By the end of 2008, 33.4 million people worldwide were estimated to be living with HIV. Figure 1 displays the prevalence of HIV in different regions of the world.

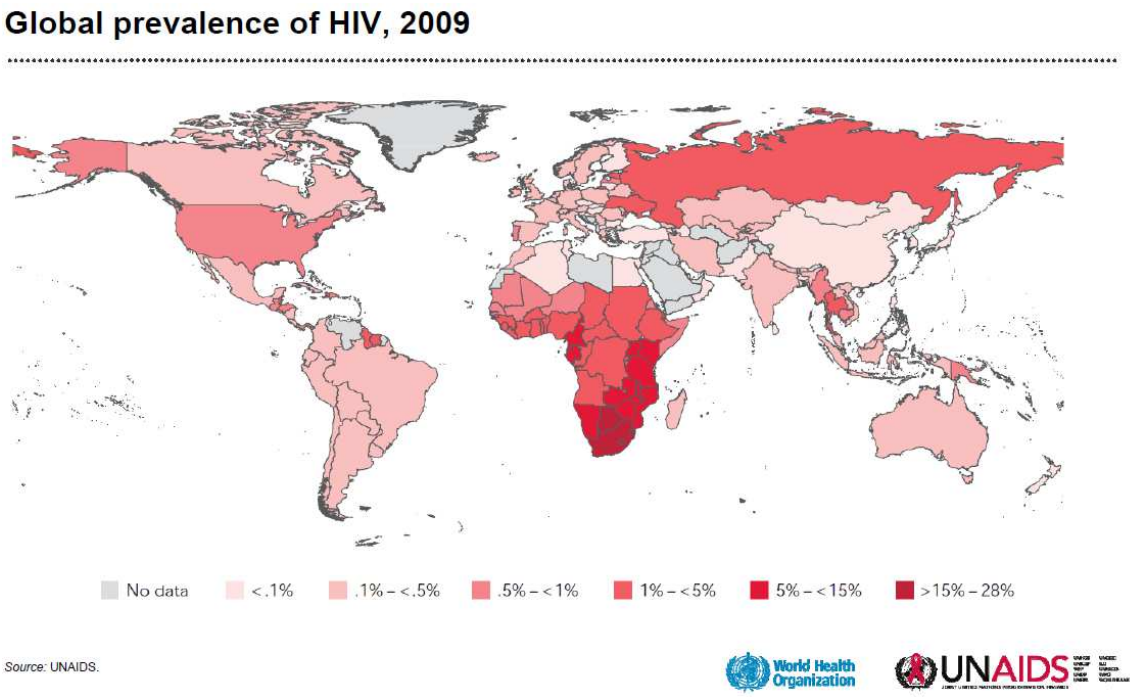

Figure 1. Global prevalence of HIV in 2009. The figure was adapted from the UNAIDS 2010 AIDS epidemic update report (www.unaids.org)

According to the UNAIDS 2010 report, in 2009, there were an estimated 2.6 million [2.3 million–2.8 million] people who became newly infected with HIV. This is nearly one fifth (19%) fewer than the 3.1 million [2.9 million–3.4 million] people newly infected in 1999, and more than one fifth (21%) fewer than the estimated 3.2 million [3.0 million–3.5 million] in 1997, the year in which annual new infections peaked .

As it can be seen from the regional profiles of HIV prevelance around the World (Figure 1), there is geographic variation between and within countries and regions. Epidemic patterns can change over time. A recent 2009 report from UNAIDS suggests that national epidemics throughout the world are experiencing important transitions. In Eastern Europe and Central Asia, epidemics that were once characterized primarily by transmission among

injecting drug users are now increasingly characterized by significant sexual transmission, while in parts of Asia epidemics are becoming increasingly characterized by significant transmission among heterosexual couples. Sub-Saharan Africa still bears an inordinate share of the global HIV burden. The epidemics in sub-Saharan Africa vary considerably, with southern Africa being the most severely affected. An estimated 11.3 million [10.6 million– 11.9 million] people were living with HIV in southern Africa in 2009, nearly one third (31%) more than the 8.6 million [8.2 million– 9.1 million] people living with HIV in the region a decade earlier. The high prevalence in sub- Saharan Africa can also be attributed to the fact that this region is believed to be the origin of HIV (Zhu *et al*., 1998). It is estimated that HIV entered the human population in 1931 through multiple infections from simian immunodeficiency virus (SIV) - infected nonhuman primates (Korber *et al*., 2000). Thus, the virus went undetected for many years after its entry into human population, until the cases of AIDS were detected in 1981. During these years, the virus could spread unrecognized, mainly because the late symptoms of AIDS coincide with symptoms of e.g. malnutrition and tuberculosis, which happen to be frequent problems in the infected population.

HIV can be divided into two major types: HIV-1 evolved from an SIV variant present in chimpanzees, whereas the other type, HIV-2 is the result of a zoonotic infection from SIV in sooty mangabeys (Heeney *et al*., 2006). HIV-1 is the most common and pathogenic strain of the virus. HIV-1 into a major group (Group M) and two or more minor groups. Group M was the first to be discovered and is the most common type of HIV, with more than 90% of HIV/AIDS cases deriving from infection with HIV-1 group M. Since its discovery it has infected at least 60 million people and caused more than 25 million deaths The M group is subdivided further subtypes. HIV-1 group M is further divided into subtypes, based on clusters typically appearing in phylogenetic analyses of genetic sequences of HIV-1 group M (Robertson *et al*., 2000). These subtypes are named A-D, F-H, J and K. In addition to these

subtypes of group M of HIV-1, there are also circulating recombinant forms (CRFs) derived from recombination between viruses of different subtypes which are each given a number. The other subtypes of HIV-1 are N, O and P which are much less prevalent than the group M.

Questions related to HIV-1 subtypes and its influence on disease progression (Kanki *et al*., 1999) and efficacy of antiretroviral treatment are still of major interest. HIV-1 subtype B is most prevalent in the developed, industrialized regions of the world, and therefore a representative of this subtype was used for development of antiretroviral drugs (Kantor *et al*., 2005). The genetic changes that distinguish B variants from non-B variants are believed to hamper the effectiveness of antiretroviral therapy (Descamps *et al*., 1998). HIV-1 subtype B is the best-studied variant of HIV-1 owing to the available resources and infrastructure for research in its region of prevalence. The other HIV-1 subtypes clearly deserve more attention than they have received so far. However, data collection efforts in regions of their prevalence (mainly Africa, South America and Asia) are less advanced than in Europe and North America. Hence, there exists a certain bias towards the HIV-1 subtype B. The diversity of HIV poses also one of the major challenges for HIV vaccine design (Walker & Burton, 2008). The sequence diversity within a single subtype, for example, can reach up to 20%. Clearly, the sequence diversity is an issue especially for antibody based vaccines that require conserved epitopes on surface proteins.

HIV-2 is much less pathogenic than HIV-1 and is restricted in its worldwide distribution. HIV-2 has remained largely restricted to West Africa, with its highest prevalence rates recorded in Guinea-Bissau and Senegal (de Silva *et al*. 2008). However, overall prevalence rates are declining, and in most West African countries HIV-2 is increasingly being replaced by HIV-1 (van der Loeff *et al*. 2006; Hamel *et al*. 2007). Most individuals infected with HIV-2 do not progress to AIDS, although those who do, show clinical symptoms indistinguishable from HIV-1 (Rowland- Jones and Whittle 2007). Thus, it is clear

that the natural history of HIV-2 infection differs considerably from that of HIV-1, which is not surprising given that HIV-2 is derived from a very different primate lentivirus.

2. Human Immunodeficiency Virus Type 1

Extensive knowledge on HIV has been accumulated and a substantial amount of literature is available (PubMed search for "The human immunodeficiency virus" extracted > 250, 000 publications). HIV is a part of the retroviruses family and, is a member of the genus of lenti-viruses, which indicates a long incubation period. Electron microscopy of particles in infected cell cultures shows spherical entities with a diameter of 100 - 120 μm (Figure 2 a). A conceptual representation of the virus architecture is depicted in Figure 2 b.

The retroviruses store their genetic information in ribonucleic acid (RNA) and thus require a mechanism to translate RNA to deoxyribonucleic acid (DNA), which is the carrier of genetic information in their hosts. Each viral particle contains two single stranded RNAs that are tightly bound to viral nucleocapsid proteins and two viral enzymes (reverse transcriptase and integrase) that are essential for a successful infection of the host cell. This complex is protected by a cone-shaped capsid comprising approximately 2,000 copies of the capsid protein (Figure 2 a).

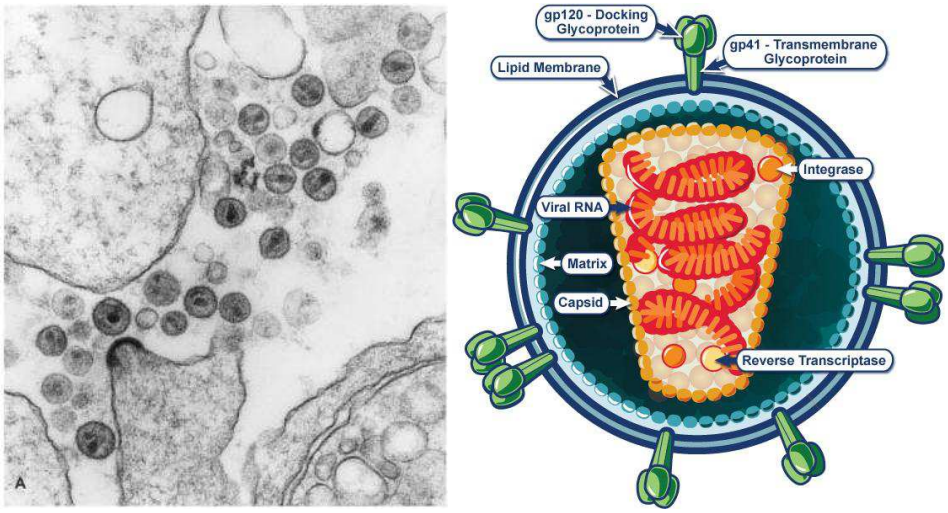

(a) (b)

Figure 2. (a) Electron micrograph of a budding HIV particle and mature HIV particles with visible viral core from Fields *et al*. (2007). (b) Schematic representation of a single HIV virion. (http://www.niaid.nih.gov/topics/hivaids/understanding/biology/pages/hivvirionlargeimage.aspx).

The viral cone is surrounded by a spherical matrix that is in turn covered by a lipid membrane. The viral spike is attached to the matrix. It is responsible for target cell recognition and cell entry. Figure 3 shows a schematic organization of the HIV genome. HIV encodes a total of 15 viral proteins in overlapping reading frames.

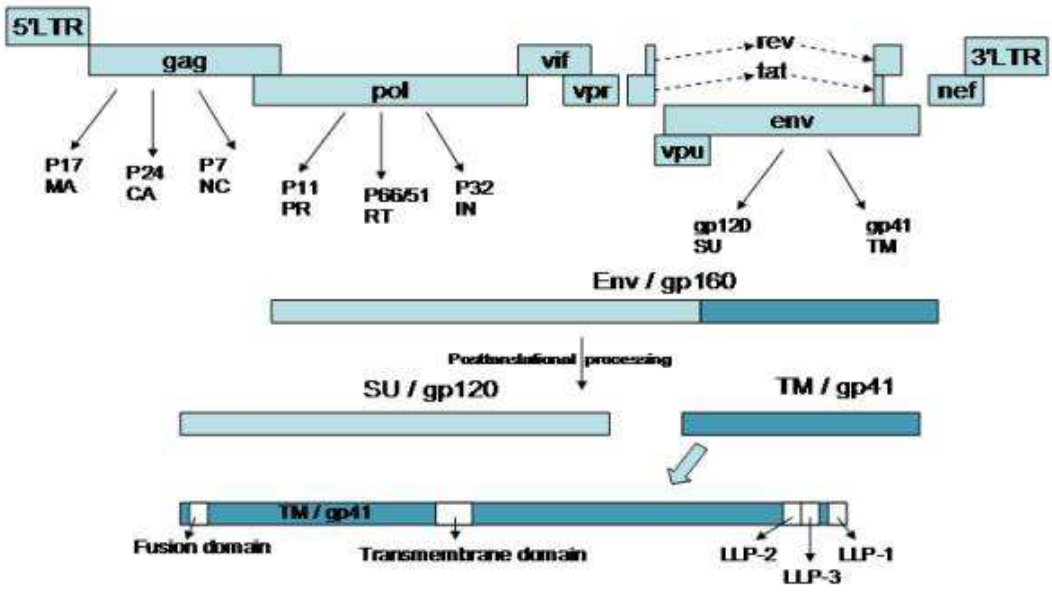

Figure 3. Depiction of the ~10 Kb HIV-1 genome showing the organization of genes and their transcriptional splicing (dashed lines) (Costin *et al.,* 2007).

HIV has several major genes coding for structural proteins. The gag (group-specific antigen) gene provides the physical infrastructure of the virus. The gag gene is the precursor of four viral structural proteins: p24 (the viral capsid), p6 and p7 (the nucleocapsid proteins), and p17 (the viral matrix). The polymerase gene (Pol) encodes for three proteins: the protease, the reverse transcriptase, and the integrase. Pol gene provides the mechanism for the retroviral reproduction. The env (envelope) gene codes for glycoprotein gp160 which acts as a precursor to the glycoproteins gp 120 and gp 41. The smaller genes encode for transactivators – Tat (Trans-Activator of Transcription), Rev (Regulator of Virion Expression), Vpr (Viral Protein R)- which enhance gene expression, and other regulatory proteins – Vif (Viral infectivity factor), Nef (Negative Regulatory Factor) and Vpu(Viral Protein U) which help the virus to be more efficient in its reproduction and to counter the defense mechanisms of the host cell.

3. HIV-1 subtypes and circulating recombinant forms

The global distribution of HIV-1 subtypes and recombinants indicated a broadly stable distribution of HIV-1 subtypes worldwide with a notable increase in the proportion of circulating recombinant forms (CRFs), a decrease in unique recombinant forms (URFs) and an overall increase in recombinants (Hemelaar *et al*., 2011). Particularly, in 2004-2007, CRF02_AG accounted for 8% of all global infections, following subtypes C (48%), A (12%) and B (11%). CRF02_AG is the predominant HIV strain circulating in West and West Central Africa (Fischetti *et al.,* 2004; Njai *et al*., 2006). Recently the recombinant CRF02-AG form was identified in the Amazon region of Brazil (Machado *et al*., 2009) and in China (Ye *et al*., 2012).

In France the frequency of antiretroviral-naive chronically HIV-infected patients infected with a non-B subtype reached 42% in 2006/2007, having increased significantly since

1998 (10%) and 2001 (33%). This evolution in subtype distribution was mainly due to a higher proportion of patients originating from sub-Saharan countries. Among these non-B subtypes, the most prevalent was CRF02-AG with a stable proportion around 20% between 2001 and 2006/2007 (Descamps *et al*., 2010).

Enzymatic and virological data support the concept that naturally occurring polymorphisms in different non-B subtypes can affect the susceptibility of HIV-1 to different antiretroviral drugs, the magnitude of resistance conferred by major mutations, and the propensity to acquire some resistance mutations (Martinez-Cajas *et al*., 2008). The genetic variation between viral isolates retroviral enzymes is estimated up to 25-35%; particularly the *pol* gene exhibits high variation, about 10-15 % for reverse transcriptase (RT) and 8-12% for integrase (IN) (Taylor *et al*., 2008). Integrase inhibitors are active *in vivo* against B and non-B subtypes. Furthermore, *in vitro* studies suggested that subtype C integrase is equally susceptible to INSTIs (Bar-Magen *et al.,* 2009). Similarly, the analysis of *pol* gene in infected patients showed that highly prevalent polymorphisms have little effect on INSTIs susceptibility (Low *et al*., 2009). Nevertheless, the comparison of IN sequences of B and CRF02_AG strains showed that CRF02_AG sequence differs from the B sequence by 13 residues (K/R14, V/I31, L/I101, T/V112, T/A124, T/A125, G/N134, I/V135, K/T136, V/I201, T/S206, L/I234 and S/G283) (Malet *et al*., 2008). Based on a model of the B HIV-1 integrase/DNA complex (Fenollar-Ferrer *et al*., 2008), it was suggested that several of these variations K/R14, T/V112, T/A125, G/N134, K/T136, and T/S206 may impact IN interaction with DNA or IN susceptibility to INSTIs. Later we compared the genetic barriers between B and CRF02_AG strains; we found that the variability between subtypes impacted the genetic barrier for G140C/S and V151I with a higher genetic barrier being calculated for subtype CRF02_AG suggesting a great difficulty in selecting these mutations for CR02_AG compared to subtype B (Maiga *et al*., 2009).

4. HIV Replication Cycle

The replication cycle of HIV is depicted on Figure 4 that represents schematically all principle steps of viral life cycle starting from cell entry to maturation of new infectious viral particles.

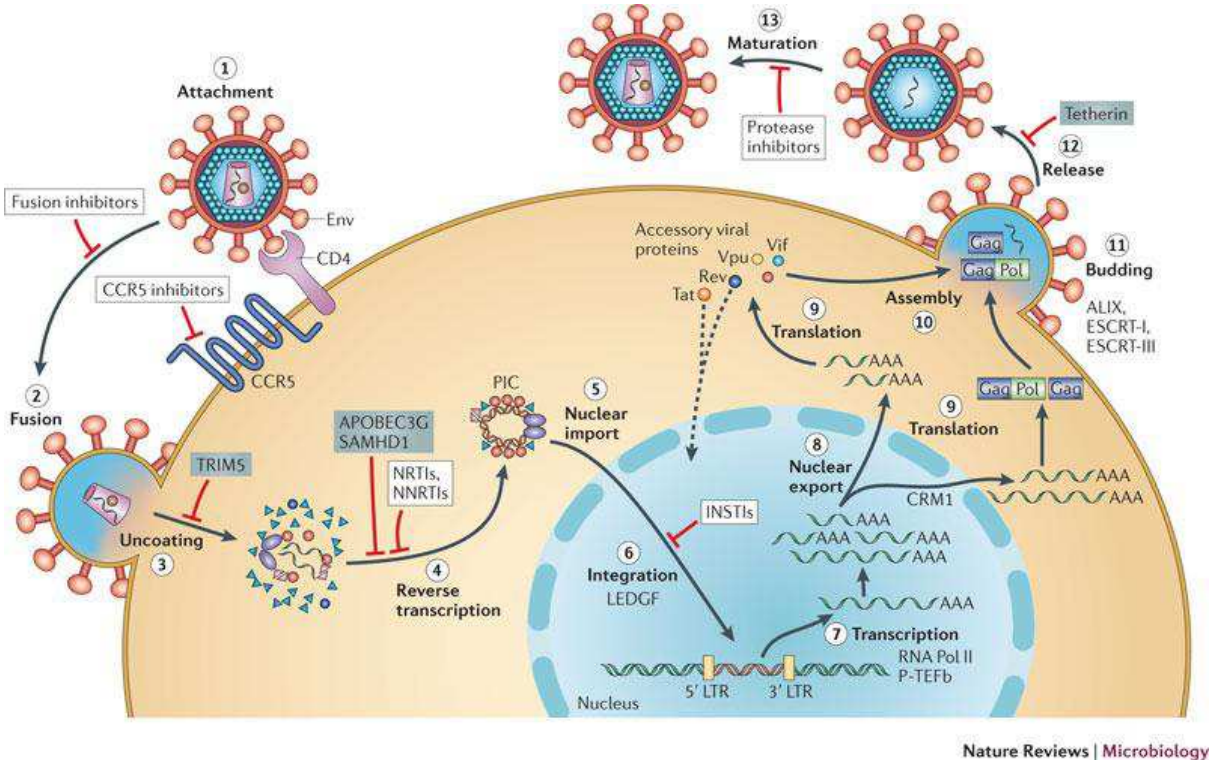

Figure 4. HIV replication cycle. The basic steps of the HIV replication cycle: viral entry, reverse transcription, integration, and formation of infectious particles (Cherepanov & Engelman 2012).

The HIV replication cycle begins when the gp120 protein on the viral surface binds to a CD4 receptor on the host cell surface by a mechanism involving conformational changes in both the CD4 receptor and the gp120 protein. The role of the CD4 receptor in HIV cell entry was identified shortly after the isolation of HIV (Dalgleish *et al*., 1984). The conformational changes in the gp120 protein leads to exposing an epitope which allows binding to a co-receptor, such as the chemokine receptors CCR5 or CXCR4, which are the most co-receptors used by HIV in-vivo. The importance of this co-receptor binding was emphasised by the compromised HIV-1 infectivity in the individuals harbouring mutant CCR5 proteins (Berger,

Murphy, & Farber, 1999). Following this, HIV is now able to enter into the cell by a process that involves fusion of the viral envelope with the plasma membrane of the host cell. Although, studies have supported the hypothesis that HIV primarily enters the target cell by endocytosis followed by fusion in the endosome and not by fusion directly at the plasma membrane (Uchil & Mothes, 2009). The entry of virus inside the host cell is followed by Reverse Transcription, catalysed by the the viral enzyme reverse transcriptase (RT), which transcribes the viral single-stranded RNA genome is converted into double-stranded DNA (dsDNA).). Together with viral and host proteins the dsDNA forms the pre-integration complex (PIC), which is guided to the nuclear pore. This is an essential step in the HIV replication cycle of HIV because it prepares the viral genome for the subsequent integration into the host chromosome. The viral enzyme Integrase is a part of the PIC which catalyzes the integration of viral DNA into the host chromosome, after the PIC has entered the nucleus of the host cell. The virus now exists as a part of the host genome and is referred to as Provirus.

The next phase of viral replication involves transcription of the integrated DNA provirus into messenger RNA (mRNA), which is then spliced into smaller pieces. The spliced mRNA fragments translated into regulatory proteins Tat and Rev, encouraging new virus production, upon being exported exported to the cytoplasm from the nucleus. The poly-proteins Env and Gag/Gag-Pol are also transported to the viral membrane where they participate in formation of new viral particles. In the final step of the viral cycle, new HIV-1 virions begin to assemble at the plasma membrane of the host cell. The Env poly protein (gp160) is transported to the golgi complex after going through endoplasmatic reticulum of the host cell. In the cell's Golgi complex gp160 protein is cleaved into two HIV envelope glycoproteins – gp120 and gp41 – which are further transported to the plasma membrane of the host cell. As the forming virion begins to bud from the host cell, Gag and Gag-Pol poly proteins associate with the the plasma membrane along with the HIV genomic RNA. The process of maturation can occur either in

the forming bud or in the immature virion after it buds from the host cell. After release, the Gag and Gag–Pol proteins are cleaved into their mature forms by the viral protease (PR) which is part of Gag or Gag–Pol polyproteins in the particle. The diverse structural entities assemble to produce a mature HIV virion which is further able to infect another cell.

II. Antiretroviral Drugs

The significant advancement in the understanding of HIV replication and its pathogenesis has helped in the identification of various pharmacological targets. The first anti-HIV agent to be licensed for clinical use was Zidovudine (AZT), in 1987. Since then, several anti-HIV compounds have been approved for the treatment of AIDS by the FDA and EMEA (European Medicine Agency) for treating HIV infections (DrugBank: http://www.drugbank.ca/). These compounds fall within different categories depending on the target within the HIV replicative cycle they interact with.

1. The Entry and Fusion Inhibitors

These inhibitors intercept the viral replication at the entry of the viral core into the cytosol of the host cell. Among all approved anti-HIV drugs, entry inhibitors are the only drugs that target a host protein rather than a viral protein. The group of entry inhibitors can be subdivided into classes of agents that act at different stages of entry: attachment and CD4 binding, co-receptor binding, and fusion. Currently, only antagonists that block CCR5 binding (Maraviroc) and fusion (Enfuvirtide) have been approved by the FDA for treatment of HIV-infected patients, although strategies to inhibit other aspects of HIV entry are under development (Tilton & Doms, 2010). In addition to maraviroc, more CCR5 and also CXCR4 inhibitors are under investigation (Este & Telenti, 2007). Prior to the use of co-receptor

blockers, it is necessary to determine the co-receptor which is being used by the virus for entering (Lengauer *et al*., 2007). Enfuvirtide (abbreviated ENF or T-20) prevents HIV from entering a target cell inhibiting fusion of virus and host cell membranes. ENF binds to a subunit of gp41 and therefore prevents the required conformational change that facilitates the fusion of host and viral membrane. Drug resistance mutations are usually located in the ENF-binding site on gp41 (direct resistance) or confer resistance indirectly via mutations in other regions of gp41 and even in gp120 (Miller & Hazuda, 2004).

2. The Reverse Transcriptase (RT) Inhibitors

The Reverse Transcriptase (RT) inhibitors interfere with the generation of a DNA copy of the viral genome. RT functions as a heterodimer to catalyze the conversion of the single-stranded genomic RNA into double-stranded DNA with duplicated long terminal repeats, which is integrated into cellular DNA by the viral integrase. RT heterodimer, comprising of p66 and p51 units (Figure 3), is generated by the viral protease from a p66/p66 homodimer by cleavage of the C terminal RNase H domain during maturation of the viral particle. The polymerase and RNase H catalytic sites are located on p66, while p51 plays a structural role (Kohlstaedt *et al.,* 1992).

There are two classes of RT inhibitors, distinguished by their mode of action. First of them is the group of nucleoside/nucleotide reverse transcriptase inhibitors (NRTIs). These are nucleoside and nucleotide analogues that are incorporated by the viral RT into the newly synthesized DNA strand. They are inactive in their parent forms and require successive phosphorylation steps by host cell kinases and phosphotransferases to form deoxynucleoside triphosphate (dNTP) analogs capable of viral inhibition. In their respective triphosphate (TP) forms, NRTIs compete with their corresponding endogenous dNTPs for incorporation by HIV RT. Once incorporated, they serve as chain-terminators of viral RT, thus, acting early in the

viral replication cycle by inhibiting a critical step of proviral DNA synthesis prior to integration into the host cell genome (Cihlar & Ray, 2010). The currently approved NRTIs are Zidovudine, Lamivudine, Didanosine, Zalcitabine, Stavudine, Abacavir, and Emtricitabine

The second group of RT inhibitors is the Non-nucleoside reverse transcriptase inhibitors (NNRTIs). They are small molecules that carry out the inhibition of RT by binding to a hydrophobic pocket in the proximity of the active site of the enzyme. After the inhibitor is bound, it impairs the flexibility of the RT resulting in its inability to synthesize DNA. Mutations can cause resistance to NNRTIs which results in reduced affinity of the inhibitor to the protein. Usually, a single mutation selected by one NNRTI is sufficient to confer complete resistance to all compounds of the drug class (Clavel & Hance, 2004).

3. The Protease Inhibitors (PIs)

Protease Inhibitors (PIs) interfere with the process of forming new infectious viral particles. The viral protease is engaged in virion maturation.

Protease targets the amino acid sequences in the gag and gag–pol polyproteins, which must be cleaved before nascent viral particles (virions) can mature. Cleavage of the gag polyprotein produces three large proteins (p24, p17 , and p7) that contribute to the structure of the virion and to RNA packaging, and three smaller proteins (p6, p2, and p1) of uncertain function. PIs are small molecules that bind to the active site of the protease and therefore compete with its natural substrates. PIs contain a synthetic analogue of the amino acid sequence of the gag–pol polyprotein at position that is cleaved by the protease. PIs prevent cleavage of gag and gag–pol protein precursors in acutely and chronically infected cells, arresting maturation and hence blocking the infectivity of nascent virions (Flexner, 1998). The resistance of HIV against PIs can be achieved by two mechanisms. The first one involves the exchange of amino acids in the protease such that the affinity to the inhibitor is

decreased while the natural substrates can be bound efficiently as opposed to the synthetic analogues (Clavel & Hance, 2004). Modifications of the affinity to the natural substrate alter also the efficiency of the protease. Thus, the second mechanism introduces compensatory mutations aiming at re-establishing the efficiency of the enzyme while maintaining resistance against the inhibitor. These compensatory mutations can occur either in the protease or in its substrate, i.e. at cleavage sites (Nijhuis *et al*., 2007). The four approved HIV-protease inhibitors are based on amino acid sequences recognized and cleaved in HIV proteins- Indinavir, Nelfinavir, Ritonavir and Saquinavir.

4. The Integrase Inhibitors (INIs)

Integrase inhibitors aim at preventing the enzyme activities, particularly integrating the viral DNA into the host chromosome. The integrase (IN) functions as a tetramer. Each monomer, which is cleaved out by the protease from the C-terminal portion of the Gag-Pol polyprotein (Figure 3), has three domains.

The N-terminal domain (NTD) contains a HH-CC zinc finger motif that is partially responsible for multimerization, optimal activity, and protein stability. The DDE motif in the catalytic core domain (CCD) forms the catalytic triad. The C-terminal domain (CTD) binds non-specifically to DNA with high affinity. The integration of the viral DNA requires three subsequent steps (Figure 4). During the 3' processing step the integrase removes a di-nucleotide from the long terminal repeat of each HIV-DNA strand. This step is followed by a process termed strand transfer occurring in the nucleus where the integrase cuts the cellular DNA and covalently links the viral DNA 3' ends to the target DNA. The final step, the required gap repair, is believed to be carried out by host DNA repair enzymes (Yoder & Bushman, 2000).

Two strategies were employed for the development of IN inhibitors. First, targeting the IN structure at the 3'-P step and the other targeting the ST step (Discussed in **III. Structure and Functions of HIV-1 Integrase**).

Currently only one FDA approved integrase inhibitor (INI) is available. Raltegravir (RAL) is a strand transfer inhibitor that interferes with the process by binding to the DDE motif in the catalytic domain (Hazuda *et al*., 2000). Successful inhibition of the integration process leaves the viral DNA in the nucleus, where it is re-circularized by the host's repair enzymes. Hence, the HIV life cycle is interrupted. Like other antiretroviral inhibitors, RAL develops/induces a resistance effect (Discussed in **III. Structure and Functions of HIV-1 Integrase**). The mechanism of resistance of HIV against INIs is still subject to investigation.

5. Highly Active Antiretroviral Therapy (HAART) and resistance effect to drugs

As discussed above, the HIV develops resistance against individual drugs and inhibitors. This problem required a new pharmaceutical strategy. An approach of combination therapy was developed which involved combining several antiretroviral compounds. This approach benefited the most from the development of drugs in NNRTIs and PI classes. Combination therapy can block the resistance effect more effectively for two reasons; first, multiple mechanisms are required for resistance to occur to all drugs in the regimen and second; multiple drugs suppress viral replication more effectively than single agents. This marked the beginning of the era of highly active antiretroviral therapy (HAART) in 1995. HAART combines a minimum of three drugs from at least two different drug classes targeting distinct proteins (Clavel & Hance, 2004). A typical HAART treatment combines two NRTIs plus either one PI or one NNRTI (Dybul *et al*., 2002). Combinations of antiretrovirals create

multiple barriers to the HIV replication process. This helps to keep the number of offspring low and reduce the possibility of a superior mutation.

In 2006, it was reported that the number of HIV related deaths declined as compared to the pre-HAART era. Despite the increasing concerns regarding antiretroviral resistance, the death rate among HIV-infected people continued to decline (Crum *et al*., 2006).

HAART suffers from certain limitations, despite of its success. HAART therapy is highly effective in delaying the onset of AIDS but its clinical utility is limited by viral resistance, non-adherence to therapy, and drug toxicity. Consequently, multidrug regimens are necessary for successful treatment. Since each HAART agent has its own unique adverse effect profile, selecting a regimen with a favourable profile may be difficult. For example, certain PIs produce adverse metabolic effects that may increase the risk of developing cardiovascular disease. On the other hand, NNRTI-based therapies may result a different side effect profile. Since each HAART agent has specific limitations, tailoring a regimen to the individual patient is of utmost importance for achieving optimal outcomes (Sension *et al.,* 2007). Once this therapy is initiated, it should never be stopped. This results from the fact that the selection pressure of incomplete suppression of viral replication in the presence of drug therapy can cause more drug sensitive strains to be selectively inhibited. In 1996, it was discovered that

In 2005-06, FDA approved Fixed-dose combinations of antiretrovirals (for example, Atripla). These are multiple antiretroviral drugs combined into a single pill, which helps to significantly simplify a drug treatment regimen by reducing the pill burden, helping to increase adherence and thus reducing potential development of viral resistance to the drugs. This may result in longer term effectiveness of the regimen. They may combine different classes of antiretrovirals or contain only a single class. Another milestone in HAART was the

discovery that the protease inhibitor ritonavir interferes with the liver enzyme cytochrome P450 (Kumar *et al*., 1996). This enzyme is involved in the metabolic processing of most protease inhibitors. Thus, the use of a small dose of ritonavir inhibits the liver enzyme, and helps to maintain optimal levels of other protease inhibitors in the patient's blood for a longer period of time. The boosting of protease inhibitors with ritonavir is standard as of 2001 – following the introduction of Kaletra (LPV+RTV) – and is usually denoted by PI/r.

II. Structure and Functions of the HIV-1 Integrase

1. Structural characterization of the HIV-1 Integrase

1.1 Experimental Data

The HIV-1 integrase is a 288-amino acid protein (32 kDa) encoded by the C-terminal part of the *pol* gene of the HIV-1 genome (Figure 3). It has three structurally independent domains: (i) the N-terminal domain (NTD) ($IN^{1–49}$) with a non-conventional HHCC zinc-finger motif, promoting protein multi-merization; (ii) the central core domain (CCD) ($IN^{50–212}$) containing a canonical D, D(35)E motif and involved in DNA substrate recognition; (iii) the C-terminal domain (CTD) ($IN^{213–288}$), which binds DNA non-specifically and helps to stabilize the IN•DNA complex (Asante-Appiah & Skalka, 1999). Neither the structure of isolated full-length IN from HIV-1 nor that of IN complex with its DNA substrate has been determined. Nevertheless, the structures of the isolated HIV-1 domains or two domains were characterized by X-ray crystallography (34 structures) and NMR analysis (9 structures) (Berman *et al*., 2000).

The structures of the isolated HIV-1 NTD ($IN^{1–49}$) and CTD ($IN^{219–270}$) domains have been determined by NMR (Cai *et al*., 1997; Eijkelenboom *et al*., 1995). The $IN^{1–49}$ polypeptide has a structure consisting of four helices stabilized by a Zn^{2+} cation in tetrahedral coordination

with the HHCC motif formed by His12, His16, Cys40 and Cys43, with the last 43–49 amino acids disordered (Figure 5).

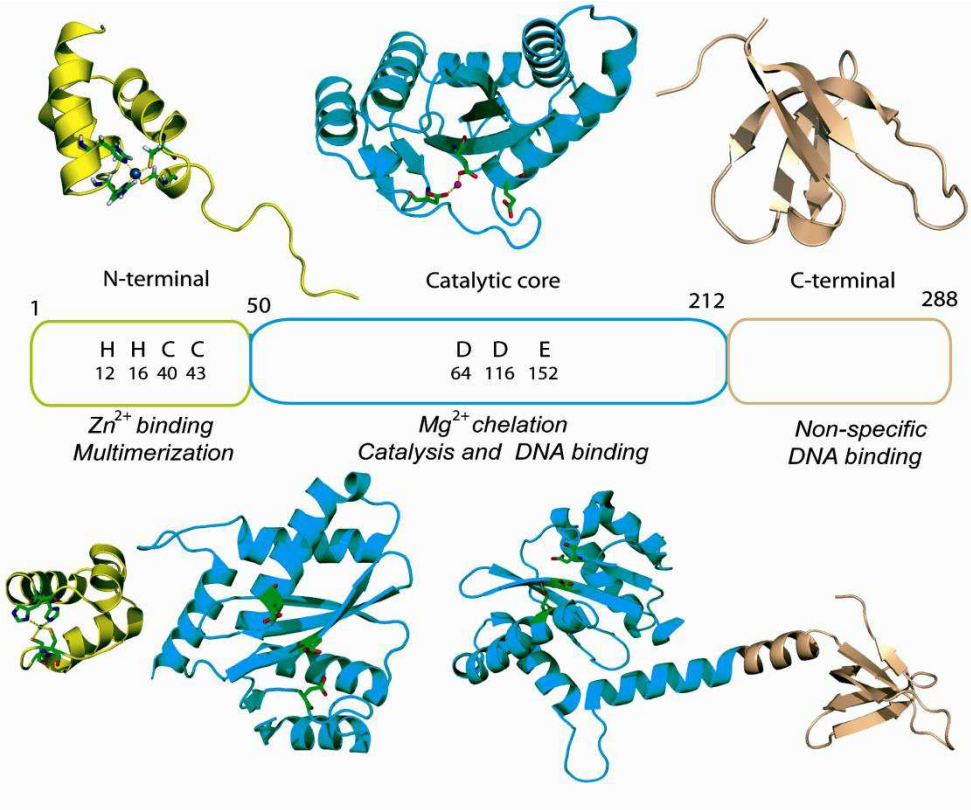

Figure 5. Structural domains of the HIV-1 integrase. (Top) N-terminal ($IN^{1–49}$, left), catalytic-core ($IN^{50–212}$, middle) and C-terminal ($IN^{219–270}$, right) domains; (bottom) left, N-terminal with catalytic-core domain ($IN^{1–212}$) and right, catalytic core with C-terminal fragment ($IN^{52–288}$). The structures are shown as cartoon with the side chains of the HHCC and DDE motifs in the N-terminal and catalytic-core domains rendered in stick and the Zn^{2+} and Mg^{2+} cations as balls; dashed lines indicate ion coordination. (Mouscadet *et al.,* 2010; Arora & Tchertanov, 2012).

The $IN^{219–270}$ structure consists of five antiparallel β-strands forming a β -barrel and adopting an SH3-like fold (Figure 5). The structure of the CCD (IN^{50-212}) has been resolved on many occasions, with W131D/F139D/F185K mutations used in each case to overcome the poor solubility of the protein. IN CCD has been characterized by X-ray analysis reported as 14 different crystal structures (1HYV, 1HYZ, 1EXQ, 1QS4, 1B92, 1B9D, 1BHL, 1BI4, 1BIS, 1BIU, 1BIZ, 1BL3, 1ITG and 2ITG). The wild-type IN was resolved with a poor precision (1ITG) ((Dyda *et al*., 1994), the other structures represent engineered mutants, either single (F185K/H) (Bujacz *et al*., 1997; Maignan *et al*., 1998; Molteni *et al*., 2001), double (W131E

and F185K; G149A and F185K or C56S and F185K) (Goldgur *et al*., 1998; Goldgur *et al*., 1999; Greenwald *et al*., 1999) or multiple (C56S, W131D, F139D and F185K) (Chen *et al*., 2006) mutants which were designed to overcome the poor solubility of the protein.

The core domain has a mixed α/β structure, with five β-sheets and six α -helices (Figure 5) (Dyda *et al.,* 1994). The active site residues D64, D116 and E152 are located in different structural elements: β-sheet (β1), coil and helix (α4), respectively. The CCD comprises a flexible 10 residues loop (140–149) that encompasses the catalytic site. Conformational changes in this loop are required for 3'-P and ST reactions (Mouscadet *et al*., 2010). The IN activities require the presence of the metallic cofactor(s), which binds to the catalytic residues D64, D116 and E152. The structures of Avian Sarcoma Virus (ASV) IN (Bujacz *et al.,* 1997) and the Tn5 transposase (Lovell *et al*., 2002) have provided evidence of a two-metal active site structure, which has been used to build metal-containing IN models (Karki *et al*., 2004; Wang *et al*., 2005). Crystallographic structures of $IN^{1–212}$ and $IN^{50–288}$ two-domain constructs have also been obtained for W131D/F139D/F185K and C56S/W131D/F139D/F185K/C180S mutants, respectively (Figure 6) (Chen *et al*., 2000; Wang *et al*., 2001). In the first of these structures, there is an asymmetric unit containing four molecules forming pairs of dimers connected by a non-crystallographic two fold axis, in which the CCD and NTD are well resolved, their structures closely matching those found with isolated $IN^{1–45}$ and $IN^{50–212}$ domains, and connected by a highly disordered linking region (amino acids 47–55). The X-ray structure of the other two-domain construct, $IN^{50–288}$, showed there to be a two-fold symmetric dimer in the crystal. The CCD and CTD were connected by a perfect helix formed by residues 195–221. The local structure of each domain was similar to the structure of the isolated domains. The dimeric interface between two CCD monomer subunits was found to be similar to the isolated CCD, whereas the dimer C-terminal interface differed from that obtained by NMR. Recently the complete structure of the HIV-1 homologue - the Primate foamy virus

(PFV) integrase complexed with the substrate DNA has also recently been reported (Hare *et al.*, 2010). All these available structural experimental data together with biochemical evidences are useful for generation of the HIV-1 IN models.

1.2 Theoretical Models

Integrase acts as a multimer (Ellison *et al*., 1995). Dimerization is required for the 3'-processing step, with tetrameric IN catalyzing the ST reaction (Faure *et al*., 2005; Guiot *et al*., 2006). Dimeric models were built to reflect the specific contacts between IN and the LTR terminal CA/TG nucleotides identified in vitro (De *et al*., 2003; Esposito & Craigie, 1998) (Figure 6 a). However, most models represent a tetrameric IN alone or IN complex with either vDNA or vDNA/hDNA, recapitulating the simultaneous binding of IN to both DNAs required for strand transfer (Figure 6 b–d). These models were either based on the partial crystal structure of IN (Gao, Butler, & Bushman, 2001) or constructed by analogy with a synaptic Tn5 transposase complex described in previous studies (Davies *et al*., 2000; Podtelezhnikov *et al*., 2003; Wielens, Crosby, & Chalmers, 2005). Most models include an Mg^{2+} cationic cofactors and take into account both structural data and biologically significant constraints. In particular, HIV-1 IN synaptic complexes (IN4•vDNA•hDNA) have been constructed to take into account the different enzymatic states occurring during the integration process (Figure 6 d) (Fenollar-Ferrer *et al*., 2008).

Such complexes have also been characterized by electron microscopy (EM) and single-particle imaging at a low resolution of 27Å (Ren *et al*., 2007). The X-ray structure of full-length integrase from Foamy Virus (PFV) in complex with its cognate viral DNA and INSTIs (particularly, RAL and ELV) has recently been reported (Figure 6 e) (Hare *et al*., 2010). In this complex, the retroviral intasome consists of an IN tetramer tightly associated with a pair of viral DNA ends.

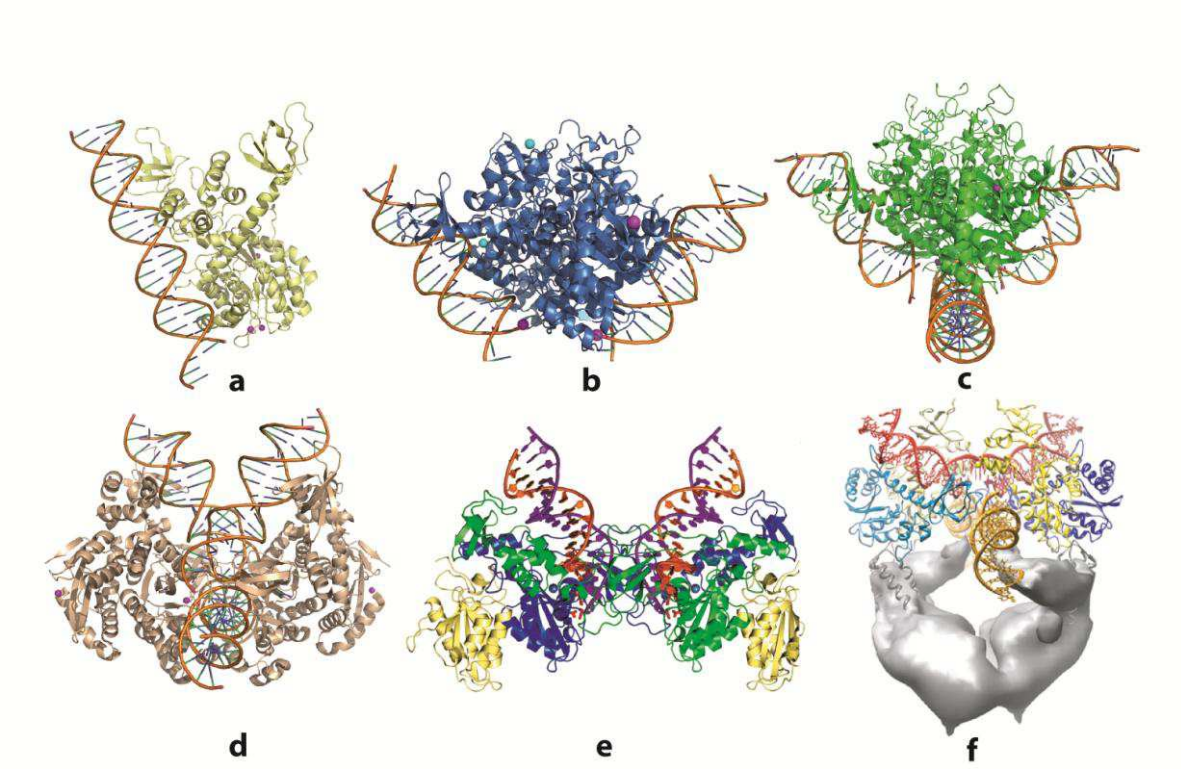

Figure 6. Integrase architecture and organization (Mouscadet *et al.,* 2010; Tchertanov & Arora, 2012). Theoretical models: (a) dimeric model of the full-length IN•vDNA complex (DeLuca et al., 2003); (b) tetramer models of the IN4•vDNA (Chen *et al*., 2006); (c and d) synaptic complexes IN4•vDNA•hDNA (Fenollar-Ferrer *et al*., 2008; Wielens *et al*., 2005); (e) X-ray structure of the PFV IN4•vDNA intasome (Hare *et al*., 2010); and (f) EM maps reconstitution of IN4•vDNA•hDNA complex with LEGDF(Michel *et al*., 2009). Protein and DNA structures are presented as cartoon with color-coded nucleotides and Zn^{2+} and Mg^{2+} cations shown as balls. The active site contains two Mg^{2+} cations in (a) and one in (b–d).

The overall shape of the complex is consistent with a low-resolution structure obtained by electron microscopy and single-particle reconstruction for HIV-1 IN complex with its cellular cofactor, the lens epithelium-derived growth factor (LEDGF) (Figure 6 f) (Michel *et al.,* 2009). The sequence identity between HIV-1 and PFV INs is low (22%), the structure-based alignment of the two proteins demonstrates high conservation of key secondary structural elements and the three PFV IN domains shared with HIV-1 IN have essentially the same structure as the isolated HIV-1 domains. This structure can be used to generate reliable HIV-1 IN models for INSTIs design, but the active site loop has a five-residue coil structure, rather than the 10 residues of the extended loop of HIV-1IN. This difference may be due to a

difference in the sequence of the two enzymes or an effect induced by DNA binding, and caution is therefore required in the use of this structure as a template for modeling biologically relevant conformations of HIV-1 integrase (Davies *et al.,* 2000; Hare *et al.*, 2010).

1.3 Structural and functional role of the Catalytic Site Loop

As was mentioned above, the catalytic site loop, comprising residues 140-149, is a crucial element of the HIV IN. This loop is known to be required for efficient IN function, but its precise role in integration in unknown. Several residues subject to primary mutations for resistance to both RAL and ELV (N155, E138, Y143, Q148) and to the secondary mutations (G140, Q146, S147) are located within the 140–149 loop of the CCD, which is required for efficient IN activity (Figure 7). The Molecular Dynamics (MD) simulation studies have demonstrated the importance of its flexibility for catalysis (Lee *et al*., 2005; Weber *et al*., 1998; Wijitkosoom *et al*., 2006). A significant conformational change, involving the E152 residue of the DDE motif, was observed upon viral DNA binding (Lins *et al*., 1999; Perryman *et al*., 2010).

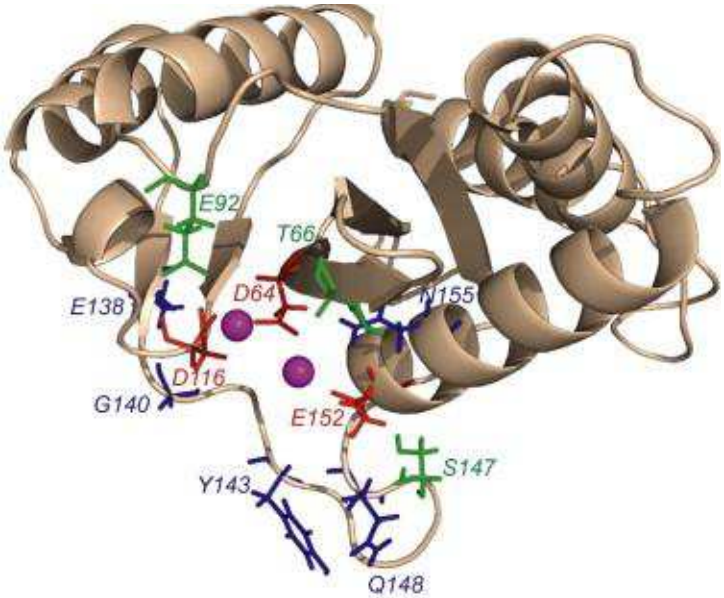

Figure 7. Main residues of the catalytic core domain mutated in the resistance pathways to RAL and ELV. Amino acids whose mutation leads to resistance to RAL (blue) or ELV (in green), and DD(35)E catalytic motif (in red) is shown as stick and the Mg^{2+} cations as balls. (Mouscadet *et al.,* 2010).

The coordination of a second Mg^{2+} cation in the active site induced a switch of E152 side chain conformation, directing this side chain towards the active site, but with no overall change in the conformation of the catalytic loop (Mouscadet & Tchertanov, 2009). This conformational flexibility is thought to be important for the catalytic steps following DNA binding, as a decrease in flexibility induced, for example, by the G140A/G149A mutations, results in lower levels of activity despite minimal effects on DNA binding (Greenwald *et al*., 1999). Moreover, several residues, particularly Q148, Q137, Q146, and N144, are predicted to constitute a DNA substrate binding site (Dolan *et al*., 2009) (Figure 8). Owing to its conformational flexibility, it has been suggested that (i), the loop is directly involved in contacts with substrates, thus playing a crucial role in the post-binding integration steps (Greenwald *et al*., 1999), and/or (ii) the conformation of the loop may depend on the presence of substrates and/or inhibitors (Hare *et al*., 2010).

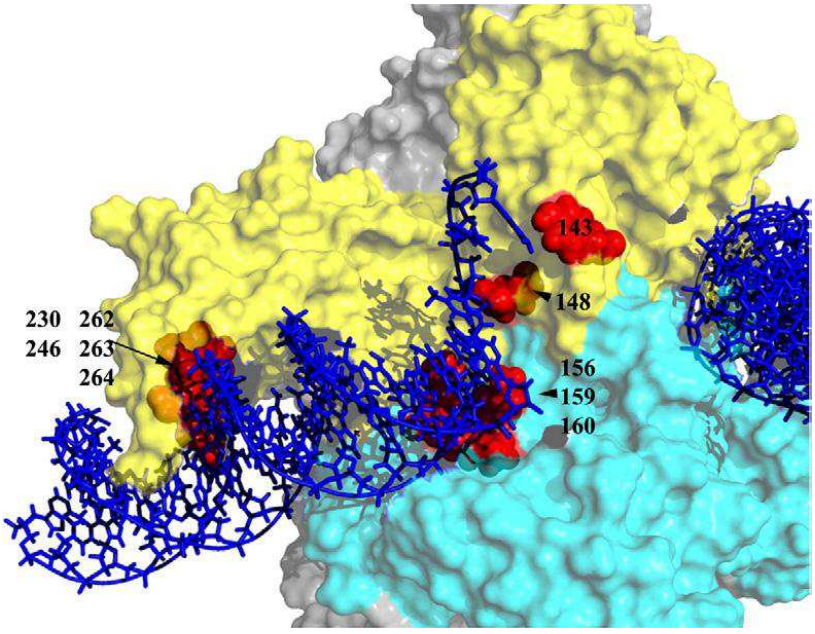

Figure 8: Residues reported in the literature to cross-link to viral LTR DNA. Interactions between viral DNA and HIV-1 IN have been demonstrated for residues Tyr143, Gln148, Lys156, Lys159, Lys160, Ser230, Glu246, Arg262, Arg263, and Lys264.33–36,38 These residues are shown in red in space-fill representation and shown only for one LTR end. (Dolan *et al*., 2009).

In all structures of single F185H, double W131E/F185K or triple G140A/G149A/F185K mutants generated to date, this flexible loop is either disordered or shows variable conformations (Figure 9 a).

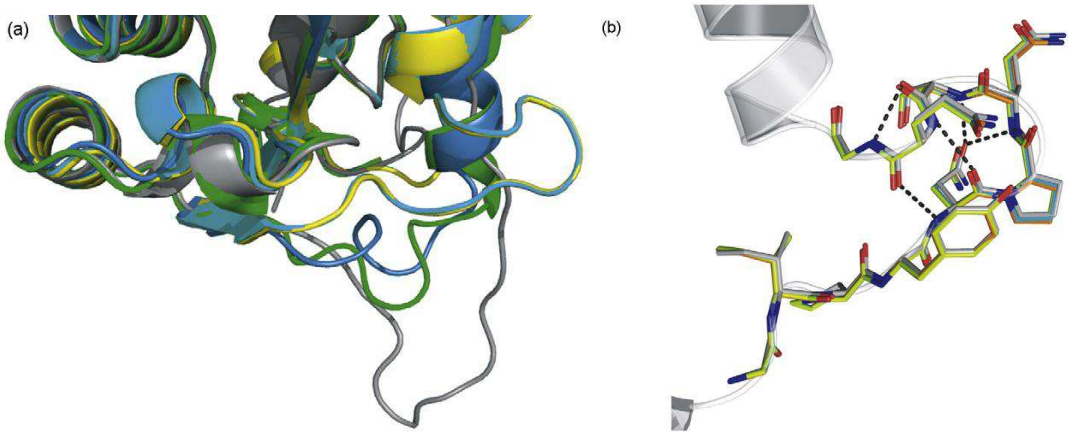

Figure 9. Structure of the HIV-1 IN catalytic site loop 140–149 (Mouscadet *et al.,* 2010; Arora & Tchertanov, 2012). (a) Superposition of catalytic loop found in 1BL3 (yellow) (Maignan *et al*., 1998), 1BI4 (cyan) (Maignan *et al*., 1998), 2ITG (gray) (Bujacz *et al*., 1996), 1BIS (blue) (Goldgur *et al*., 1998) and 1B9F PDB structures (green) (Greenwald *et al.*, 1999). (b) Theoretical modelof the catalytic site loop displaying the Ω-shaped hairpin structure (Mouscadet *et al*., 2009). The stabilizing H-bonds are indicated by dashed lines.

However, a secondary structure organization displaying a Ω-shaped hairpin motif that can move in a gate-like manner towards the active site has been observed (Figure 9 b) (Mouscadet *et al*., 2009). Modeling of the impact of RAL-selected mutations on IN structure and, particularly, on the structure of the 140–149 loop, indicated a strict conservation of IN CCD structure, including the Ω-shaped hairpin in the active site loop (Mouscadet *et al*., 2009). Finally, the dynamics of the HIV-1 IN CCD has been described for the wild type (WT) enzyme and few mutants, including the T66I/M154I and G140A/G149A mutants, in particular (Brigo *et al*., 2005; Lee *et al*., 2005; Lins *et al*., 1999). It has been shown that the dynamic behaviour of IN T66I/M154I mutants is not significantly different from that of the wild-type integrase, whereas the G140A/G149A IN mutant displayed major dynamic differences from the WT enzyme, again concentrated within the catalytic site loop region. A study based on the enhanced sampling technique reversible digitally filtered molecular dynamics (RDFMD) has

been applied to the CCD of the WT and G140A/G149A mutant enzymes. This study highlighted significant differences between in the behaviour of the catalytic site loop, potentially accounting for the decrease in activity observed in experimental studies of this mutant (Williams & Essex, 2009).

These results have highlighted the role of the flexibility of the loop in the development of resistance. In particular, they demonstrate the interdependence of residues G140 and Q148 for IN catalytic activity (Metifiot *et al*., 2010). Indeed, the Q148H mutation, which strongly affects IN catalytic activity, can be rescued by the compensatory G140S mutation, which restores an active configuration of the flexible loop (Delelis *et al*., 2009). The G140 residue is not directly involved in the cooperative flexibility of the catalytic loop, but plays a critical role in controlling the overall motion of the loop and its precise position relative to the phosphodiester bond to be cleaved (Mouscadet *et al*., 2009). The G140 residue participates in catalytic loop hinge formation and its mutation may restore specific contacts required for catalysis, between the loop of the double mutant and the end of the viral DNA.

1.4 Molecular Dynamics Simulation of HIV-1 Integrase

Structural data describes the protein in a static state and provides no time-dependant information about conformational flexibility. Molecular Dynamics (MD) simulations provide very useful information on the dynamic properties of IN and insight into the enzyme-substrate or enzyme-inhibitor complex interactions. The first study by (Weber *et al*., 1998) was performed for IN without the metal cations in the IN active site and it provides ideas about the slow-motion dynamics of the loop. Later MD simulations, performed on completely hydrated model of CCD with no metal cations, with one and with two metal cations have been reported a significant conformational change, involving the catalytic site loop and the E152 residue of the DDE motif, to occur when a second metal ion is included (Lins *et al*., 1999; Lins *et al*.,

2000; Lins, Straatsma, & Briggs, 2000). In contrast, the "rigid" molecular modelling shows that metal coordination does not affect the conformation of the catalytic loop (Mouscadet *et al.*, 2009) and fixation of the second Mg^{2+} ion in the active site induced a switch of E152 side chain conformation to those directed towards the active site (Savarino, 2007). The study of structural and dynamic properties of HIV-1 integrase reports the difference in the molecular properties of the full-length enzyme due to different construction methods or simulation techniques applied as well as the effects of two terminal domains, the NTD and CTD, on the CCD (Wijitkosoom *et al*., 2006).

The comparison of HIV-1 IN model structures derived from hybrid MD simulations, including classical and quantum mechanical/molecular (QM/MM) approaches, reveals two notable differences for two CCD loops, 116-119 and 140-149 (Nunthaboot *et al*., 2007). In the conventional MD, residues 116-119 show high mobility, however, this loop was quite rigid in QM/MM simulation. Differences in the dynamics of loop 140-149 lead to substantially different orientations of key amino acids, particularly K159 in the α4-helix resulted in two types of calculations.

The dynamic behaviour of the HIV-1 IN CCD has been described for the WT enzyme (Lins *et al*., 1999) and for the mutants, T66I/M154I (Brigo *et al*., 2005) and G140A/G149A (Lee *et al*., 2005). It has been shown that the dynamic behaviour of IN T66I/M154I mutant does not display significant differences (Brigo *et al*., 2005) with respect to the behaviour of the WT IN described by Lins (Lins *et al*., 1999), while the G140A/G149A mutant showed the important dynamic differences which were mainly concentrated in the catalytic loop region (Lee *et al*., 2005). This method was applied for study of enzyme complexed with the inhibitor 5CITEP (Nunthaboot *et al*., 2007; Barreca *et al*., 2003; Ni, Sotriffer, & McCammon, 2001; Nunthaboot *et al*., 2007) showed that the mobility of the loop is constrained due to the presence of the 5CITEP inhibitor.

Subsequent studies of the dynamic behaviour of the 140-149 loop as a function of the presence/absence of the vDNA demonstrated a markedly different behaviour of the residues in the loop in the chains A (contacting with viral DNA) and B (no contacts exist between CCD and vDNA) (De Luca *et al*., 2005). MD studies also demonstrate the importance of the flexibility of the 140-149 loop for catalysis (Lee *et al*., 2005). Moreover, in recent theoretical predictions it has been shown that the active site loop residues constitute a vDNA substrate binding site that include Q148, together with Q137, Q146 and N144 (Dolan *et al*., 2009; Chen *et al*., 2008). The large scale conformational dynamics and clustering analysis performed by Lee (Lee *et al*., 2005) permits to identify different conformational states of the WT catalytic loop, particularly, the open and closed conformations. The dynamics of Y143 in these simulations indicate the mobility allowing this residue to access the substrate easily.

2. HIV-1 Integrase functions

2.1 Integrase Activity

The HIV-1 integrase (IN) is a key enzyme in the replication mechanism of retroviruses, catalyzing the covalent insertion of the reverse-transcribed DNA into the chromosomes of the infected cells (Brown, 1990). Once integrated, the provirus persists in the host cell and serves as a template for the transcription of viral genes and replication of the viral genome, leading to the production of new viruses. Two reactions are required for the covalent integration of vDNA into host DNA (hDNA). The integrase first binds to a short sequence located at either end of the long terminal repeat (LTR) of the vDNA and catalyze an endo-nucleotide cleavage. This process is known as 3'-processing (3'-P) and results in the elimination of a di-nucleotide from each of the 3' ends of the LTR. The resulting cleaved DNA is then used as a substrate for integration or Strand Transfer (ST) reaction leading to the covalent insertion of the vDNA into the genome of the infected cell (Brown, 1990). This second reaction occurs

simultaneously at both ends of the vDNA, with an offset of precisely five base pairs between the two opposite points of insertion. The integration process is completed by the removal of unpaired di-nucleotides from the 5'ends of the vDNA, the filling in of the single-strand gaps between viral and target DNA (hDNA) and ligation of the 3'ends to the 5'ends of the hDNA (Brown, 1990; Chiu & Davies, 2004).

2.2 Role of the cationic co-factors

All integrase activities strictly require the presence of the metallic cationic cofactors, which are coordinated by residues of the catalytic triad (D64, D116 and E152 for HIV-1 IN) (Sante-Appiah & Skalka, 1999). The catalytic cation may be either Mn^{2+} or Mg^{2+} *in vitro*, but Mg^{2+} is the cofactor required *in vivo* and Mg^{2+} dependent activities also reproduce physiological activity more faithfully *in vitro*. IN displays non specific nuclease activity in the presence of Mn^{2+} and the Mg^{2+} containing enzyme is much less tolerant of sequence variations at the ends of the LTR than the Mn^{2+} enzyme (Esposito & Craigie, 1998). Several mutations are known to have no effect on IN activity in Mn^{2+}- dependent assays, whereas they do affect IN activity in Mg-dependent assays. For example, mutations of the HHCC domain known to be detrimental for the virus *in vivo* alter 3'processing *in vitro* in the presence of Mg^{2+}, but not in the presence of Mn^{2+} (Lee & Han, 1996). In addition, factors promoting integrase multimerization, such as Zn^{2+}, also specifically stimulate the Mg^{2+}-dependent activity of the enzyme, consistent with the multimeric nature of the functional enzyme (Leh *et al*., 2000). These differences between cofactor activities have resulted in pharmacological discrepancies, as some early IN inhibitors identified on the basis of Mn^{2+}-dependent assays were not active against the Mg^{2+} enzyme. Based on a model of another phosphatidyl transferase, the 3'-5' exonuclease of *E. coli* DNA polymerase I (Beese & Steitz, 1991), it was suggested early on that the retroviral integrase might contain two metal cation cofactors. As it

was mentioned above, the 3D structures of ASV integrase and the Tn5 transposase alone or in complex with DNA have provided structure-based evidence for a two-metal active site structure for retroviral integrases (Bujacz, Alexandratos, & Wlodawer, 1997; Lovell *et al*., 2002). Hypothesis of two-cations IN active site eventually led to a pharmacological strategy based on incorporation of Mg^{2+}-chelating pharmacophores for the rational design of IN inhibitors. Such pharmacopohores are present in all effective IN inhibitors, including RAL (Grobler *et al*., 2002).

2.3 Mechanisms of inhibition and target-inhibitors interactions

In terms of pharmacological development, two principal strategies have been considered for the development of IN inhibitors: one based on the free, unbound protein and the other on the preformed IN•vDNA complex. Both approaches were demonstrated to be feasible, with the inhibitors identification targeting either 3'-P, such blocking the binding of IN to the vDNA, or blocking the strand transfer reaction, targeting the IN•vDNA complex. Since the early 1990s, a number of compounds inhibiting one or other of these reactions have been identified *in vitro* (Semenova, Marchand & Pommier, 2008). However, the pre-integration complex (PIC) resulting from the association of integrase with viral DNA whether isolated from infected cells , or reconstituted *in vitro*, is highly stable, keeping the complex together for long enough after the 3'-processing reaction for subsequent integration to occur (Lee & Craigie, 1994). This complex has an intrinsically slow catalytic activity and does not dissociate after 3'-processing, limiting multiple turnover (Smolov *et al*., 2006). This weak catalytic activity is not detrimental in host cells, because a single integration event is sufficient for overall function, but it makes it difficult to develop competitive inhibitors of free IN. For these reasons, the Merck's team lead by D. Hazuda suggested in the middle of 1990s that the PIC would be a more suitable target for inhibitors

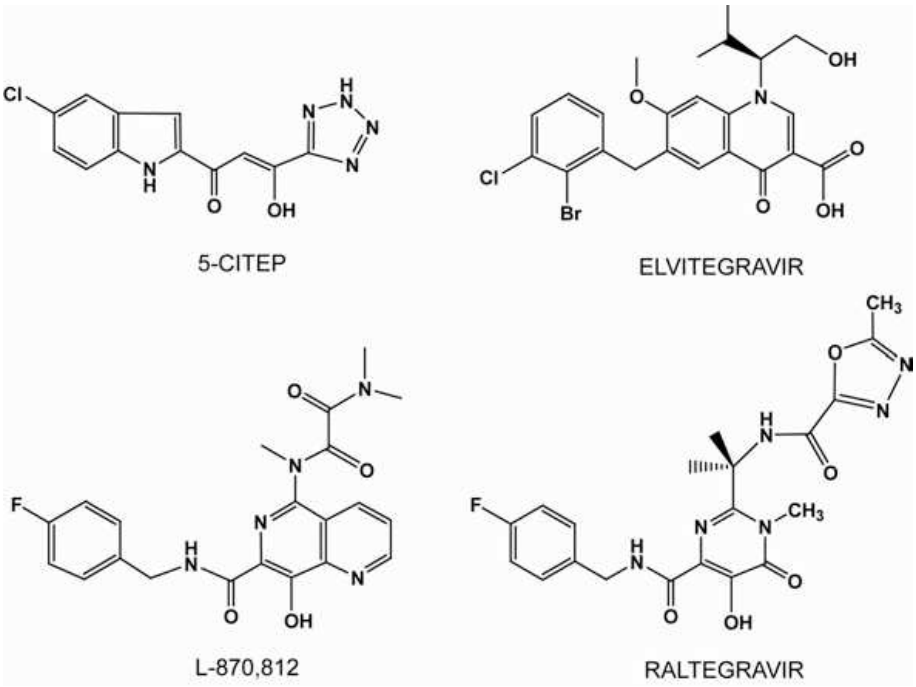

Figure 10. Integrase strand transfer inhibitors.

.This hypothesis proved to be correct, particularly given that PIC formation probably occurs within a capsid that is not fully dissociated, thus precluding easy access to free IN (Arhel *et al*., 2007). The design of new assays for screening ligands of the IN•vDNA complex eventually led to the identification of the first strand transfer inhibitors, L-731,988 and L-708,906 at the turn of the century (Hazuda *et al*., 2000). These compounds compete with the target DNA by binding to the IN•vDNA complex. They recognize a specific site close to the catalytic triad of CCD, which opens following a change in conformation induced by the binding and 3'-processing of the vDNA (Espeseth *et al*., 2000). The first selective ST inhibitors to be identified were diketoacids (DKAs) (Hazuda *et al*., 2000). Such compounds based on the β-ketoenol fragment efficiently chelate the Mg^{2+} cation required for the IN activity and their overall affinity for the target depends on their surrounding substituent groups (Figure 11 b) (Kawasuji *et al*., 2006; Tchertanov & Mouscadet, 2007). The prerequisites for a specific ST inhibitor include the presence of a chemical group including the heteroatoms, nitrogen or oxygen, capable of binding two divalent cations , and a hydrophobic

aromatic part to bind and stabilize the IN•vDNA complex, forming an active pharmacophores responsible for the activity of all integrase ST inhibitors (Barreca *et al*., 2005; Kawasuji *et al*., 2006). Compounds with these properties selectively target and bind to the IN•vDNA complex, close to the 3' end of the donor vDNA, thereby inhibiting target v or h DNA binding, resulting in selective inhibition of the ST process with no significant effect on the 3'-processing reaction (Pommier, Johnson & Marchand, 2005). They therefore act as IN•DNA interfacial inhibitors, and are known as Integrase Strand Transfer Inhibitors (INSTIs). The replacement of the carboxylate group by its tetrazolium bioisostere led to the development of 5-CITEP (Figure 10) and its analogue, S-1360.

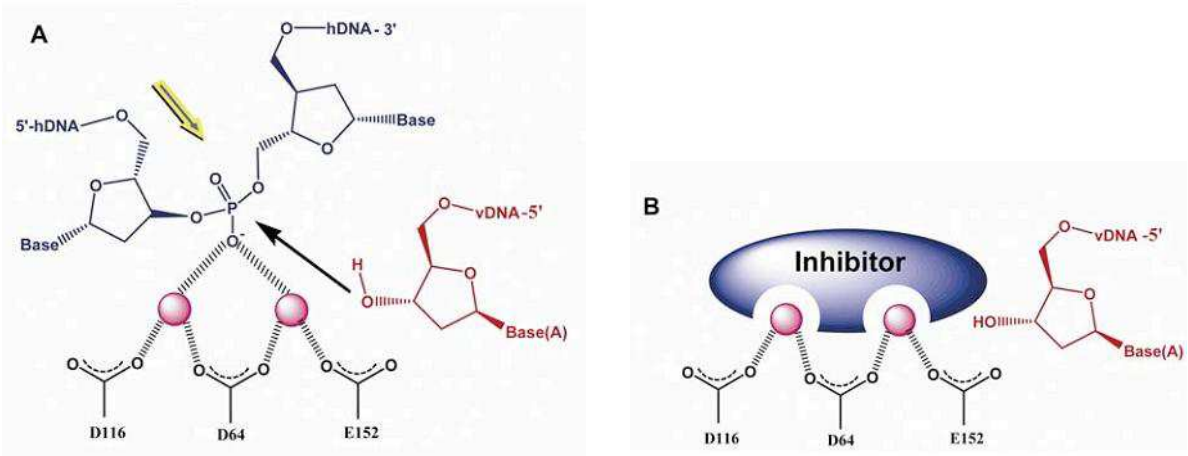

Figure 11. Strand transfer reaction and proposed mechanism of IN inhibition by INSTIs. a) A trans-esterification reaction involving a nucleophilic attack on the 3' hydroxyl group of the two newly processed 3' viral DNA ends on the phosphodiester backbone of the host DNA. The host DNA and viral DNA are shown in blue and red, respectively; the yellow arrow indicates the scissile phosphodiester. b) IN strand transfer inhibitors may chelate the two metal ions in the catalytic site, thereby blocking the binding of host DNA (Mouscadet & Tchertanov, 2009).

Despite the weak activity of these molecules against IN, the structure of the IN/5-CITEP complex has been determined, making it possible to construct a model of the inhibitor binding to the active site metal cation (Goldgur *et al*., 1999). Modifications to the β, γ-diketoacid part

of the molecule initially led to the replacement of this group by 8-hydroxy quinoline, to increase antiviral activity and to overcome pharmacological limits, such as serum protein binding (Zhuang *et al*., 2003). Compounds from this family, such as Merck L-870,812 (Figure 10), have potent antiviral activity, providing the proof-of-concept for INSTI activity *in vivo* despite their toxicity *in vivo* (Hazuda *et al*., 2004). The L-870,812 series of compounds was not developed further, but the dihydroquinoline JTK303/GS9137 derived from quinolone antibiotics was used for further drug development and is now at the advanced clinical development stage, under the name of Elvitegravir (ELV) (Figure 10) (Sato *et al*., 2006).

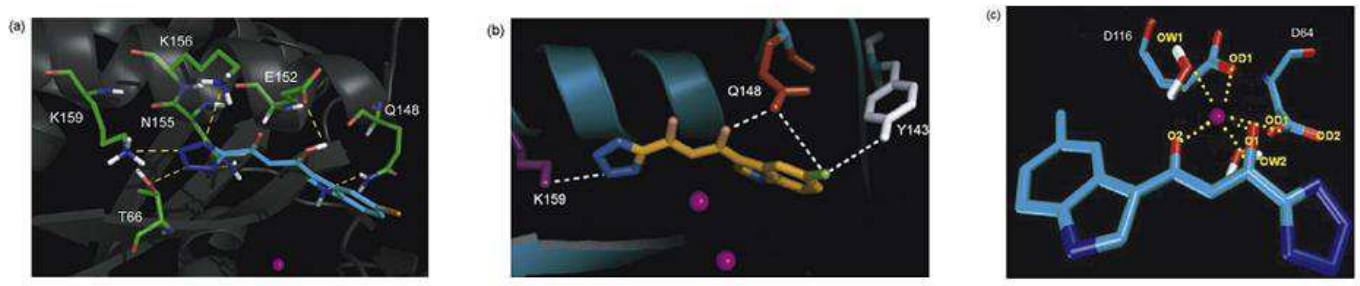

Figure 12. 5-CITEP binding to the HIV-1 IN (Mouscadet *et al.,* 2010). (a) X-ray structure (Goldgur *et al*., 1999); (b) theoretical modeling (Savarino, 2007); (c) hybrid QM/MMMD simulations of IN complexed with the inhibitor (Nunthaboot *et al*., 2007). H-bonds are indicated by dashed lines in (a and b); coordination bonds and H-bonds by dotted lines in (c).

The cavity formed by residues D64, C65, T66, H67, E92, N120, F121 and D116 defines the active site for the 3'-P reaction, whereas residues Q62, I141, P142, Y143, Q148, I151, E152, N155, K156 and K159 define the ST cavity. Theoretical studies have predicted that the Q146, Q148 and N144 residues of the loop form a DNA binding site (Agapkina *et al*., 2006; Dolan *et al*., 2009). An early INSTI, 5-CITEP was co-crystallized in the centre of the active site, lying between the D64, D116 and E152 residues. Its tetrazolium moiety forms H-bonds with T66, N155, K156 and K159, the ketoenol motif being H-bonded with E152, whereas the indol ring of the inhibitor points toward the Q148 residue (Figure 12 a) (Goldgur *et al*., 1999). A docking study positioned 5-CITEP close to Y143 and Q148 (Figure 12 b). Hybrid QM/MM simulations showed that 5-CITEP interacted directly with the Mg^{2+} cation

via its ketoenol fragment whereas the tetrazole ring points toward residues N155, K156 and K159 (Figure 12 c) (Nunthaboot *et al*., 2007). Finally, a MD study of 5-CITEP bound to IN showed that the mobility of the 140–148 loop is constrained by the presence of the inhibitor (Barreca *et al*., 2003). Rigid or semi-rigid docking of RAL and ELV onto the CCD confirmed that both inhibitors chelate the Mg^{2+} cation via coplanar β-ketoenol fragments (Figure 13 b) (Barreca *et al*., 2006) and that ELV may also chelate the cation in a non-coplanar metal-binding mode (Savarino *et al*., 2007) (Figure 14 b).

A similar study demonstrated that RAL contacts the three catalytic residues, D64, D116 and E152, and interacts with the five residues, T66, E92, Y143, Q148 and N155, involved in primary resistance (Figure 13 a) (Serrao *et al*., 2009) (Table 1). Like RAL, ELV was found in the vicinity of T66, E92, G140, Y143, Q148 and the catalytic residues D116 and E152 (Figure 13 a). In another theoretical study, two different modes of binding were reported for RAL (Loizidou *et al*., 2009) (Figure 13 c d), corresponding to different modes of Mg^{2+} chelation and an absence of direct contacts with Y143 or N155 and Q148 residues. The authors also reported only one conformation observed for ELV, which displayed tolerant contacts with residues D64, D116, E152, N155, G140 and T66 and made additional contact with residues C65, H67, N117 and G118 (Figure 14 c).

A comparative residue interaction analysis (CoRIA) allowing evaluation of the non-bonded interaction energies of integrase inhibitors with individual active sites suggested that D64, T66, V77, D116, E152 and K159 were the key residues influencing the binding of ligand to the integrase (Dhaked *et al*., 2009). However, the exact modes of binding of both inhibitors remain a matter of debate. ELV was also docked onto the Tn5 transposase•DNA complex, which is considered as a surrogate model for studying the mechanism of action of INSTIs (Pasquini *et al*., 2008; Ason *et al*., 2005).

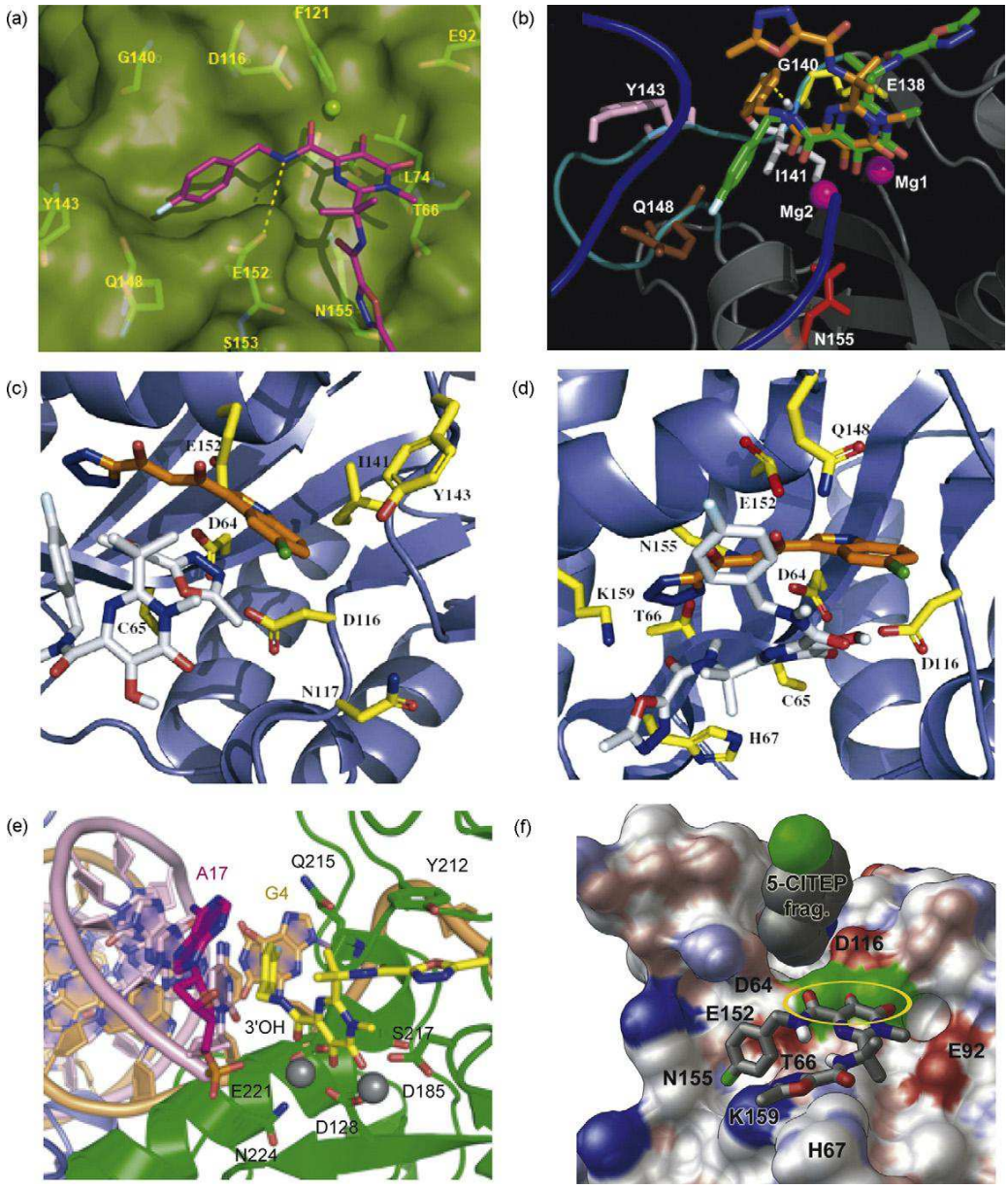

Figure 13. Binding modes of raltegravir (Mouscadet *et al.,* 2010). (a) Raltegravir docking (GOLD 3.2) on 1BL3 structure (Serrao *et al*., 2009). RAL (magenta) and residues in close contact (green) are indicated as sticks; (b) RAL induced-fit docking on the IN•DNA complex (Barreca *et al*., 2009). Two poses of RAL (orange) and (green) and residues in closed contact are indicated as sticks and the protein is shown as a secondary structure cartoon; (c) two different conformations of RAL obtained by docking (Autodock 4.0) on the 5-CITEP•IN complex (Loizidou *et al*., 2009). RAL and residues in close contact are indicated as sticks and the protein is shown as a secondary structure cartoon. 5-CITEP indicating the terminal portion of 3'-processed viral DNA, RAL, the catalytic triad (D64, D116 and E152) and interacting key residues are shown as orange, gray and yellow carbon backbone representations, respectively. (e) RAL (yellow) binding determined in X-ray structure of the PFV IN•DNA complex. Protein (green) and DNA (rose and orange) are shown as cartoons, with A17 and the side chains of indicated amino acids as sticks; (f) RAL (gray sticks) binding mode in 5-CITEP•IN complex predicted by dynamic approach (Perryman *et al*., 2010). A solvent-accessible surface is shownwith labels for key residues and 5-CITEP.

The binding mode proposed was highly consistent with mutation profile of Tn5 transposase•DNA complex (This will be discussed below, in paragraph 3. **Resistance to Integrase Strand Transfer Inhibitors**).

These residues are equivalent to the active site residues in the CCD of HIV-1 IN. Moreover, the hydroxyl group of the N-1 chain formed two H-bond interactions with S100. Finally, the 2-F and 3-Cl substituted benzyl group was perpendicular to the quinolone ring, establishing favourable van der Waals interactions with E190 and D188. When flexibility of inhibitor was taken into account through the induced-fit docking (IFD), two different binding modes common to INSTIs were identified, involving two-metal chelation with aromatic groups directed toward the active site catalytic loop (Barreca *et al*., 2009). The best-ranked model of RAL binding was characterized by a similar two-metal-binding mode, with the fluorobenzyl group pointing toward the Q148 residue and establishing interactions with the terminal adenine of the 3'-processed vDNA (Figure 13 b). Moreover several residues, particularly E92, K159, Y143, N155, Q148 and S143, underwent marked changes during the IFD run. The second type of complex also highlighted the residues H67, D116, Y143 and Q148 as the location of the most significant change during the IFD.

ELV pose obtained by IFD shows that inhibitor is pointed to either a one-metal-binding mode with three H-bonds stabilizing the IN-ELV complex (Figure 14 f) or a two-metal-binding mode differing in the orientation of the halogenated benzyl group. No direct contacts between the inhibitors and residues involved in resistance were observed, but inhibitors were consistently found in the close vicinity of these residues. From this study, it may be hypothesized that the difference between the resistance pathways for RAL and ELV may be related to alternative modes of inhibitors binding. RAL was docked to a set of conformations including different backbone and side chain conformations from MD simulations (Perryman *et al*., 2010).

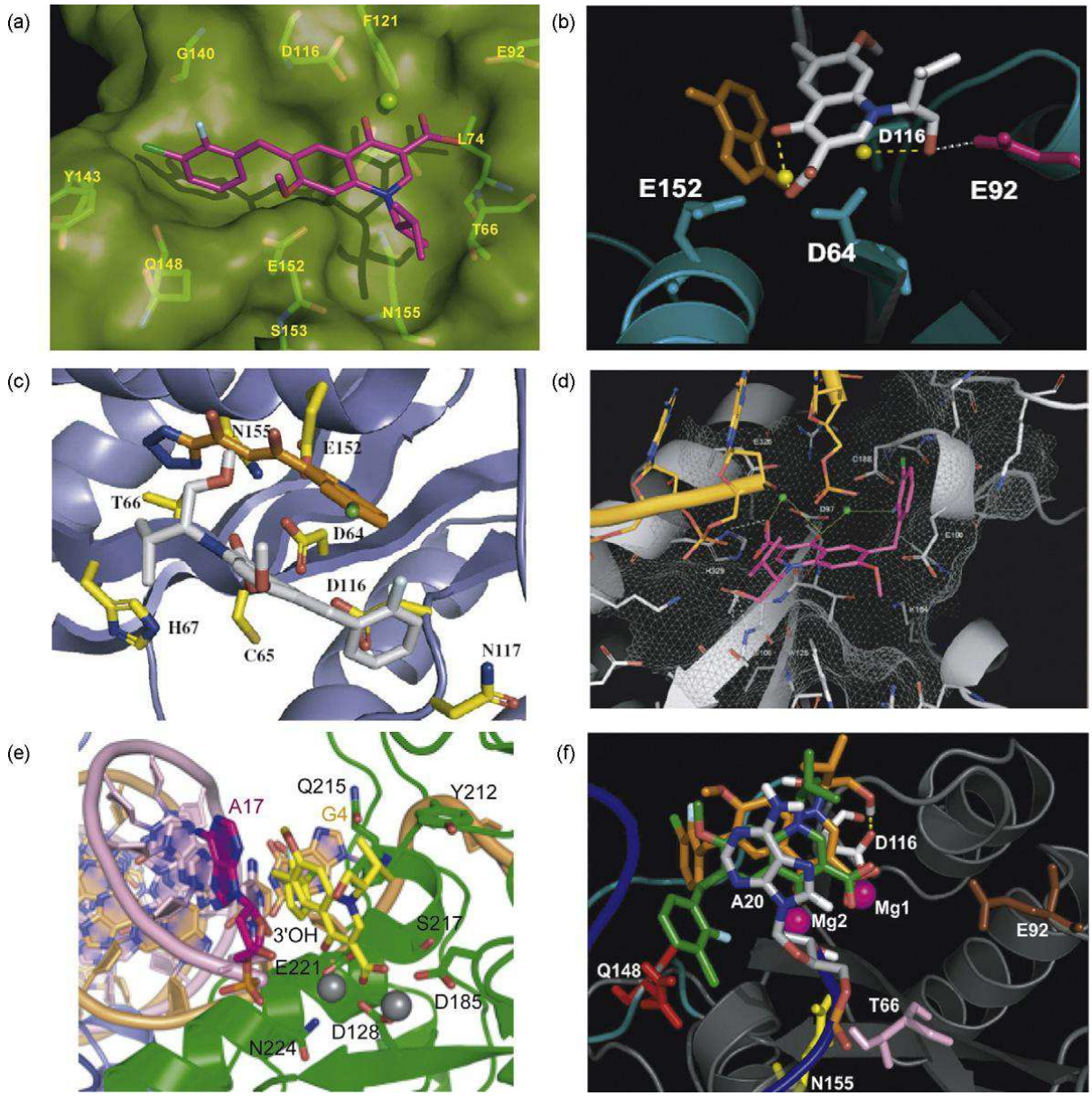

Figure 14. Binding modes of elvitegravir (ELV) (Mouscadet *et al.,* 2010). (a) ELV docking (GOLD 3.2) on the 1BL3 structure (Serrao *et al*., 2009). ELV (magenta) and residues in close contact (green) are indicated as sticks; (b) ELV docking (GOLD 3.1) on the modified 5-CITEP•IN complex (two Mg^{2+} cations in the active site and 5-CITEP replaced by the adenine) (Savarino, 2007). ELV (gray), adenine (orange) and residue in close contact (magenta) are indicated as sticks, Mg^{2+} cations as balls. c) ELV conformation obtained by docking (Autodock 4.0) on the 5-CITEP•IN complex (Loizidou *et al*., 2009). ELV (gray), 5-CITEP (orange), catalytic site rsidues and residues in close contact (yellow) are indicated as sticks. (d) ELV docking (GOLD 3.0) on Tn5 transposase•DNA complex (Pasquini *et al*., 2008). Mg^{2+} cations are presented as green balls, ELV (magenta), DNA (yellow) and Tn5 Tnp residues in close contact (gray) indicated as sticks. Tn5 Tnp/ELV interactions are shown as dashed lines. (e) ELV (yellow) binding observed in X-ray structure of the PFVIN•DNA complex (Hare *et al*., 2010). Protein (green) and DNA (pink and orange) as cartoons, with A17 and the side chains of indicated amino acids as sticks; (f) ELV induced-fit docking on the IN•DNA complex (Barreca *et al*., 2009). Two positions of ELV (orange) and (green) and residues in closed contact are indicated as sticks; H-bond represented as yellow dashed lines. The divalent metal ions are shown as magenta balls, the active site loop is highlighted in cyan, and the viral DNA backbone is depicted in blue.

The best binding mode involved close contact between both Mg^{2+} ions and the His67 residue and important interactions with T66, K159 and N155. An alternative, less favourable, flipped mode yielded contacts with the E92 accounting for the possible involvement of this residue in an alternative resistance pathway (Figure 13 f). In the G140S/Q148H mutant, as in the WT and primary mutants, RAL coordinates two Mg^{2+}cations.

3. Resistance to Integrase Strand Transfer Inhibitors (INSTIs)

3.1 Resistance phenomenon

As with other antiretroviral drugs, resistance to INSTIs emerges through the selection of mutations in the IN-coding region of the *pol* gene that affect the susceptibility of the virus to the inhibitors. More than 60 mutations have been specifically associated with resistance to INSTIs *in vitro* and *in vivo* (Ceccherini-Silberstein *et al*., 2009). Resistance to RAL *in vivo* has been associated, to different degrees, with 14 mutations, but the virologic failure of RAL treatment initially observed during the BENCHMRK trials was unambiguously associated with two principal independent genetic pathways involving primary mutations affecting the N155 (N155H) and Q148 (Q148K/R/H) residues carried by 68% of subjects (Cooper *et al*., 2008). Clonal analysis of the viral populations in patients displaying treatment failure on RAL showed that no viral clone carried mutations simultaneously at positions 148 and 155, demonstrating the independence of the two main pathways (Table 1). A third pathway, involving the Y143R/C/H mutation and conferring a large decrease in susceptibility to the inhibitor, was subsequently described (Delelis *et al*., 2010; Sichtig *et al*., 2009). Y143R/C/H mutations occur less frequently and later than the other two mutations described above (Croxtall & Keam, 2009). Phenotypic analysis showed that the presence of the mutation at position 148, together with one or more secondary mutations, resulted in greater resistance to RAL than observed for viruses carrying the N155H mutation. The level of phenotypic

resistance to RAL associated with the Q148 or Y143 mutation is always much higher (>100 times higher) than that associated with N155H (Hatano *et al*., 2010). These mutations were not detected in various studies on IN polymorphism in INSTI-naive patients, confirming their likely role in conferring resistance to this class of drugs (Lataillade, Chiarella & Kozal, 2007; Rhee *et al*., 2008). Secondary mutations increasing the fitness of the resistant viruses have been identified and include L74 M, E138A/K and G140A/S for the Q148H/R/K pathway and L74 M, E92A/Q, T97A, Y143H/C, V151I, G163K/R and D232N for the N155H pathway (Table 1) (Mouscadet *et al*., 2010). In particular, the G140S mutation rescues a replication defect resulting from the Q148H primary mutation (Delelis *et al*., 2009). The change in IC_{50} was found to be largest in patients carrying viruses following the 148 pathway, with secondary mutations increasing resistance from a factor of 10 (Q148H) to a factor exceeding 500 (Q148H + G140S and Q148K + E138A + G140A). A small number of mutations involving residues E92, E157 or T97A/G163R may lead to alternative pathways of resistance (Ceccherini-Silberstein *et al*., 2009; Ghosn *et al*., 2009). Other double mutations conferring substantial resistance *in vitro* to RAL, such as T66I/E92Q, T66K/L74 M and F121Y/T125K, have been identified *in vitro* (Table 1). It was recently confirmed *in vivo* that some double or triple combinations of secondary mutations, such as T97A/G163R, V72I/T97A/G163R, V72I/L74 M/T97A or L74 M/T97A/V151I, may lead to moderate resistance to RAL in the absence of primary mutation (2<FC<5). The resistance mutations identified in a phase II study of ELV included E92Q, T66I/A/K, E138K, S147G, Q148R/H/K and N155H (Mccoll *et al*., 2007). The Q148R/H/K and N155H, E92Q and T66I substitutions were the principal causes of ELV resistance (Goethals *et al*., 2008) summarising in (Table 1). *In vitro* susceptibility assays with recombinant clones indicated that two other mutations, Q146P and S147G, conferred a significant but more moderate decrease in ELV susceptibility (decrease by a factor of 11), suggesting that these mutations may also be primary mutations involved in resistance to this

compound (Shimura *et al*., 2008). Other mutations — the H51Y, Q95K, and E157Q substitutions — confer smaller decreases in ELV susceptibility, but increased resistance further when combined with the T66I or E92Q mutations, suggesting that these mutations constitute secondary resistance mutations. H114Y, L74 M, R20K, A128T, E138K and S230R were observed in another in vitro study, in association with one or more of the four primary mutations (Goethals *et al*., 2008) (Table 1). As single mutations, they had little effect on susceptibility to either ELV or RAL. The accumulation of these inhibitors selected IN mutations resulted in a significant decrease in the rate of viral replication. Thus, the emergence of resistance to IN inhibitors maybe associated with a decrease in viral fitness. Selection experiments with S/GSK1349572 resulted in the selection of T124A, S153A, T124A/S153A and L101I/T124A/S153F mutants (Table 1), although the fold change (FC) in susceptibility was low (FC < 5) (Emiliani *et al*., 2005). *In vitro*, only small changes (FC < 5) in S/GSK1349572 (a new potent IN inhibitor, in stage 2 of clinical trials) activity were observed with a broad range of single mutants, with the exception of S153A and double mutants resistant to INSTIs, including RAL- and ELV-induced recombinant viruses. In particular, Y143R/C and N155H viruses remained fully susceptible to S/GSK1349572. For 21 double mutants, a low FC (<5) in S/GSK1349572 activity was observed against all but the E138K/Q148K, G140S/Q148R and Q148R/N155H mutants.

These data suggest that S/GSK1349572 has a resistance profile different from those of RAL and ELV. Nevertheless, G140/Q148 double mutants displayed a low, but significant FC in activity, ranging from 2 to 10, with a FC between 10 and 20 for E138K/Q148K; the addition of T97A, M154I or V201I to G140S/Q148H also increased S/GSK1349572 resistance (Seki, 2010). Furthermore, multiple mutations identified during passage. Q148H/R, used as a starting point, gave rise to resistant profiles, such as V75I/E138K/G140S/Q148H/M154I, conferring resistance to both S/GSK1349572 and RAL.

Table 1. Resistance mutations selected either in vitro (black) or in vivo (red) by raltegravir (RAL), elvitegravir (ELV), and S/GSK1349572 (GSK572). Summary of the environments around the inhibitors determined by molecular modeling. (Mouscadet *et al.,* 2010).

Integrase inhibitor	IN mutations	Target residues within 5Å of inhibitor	Method	References
RAL	**N155H** **Q148K** **Q148R** **Q148K/E138K** **Q148R/E138K** **Q148R/G140S** **Q148H/G140S** **Y143R** **Y143H**/L740M/E92Q/T97A N17S/**Q148K**/G163R G140C/**Q148K**/G163R **E138K/Q148K**/G163R E92Q/E138K/Q148K/M154I **N155H**/I204T **N155H/V151I** T124A **N155H/V151I**/T124A	**D64**, T66, L74, E92, **D116**, F121, **Y143**, **Q148**, **E152** and **N155** (I) **D64**, C65, **D116**-S119, P121, T122, I141, **Q148**, G149, **E152** and C19, A20, G24, C25 (II) **D64**, C65, **D116**-S119, P121, **G140-Y143**, **Q148**, G149, **E152** and A20*, G24*, C25* (I) **D64**, C65, **D116**, N117, I141, **Y143**, **E152** (II) **D64**, C65, T66, H67, **D116**, **Q148**, **E152**, **N155**, K159 (i)**D128**, **D185**, Y212, P214, Q215, S217, **E221**, N224 and A17*, G4* T66, H67, E92, **D116**, **E152**, **N155**, K159	Docking Induced-fit docking Docking X-ray Molecular Dynamics	Serrao *et al*., 2009 Barreca *et al*., 2009 Loizidou *et al*., 2009 Hare *et al*., 2010 Perryman *et al*., 2010
ELV	**E92Q** **E92Q/N155H** **E92Q/T66A** **N155H** **N155H/T66I** **N155H/E138K** **Q148K** **Q148R** **Q148R/S147G/E138K** **Q148R/H/K** and **G140C/S** **Q148R**/T124A **T66I**/T124A **T66K**/T124A T124A P145S E92V/T124A P145S/T124A Q146L/T124A **T66I**/V72A/A128T **T66I/E92Q**/T124A **T66I**/T124A/Q146L	**T66**, L74, **E92**, **D116**, F121, G140, Y143, **Q148**, **E152**, **N155** **T66**, L74, E92, F121, **D116**, G140, Y143, Q148, **E152** **D64**, C65, T66, H67, **D116**, N117, **E152**, **N155** (i)**D128**, **D185**, Y212, Q215, S217, **E221**, N224 and A17*, G4* (ii)**D97**, S100, W125, K164, **D188**, E190, **E320**, H329 and DNA** (I) **D64**, C65, **T66**-L68, V72, **E92**, **D116**, G118, P121, **E152**, K159 and G18*-A20* (II) **D64**, C65, **D116**-G118, I141, **Q148**, G149, **E152**, K156 and G18*-A20*, G24*, C25* (III) **D64**, C65, **D116**-S119, P121, G140-Y143, **Q148**, G149, **E152** and A20*, G24*, C25*	Docking Docking Docking X-Ray Docking Induced-fit docking	Serrao *et al*., 2009 Savarimo, 2007 Loizidou*et al*., 2009 Hare *et al*., 2010 Pasquini *et al*., 2008 Barreca *et al*., 2009
GSK572	T124A S153Y T124A/S153L101I/T124A/S153F			

Active site residues in bold black; *DNA nucleotide bases; **DNA backbone chain: (i) the sequence corresponds to PFV IN; (ii) the sequence corresponds to Tn5 transposase

Finally, it has also been shown that mutations conferring resistance to S/GSK1349572 *in vitro*, such as T124A and L101I/T124A, may also be present in INI-naive and RAL-experienced patients. In particular, the T124A mutation, which was identified *in vitro* in a resistance selection assay with S/GSK1349572, seems to be involved in the first step in the development of resistance to this compound (Marcelin, 2010). Thus, the virological response

to S/GSK1349572 should be investigated further in patients with previous treatment failure on RAL or ELV and with various profiles of resistance mutations to INSTI subsequently treated with S/GSK1349572.

3.2 Polymorphism effect

The contribution of clade-specific polymorphisms of the IN gene to phenotypic susceptibility to IN inhibitors was assessed in 137 clinical isolates, 60 of which were non-clade B strains (Van Baelen *et al*., 2008). Phenotypic testing demonstrated that clade-specific IN polymorphisms made no significant contribution to susceptibility to IN inhibitors. *In vitro* studies comparing the enzymatic activities of HIV-1 INs from subtype B and C viruses, and their susceptibility to various IN inhibitors (RAL, ELV and MK-2048) confirmed that the catalytic activities of the enzymes of these two subtypes were similar and that the various INSTIs used inhibited both types of enzyme to a similar extent (Bar-Magen *et al*., 2009). In another study, IN genotyping was performed on patients with experience of multiple treatments that had received RAL. No primary and very rare secondary RAL mutations (T97A, G140A, V151I, G163R) were observed at baseline (Ceccherini-Silberstein, 2010). The presence of these secondary mutations was not specifically associated with progression to specific primary RAL resistance mutations. It was also confirmed that mutations altering susceptibility to ELV *in vitro*, such as Q95K, H114Y, F121Y, T125K, Q146P, S153Y, were not prevalent. Nevertheless, although the positions subject to primary mutations — E92Q, Q148K/R/H, N155H and E157Q — are highly conserved and subject to similar genetic barriers in subtypes B and CRF02 AG, it has been suggested that the CRF02 AG subtype has a stronger genetic barrier to the acquisition of mutations of residue G140 than subtype B (Maiga *et al*., 2009). Another study showed that treatment failure on RAL occurred more rapidly in patients infected with non-B subtype viruses, indicating a possible impact of non-B-associated polymorphisms on the genetic barrier to RAL (Sichtig *et al*., 2009). The dynamics

of resistance mutations is very complex *in vivo*. High levels of resistance are always associated with the emergence of primary resistance mutations, but treatment failure on IN inhibitors is common in patients infected with WT virus. Nevertheless, maintaining INI treatment in patients with treatment failure but no IN mutations, invariably leads to emergence of a high level of resistance (Hatano *et al*., 2010). Furthermore, in addition to the stepwise accumulation of primary and secondary mutations under constant RAL pressure, as observed with other antiretrovirals a switch from one resistance mutation pattern to another is also commonly observed (Malet *et al*., 2009). The switch of resistance profile from residue N155 to residue Q148 mutations may occur due to the higher level of resistance to RAL conferred by pathways associated with Q148R/H mutation and the greater instability of the pathways associated with residue N155 (Malet *et al*., 2009). As it has been shown for RAL that no relevant antiviral activity persists *in vivo* for viruses harbouring N155H mutations, and given the risk of an accumulation or switching of mutations towards higher levels of resistance and cross-resistance to other INSTIs, it would appear to be inadvisable to maintain INI treatment in patients with treatment failure (Wirden *et al*., 2009).

IV. Raltegravir- the first clinically used Integrase specific drug

1. Discovery and development of Raltegravir.

As was mentioned above, (**II. Antiretroviral Drugs,** 4. Integrase Inhibitors) the discovery of RAL stemmed from investigations of a series of HCV polymerase inhibitors. The architecture of the catalytic site and the arrangement of the metal cations are very similar in integrase and the HCV NS5b RNA dependent RNA polymerase. These similarities led the Merck team to test HCV polymerase inhibitors originally designed as drug-compliant DKA replacements (Summa *et al*., 2008). This led to the identification of a compound with activity

in the enzymatic assay, which was further optimized in cell culture (Pace *et al*., 2007). RAL is a very potent inhibitor of the replication of HIV-1 and HIV-2 *in vitro* (Roquebert *et al*., 2008). It is more than 1,000 times more selective for integrase than for other phosphatidyl transferases, such as HIV-1 RNAseH and human polymerases. It has an IC_{50} of 2 to 7nM for the inhibition of recombinant IN-mediated strand transfer *in vitro* and an IC_{95} of 0.019 and 0.031 μM in 10% FBS and 50 % NHS, respectively, in a cell-based assay (Summa *et al*., 2008). Due to its mode of action, it is independent of HIV-1 tropism (CCR5 and CXCR4) and active against viruses resistant to other classes of antiretroviral drugs, such as nucleoside RT, PR fusion and entry inhibitors (Grinsztejn *et al*., 2007).

2. Efficiency of Raltegravir

2.1 Antiviral activity *in vivo*

Phase II and III clinical trials demonstrated a remarkable potency of combinations of RAL and other ARVs in treatment-experienced patients (Cooper *et al*., 2008; Grinsztejn *et al*., 2007). The first phase II assay was a dose-ranging study in patients with documented resistance to at least one drug in each of the three classes of ARVs. This population had considerable experience of treatment and a very high level of drug resistance.

There was an approximate 2.0 log copies/ml drop in plasma HIV RNA levels by week 24 in the RAL group, versus only 0.35 log with optimized therapy alone plus placebo, with no significant difference in viral efficacy between the three dosage groups studied (200, 400, 600 mg) (Grinsztejn *et al*., 2007). For the subsequent double blind phase III BENCHMARK I and II studies, in which 699 patients with considerable experience of treatment were enrolled, the combined analysis at 48 weeks showed that 72.3% and 62.1% of RAL treated patients had HIV RNA levels of less than 400 and 50 copies/ml, respectively, whereas such levels were found in only 37.1% and 32.9%, respectively, of the patients in the placebo group. The 48-

week results recently obtained for the phase III STARTMRK study comparing RAL-based and Efavirenz-based (RT inhibitor) combination regimens as initial treatment demonstrated that RAL suppressed HIV replication more rapidly than Efavirenz, this rapid viral decay being of unknown origin (Lennox *et al*., 2009). Moreover, preliminary results from a non inferiority study of the use of RAL to replace Enfuvirtide in patients intolerant to Enfuvirtide have shown RAL to be virologically effective for sustained periods, with good tolerance for up to 48 weeks. Conversely, the SWITCHMRK 1 and 2 trials, designed to examine the benefit of replacing a protease inhibitor with RAL, suggested that the RAL combination might not inhibit HIV replication more efficiently. In situations of resistance due to prior treatment failure, switching to RAL amounts to monotherapy, with the rapid selection of RAL-resistant HIV strains, as the genetic barrier to RAL is easily overcome. Nevertheless, these results suggest that RAL is an important additional drug for the initial treatment of HIV-1 infection.

2.2 Safety

Preclinical studies of toxicity by repeated administration, genotoxicity and toxic effects on development have been conducted with RAL, in mice, rats, dogs and rabbits. No mutagenic or teratogenic effect was observed. The effects observed at levels exceeding actual exposure levels revealed no likelihood of a clinical risk in humans (Summa *et al*., 2008). RAL is well tolerated and adverse events are rare. Most frequent drug-related clinical events, such as diarrhoea, nausea, headache and fatigue, were moderate and transient (Iwamoto *et al*., 2008). Laboratory abnormalities included an increase in serum lipid, amino-transferase and creatinine concentrations. Increases in creatinine phosphokinase levels, although not statistically significant, led to a cautious recommendation not to use RAL concomitantly with other drugs known to increase these levels. In phase II and phase III trials, the frequency of clinical and laboratory adverse events was similar in the RAL and placebo groups. In the

STARTMRK trial, significantly fewer drug-related clinical adverse events occurred in patients on RAL than in those on Efavirenz (Lennox *et al*., 2009). The BENCHMRK trial suggested a small increase of the risk of cancer in the RAL arm, with a relative risk of 1.5, but a recent analysis of all the available data concluded that the relative risk was actually less than 1 (Chirch, Morrison & Steigbigel, 2009).

2.3 Pharmacokinetics

RAL is administered orally and is rapidly absorbed. Its absolute bioavailability has yet to be determined, but the administration of 400 mg per day results in steady-state levels of the drug in the body within two days, as demonstrated by pharmacokinetics studies. About 83% of the RAL ingested binds to plasma proteins. Animal studies have shown RAL penetrate the stomach, liver, small intestine, kidney and bladder effectively, but have suggested that penetration into the brain is limited. Considerable intra- and inter individual variability was observed. RAL is a substrate, but not an inhibitor of P-glycoprotein (Pgp). There is currently no evidence to suggest that inhibitors or inducers of Pgp could affect RAL, but this property may affect its absorption (Sante-Appiah & Skalka, 1999). It could also account for the limited diffusion of this drug into the central nervous system. No effect of age or sex has been identified in studies of the pharmacokinetics of RAL (no data are available for children) (Iwamoto *et al*., 2008). The half-life of RAL in the body is about nine hours, with an initial phase of rapid elimination lasting about 1 hour. At steady state, a slight increase in residual concentrations of the drug is observed, but with no effect on the maximum concentration, making it possible to administer RAL twice daily. RAL is mostly metabolized in the liver, through glucuronidation by uridine diphosphate-glucuronolsy- transferase 1A1 (UGT1A1) to generate a single metabolite, M2. RAL is neither a substrate nor an inhibitor of the cytochrome P450 enzymes, consistent with a lack of interaction with drugs metabolized by

P450 isoenzymes, including PR inhibitors. It does not inhibit either UGT1A1 or 2B7 and does not induce CYP34A. As RAL is mostly metabolized by UGT1A1, it should be used with caution when co-administered with strong inducers of UGT1A1, such as Rifampicin. This antibiotic has been shown to reduce plasma concentrations of RAL, although its impact on the efficacy of RAL is unknown. A mutation of the UGT1A1 gene resulting in the production of an inactive enzyme has been identified. Two studies have shown in the concentration of RAL to be higher in patients with a homozygous mutant genotype. This genotype seems to be an important factor in interindividual variability, but its clinical relevance, in terms of efficacy and toxicity, is unknown (http://www.emea.europa.edu). Finally, Atazanavir, a PR inhibitor affecting glucuronidation, decreases the formation of RAL glucuronide and induces a moderate increase in RAL concentration (Grinsztejn *et al*., 2007).

3. Viral Resistance to Raltegravir

As with other antiretroviral drugs, resistance to INI emerges through the selection of mutations in the integrase gene affecting the susceptibility of the virus to INI. More than 40 mutations have been specifically associated with resistance to INSTIs *in vitro* and *in vivo* (Ceccherini-Silberstein *et al*., 2009) (Table 1). Resistance to RAL *in vivo* has been associated with 14 mutations, to different degrees, but the virologic failure observed during the BENCHMRK trials was unambiguously associated with two principal independent genetic pathways involving primary mutations of residues N155 (N155H) and Q148 (Q148K/R/H) (Cooper *et al*., 2008; Steigbigel *et al*., 2008). These mutations were not detected in the various studies on integrase polymorphism in INI-naive patients, confirming their likely role in conferring resistance to this class of drugs. Secondary mutations increasing the fitness of the resistant viruses were identified in both pathways. In particular, the G140S mutation rescues a replication defect resulting from the primary mutation Q148H (Delelis *et al*., 2009)

phenotypic analysis showed that the presence of the mutation at position 148 together with one or more secondary mutations resulted in greater resistance to RAL than observed for viruses carrying the mutation N155H. Clonal analysis of the viral populations in 11 patients with treatment failure on RAL showed that no viral clone simultaneously carried mutations in position 148 and 155, demonstrating the independence and exclusivity of the two main pathways. Moreover, a switch of resistance profile from residue 155 to residue 148 mutations may occur due to the higher level of resistance to RAL conferred by the pathways associated with residue 148 mutation and the greater instability of the pathways associated with residue 155 (Delelis *et al*., 2009; Malet *et al*., 2009). A small number of mutations involving residues E92, E157 and Y143 might constitute another pathway of resistance. There is some debate about whether the first two of these mutations are true primary mutations for RAL resistance, whereas the Y143 mutation has been shown to confer a real decrease in susceptibility to the inhibitor (Sichtig *et al*., 2009). Y143R/C/H mutations occur less frequently and later than the other two mutations (Croxtall & Keam, 2009). The major IN mutations E92Q, Q148K/R/H, N155H and E157Q are highly conserved and subject to similar genetic barriers between subtypes B and CRF02_AG. However, the CRFO2_AG subtype has a stronger genetic barrier to the acquisition of mutations of residue G140 than subtype B (Maiga *et al*., 2009). Another showed that treatment failure on RAL occurred more rapidly in patients infected with non B subtype viruses, indicating a possible impact of non B-associated polymorphisms on the genetic barrier to RAL (Sichtig *et al*., 2009).

V. Molecular Modeling Approaches

Molecular modeling encompasses all theoretical methods and computational techniques used to model the biological or chemical molecules and mimic or simulate their

behaviour. The techniques are used in the fields of computational chemistry, biology and materials science for studying molecular systems ranging from small chemical molecules to large biological systems and molecular or material assemblies. The structural properties of chemical and biological molecules are characterized mainly by X-ray analysis. Although crystallographic data yield valuable insights into such structural rearrangements, they represent only average conformation for a given set of crystallization conditions. Alternative experimental techniques, such as NMR spectroscopy, and computational approaches, such as molecular dynamics (MD) and normal mode analysis (NMA), provide a way to better understand the structure-dynamics-function relationships at the atomic level and further characterize the protein structure alteration and internal dynamics induced by exogenous factors.

The common feature of modeling techniques is the atomistic level description of the molecular systems; the lowest level of information is individual atoms. The benefit of molecular modeling is that it reduces the complexity of the system, allowing many more particles to be considered during simulations. Molecular modeling studies are useful in as much as they may allow us particularly, to understand the activity and selectivity of currently existing therapeutic agents, and, furthermore, may help in the design of novel effective therapeutic agents. These theoretical methods also enable to describe intermediate conformational states that can be used to guide the design of specific inhibitors acting as modulators of the enzymatic function by targeting putative allosteric sites.

In the present work, we employed a series of molecular modeling approaches in order to characterise the conformational flexibility of raltegravir, to build the structural models of the HIV-1 integrase and to study the interactions between RAL and its viral targets, IN, viral DNA and IN•vDNA complex.

1. Ab-initio Methods

Quantum mechanical (QM) calculation of macromolecular interaction energy presents a grand challenge in theoretical chemistry and computational biology. Due to the large number of atoms present in biological macromolecules (proteins, DNA), standard application of quantum chemistry methods to computing interaction energy of biological molecules is beyond the reach of computations due to steep computational scaling with the system size. At present, the overwhelming computational studies of biological molecules employ molecular force fields to calculate interaction energies of biological molecules (Brooks *et al*., 1983; Brendesen, 1984; Brendesen, 1984).

The *ab initio* quantum mechanical methods are readily used in drug metabolism studies. These methods require only the positions and atomic numbers of the atoms to be specified and offer greater transferability than conventional molecular modeling techniques. This fact permits computational experiments to be performed, allowing details of reaction mechanisms to be understood (Segall, Payne, Ellis, Tucker, & Boyes, 1997).

Despite the great success of force field methods in biological applications, quantum mechanical or *ab initio* computation of interaction energy is more desirable due to limitations of the classical force field approach. The introduction of QM calculation of electronic energy into biological molecules is of paramount importance for accurate prediction of chemical and biological properties of complex biological systems (Chen & Zhang, 2004)

2. Fragment-based Structural Analysis

Drugs are typically discovered by identifying active compounds from screening chemical libraries or natural products and optimizing their properties through the synthesis of structurally related analogues. This is a costly and time-consuming process. Suitable compounds with the requisite potency, compound availability, or desired chemical and

physical properties cannot always be found. Furthermore, even when such compounds are found, optimization often requires the synthesis of many analogues (Shuker, Hajduk, Meadows, & Fesik, 1996). The fragment-based structure design focuses on a relatively new concept within the domain of drug discovery. The fragmentation of drug leads into smaller pieces, or even into discrete functional groups (for example, carboxylate, amine, aryl group), has been used for some time to simplify the computational analysis of ligand binding and to map out different pharmacophoric elements required for high-affinity binding (Bohm, 1995; Miranker & Karplus, 1991). These fragments are usually endowed with reduced affinities but are better suited for chemical modifications aimed at producing novel drug candidates.

Since its onset, the technique has experienced a soaring success in large pharma, small biotechs, and academia (Hajduk & Greer, 2007). Fragments can sample chemical space more effectively than regular ligands do and fragment docking clearly outperforms traditional high-throughput screening in terms of hit rates. Parallel to the purposeful deployment of customized software, some other computational techniques have been adapted to handle fragments, in particular those that attempt to yield ligands by starting off from these building blocks. Fragments can evolve virtually, be linked (to join two or more fragments that occupy different regions of the binding site), self-assemble (through direct bond formation, linkers, between different reacting fragments), and/or be optimized to better fulfil drug-like properties. Fragments are usually docked and scored, but due to the fact that their volumes are smaller than the binding site cavity erroneous binding modes can be obtained. Besides, scoring functions need to be tuned as they are parameterized for much larger molecular entities. Nonetheless, despite these deficiencies, much progress has been made in the field and fragment-based ligand design (FBLD) has become a routine tool nowadays. Fragments can be designed *de novo* or obtained from ligand databases by chemical dissociation (i.e. fragmentation) (Cortes-Cabrera, Gago, & Morreale, 2012).

3. **Docking**

3.1 Protein-Ligand Docking

Protein–ligand docking is a molecular modeling technique aimed to predict the position and orientation of a small molecule (ligand, inhibitor, cofactor) when it is bound to a protein or enzyme. Computational structure prediction of ligand-protein complexes by the use of molecular docking simulations has led to great advances in understanding of the molecular recognition phenomenon and has become a vital tool in drug discovery by facilitating structure-based ligand design (Jones & Willett, 1995; Gschwend, Good, & Kuntz, 1996). Docking simulations require the energy of the ligand-protein complex crystal structure to be the global minimum on the binding energy landscape, that represents a thermodynamic condition on the employed in simulations energy function.

Docking simulations usually determine a single structure of the molecular complex with the lowest energy and postulate that the lowest energy conformation corresponds to the wild-type structure. The number of low energy structures is usually very large and a computationally demanding task of finding the lowest energy structure does not imply its thermodynamic stability. Nevertheless, the structure prediction problem implies determination of the ensemble of many similar conformations, which describe the thermodynamically stable native basin of the global energy minimum, rather than a single structure (Verkhivker *et al*., 2000).

The key characteristic of a good docking program is its ability to reproduce the experimental binding modes of ligands. To test this, a ligand is taken out of the X-ray structure of its protein–ligand complex and docked back into its binding site. The docked binding mode is then compared with the experimental binding mode, and a root-mean-square distance (RMSD) between the two is calculated; a prediction of a binding mode is considered

successful if the RMSD is below a certain value. Another characteristic of a good docking program is the ability of its scoring function to score and rank ligands according to their experimental binding affinities. To test this, the predicted binding affinities, or scores, are plotted against the experimental binding affinities; the key indicator for the quality of the predicted affinities is the standard deviation. An important use of protein–ligand docking programs is virtual screening, in which large libraries of compounds are docked into a target binding site and scored. For this purpose, the docking needs to be quick. Speeding up a docking protocol is often done at the cost of sampling fewer binding modes, and, as a result, reduces the success rates. It is therefore important that search parameters are chosen that give docking speeds useful for virtual screening applications, with an acceptable loss in docking accuracy (Verdonk, Cole, Hartshorn, Murray, & Taylor, 2003).

3.2 Protein-DNA Docking

Protein-DNA interactions regulate many cellular processes involving gene expression, DNA replication and repair. The recognition process can either be specific or non-specific depending on functional requirements. Although several structural studies have been performed to understand the specificity of the recognition process, the mechanism is still elusive and a simple code for DNA recognition by proteins does not seem to exist (Matthews, 1988; Lavery, 2005). Protein-DNA docking is a very challenging problem in bioinformatics and has important implications in a number of applications (e.g. rational drug design).

Computational docking methods can provide structural models of molecular complexes in cases where it is difficult or impossible to obtain an experimental complex structure. It is a predictive approach based on the structures of the individual partners. Several methods for protein-ligand and protein-protein docking have been developed and used extensively for the prediction of these complexes. However, much fewer methods for systematic docking to

predict the structure of protein-DNA complexes have been published so far (Setny, Bahadur, & Zacharias, 2012). This includes Fast Fourier correlation techniques (Aloy *et al*., 1998) and the geometric hashing method - ParaDock (Banitt & Wolfson, 2011). Another program, HADDOCK (van, van Dijk, Hsu, Boelens, & Bonvin, 2006; van & Bonvin, 2010) includes conformational changes at some stage of a multi-start docking search has been used to tackle the prediction of protein-DNA complexes.

4. Molecular Dynamics

Molecular Dynamics (MD) is a simulation of the physical movements of atoms and molecules in a given system. These atoms and molecules are allowed to interact for a period of time, producing a view of the atoms motion. The trajectories of these entities are determined by solving the Newton's equations of motion for a system of interacting particles, where forces between the particles and potential energy are defined by molecular mechanics force fields.

The conformational dynamics of protein molecules is encoded in their structures and is often a critical element of their function. A fundamental appreciation for how proteins work therefore requires an understanding of the connection between three-dimensional structure, obtained with increasing rapidity by X-ray crystallography or nuclear magnetic resonance (NMR spectroscopy), and molecular dynamics, which is much more difficult to probe experimentally. MD simulations provide powerful tools for the exploration of the conformational energy landscape accessible to these molecules, and the rapid increase in computational power coupled with improvements in methodology makes this an exciting time for the application of simulation to structural biology (Karplus & Kuriyan, 2005). MD simulations provide links between structure and dynamics by enabling the exploration of the conformational energy landscape accessible to protein molecules (Karplus, 2002; Wang,

Donini, Reyes, & Kollman, 2001). The first MD simulation of a protein was reported in 1977 and consisted of a 9.2-ps trajectory for a small protein in vacuum (McCammon, Gelin, & Karplus, 1977). The increase in computing power since then now makes it possible to run simulations of much larger proteins, in various environments.

Molecular dynamics simulations can provide the ultimate detail concerning individual atomic motions as a function of time; thus, they can be used to answer specific questions about the properties of a model system often more readily than experiments (Karplus & Kuriyan, 2005).

5. Homology Modeling

Homology modeling allows construction of a three-dimensional (3D) model of the protein at the atomic level (target) from its amino acid sequence and an experimental 3D structure of a related homologous protein (template). It relies on the identification of one or more known protein structures likely to resemble the structure of the target sequence, and on the production of an alignment that maps residues in the target sequence to residues in the template sequence. It has been shown that protein structures are more conserved than protein sequences amongst homologues (Chothia & Lesk, 1986).

3D protein structures provide invaluable insights into the molecular and structural basis of protein function. Although great progress was made in the field of experimental structure solution by X-ray crystallography and NMR spectroscopy, it is still a time-consuming process with no guarantee of success.

Protein Data Bank (PDB) currently contains about 84 645 experimentally characterized protein structures (Westbrook, Feng, Chen, Yang, & Berman, 2003; http://www.rcsb.org/pdb/). Whereas, the number of known protein sequences in SWISS-

PROT and TrEMBL databases is much more (about 850,000 sequence entries) than number of known different structures (Boeckmann *et al*., 2003). Hence, no structural information is available for a vast majority of proteins. There exists a gap in the structure knowledge and computational methods for protein structure prediction have helped in filling this gap, in recent years. Among all current theoretical approaches, comparative homology modeling is the only method that can reliably generate a 3D model of a protein (target) from its amino acid sequence (Schwede, Kopp, Guex, & Peitsch, 2003). Successful model building requires at least one experimentally solved 3D structure (template) that has a significant amino acid sequence similarity to the target sequence. Homology modeling typically involves four steps (Sanchez & Sali, 1997; Marti-Renom *et al*., 2000): (1) identification of protein homologs that can be used as template(s) for modeling; (2) alignment of the target sequence to the template(s); (3) building a 3D model for the target based on the information from the alignment(s); and (4) evaluation of the model. Finally, all four steps can be repeated until a satisfactory model is obtained. The elucidation of experimental structures and homology modeling complement one another in the exploration of the protein structure space. The growing number of structural templates brings a steadily increasing number of sequences into 'modeling distance' for comparative modeling. (Schwede *et al*., 2003)

Chapter 2. **RESULTS**

I. Raltegravir conformations in gas, water solution and solid state

RAL consists of three aromatic cycles possessing distinct electronic properties and connected by aliphatic linkers. Each linker contains four single bonds providing a large conformational flexibility of the inhibitor. Structural versatility of RAL is enriched by a capacity of two moieties, 1,3,4-oxadiazole-2-carboxamide (**1**) and carbonylamino-1-N-alkyl-5-hydroxypyrimidinone (**2**), to constitute either the Z- or E- isomer stabilized by intramolecular H-bonds (**Chart 1**) (Mouscadet *et al*., 2009 ; Arora & Tchertanov, 2012; Arora *et al*., 2012).

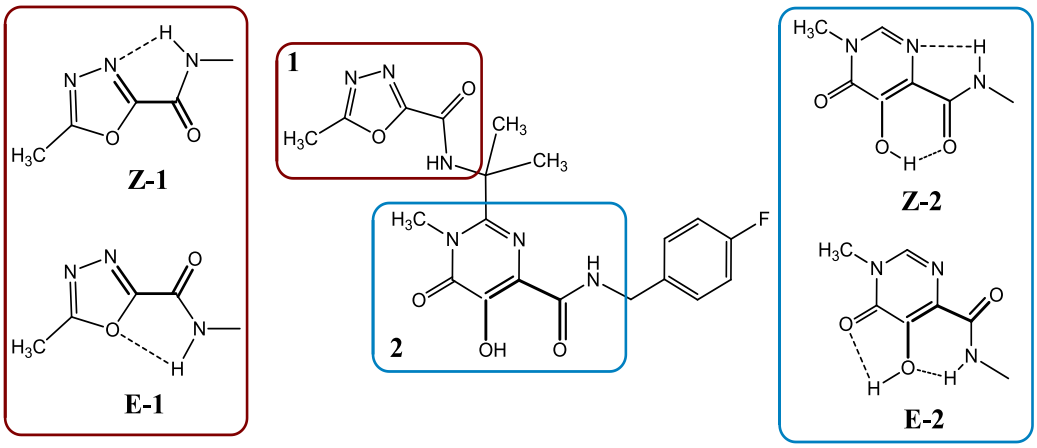

Chart 1. RAL structure. The E- and Z-isomers of carbonylamino-1-N-alkyl-5-hydroxypyrimidinone (**1**) and 1,3,4-oxadiazole-2-carboxamide (**2**) pharmacophores are stabilized by intramolecular H-bonds. (Arora & Tchertanov, 2012).

Each peptide-like carboxamide moiety of RAL is planar. Consequently the conformational flexibility of each isomer of RAL is determined by rotation around the other 4 aliphatic single bonds of the linkers. RAL features a set of multiple H-bond donor (HBD) and H-bond acceptor (HAD) groups; 3 and 8 in the protonated state and 2 and 9 in a

pharmaceutically acceptable potassium (K) salt, respectively, which could affect RAL affinity for its target.

The intrinsic conformational features of RAL have been investigated in the gas phase, in the water solution and the solid state.

1. Raltegravir conformations in the gas phase

First, the geometry and energetic of the protonated RAL was considered in the gas phase. The *ab initio* calculations were performed at the Hartree Fock (HF) level of theory. The RAL structure from crystallographic data characterized the PFV IN in complex with the viral DNA and RAL (PDB code: 3OYA, 2.65Å resolution) was used as initial template. Full geometry optimization and energy calculations were carried out for the four RAL isomers: Z-1/Z-2, Z-1/E-2, E-1/Z-2 and E-1/E-2 (**Chart 1**). Following the geometry optimization, the RAL conformations were generated for the four configurations by relaxed scan around four aliphatic single bonds of the linkers, characterized by torsion angles τ1-τ4 respectively, with an increment step of 30°. The energy profiles of generated RAL conformations differ strongly in terms of energy value, while the local minima and maxima are localized within the approximately same ranges of torsion angles in all configurational states (Figure 15 a-d). The energetic profiles of free rotation describing conformational flexibility of two substituents relatively to pyrimidine cycle (torsion angles τ1 and τ2, in blue and red colours respectively), are quite indicative and discriminative for selection of the energetically favourable RAL configuration. Energy profile describing rotation of oxadiazole-carboxamide (torsion angle τ3, in green color) is very similar in Z-1/Z-2 and E-1/Z-2 isomers and represents the energy values varied weakly within a large torsion angle range from 30 to 330°. The max and min values are observed at 0 and 360° respectively. In the two other configurational isomers, Z-1/E-2 and E-1/E-2, their profiles are slightly different. Energetical profile of the fluorobenzyl

fragment rotation (torsion angle τ4, in violet color) is nearly similar in all RAL configurations: its energetical impact is minimal in the wide range from 100 to 300°; two maxima in the ranges 0-70° and 320-360° are observed.

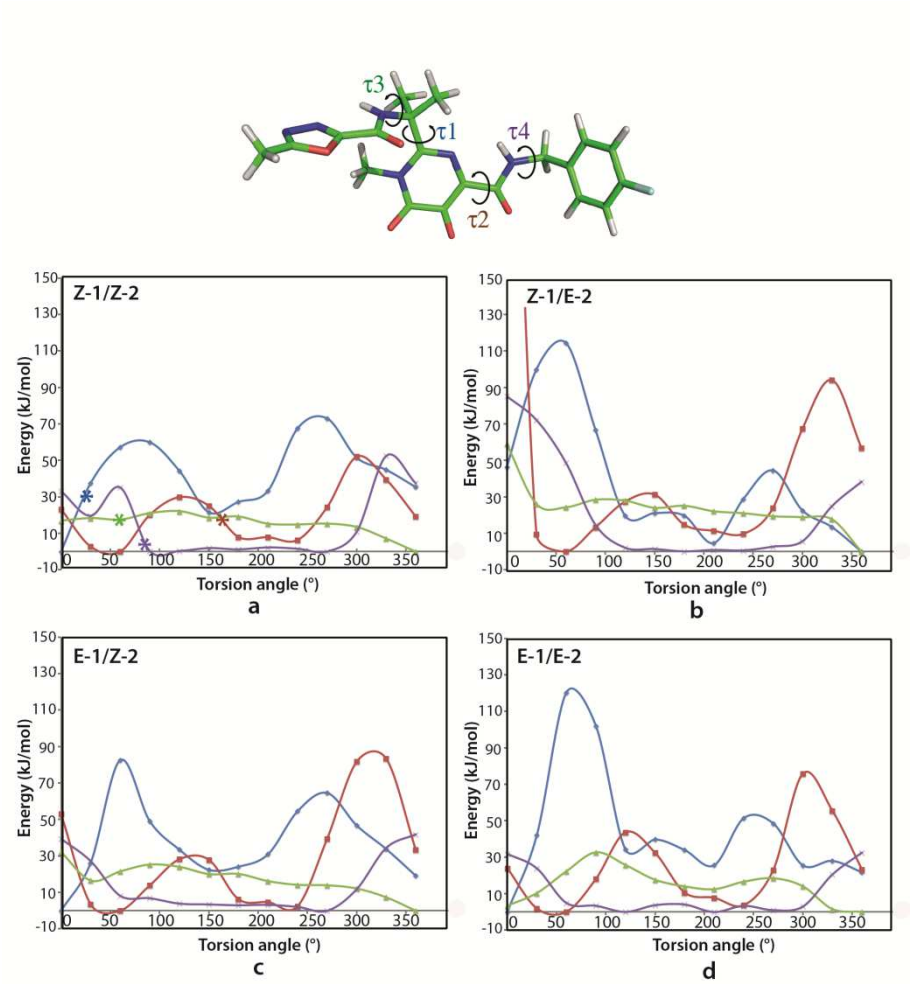

Figure 15. RAL conformations in the gas phase. The free energy profiles obtained by relaxed scan of molecular fragments from 0° to 360° with an increment step of 30° around the single bonds of the RAL isomers: (**a**) Z-1/Z-2, (**b**) Z-1/E-2, (**c**) E-1/Z-2 and (**d**) E-1/E-2. The curves representing rotation described by torsion angles τ1, τ2, τ3 and τ4 are shown in blue, red, green and violet colours. The value of torsion angles τ1, τ2, τ3 and τ4 observed in RAL crystal structure are indicated by asterisks. (Arora *et al*. 2012).

We found that in the gas state, the Z-1/E-2 and Z-1/Z-2 configurations show the energetical profiles characterizing the most unstable and the most energetically favorable RAL conformations, respectively (Figure 14 a, b, d). The energy of E-1/E-2 and E-1/Z-2

configurations display the intermediate values with the profiles closed to Z-1/E-2 and Z-1/Z-2, respectively (Figure 15 c, d). The relative stability of the four RAL isomers may be represented as follows: Z-1/Z-2 ≥ E-1/Z-2 >> E-1/E-2 >> Z-1/E-2 for all considered conformers. These results indicate that the Z-1/Z-2 configuration of RAL is the most preferable energetically. The energetical profile of deprotonated species is very similar to that in the neutral molecule (data not shown).

According to the crystallographic data, RAL structure in the PFV IN molecular complex is stabilised as the Z-1/Z-2 isomer, corresponding to the most stable RAL configuration observed in the gas phase. The values of torsion angles τ1−τ4 observed in the X-ray RAL structure do not exactly correspond to the minimum on energey profiles characterised the free rotation around the single bonds (Figure 15 a). Such conformational difference is probably caused by the influence of the crystal environment on RAL.

2. Molecular dynamic simulations of Raltegravir in water solution

Further the RAL crystallographic structure was used as initial template for MD simulations in explicit solvent. Three trajectories of 10 ns of the deprotonated RAL, each following an equilibration of 2 ns, were run to explore the conformational flexibility of the molecule in water. The four torsion angles, τ1 – τ4 (Figure 15), describing the RAL flexibility were analysed throughout the MD simulations. The root mean square deviations (RMSDs) of the RAL atoms revealed a high degree of atomic deviations between the coordinates sequentially stored along 10-ns trajectories and the starting coordinates. All three trajectories display comparable conformational drifts with RMSD values of 0.16 ± 0.06 nm (Figure 16 a).

The root mean square fluctuation (RMSF), a measure of the average atomic mobility of RAL atoms during the MD simulations, as it was expected, shows that the most fluctuating atoms are the RAL non-hydrogen atoms of fluorophenyl fragment and methyl groups and also the hydrogen atoms (Figure 16 b).

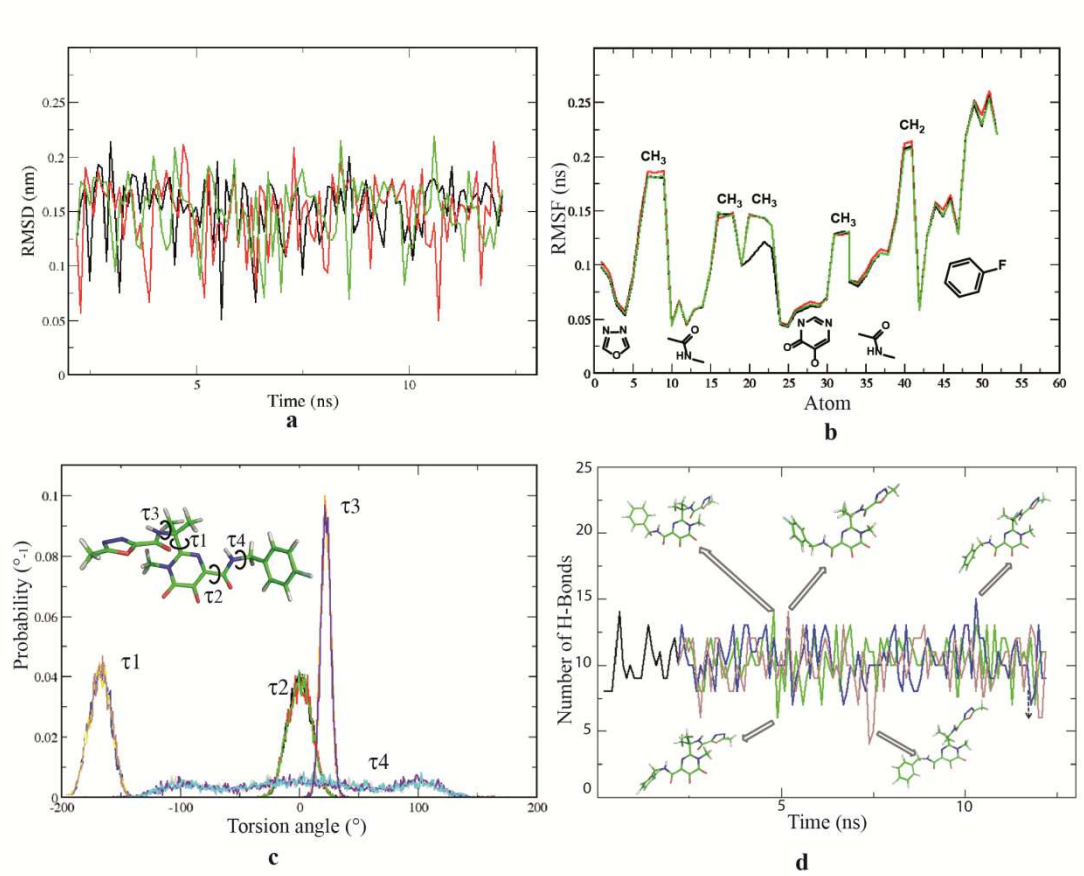

Figure 16: (a) The root mean square deviations (RMSDs, nm), (b) the root mean square fluctuations (RMSFs, nm) and (c) normalized probability distributions of torsion angles were calculated from MD simulations of RAL. The 1, 2 and 3 replicas of 10-ns simulations are shown by red, green and black colours. (d) The RAL H-bonding with the solvent water molecules recovered during MD simulations over the 2 ns equilibration step (in black), common for all the three trajectories, is shown by green, blue and brown colours. The representative RAL conformations forming the maximum and the minimum number of H-bonds are shown as the inserts. (Arora *et al*. 2012).

The torsion angles τ1 – τ4 occurrences recovered during simulations show excellent agreement between the three replicates (Figure 16 c). The torsion angels τ1, τ2 and τ3 are represented by the Gaussian-like distributions. The torsion angle τ3 mostly displays values in

a narrow range, from 10 to 30°. Values for the torsion angles τ1 and τ2 ranged from -190 to -150° and -25 to 25° respectively. The τ4 values are largely/widely distributed from -130^0 to 130^0.

The RAL H-bonding recorded during MD simulations indicates a very high capacity of the molecule to bind water molecules (Figure 16 d). The number of H-bonds formed by RAL varies from 4 to 15 with mean value of 11. In the majority of RAL conformations the eight acceptor and two donor groups of RAL are exposed to the solvent accessible at the same time, hence each such group is capable to form one or two H-bonds with the water molecules. Most of these H-bonds are strong in terms of their length. The RAL involved in multiple H-bonds may strongly affect the molecular conformation in solution compared to those observed in the crystal (PDB code: 3OYA) and in the gas phase (Figure 15 a).

3. Fragment-based structural analysis

3.1 Raltegravir configuration/conformation properties

We analyzed the conformational properties of RAL in the solid state using the structural data of the building stones of RAL, the 1,3,4-oxadiazole-2-carboxamide (**1**), carbonylamino-1-5-hydroxypyrimidinone (**2**) and 4-fluorobenzylcarbamoyl (**3**) derivatives in crystals. The Cambridge Structural Database (CSD) (Allen, 2002) search for the molecules based on the each pharmacophore produced no hits for the **1**, only 3 structures for the **2** and X structures for the **3** (**Table 2**). The absence (**1**) or limited data (**2** and **3**) required the search for the more general fragments and resulted in statistically relevant data (**Table 2**).

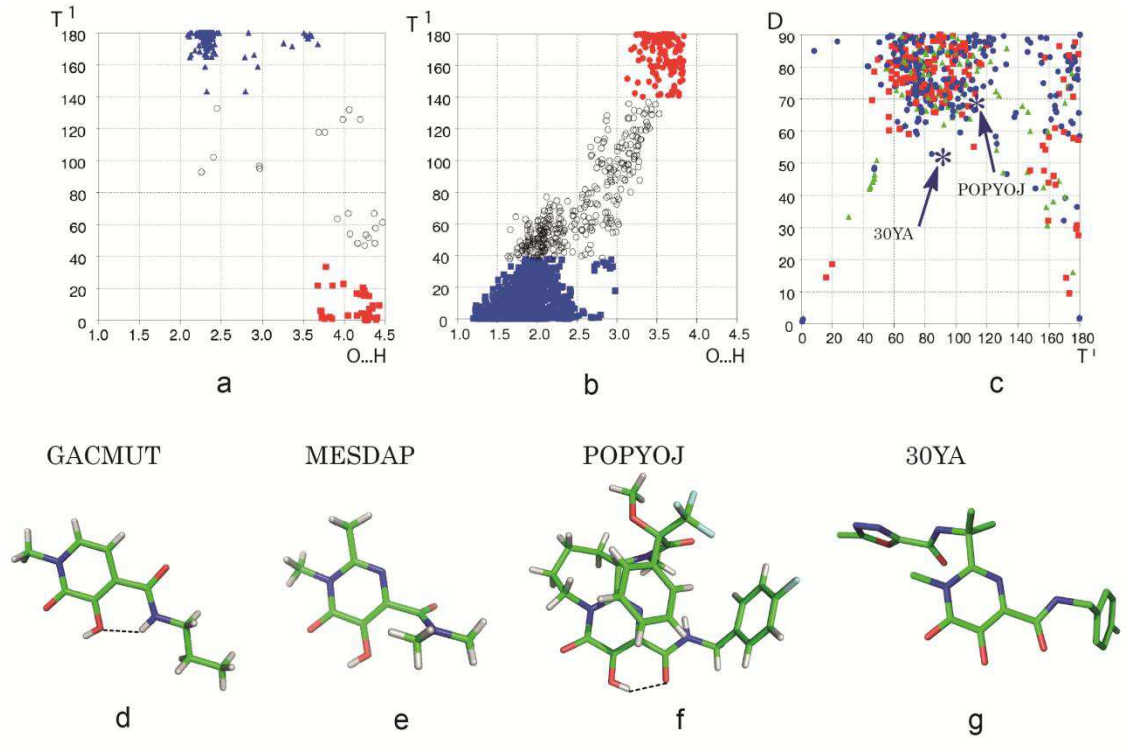

Figure 17. RAL conformations in the solid state. CSD fragment-based analysis of the RAL subunits as defined in Table 1. (a) F1: Scatter plots of the absolute value of torsion angle T^1 *vs* intermolecular distance O···H. The E- (blue triangles) and Z- (red squares) conformations are indicated by closed symbols. Intermediate conformations are shown as hollow symbols. (b) F2: Absolute value of torsion angle T^1 *vs* intermolecular distance O···H. The E- (red circles) and Z- (blue squares) conformations are indicated by closed symbols. Intermediate conformations are shown as hollow symbols. (c) F3: Absolute value of torsion angles T^1 *vs* T^2. The data representing F (blue circles), Cl (red squares) and Br (green triangles) substituent at the phenyl ring. The RAL and POPYOJ crystal structure parameters are indicated by asterisks. (Arora *et al*. 2012).

The torsion angle T^1 describing the relative position of the O or N vicinal atoms and the intramolecular contact O···H were used to distinguish between the **F1** conformations. A scatter plot of absolute values of torsion angle and O···H-N distance (T^1 *vs* O···H) revealed three major clusters and a limited number of randomly distributed observations (Figure 17 a) Torsion angles within the range 0 to 25° and to 145 to 180° were considered to meet the criteria for Z- and E-configuration, respectively. Bases on this definition, the one cluster with $T^1 \sim 0°$ was attributed to the Z- and two distinct clusters with T^1 ~180 to the E-configuration. The randomly distributed points corresponding to intermediate conformations were not

considered. The populations of the different clusters were not identical, with most of the **F1** fragments in crystals adopting E-conformation (~ 75%). The intramolecular O···H distance was correlated with the **F1** conformation. The O···H distance ranges from 2.0 to 2.5 Å and corresponds to stabilising the E-configuration intramolecular H-bonds (IHB). The small cluster with T1 ~ 180° and O···H distances from 3.35 to 3.65 Å represents also the E-conformation, but the amino H-atom position is not favourable to form IHB.

This structural fragment-based analysis indirectly indicates a higher probability of the E-conformation in the 1,3,4-oxadiazole-2-carboxamide derivatives than the Z-conformation. The stability of such configuration can be attributed to the intramolecular H-bonding or steric and/or other electronic molecular factors. Nevertheless the Z-conformation is observed in ~20% of related structures.

Retrieved carbonylamino-1-5-hydroxypyrimidinone (**2**) derivatives were synthesized recently and represent a new class of heterocyclic ligands (Xu, Whisenhunt, Veeck, Uhlir, & Raymond, 2003; Sunderland, Botta, Aime, & Raymond, 2001). These ligands were synthesised by a two-step procedure to provide the desired flexibility and were characterized by X-ray analysis (CSD refcodes: GACMUT and MESDAP). GACMUT shows a planar structure stabilized in the E-configuration by N–H···O intramolecular H-bonding with H···O of 2.02 Å (Figure 17 a). To avoid the H-bond induced stabilization of the E-configuration H atom was replaced by methyl group. Produced molecule, MESDAP, conserves its E-conformation but not planarity: carbonylamino group is turned at 70° relatively hydroxypyrimidinone ring to resolve the steric constrains. Later a multi-steps procedure was applied to synthesized a RAL prototype, flurobenzyl derivative of carbonylamino-1-5-hydroxypyrimidinone, POPYOJ (Zhong *et al*., 2009), lead to RAL synthesis which was finalized by a manufacturing route for the synthesis of RAL potassium salt (Humphrey *et al*., 2011). Carbonylamino-1-5-hydroxypyrimidinone moiety of POPYOJ is stabilized in a planar

Z-configuration by strong O–H···O intramolecular H-bond with H···O bond distance of 1.86 Å (Figure 17 b). Consequently in the solid state carbonylamino-1-5-hydroxypyrimidinone moiety shows two different configurations, E- and Z (**Chart 1)**.

To enrich the structural data related to carbonylamino-1-5-hydroxypyrimidinone moiety we referenced to the β-ketoenol fragments, **F2**, a very important pharmacophore and corner stone of (**1**) and numerous biologically active molecules. F2 has been previously characterized in details (Tchertanov & Mouscadet, 2007). We had shown that the vast majority of β-ketoenols (96%) were stabilized by very strong intramolecular H-bonding in Z-configuration. At the present work we performed the last update of the data with recent version of CSD (Figure 17 b).

The halogenated aromatic rings are widely present in the drugs. Fluorine is the smallest halogen, strongly electronegative and can interact with the H-atom donors in the enzyme as well as contribute to an enhancement of the inhibitor lipophilicity that in turn effects on improvement in cell permeability.

The CSD search was performed for more generalized fragment **F3** based on benzylcarbamoyl derivatives with a halogen atom (Hal =F/Cl/Br) at the *para* position. The rotation of the aromatic ring relatively carbamoyl fragment was described with torsion angle, T^1 and dihedral angle D formed by two planes P^1 and P^2 defined in **Table 2.** A type of the halogen atom was taken into consideration. A scatter plot of absolute value of torsion angles T^1 *vs* D reveals a dense cluster for T^1 ranging from 60° to 120° and D from 65° to 90°. The second and diffused cluster is in the range of T1 from 160 to 180° and D of 0° to 90°. Such distribution indicates a very large conformational freedom of benzylcarbamoyl derivatives with a halogen atom at the *para* position (blue circles for F, red squares for Cl and green triangles for Br).

Table 2. RAL conformations in the solid state: CSD fragment-based search for the RAL pharmacophore subunits. (Arora *et al*. 2012).

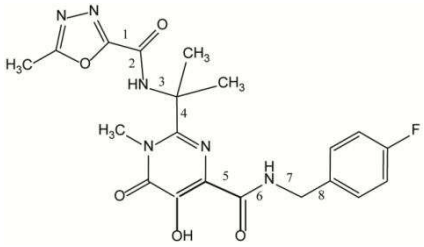

	1,3,4-oxadiazole-2-carboxamide	carbonylamino-1-5-hydroxypyrimidinone	4-fluorobenzylcarbamoyl
Pharmacophore	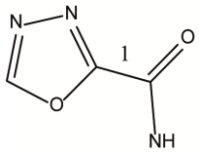	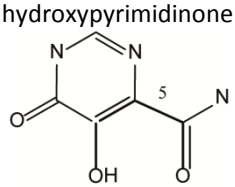	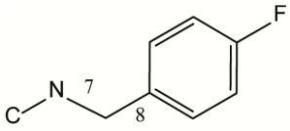
N Hits/Fragments	non	3/3	83/239
	F1	F2	F3
Fragment	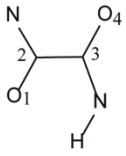	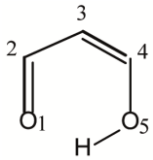	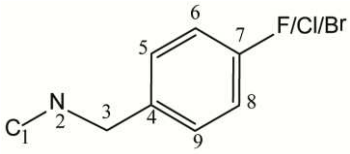
N Hits/Fragments	194/310	1785/2336	200/521
Parameters	$T^1[O_1C_2C_3O_4]$,° D^1 [O_1...H], Å	T^1 [$O_1C_2C_3C_4$],° T^2 [$C_2C_3C_4O_5$],° D^1 [O_1…H], Å	T^1 [$C_1N_2C_3C_4$],° D = P^1/P^2,˚; P^1 [$C_1N_2C_3C_4$] P^2 [C^4-C^9]
Conformation	E ~75%, Z ~20%	E~ 2%, Z ~ 95%	T^1 : 60°-120°, 160°-180° D : 65°-90°, 0°-90°

Conformation of the benzylcarbamoyl fragment from POPYOJ and 3OYA is shown in Figure 17 f as asterisks. Both structures display the T1 values either at extremity of a dense cluster.

3.2 Probing of the Raltegravir coordination to biologically relevant cations – Mg, Mn and K

The HIV-1 integrase requires Mn or Mg cations for activities *in vitro* (Feng *et al*., 2004) and *in vivo* (Neamati *et al*., 2002). The conformation of the active site of the HIV-1 integrase may differ according to whether it contains Mn^{2+} or Mg^{2+}, consequently the mode of interaction between inhibitor and ion-loaded active site may vary. RAL is used as a pharmaceutically acceptable potassium (K) salt. We focused here on the interaction of 1,3,4-oxadiazole-2-carboxamide (**1**) and carbonylamino-1-N-alkyl-5-hydroxypyrimidinone (**2**) moieties with K, Mg and Mn. Each pharmacophore, **1** and **2**, is polydentate, and binds metals either *via* a single atom or through chelation. **1** and **2** possess chelating fragment(s) differed in the Z- and E-conformations (**Chart 2**).

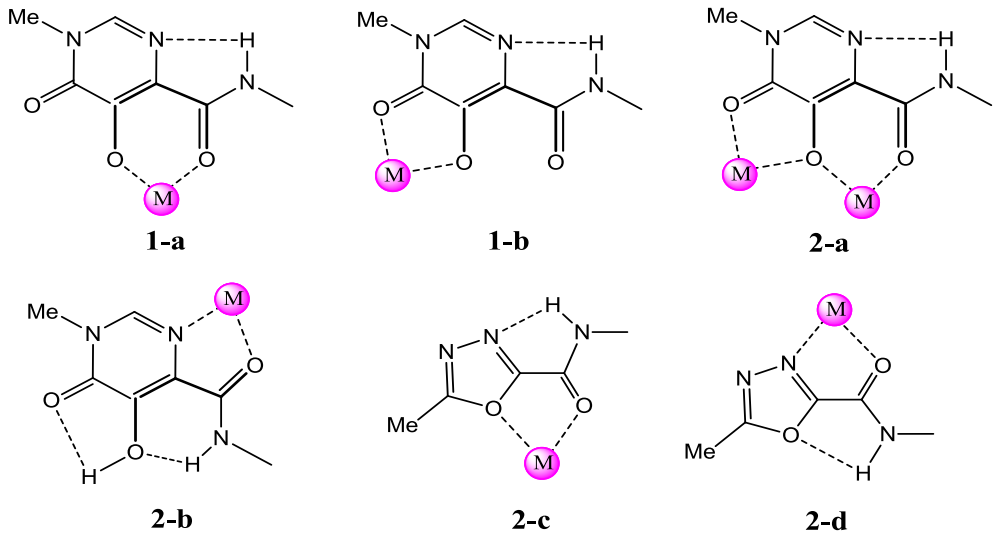

Chart 2. Metal chelating properties of 1,3,4-oxadiazole-2-carboxamide (1) and carbonylamino-1-N-alkyl-5-hydroxypyrimidinone (2) moieties (Arora *et al*. 2012).

Vicinal 1–4 oxygen atoms of hydroxypyrimidinone and β-ketoenolate can chelate two metal cation simultaneously. Chelation gives more stable complexes and is therefore the only mode of coordination considered here.

The 5- and 4-atoms based ligands with either two oxygen ligating atoms (L1 and L3) or heteroatoms O/N (L2 and L4) were used for retrieving and analysis of the M-L complexes (M = K , Mg and Mn) (Table 3). Number of crystal structures containing both, a metal atom (K, Mg or Mn) and a ligand with identical ligating atoms (L1 and L3) are three times more common respectively to those containing heteroatomic ligand (L2 and L4); obvious predominance between structures based on L1 or L3 ligands (M/L1 : M/L3 ratio of 3 : 1) is observed, while a quantity of structures based on ligands L2 and L4 differ less significantly (M/L2 : M/L4 ratio of 1 : 1.5). A proportion of the metal-ligand complexes in which the metal is chelated by ligand L1 or L3 and L2 or L4 is approximately the same. The metals are fond with occurrences showed K:Mg:Mn ratio of 8:1:5 for all analysed structures while the ratio of metals chelated with all ligands L1–L4 are K:Mg:Mn of 1.5:1:6. L1 and L4 appear to display preferential binding to Mn, while L4 chelates better K. M–O coordination bond distances in M-L1 complexes forms four clusters on the scatter plot (Figure 17a). Three dense clusters correspond to MnIII/MnIV (MnIII and MnIV complexes considered together), MgII and MnII complexes respectively. Mn/Mg···O bond distances were well characterized in details (Tchertanov & Mouscadet, 2007). The M···O bond distances, with mean value of 1.909 2.150 and 2.052 Å for MnIII/MnIV, MnII and MgII respectively were correlated with the oxidation number of the metal ion (MnII or MnIII/MnIV) and its size (Mg or Mn). The last update of the data with recent version of CSD confirmed the earliest finding. The diffused cluster on the scatter plot is composed with K complexes. K···O bond distances range from 2.6 to 3.6 Å indicating on weak or very weak ionic interactions.

Table 3. Probing of the RAL coordination to Mg, Mn and K cations: CSD fragment-based search. $N_{Total}/N_{Fragments}$ represent the total number of crystal structures (hits) where the both metal cation and ligand are present (N_{Total}) and the number of fragments corresponding to the metal-ligand complexes ($N_{Fragments}$) ; metal-ligating atom distance (M – O/N, Å). (Arora *et al*. 2012).

	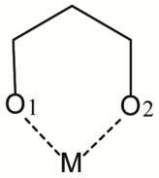	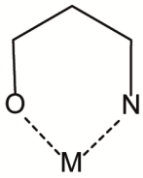	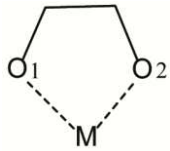	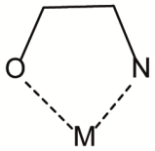
M/L	L1	L2	L3	L4
K	3504/36 M – O1 = 2.808 M – O2 = 2.802	452/0	2126/181 M – O1 = 2.830 M – O2 = 2.826	1338/4 M – O = 2.799 M – N = 2.957
Mg	649/74 M – O1= 2.055 M – O2= 2.063	162/26 M – O = 1.958 M – N = 2.136	80/29 M – O1 = 2.129 M – O2 = 2.104	143/14 M – O = 2.099 M – N = 2.240
Mn	2918/469 M – O1 = 2.043 M – O2 = 2.054	753/149 M – O = 1.963 M – N = 2.027	331/82 M – O1 = 2.138 M – O2 = 2.130	543/149 M – O = 2.116 M – N = 2.190

Distribution of M–O coordination bond distances in M–L3 is similar to that observed in M–L1 complexes (Figure 18 a, c). However, M–O bond distances were more symmetric and cluster formed with K–L3 complexes was more populated. Mg–L3 appears to display two separated clusters, corresponding to six- and seven-coordinated complexes with Mg–O bond distance of 2.065 Å and 2.170 Å respectively. M–O *vs* M–N scatter plot characterising M–L2 complexes contains only two clusters composed with MnIII/MnIV and MnII separated by Mg–L3 containing cluster (Figure 18 b). In M–L4 complexes, M–O *vs* M–N scatter plot is

similar to that in M–L3, but density of clusters is different, the higher for Mn and the lower for Mg cations (Figure 18 d).

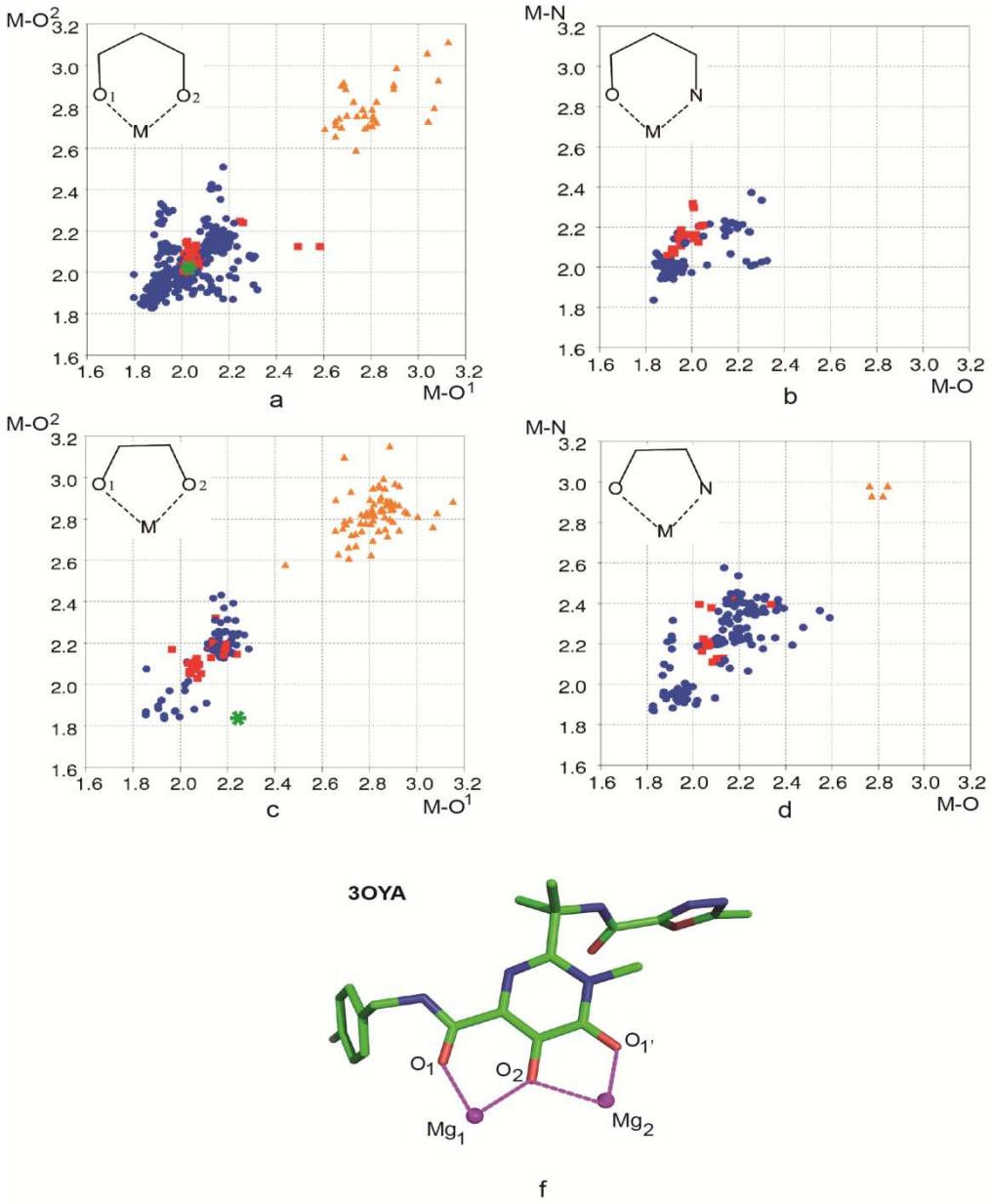

Figure 18. Probing of ligand interactions with Mg, Mn and K: CSD fragment-based search as defined in Table 2. Scatter plots of M-O^1 *vs* M-O^2 distances in M-L1 (a), M-L2 (c) and M-O *vs* M-N distances in M-L3 (b) and M-L4 (d) complexes. Metal complexes are indicated by bull symbols: red squares (Mg), blue circles (Mn) and orange triangles (K). The RAL crystal structure parameters are indicated by asterisks. (Arora *et al*. 2012).

Limited number of points with M–O/M–N bond distances of 2.80/2.90 Å corresponds to K–L4 complexes. In RAL co-crystallized with the PFV IN•vDNA complex (PDB code:

3OYA) the coordination bonds M–O correspond very well to statistical observations for M-L1 complexes, while these distances are strongly asymmetric and differ from corresponding statistical data for M–L3 complexes (Figure 18 a, c). Both Mg^{2+} cations in the active site are fixed as two-atom cluster by means of D64 residue that plays a role of the bridge. The sterical conditions in the active site and conjugated effect in RAL may be the major factors for such distorted coordination geometry.

4. Discussion

In the context of drug design, the conformation an inhibitor adopts when bound to a target is of fundamental importance. The variety of inhibitor conformations observed in different conditions may arise from interactions with a local environment and frequently differ from the bioactive conformation. Systematic differences may occur between the solid state conformation and those observed in solution or gas phase. Our conformational analysis of the different isomeric states of RAL in the gas phase indicates a small difference between the energy profiles of the Z-1/Z-2 and E-1/Z-2 isomers suggesting a relatively low energetical barrier between these two inhibitor states. A slight preference for the Z-configuration of carbonylamino-hydroxypyrimidinone pharmacophore in the gas phase was observed, in coherence with the established predisposition of β-ketoenols – a principle corner stone of this pharmacophore – to adopt the Z-isomer in the solid state (Tchertanov & Mouscadet, 2007). The preference of aliphatic β-ketoenols to form energetically favourable Z-configuration has been predicted early by *ab initio* studies at the B3LYP/3-G** level of theory (Schiavoni *et al*, 2001). Our structural databank search based on molecular fragments mimicking the two RAL pharmacophores statistically demonstrates the preferential Z-configuration of carbonylamino-

hydroxypyrimidinone-like molecules and the E-configuration of oxadiazole carboxamide–like molecules in the solid state.

Synthesized as a metal cations chelating ligand, RAL can bind the metal by both pharmacophores in the different isomerisation states. Probing of the RAL chelating features with the relevant cations, K, Mg and Mn, we evidenced that in the majority of metal complexes, the carbonylamino hydroxypyrimidinone-like fragments are observed in the Z configuration in the solid state. The oxadiazole carboxamide-like pharmacophore is observed in the metal complexes as two isomers and demonstrates a strong selectivity to the metal type : the Z isomer binds K and Mg while the E isomer binds mainly Mn. The higher probability of Mg^{2+} cation coordination by the Z-isomer of both pharmacophores indicates that the presence of two Mg^{2+} cations at the integrase binding site may be a decisive factor for stabilisation of the Z/Z configuration of RAL which is observed in the PFV intasome complex (Hare *et al*., 2010 a; Hare *et al*., 2010b).

Therapeutically used RAL is in deprotonated state neutralised by K cation. Such drug formula corresponds to the optimal condition allowing efficient cations replacement in cells. The significantly higher affinity of both parmacophores to Mg relatively to K permits a positive competition between these cations, resulting in the change of RAL composition from a pharmaceutically acceptable potassium (K) salt to a biologically relevant Mg complex. To describe the pharmacological properties of a given inhibitor, the knowledge of the site where the inhibitor is to bind in the target and of the interaction(s) that control the specific recognition of the inhibitor by its target(s), represents a corner stone factor. Only a limited number of target-ligand molecular complexes are characterized experimentally at the atomic level (X-ray or NMR analysis). Part of them characterize the binding of therapeutically relevant ligands to biologically non-relevant and non-pertinent targets, for example, the HIV-1 integrase specific inhibitor RAL was published as a ligand fixed to the PFV intasome (Hare *et*

al., 2010a; Hare *et al*., 2010b). Consequently, a large quantity of reliable information on target-ligand binding is based on molecular docking methods which generate insights into the interactions of ligands with the amino acid residues in the binding pockets of the targets, and also predict the corresponding binding affinities of ligands (Krovat, Steindl & Langer, 2005). The first step of a docking calculation consists in the choice or generation/construction of the therapeutically appropriate target.

II. Targets models, representing the HIV-1 Integrase and viral DNA before and after 3'-processing

1. Modeling of the biologically relevant HIV-1 targets

Four integrase models were generated by homology modeling (Figure 19). Models **1A** and **1B** (Figure 19 a) represent the unbound homodimer of the full-length integrase (IN^{1-270}), which plausibly depicts the conformational state of the enzyme before the 3'-processing of vDNA (unbound state of IN). The models differ by the number of Mg^{2+} atoms localized in the active site (one and two Mg^{2+} cations in model **1** and 2 respectively). Model **2A** (Figure 19 b) represents the IN homodimer in complex with two double-strand vDNA, which likely depicts the active unit of the IN•vDNA strand transfer intasome; models **2B** (not shown) was derived from model **2A** by removing vDNA.

1.1. Models of the unbound Integrase

The models **1A** and **1B** did not show any significant structural change induced by the different number of Mg^{2+} cations in the active site. This finding is coherent with our early published results for the catalytic core domain (CCD) where we reported that a second Mg^{2+} ion would likely enter the active site upon movement of the E152 side chain toward the active

site conserving the overall structure of CCD (Mouscadet *et al*., 2009; references therein). Therefore only the model **1A** is presented on Figure 19 a.

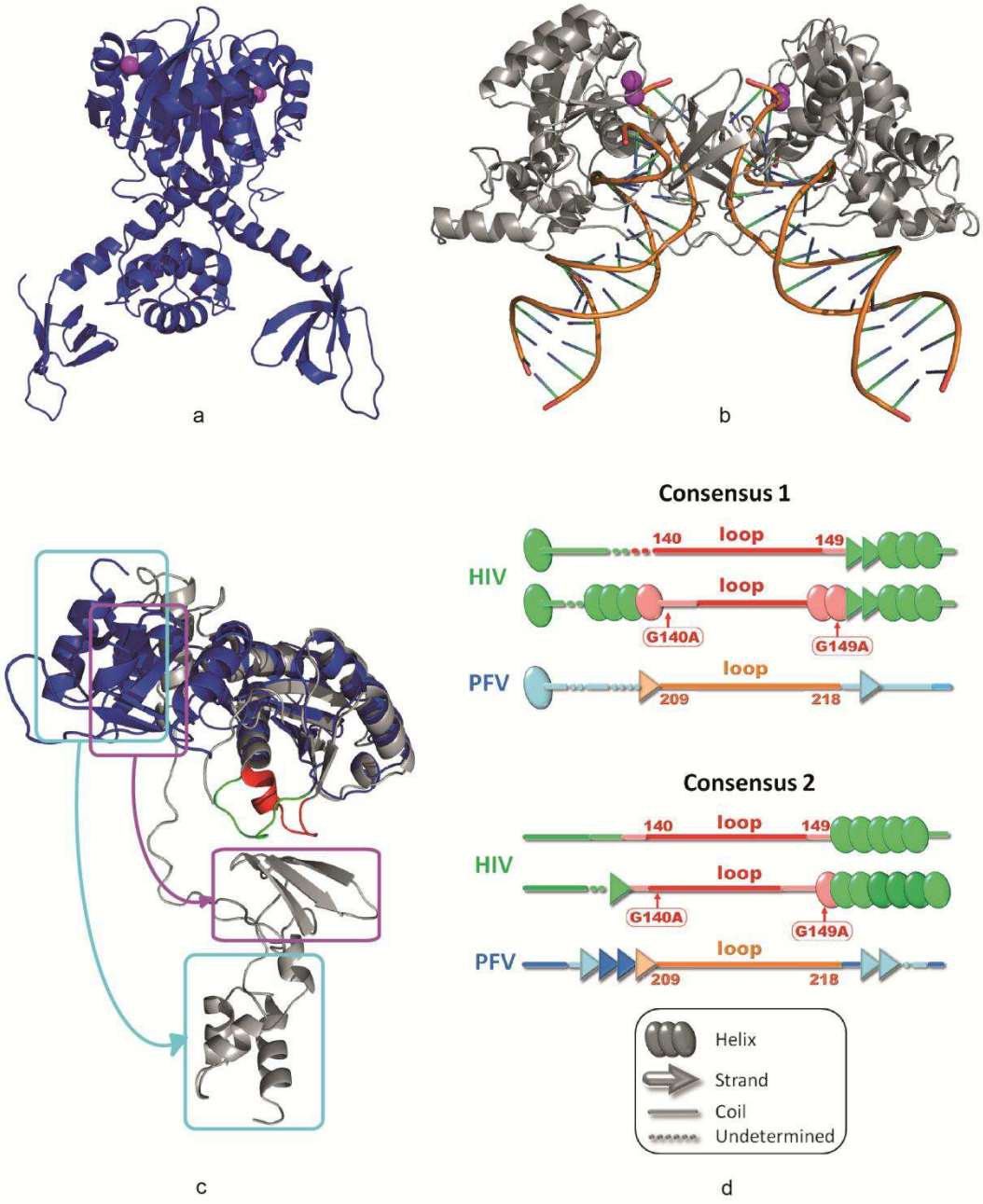

Figure 19. Structural models of the HIV-1 integrase. (a) Model 1A, representing the homodimeric enzyme before the 3'-processing; (b) Model 3A, representing the simplified IN-DNA pre-integration complex (dimeric form); (c) Superimposition of monomeric subunits from models 1A and 2A. The proteins are shown as cartoons, Mg^{2+} ions as spheres (in magenta). (d) Schematic representation of the HIV and PVF active site loop secondary structure prediction, according to consensus 1 and consensus 2. (Arora & Tchertanov, 2012).

It will be useful to note that the Normal Modes Analysis (NMA) shows that in unbound IN with two Mg^{2+} cations the active site is more rigid due to the stabilising role of the coordination of the Mg^{2+} cations by three active site residues –D64, D116 and E152 – whereas the catalytic site loop flexibility increases significantly (S. Abdel-Azeim, personal communication).

1.2 Models of the IN•vDNA complex

Model **2A** was generated from the X-ray structure of the PFV intasome (Hare *et al*., 2010). As we reported, despite the very low sequence identity (22%) between the HIV-1 and PFV INs, the structure-based alignment of the two proteins demonstrates high conservation of key secondary structural elements and the three PFV IN domains shared with HIV-1 IN have essentially the same structure as the isolated IN domains from HIV-1 (Ni *et al*., 2012). Moreover, the structure of the PFV intasome displays a distance between the reactive 3' ends of vDNA that corresponds to the expected distance between the integration sites of HIV-1 IN target DNA (4 base pairs). Consequently, we suggested that the PFV IN X-ray structure represents an acceptable template for the HIV-1 IN model generation (Yin & Craigie, 2010). We supposed that a simplified dimer model of the IN•vDNA complex (Figure 19 b**)** will be appropriate for the docking procedure.

It is worth noting large structural and conformational changes observed between the unbound (model **1A**) and vDNA-bound (model **2A**) integrase states regarding the relative positions of the IN domains (RMSD of 31 Å, based on C_α) (Figure 19 c). These structural modifications result in different contacts between the IN domains. As such, in the model **1A** no interaction was detected between CTD and CCD whereas the two domains interact tightly in model **2A**. The NTD-CCD interface also exhibits substantial changes: in the unbound form

the NTD-CCD interface belongs to the same monomer subunit whereas in the vDNA-bound form the interface is composed of residues from the two different subunits.

Moreover, in the homology modelled IN•vDNA complex, IN undergoes important structural transformation leading to structural re-organisation of the catalytic site loop; the coiled portion of the loop reduces from 10 residues (140 -149 aas) in the unbound form to 5 residues (140-144 aas) in the vDNA-bound form. Two hypotheses were proposed: (i) such effect may be induced by the vDNA binding, or (ii) it is an artefact derived from homology modeling with the structural data of the PFV IN in which the shorter loop may be a natural fold of the PFV IN sequence.

To explore the influence of the sequence on the loop folding we used a large range of algorithms designed to predict secondary structure elements. Efficiency of secondary structure prediction tools has been recently improved by the use of evolutionary information from multiple alignments: the query sequence is aligned with homologous sequences taken from a protein structures database, and the experimental structures of the homologous sequences are considered in the prediction. Such method can produce biased results, particularly in the case studied here. To avoid this discrepancy we considered consensus predictions derived from two sets of prediction tools (see Chapter 4. **MATERIAL AND METHODS**).

Three amino acid sequences $IN^{133-155}$of the wild-type (WT) and the double mutant G140A/G149A IN from HIV-1 and the WT IN from PFV were considered. The secondary structure prediction shows that in HIV-1 WT the sequence segment $IN^{150-155}$, a part of the α-helix $IN^{150-166}$, is preceded by a random coil composed of 10 residues, $IN^{140-149}$, while in the double mutant G140A/G149A a reduced coil formed by only 7 amino acids, $IN^{141-147}$, and an increased α-helix $IN^{148-166}$ are observed (Figure 19 d). Mutation G140A also influences the secondary structure of the $IN^{133-139}$ sequence segment, improving a β-sheet structure

respectively to those in the WT. Prediction results obtained with high reliability (>75%) correlate perfectly with the X-ray data characterising the WT HIV-1 integrase (PDB code: 1B3L) (Maignan *et al*., 1998) and its double mutant G140A/G149A (PDB code: 1B9F) (Greenwald *et al*., 1999).

Prediction for the PFV IN indicates a high probability of a two β-strands organisation of sequence segments $IN^{204-208}$ and $IN^{220-222}$ (corresponding to $IN^{135-139}$ and $IN^{151-153}$ in the HIV-1), linked by a random coil including 10 residues, $IN^{209-219}$, ($IN^{140-152}$ in the HIV-1) (Figure 19 d). Consequently, the secondary structure prediction shows that the WT $IN^{133-155}$ sequence segment from HIV-1 and corresponding $IN^{202-224}$ sequence segment from PFV should naturally fold in different and unlike structural elements. Crystallographic data characterising the unbound PFV IN reports that $IN^{210-220}$ residues were not identified (PDB code: 3DLR) (Valkov *et al*., 2009). Apparently this sequence represents a strongly flexible coiled structure as we observed in our prediction. In contrast, the X-ray structure of the PFV IN bound to the vDNA shows a shortened coil and a long well-organized α-helix in $IN^{214-234}$ sequence (PDB code: 3L2U) (Hare *et al*., 2010b). This partial folding of the catalytic site loop is stabilized through intra-IN domain-domain interactions and interactions with vDNA that probably contribute to stabilisation and elongation of the α4-helix.

To complete the RAL targets definition, structural models representing the non-cleaved and cleaved HIV-1 viral DNA (model **3A** and **3B** respectively) were constructed as described in Chapter 4. **MATERIALS AND METHODS** and represent the double strands helix which is slightly distorted at 3'-end in **3A** model (Figure 21 a,b).

III. Raltegravir – targets recognition

The characterization of RAL recognition by it viral targets were performed as follows. First, RAL in each conformation generated starting from crystallographic structure (PDB ID: 3OYA) represented the Z-1/Z-2 isomer, was docked onto the active site of three targets, unbounded IN with the one and two Mg^{2+} cations at the catalytic site (models **1A** and **1B**) and onto IN•vDNA pre-integration complex (model **2A**). RAL was considered in its deprotonated form, as it is pharmaceutically acceptable as the potassium (K) salt.

Four different software were used for the docking procedure, AutoDock, Glide, Vina and SurFlex. Such routine allows (i) to optimize the algorithm choice to dock the flexible inhibitor and (ii) to evaluate RAL binding with different kind of the targets, flexible (unbounded IN with the one Mg^{2+} cations at the catalytic site), semi-flexible (unbounded IN with the two Mg^{2+} cations at the catalytic site) and rather rigid (IN•vDNA complex).

To distinguish between the RAL conformations we will referred crystallographic structure of RAL as the "crystallographic conformation", the conformations generated by relaxed scan from crystallographic structure of RAL as the "generated conformations" and RAL conformations produced by docking to targets as the "docked conformations".

1. Docking poses and conformations

The docking conformations of RAL produced by docking of the generated conformations onto the unbounded IN with a single Mg^{2+} cation within the catalytic site are positioned mainly at the space (region) delimited by the catalytic site loop in extended (open) conformation (Figure 20). They differed strongly from the generated conformations and their isomeric state is frequently not coincident with the initial crystallographic Z-1/Z-2 isomer.

The binding energy values obtained by all applied software are ranged from -8.8 to -5.3 kcal/mol (Figure 20).

Docking of the same RAL conformations onto the unbounded IN with two Mg^{2+} cations within the catalytic site shows that the molecule is re-positioned from the loop towards the active site (Figure 20). The binding energies are ranged from -9.8 to -6.5 kcal/mol. Similarly to the docking of RAL onto the unbounded IN with a single Mg^{2+} cation a large variety of isomers/conformers is realized. The RAL is oriented rather randomly respectively the active site and loop.

Docking of the RAL conformations onto the IN•vDNA model resulted in RAL binding modes with significantly higher scores (from -11.9 to -7.8 kcal/mol) than those found for the unbounded IN with different Mg^{2+} cations population at the active site. RAL is positioned in the catalytic site of pre-integration complex and chelates the Mg^{2+} cations in agreement with the mechanism of action of the integrase inhibitors blocking strand transfer reaction. Consequently, according to the data obtained by four different docking algorithms, the Z-1/Z-2 isomer of RAL in all generated conformations bound most efficiently to the IN●vDNA model. Nevertheless, the docking conformations show some differences.

The docking conformations of RAL differ strongly from the generated conformations of the Z-1/Z-2 isomer of RAL. Moreover, some of them represent alternative isomers (Figure 20).

2. Evaluation of the docking algorithms

We also analysed the docking results individually for each docking method and compared the efficiency of docking algorithms taken into consideration the target.

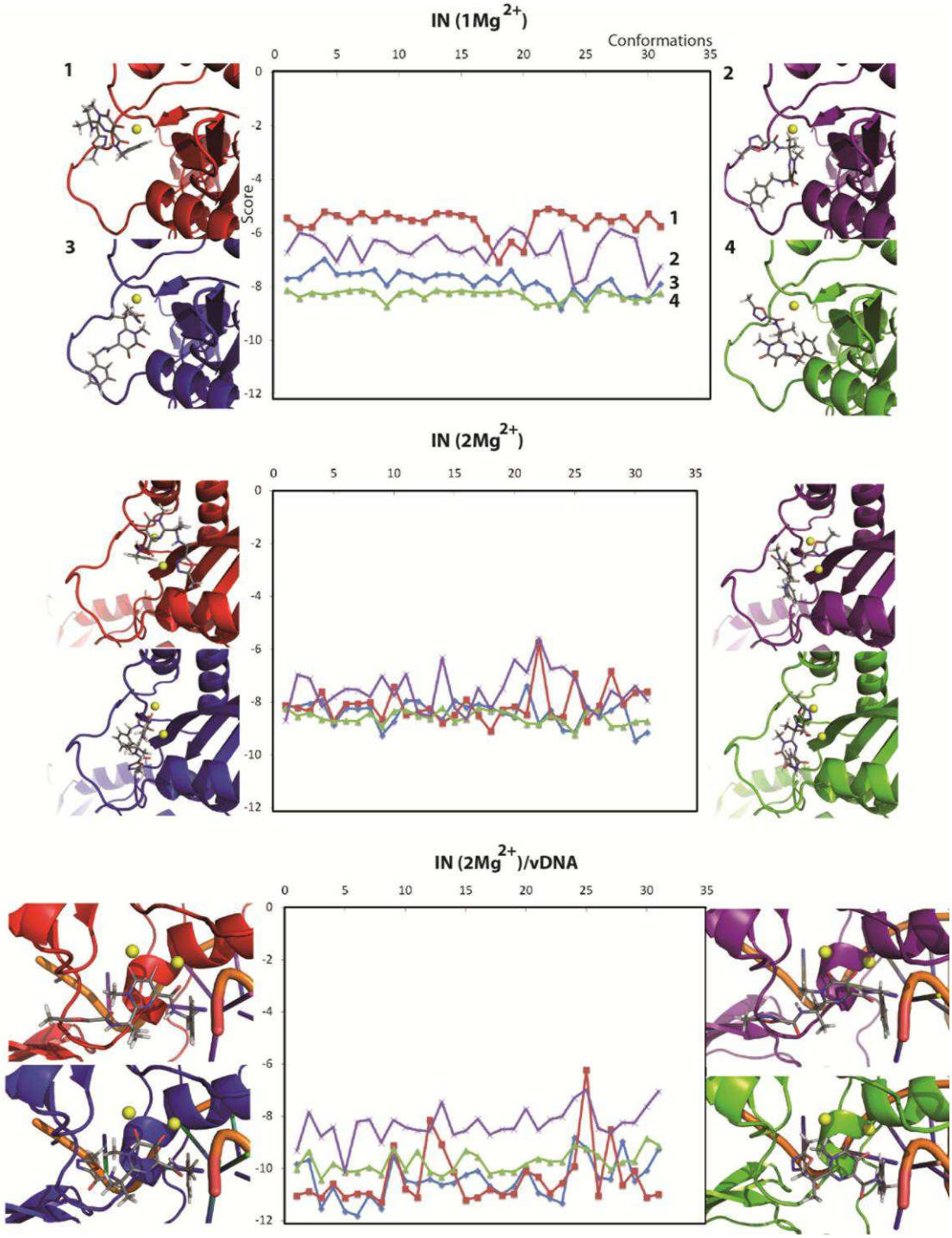

Figure 20. RAL–Integrase binding predicted by docking. The docking of RAL generated conformations for the Z-1/Z-2 isomer onto the unbound IN with a single Mg^{2+} cation within active site (model 1A), with two Mg^{2+} cations within the active site (model 1B), and the IN•vDNA complex (model 3A) are presented at the top, middle and bottom panels, respectively. The graphs in the middle column shows the score profiles obtained by docking with using of four algorithms – GLIDE (in red, line 1), SurFlex (in violet, line 2), AutoDock (in blue, line 3), and VINA (in green, line 4). Snapshots on the right an on the left show the representative poses of RAL obtained by docking onto the targets 1A, 1B and 3A by using the four different programs Numeration of the scores curves and snapshots showed on the top panel is valid for other panels. The proteins are shown as cartoons with a colour coded the used docking program, Mg^{2+} ions as spheres (in yellow) and RAL as sticks. (Arora *et al*. 2012).

The score profiles obtained for the RAL docking onto the same target by the different software are altered significantly (Figure 20, middle column). For RAL docking onto unbounded IN with a single Mg^{2+} cation the best scores were obtained with VINA. Binding energies for all RAL conformations are very similar and ranged in a very narrow interval (from -7.9 to -7.6 kcal/mol) (Figure 20). The results obtained with Autodock are very close to those obtained with VINA and show only very slight increase of binding energies (from -7.9 to -7.2 kcal/mol). Binding energies obtained with SurFlex are characterized by more important fluctuations and ranged from -8.0 to - 6.3 kcal/mol. Docking with Glide produced the poor scores nearly for all docked RAL conformations.

The RAL docking conformations obtained with VINA, AutoDock and Glide docking onto unbounded IN with two Mg^{2+} cations show very small fluctuations of binding energies (Figure 20). They score value profiles superimposed perfectly with mean value of 8.5 kcal/mol. Binding energies obtained with SurFlex fluctuates significantly and show slightly decreased values.

RMSDs between generated, docked and crystallographic conformations in these experiments of RAL docking onto unbounded IN with either a single Mg^{2+} cation or two Mg^{2+} cations and IN•vDNA complex revealed a very high degree of the average RAL atomic fluctuations for all applied software for exception of only rare docking conformations obtained with Glide (data not shown).

As was mentioned above, the RAL docking onto the IN•vDNA model results the best binding score with all applied algorithms. Particularly the best scores were obtained with AutoDock and Glide as compared to the other two docking algorithms, VINA and SurFlex (m.v. of -11.4, -11.1 , -9.8 and of -8.3 kcal/mol respectively).

We generated the others RAL isomers, E-1/Z-2, Z-1/E-2 and E-1/E-2. The RAL conformations were derived for each isomer similarly to the procedure applied to Z-1/Z-2. As the best results were obtained with Glide, we further used this software to dock the RAL generated conformation onto the IN targets applying the same strategy as for docking trials of Z-1/Z-2 isomer generated conformations. The obtained results show a general similarity with the docking data observed for Z-1/Z-2 isomer, nevertheless the score values in majority of cases are lower and the RAL binding poses show rarely chelation with the Mg^{2+} ion(s) in the active site of the IN targets (data not shown).

3. The viral DNA as a putative Raltegravir target

Quite recently it was reported that unprocessed viral DNA could be the primary target of RAL (Ammar *et al*., 2012). This study is based on the PFV DNA and several oligonucleotides mimicking the HIV-1 DNA probed by experimental and computing techniques.

To provide further data concerning RAL recognition by the HIV-1 viral targets, we docked inhibitor onto the uncleaved and cleaved viral DNA (the terminal GT nucleotides at 3'-end were removed) by using Glide. The docking pose of RAL docked onto the un-cleaved vDNA represents the molecule positioned in the major (minor) groove of substrate (Figure 21 c,d). The chelating centers of molecule are oriented towards (inside) the helix centre; stabilizing interactions between the partners, RAL and vDNA, were not observed.

In contrast, RAL docked onto the cleaved vDNA is located at position of the removed di-nucleotides (Figure 21 a,b). The best score corresponds to the Z-1/Z-2 isomer of RAL with all chelating centres oriented outside of the vDNA helix (Figure 21 b). Such orientation is stabilized by H-bonds with unpaired cytosine. The nitrogen atom of RAL oxadiazole cycle interacts with amino group of cytosine (N-H···N distance of 2.85) forming

the strong H-bond. The NH group from adjacent (neighbouring) carbonylamine fragment interacts with the oxygen atom from cytosine (N-H···O distance of 2.43 Å). First, these two strong H-bonds characterized the high and specific affinity between RAL and unpaired cytosine and secondly such type of interactions is identical to those stabilized the bases pair G-C. The additional pair of N-H···N contacts with distances of 3.29 and 3.50 Å should contribute in stability of RAL···Cytosine interactions. Consequently, RAL play the role of removed guanidine.

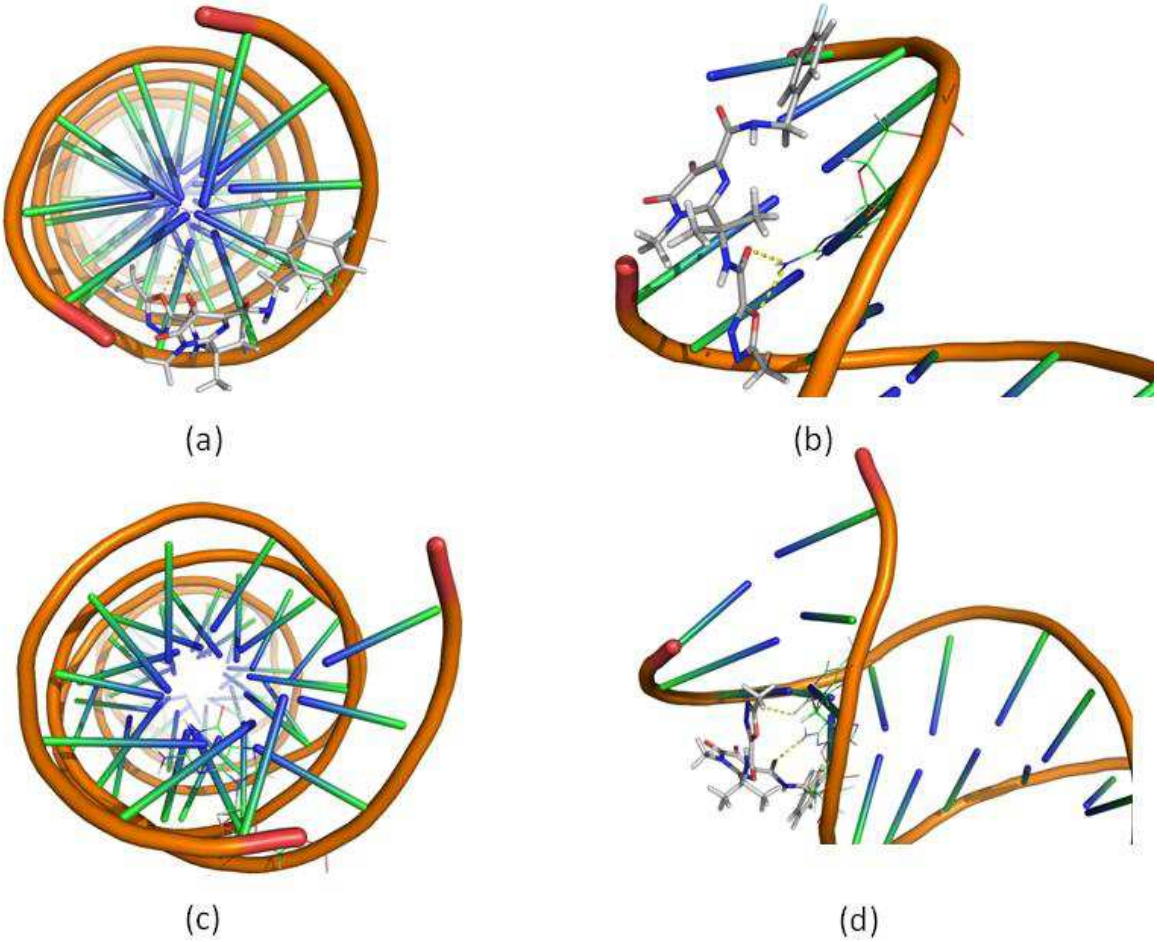

Figure 21. RAL – viral DNA recognition. The inhibitor docked onto the viral non-cleaved (a and b) and cleaved DNA (c and d). The vDNA is shown as cartoons, the guanine and RAL are shown as thing lines and sticks respectively. (Arora *et al*. 2012).

4. Discussion

The structural models reported here were generated by homology modeling and represent with a certain level of reliability two different enzymatic states of the HIV-1 IN that can be explored as RAL biological relevant targets. All generated models are based on the experimental data characterising either the partial structures of IN from HIV-1 or full-length IN from PFV. The models of the separated full-length HIV-1 integrase represent the unbound homodimers of IN (IN^{1-270}) containing either one or two Mg^{2+} cations in the active site – a plausible enzymatic state before the 3'-processing. The catalytic site loop encompassing ten residues forms the boundary of the active site. This loop shows either a coiled structure (Bujacz *et al*., 1996; Goldgur *et al*., 1998; Maignan *et al*., 1998) or contains an Ω-shaped hairpin (Mouscadet *et al*., 2009;). Our simplified model of the HIV-1 IN•vDNA pre-integration complex represents the homodimer of integrase attached non-covalently to the two double strains of the viral DNA with two removed nucleotides GT at each 3'-end.

Two models of different states of the HIV-1 IN show a strong dissimilarity of their structure evidenced by divergent relative spatial positions of their structural domains, NTD, CCD and CTD. These tertiary structural modifications altered the contacts between IN domains and the structure and conformation of the linker regions. Moreover, IN undergoes important structural transformation leading to structural re-organisation of the catalytic site loop; the coiled portion of the loop reduces from 10 residues in the unbound form to 5 residues in the vDNA-bound form. Such effect may be induced either by the vDNA binding or it can derived as an artefact produced from the using of structural data of the PFV IN as a template for the model generation**.** Prediction of $IN^{133-155}$ sequence secondary structure elements indicates a more significant predisposition of IN from HIV-1 to be folded as two helices linked by a coiled loop than the IN from PFV. The helix elongation accompanied by

loop shortening may be easily induced over the enzyme conformational/structural transition between the two integration steps prompted by substrate binding.

The docking calculations of RAL onto each model evidenced that (i) the large binding pocket delimited by the active site and the extended catalytic site loop in the unbound IN can accommodate RAL in distinct configurational/conformational states showing a lack of interaction specificity between inhibitor and target; (ii) the well defined cavity formed by the active site, vDNA and shortened catalytic site loop provides a more optimised RAL binding site where the inhibitor is stabilised by coordination bonds with Mg^{2+} cations in the Z/Z-configuration. Additional stabilisation of RAL is provided by non-covalent interactions with the environmental residues of IN and the viral DNA bases. We suggested earlier the stabilizing role of the vDNA in the inhibitors recognition by IN•vDNA pre-integration complex (Ni *et al*., 2012). The role of the viral DNA in RAL recognition was further evaluated in the present study. In the processed vDNA the Z/Z isomer of RAL takes place of the remote GT based and is stabilised by strong and specific H-bonds with the unpaired cytosine. These H-bonds characterize the high affinity and specific recognition between RAL and the unpaired cytosine similarly to those observed in the DNA bases pair G-C.

Based on the docking results we suggest that the inhibition process may include as a first step the RAL recognition by the processed viral DNA. RAL coupled to vDNA shows an outside orientation of all oxygen atoms, excellent putative chelating agents of Mg^{2+} cations, which could facilitate the insertion of RAL into the active site. The conformational flexibility of RAL further allows the accommodation/adaptation of the inhibitor in a relatively large binding pocket of IN•vDNA pre-integration complex thus producing various RAL docked conformation. We speculate that such variety of the RAL conformations contributing alternatively to the enzyme residue recognition may impact the selection of the clinically

observed alternative resistance pathways to the drug (Mouscadet, Delelis, Marcelin, & Tchertanov, 2010 and references therein).

The other question considered in our work relates to the choice of the more adapted molecular docking method to study a very flexible inhibitor – RAL in the given case – with flexible and relatively rigid targets represented here by the HIV-1 IN unbound and bound to the viral DNA, respectively.

Every protein-ligand docking program consists of two essential components, sampling and scoring. Sampling refers to the generation of putative ligand binding orientations/conformations at the proximity of a binding site of a protein and includes two aspects, ligand sampling and protein flexibility. Scoring predicts the binding tightfistedness for distinct ligand orientations/conformations (binding poses) with an energy function value and the binding pose with the lowest energy is considered as the most favorable one (Hu, Balaz, & Shelver, 2004). The recent methodological advances in protein-ligand docking are reviewed in (Huang & Zou, 2010). Although the docking problem seems intuitively easy, searching the space of all possible 3-dimensional protein–ligand conformations and determining the energetically most favorable solution is a hard computational problem. In case where both the protein and ligand are kept rigid, (wherein only the translational and rotational degrees of freedom are considered), the docking problem is six-dimensional (Thomsen, 2003). However, if flexibility in either the ligand or the receptor or both, is allowed during the search process, the dimensionality of the problem increases with the number of "rotatable" bonds. This generates an enormous search space attributed to the possible conformations of the flexible ligand.

The docking studies reported RAL located within the active site of either unbound IN or IN•vDNA complex. Distinct poses of RAL representing different RAL configuration and

modes of Mg^{2+} cations chelation were observed (Barreca *et al*., 2009; Loizidou *et al*., 2009; Perryman *et al*., 2010; Serrao *et al*., 2009).

Our trials to dock the generated RAL conformations demonstrate that the four used programs produce different results which in turn depend more on the targets choice than the exact information on the initial configurational/conformational state of the flexible inhibitor. Docking of the flexible RAL onto the flexible target (the unbound IN either with a one or two Mg^{2+} ion(s) in the active site) with an extended and poor-defined (deleterious) binding pocket produced contradictory results with all used algorithms. The programs were not capable to discriminate between the docked conformations using the scoring functions. RAL docking onto the IN•vDNA model systematically generated the RAL chelated to Mg^{2+} cations at the active site by the oxygen atoms of carbonylamino hydroxypyrimidinone moiety. The best binding energy was systematically obtained with GLIDE and AutoDock and the pharmacologically relevant poses were identified with GLIDE.

The binding of strand-transfer inhibitors displaces the reactive vDNA end from the active site, disarming the viral nucleoprotein complex. The early reported data and our results indicate as "interacting" with the strand-transfer inhibitors a large number of the IN residues forming the cavity defined as the active site for the strand-transfer reaction (Agapkina *et al*., 2006)·(Dolan *et al*., 2009) (Dhaked *et al*., 2009) (Ni *et al*., 2012). The identification of IN residues specifically interacting with RAL by docking algorithms is likely a very difficult task and the exact modes of binding of this inhibitor remain a matter of debate. Most probably the flexible nature of RAL results in different conformations and the mode of binding may differ in terms of the interacting residues of the target, which trigger the alternative resistance phenomenon.

IV. Comparison of Integrase structure from the HIV-1 subtypes B and CRF02_AG and its susceptibility to Integrase Strand Transfer Inhibitors

1. Structural analysis of Integrase from B and CRF02_AG strains

Comparative structural analysis of IN from two strains and study of the inhibitors binding were performed considering 6 IN models generated by homology modelling (Figure 22). Models 1 (B) and 2 (CRF02_AG) (Figure 22 a) represent the unbound homo-dimer of integrase (IN^{1-270}), which depicts the conformational state of the enzyme just before the 3'-processing of vDNA (apo state); models 3(B) and 4 (CRF02_AG) (Figure 22 b) represent the IN dimer in complex with vDNA (holo state), which depicts the active unit of the IN•vDNA strand transfer intasome; models 5 (B) and 6 (CRF02_AG) (not shown) were derived from models 3 and 4 by removing vDNA.

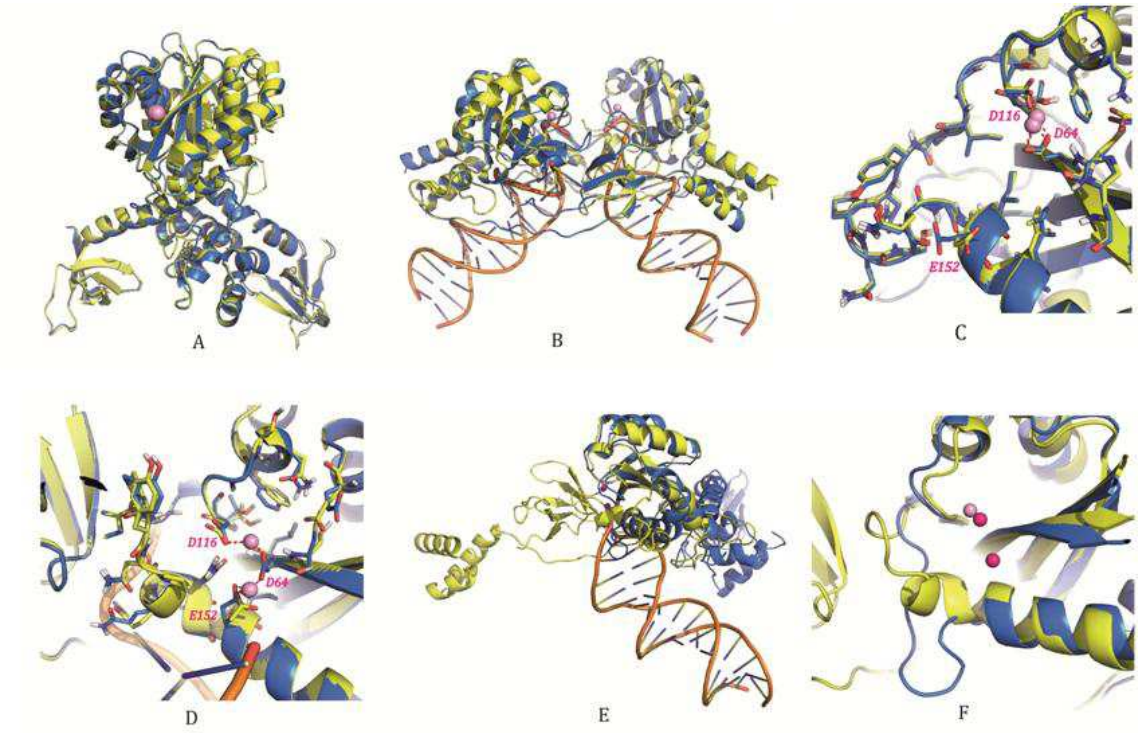

Figure 22: Structural models of the HIV-1 INs from B and CRF02 AG strains. (a) Superimposition of models 1 and 2, representing the enzyme before the 3'- processing from B (in blue) and CRF02 AG (in yellow) strains; (b) Superimposition of models 3 and 4, representing the IN·DNA pre-integration

complex from B (in blue) and CRF02 AG (in yellow) strains; (c) and (d) Comparison of the catalytic site and loop 140–149 structure in models 1/3 (in blue) and 2/4 (in yellow) respectively. The proteins are shown as cartoons, Mg^{2+} ions as spheres (in pink). (e and f) superimposition of the structural subunits from models 1 (in blue) and 3 (in yellow) and the structural details of the active site and loop 140–149.(Ni *et al*. 2012).

Models 1 and 2 were constructed from the crystallographic structures of HIV-1 IN isolated domains or pairs of domains. Overall, the analysis of the models representing the HIV-1 IN conformational state before 3'- processing (apo state), did not show any significant structural change between the two subtypes (Figure 22 a, c).

Models 3 and 4 were constructed from the crystallographic structure of the IN•vDNA complex of the PFV intasome. Although the sequence identity between HIV-1 and PFV INs is low (22%), the structure-based alignment of the two proteins demonstrates high conservation of key secondary structural elements and the three PFV IN domains shared with HIV-1 IN have essentially the same structure as the isolated HIV-1 domains. Moreover, the structure of the PFV intasome displays a distance between the reactive 3' ends of vDNA that corresponds to the expected distance between the integration sites of HIV-1 IN target DNA (4 base pairs). Consequently, we are confident that the PFV IN X-ray structure represents a good template for the HIV-1 IN model generation. To obtain a robust alignment, we adjusted the targets (HIV-1 INs from B and CRF02_AG subtypes) and template (PFV IN) sequences manually, considering each structural domain separately, in order to take into account the conservation of the secondary structure (see Chapter 4. **MATERIAL AND METHODS**).

Again, models 3 and 4, representing the IN•vDNA intasomes of both strains, superimposed perfectly and no structural dissimilarity was observed (Figure 22 b d). Most of the variations are located far from the active sites and the nearest two mutated residues to the active site, at positions 134 and 136, are exposed to the solvent and apparently did not affect significantly the structure. Similarly for 3'-processing, strand transfer activities of B and

CRF02_AG recombinant proteins were assayed and compared. In agreement with the modeling results, activities of both INs were comparable.

It is worth noting large structural and conformational changes observed between the apo (models 1 and 2) and holo (3 and 4) states regarding the relative positions of the IN domains (RMSD, root mean square deviation, of 31 Å, based on C_α) (Figure 22 e). These structural modifications result in different contacts between IN domains, N-terminal domain (NTD), catalytic core domain (CCD) and C-terminal domain (CDD). As such, in models 1 and 2 (apo state) no interaction was detected between CTD, and, CCD, whereas the two domains interact tightly in models 3 and 4 (holo state). The NTD-CCD interface also exhibits substantial changes: in the apo form the NTD-CCD interface belongs to the same monomer subunit whereas in the holo form the interface is from two different subunits. Moreover, IN undergoes important structural transformation leading to structural re-organization of the catalytic site loop upon vDNA binding ; the coiled portion of the loop reduces from 10 residues (140 -149 aas) in the apo form to 5 residues (140-144 aas) in the holo form (Figure 22 f). This partial folding of the catalytic loop is probably stabilized through intra-IN domain-domain interactions and interactions with vDNA which contribute in the helix α4 elongation.

2. The INSTIs recognition by Integrase from B and CRF02_AG strains

Although B and CRF02_AG INs are structurally similar, residue variations may impact the interaction and subsequent activity of the inhibitors. To address this hypothesis, the three inhibitors RAL, ELV and L731,988 (**Chart 3**) were docked onto INs by using two different docking algorithms, Glide and Autodock. RAL and ELV coordinates were taken from the crystallographic structures of PFV intasome co-complexes (Hare *et al*., 2010a), L731,988 was built from scratch (see Chapter 4. **MATERIALS AND METHODS**). The three compounds were considered in their deprotonated form, as it has been clearly established that diketo acids

(DKAs) mainly exist in this form in solution (Maurin *et al*., 2004). The binding energies obtained by Glide and Autodock scoring functions are reported in Table 4. The inhibitors were first docked onto the unbound IN, models 1 and 2 (apo state), with a single Mg^{2+} ion within the catalytic site. All three inhibitors are positioned at the catalytic site far from the catalytic site flexible loop. For subtype B, values of binding energies obtained with Glide range in a relatively narrow interval from -8.49 to -7.42 kcal/mol while those obtained with Autodock range from -8.72 to -6.65 kcal/mol. Scores obtained for a given inhibitor display some variations from one strain to another and between the two docking programs. ELV best pose in model 1 (B subtype) predicted by Glide is very close to that in model 2 (CRF02_AG subtype).

Table 4. Docking binding energies of RAL, ELV and L731,988 on the HIV-1 IN from B and CRF02 AG strains predicted by Autodock and Glide. The targets are the IN model with one Mg^{2+} cation in the active site (apostate, models 1 and 2) and IN·DNA model with two Mg^{2+} cations (holo state, models 3 and 4). (Ni *et al*. 2012).

Target		The free binding energies (kcal/mol)	
	Inhibitor	Autodock	Glide
IN B (apo)	RAL	−6.83	−8.05
	ELV	−8.22	−7.42
	L731,988	−7.81	−8.49
IN CRF02_AG (apo)	RAL	−6.65	−7.68
	ELV	−8.72	−8.20
	L731,988	−8.31	−7.85
IN·DNA_B (holo)	RAL	−11.43	−10.22
	ELV	−12.45	−9.17
	L731,988	−11.50	−8.73
IN·DNA CRF02_AG (holo)	RAL	−11.11	−9.98
	ELV	−13.45	−9.16
	L731,988	−11.93	−8.82
IN* B (holo)	RAL	−8.29	−8.36
	ELV	−11.62	−8.92
	L731,988	−12.19	−8.96
IN* CRF02_AG (holo)	RAL	−7.98	−8.46
	ELV	−11.80	−8.93
	L731,988	−11.58	−8.82

Small differences relate to an improved affinity of ELV to model 2 evidenced by a better score (-8.20 kcal/mol) and by the formation of an additional H-bond between the hydroxy group of ELV and E152 side chain (Figure 23 a, b). RAL poses in models 1 and 2

differ strongly. In both cases RAL coordinates similarly the Mg^{2+} cations by its ketoenolate functionality, but the inhibitor adopts opposite positions, more specifically in model 1 its flurobenzyl ring is oriented towards Y143, while in 2 towards Q148. L731,988 poses are also different in models 1 and 2, characterized by distinct pyrrole ring positions, close to E152 in 1 and to Y143 in 2. Such presence of alternative poses is likely due to a large pocket formed by the accessible active site and the open conformation of the folded loop which allow a large number of conformations and orientations with equivalent binding affinity for the flexible RAL and L731,988 molecules. Consequently no significant difference can be assessed between the binding of the three studied inhibitors to the unbound IN from strains B and CRF02_AG.

Further the inhibitors were docked onto models 3 and 4 representing pre-integration complexes, IN•2Mg^{2+}•DNA, from B and CRF02_AG subtypes respectively. Docking resulted in a binding for the three inhibitors with significantly higher scores than those found for the apo IN. Glide scores ranked in a range from -10.22 to -8.73 kcal/mol, while Autodock scores range from -13.45 to -11.11 kcal/mol. Comparison of the poses produced by the two docking software were found similar, and consequently we focus here on the analysis of Glide results.

The three compounds are positioned in the catalytic site and chelate the Mg^{2+} cations in agreement with the mechanism of action of these molecules, which are strand transfer inhibitors (Mouscadet *et al*., 2010). RAL binding mode is characterized by higher scores in both models 3 (B subtype) and 4 (CRF02_AG subtype) respectively to the other two inhibitors. RAL predicted poses are identical in models 3 and 4.

It binds bidentantly both metal cofactors of the active site acting as a 1-5 and 1-4 type ligand, with the enolic oxygen atom as an oxo-bridge between two Mg^{2+} cations.

Additional stabilization of inhibitor RAL is achieved by stabilization of inhibitor Mg a 1-5 and similarly to RAL, ELV coordinates the Mg^{2+} cofactors bidentantly through the 1-5

type β-ketoenolate moiety and 1-3 geminal carboxylic oxygen atoms, with a carboxylic oxygen atom as an oxo-bridge at the bicationic cluster. A few differences of ELV binding in model 3 and 4 refer to slightly different conformation of the chloroflurobenzyl moiety.

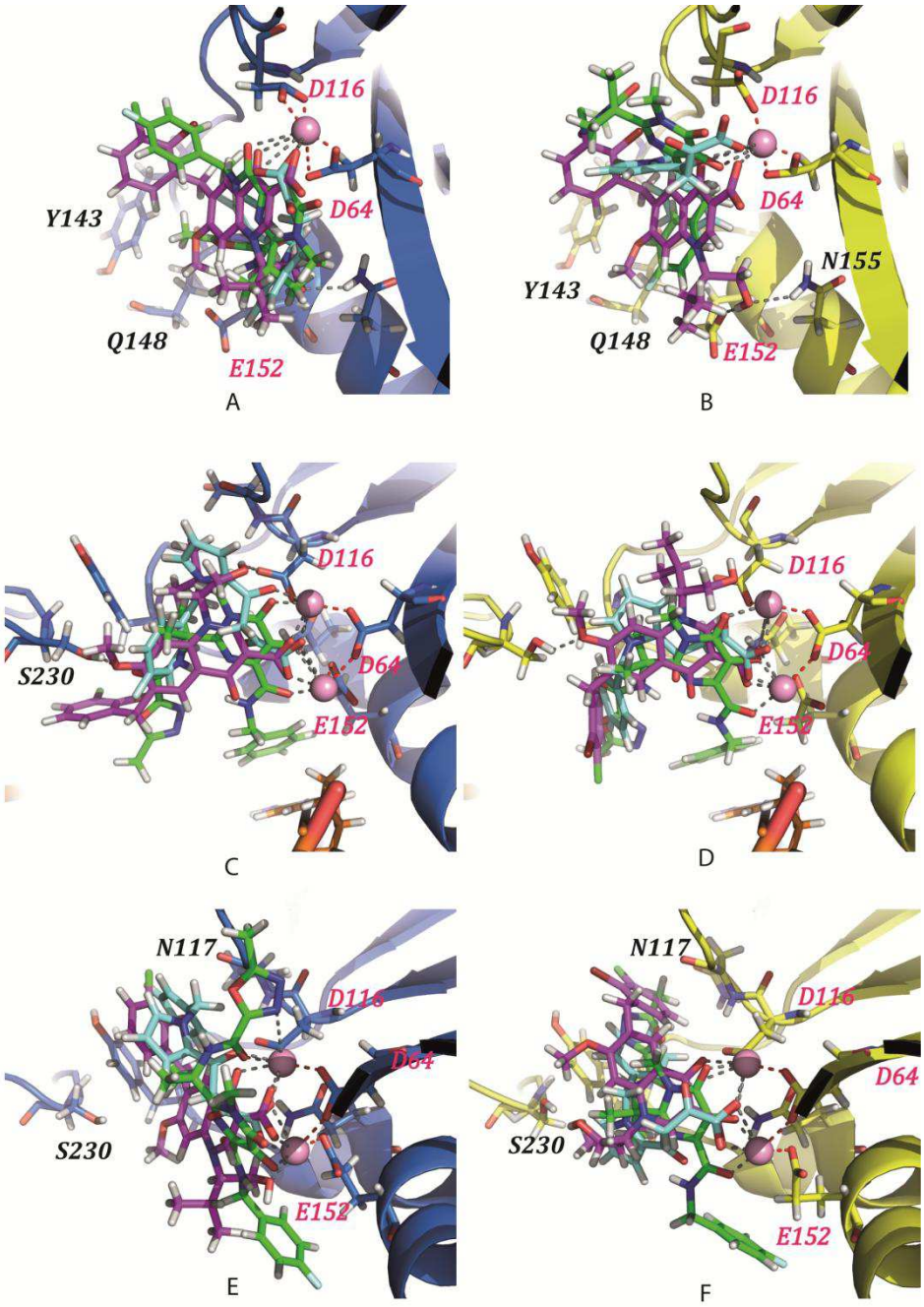

Figure 23. RAL (green), ELV (magenta), and L731,988 (cyan) best poses predicted by Glide. The inhibitors were docked into the active site of unbound IN (top) and IN·DNA complex (middle) and IN in holo conformation without DNA (bottom) from of the B (in blue) and CRF02 AG (in yellow). Proteins and DNA are shown as cartoons, inhibitors as sticks, and Mg^{2+} cations as balls. (Ni *et al*. 2012).

. L731,988 molecule shows different binding poses in models 3 and 4. In model 3 (B subtype) L731,988 coordinates bidentately one Mg^{2+} cation by the oxygen atoms from keto functionality of ketoenolate and carboxylate groups, acting as a ligand of 1-6 type. The second Mg^{2+} cation is coordinated only by the carboxylate oxygen atom. In model 4 (CRF02_AG) L731,988 inhibitor shows exclusively one coordination to the one Mg^{2+} cation.

3. Discussion

The predicted binding poses of RAL correlate well with those observed in the X-ray structure of the PFV intasome complex (Hare *et al*., 2010a; Hare *et al*., 2010b). Undoubtedly, the presence of the second catalytic Mg^{2+} cation, the partial loop folding and the DNA substrate bearing are presumably the driving determinants for the tight binding of ST inhibitors in the catalytic site. It was perfectly evidenced by Cherepanov that a series of INSTIs fixed similarly to the PFV intasome (Hare *et al*., 2010a). Apparently the crystallographic data or static models derived from these data are not suitable means to explain the specificity of inhibitor recognition by a target. Consequently, considering the similar scoring values for a given inhibitor and closed poses no significant dissimilarity can be assessed between the binding of studied inhibitors to the IN•2Mg^{2+}•DNA complex from strains B and CRF02_AG.

To validate the *in silico* predictions regarding the susceptibility of subtypes B and CRF02_AG INs, the efficiency of INSTIs (RAL, ELV and L731, 988) on recombinant INs proteins were determined by *in vitro* strand transfer assay in the presence of increasing concentration of INSTI (see **MATERIALS AND METHODS**). As to all the three studied INSTIs, no significant difference in IC_{50} values against recombinant HIV-1 INs from B and CRF02_AG strains was observed (Ni *et al.* 2012). IC_{50} of RAL, ELV and L731,988 against HIV-1 INs from B and CRF02_AG strains are 41.8, 93.4, 855 nM and 13.7-25.9, 48.9-

66.8,193-291 nM, respectively (Ni *et al.,* 2012). The experimental ranking of the three compounds was predicted correctly by Glide scoring function.

The docking calculations evidenced that (i) the IN•DNA complex represents the best target for the studied inhibitors and (ii) the co-complexed vDNA partially shapes the inhibitors binding site. To further explore the role of vDNA, substrate was removed from the IN•vDNA complex and inhibitors were docked again on unbound IN with a fold corresponding to the holo state, models 5 and 6. The binding energies of RAL are depreciated upon vDNA removal in B and CR02_AG subtypes while ELV and L731,988 binding scores are less affected.

Docking scores are nearly similar between the two strains while poses display some variations, as already observed on the apo form. Surprisingly, the Autodock results show the lower score for RAL binding to both models 5 and 6, while the binding of the two other inhibitors are characterized by better scores, closer to those obtained with models 3 and 4. In contrast the scores produced by Glide are identical between the inhibitors and the subtypes. Chelation of the Mg^{2+} ions by the inhibitors is still maintained but the interaction patterns differ from those predicted in models 3 and 4. Indeed, in model 5 (B subtype) RAL chelates the first Mg^{2+} cation through the nitrogen atom of the oxadiazol ring and the oxygen atom of the carboxamide moiety; the second Mg^{2+} is coordinated by 1-4 oxygen atoms of pyrimidinone fragment. In model 6 RAL mode of coordination resembles that observed in model 4, however stabilizing π-stacking interactions were vanished. Again, the large volume of the binding pocket and the lack of stabilizing protein-ligand and DNA-ligand interactions can explain such variety. Consequently, unbound IN in the holo conformation, as unbound IN in the apo conformation, does not appear as a suitable target for the inhibitors RAL and ELV. L731,988 appears as a weaker binder, as confirmed by the experimental IC_{50} values.

Molecular modeling approaches were used to investigate the effect of the natural variations showed by CRF02_AG strain on the *in vitro* activities of the enzyme and its susceptibility to INSTIs as compared to the ones of the consensus B integrase. We found that the structural models of unbound and viral DNA-bound integrase showed very similar folding and tertiary structure for the two studied strains. The structural models of the IN•vDNA complex, superimposed perfectly. This similarity was confirmed by comparable strand transfer activity for IN variants in 14, 112, 125, 134, 136, 206 and 283 positions. Consequently, the naturally occurring variations in the HIV-1 IN subtype CRF02_AG – K14R, V31I, L101I, T112V, T124A, T125A, G134N, I135V, K136T, V201I, T206S, V234I and S283G, which were suggested to modify IN structure do not affect significantly *in vitro* DNA binding activity, either 3'-processing or strand transfer reaction. Furthermore, docking results revealed that the modes of binding and docking conformations of three studied inhibitors are comparable for B and CRF02_AG strains and these INSTIs possessed similar IN inhibitory activity against B and CRF02_AG HIV-1 strains. Altogether these results demonstrate the absence of difference in susceptibility and confirm previously reported observations for subtype B and C HIV-1 IN (Bar-Magen *et al*., 2009). Thus, in contrast to the lower baseline susceptibilities of recombinant A/G subtype virus to protease inhibitors (PIs) and reduced susceptibility of some A/G isolates to abacavir, INSTIs potentially provide an excellent therapeutic option for the treatment of HIV-1 subtype CRF02_AG infected patients (Martinez-Cajas *et al*., 2008).

In the targets all three molecules are positioned similarly with ketoenol moiety in an orientation encouraging coordination of the two metal cofactors in the active site. Furthermore, independently of the method, the three INSTIs displayed a more favorable binding onto the IN•vDNA complex than on the unbound enzyme, in good agreement with their mechanism of action (Kawasuji *et al*., 2006). Same difference in theoretically predicted

modes of RAL binding was reported early by Loizidou (Loizidou *et al*., 2009). The observed conformational and structural transformation of IN upon DNA binding led to an important change in the folding and conformation of the catalytic site loop which in turn favours a formation of the binding pocket accommodating the INSTIs. The binding modes of ELV and L731,988 were practically not altered by the removal of the viral DNA. Conversely removing vDNA had a significant effect on the docking results RAL, thereby highlighting the role of vDNA for RAL recognition most likely due to the halogenated benzyl moiety that displaces the unpaired 5'adenine and stacking with the Cyt16 through π-π interactions. Although such interaction is thought to be involved in all the IN strand transfer inhibitors examined (Hare *et al.*, 2010), our results suggest that ELV and L731,988 binding determinants differed in part from the ones of RAL.

It should be noted that slight differences were observed between the results obtained with Glide and Autodock scores, which can be ascribed to the impact of electrostatic interactions in the studied molecular systems. Indeed Glide uses higher negative charge localized on the two oxygen atoms of the hydroxypyrimidinone of RAL than Autodock (-1.22 and -0.5 e versus -0.183 and -0.265 e). Also, within Autodock scoring function, the carboxylate charges used for ELV (2 x -0.64 e) and L731, 988 (2 x -0.62 e) are more than two oxygen atoms attached to the pyrimidine cycle of RAL. To verify this hypothesis, we repeated the docking calculations of ELV and L731,988 using the charges of two oxygen atoms attached to the pyrimidine ring of RAL instead of those assigned by Gasteiger charges. The new binding energies of both inhibitors increased from -12.45 and -11.50 to -7.95 and -7.80 kcal/mol for ELV and L731,988 respectively. Since these atomic charges contribute highly in the binding energy as the atoms coordinate Mg^{2+} ions, they are likely responsible for the discrepancies found between the theoretical binding energies and the experimental IC_{50} values. The experimental ranking of the three inhibitors based on IC_{50} is, RAL > ELV > L731,988, as predicted by

Glide while the ranking predicted by Autodock is ELV > L731,988 ≥ RAL The high negative charges of the carboxylate oxygen atoms of ELV and L731,988 may be the obstacle to have inhibitory actions on integrase, as efficient as RAL, since these charges increase the desolvation free energy and so increase the binding penalty for these inhibitors.

V. Alternative molecular recognition of DNA induced by Raltegravir resistance mutations

1. Evidence of a Stable Ω-shaped Hairpin in the catalytic site loop

As discussed above, the catalytic core domain encompasses a flexible loop comprising residues 140–149. This loop is known to be required for efficient IN function, but its precise role in the process of integration is unknown.

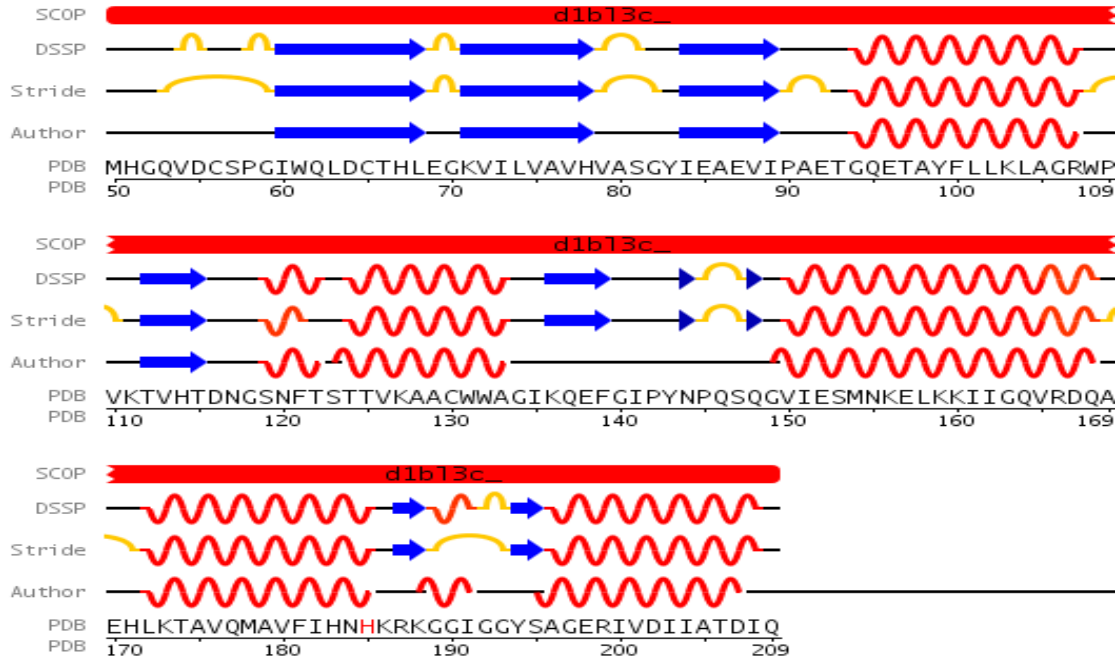

Figure 24. Secondary structure of the IN^{50-209} in 1BL3 structure (chain C) determined by DSSP (first line, Kabsch & Sander, 1983), Stride (second line, Frishman & Argos, 1995) or was recovered from structure by authors (third line, Maignan *et al*., 1998).

We began by carrying out secondary structure assignment for the 1BL3 (chain C) structure with SCOP and DSSP, comparing the results obtained with previous interpretations (Figure 24). The two methods predicted a similar fold for residues 140–149, but this fold was different from that previously reported (Maignan *et al*., 1998). We then used the complete (47–212 aa) and partial sequences (140–151 aa) of WT and mutant IN to predict the 2D structure (helix, strand, and coil) and substructural motifs (γ-, β-, α-, π-turns and hairpins; see Chapter 4. **MATERIALS AND METHODS**). Secondary structure prediction confirmed the presence of a coil domain extending from residue 140 to residue 149. Substructural motifs within the loop were indicative of a hairpin with a three-residue turn stabilized twice by i→ i±4 H-bonding involving the N144 and Q148 backbone (Figure 36 a (i)). This turn, connecting the helix to the b-sheet, corresponds to the ‘‘a–b-arch’’ described by Efimov (Efimov, 1993) as a standard structure in proteins. Thus, structure-based assignment and sequence-based 2D prediction both suggested that the catalytic active site loop contained two distinct structures: a random coil formed by the highly hydrophobic residues in positions 140–143 and a hairpin composed mostly of the hydrophilic amino acids in positions 144–148, stabilized by double across-loop backbone– backbone H-bonds. The G140A/S and Q148H/R/K mutations did not affect this structure (Figure 26 a (ii)). The 3D structure of the loop was built with two independent algorithms: a loop search based on structural data from PDB (a knowledge-based method) and *ab initio* loop generation (conformational search). Both methods identified a loop with a similar supersecondary local structural motif: a hairpin with an Ω-shaped body stabilized by the pair of backbone–backbone and three backbone–sidechain H-bond interactions, shaped like a doughnut and covering an area of 40–44Å (Figure 26 d) (Tchertanov, Delelis, & Mouscadet, 2007). This loop was recently identified in the IN/DNA complex structure, but no specific structure was discussed (Chen *et al*., 2008). The formation of this hairpin is due to the presence of N, Q, S, G, and P, matching statistical preferences for

amino acid type within particular turns (Levitt & Warshel, 1975; Hutchinson & Thornton, 1994). G and P are characteristic of reverse turns, as they confer conformational flexibility and cannot form hydrogen bonds. The importance of loops has been confirmed experimentally. Many enzymes use flexible loops that change conformation upon substrate binding to form a catalytically competent active site. Indeed, 57% of catalytic residues are located in or close to such loops (P. Aloy, personal communication). Ω–loops constitute a relatively new category of secondary structures (Leszczynski & Rose, 1986; Fetrow, 1995; Street *et al.*, 2007) and appear to be important for substrate or inhibitor binding and/or protein–protein recognition (Strobel & Ryder, 2001).

2. Modeling of the catalytic site structure of the HIV-1 integrase

According to X-ray structure data, Mg, coordinated by D64 and D116, does not affect the conformation of the catalytic loop (Maignan *et al.*, 1998). A second Mg^{2+} ion would be likely to enter the site upon movement of the E152 side chain toward the active site. However, this does not appear to alter the conformation of the loop (Savarino, 2007). Conversely, MD simulations demonstrated a significant conformational change involving the catalytic loop and E152 of the DDE motif in the presence of the second cation (Lins *et al.*, 2000). This conformational change occurred earlier in the simulation, when hydrogen phosphate was included to mimic DNA, suggesting that the binding of the second cation and the resulting conformational change occurred upon DNA binding. We investigated the effect of the metal cofactor further, by constructing models of the core domain with no cation (0LJ), one (1LJ) or two Mg^{2+} cations (2LJ–5LJ), starting from the 1BI4 and 1BL3 templates, as described in the Methods section (Figure 25). In the 2LJ and 3LJ models, the binuclear Mg^{2+} cluster was symmetric, with each Mg^{2+} ion coordinated by the D116 and E152 residues in either a monodentate (2LJ) or a bidentate (3LJ) mode. In the 4LJ and 5LJ models, the binuclear Mg^{2+}

cluster was asymmetric, with each Mg^{2+} cation coordinated by D116 and E152 in either a mono- or bidentate mode. All the 3D models had similar topologies (Figure 26 b). The first two models, 0LJ and 1LJ, did not differ from their templates: Mg^{2+} was coordinated by D64 and D116 and the other positions were occupied by water molecules, constituting pseudo-octahedral Mg coordination. The other models had a binuclear Mg^{2+} core with two non-identical bridges, the D64, and the μ-aqua bridge, with the water molecule bridging the gap between the two coordination centers. These binuclear models differed in the mode of chelation of D116 and E152. Based on the total energy values of the complexes modeled, the 3LJ and 5LJ models were excluded from further analysis due to their low probability.

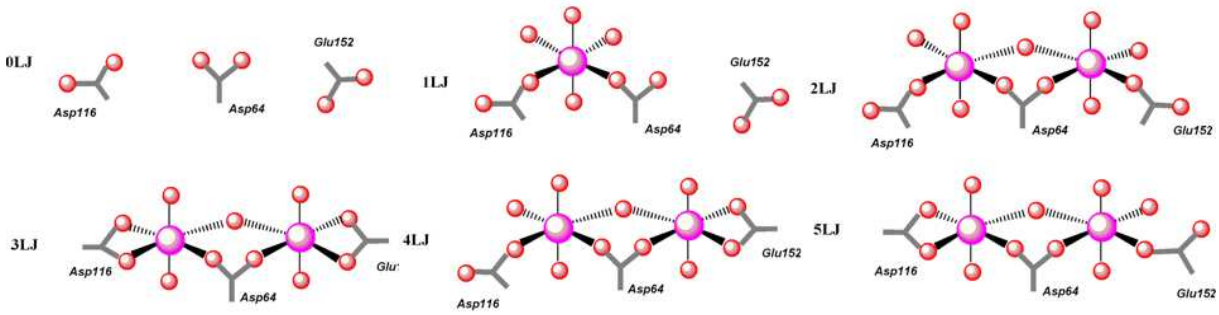

Figure 25. Constructed models of the core domain of IN with no cation (0LJ), one (1LJ), or two Mg^{2+} cations (2LJ–5LJ). In 2LJ and 3LJ, the binuclear Mg^{2+} cluster was symmetric, with each Mg^{2+} coordinated with D116 and E152 in either the monodentate (2LJ) or the bidendate (3LJ) mode. In 4LJ and 5LJ, the binuclear Mg^{2+} cluster was asymmetric; each Mg^{2+} cation was coordinated with D116 and E152 in either mono- or bidentate mode. (Mouscadet *et al*. 2009).

D64 and water stabilize the binuclear complex, with a Mg…Mg distance of 4.2 A for both the 2LJ and 4LJ models. This distance is slightly smaller than the equivalent distance in the 1SA model (4.5 A) (Savarino, 2007) and greater than that in the 1WKN model (3.9 A) (De Luca *et al*., 2005). All side chains of the catalytic amino acids involved in coordination are in a cis-position relative to the Mg…Mg axis, with E152 arranged in the equatorial and D116 in the axial position (Figure 26 c). In two-cation models, the D64 carboxylate group was rotated by about 308 relative to the Mg…O… Mg plane, corresponding to the D64 configuration in the cation-free and one-cation models. Thus, the conformation of bridged D64 was not

affected by the second Mg^{2+}. By contrast, the binding of the second Mg^{2+} ion required a major change in the conformation of the E152 side chains: the Chi1, Chi2, and Chi3 angles were -167, 169, and -38 in 1LJ and -174, 58, and 56^0 in 2LJ models. The binding of the second cation also required a slight alteration to both the D116 side chain and the first Mg^{2+} ion relative to its position in the one-cation model. Two modes of Mg coordination by E152 were possible (monodentate for 2LJ and mixed for 4LJ), but the type of coordination had no significant effect on the two-cation model. Finally, the Mg^{2+}…O distances corresponded to typical coordination bonds in Mg-containing complexes. Based on the covalent and ionic radii of the Mg and O atoms, the chelation of Mg^{2+} was essentially ionic.

The N155 residue, in the α4 helix, is a primary site of mutation leading to RAL resistance. The position and orientation of N155 relative to D64 favors $-(NH_2)_{N155}\ldots O_{=D64}$ H-bonding (Appendix of the paper, Figure 1). In cation-free and one-cation models, this H-bond was bifurcated and involved both H atoms of the 155 NH_2 group, which was also H-bonded to a carbonyl oxygen atom of the D64 backbone. Only the $N\text{-}H_{N155}\ldots O_{=E152}$ backbone–backbone interaction was involved in stabilizing the a4 helix, the distances between the N155 and E152 side chains being greater than for van der Waals (VdW) contacts. In the two-cation model, the E152 residue complexed with Mg^{2+} is oriented in a position favoring H-bonding with N155. Consequently unlike the H-bonding involving two partners in cation-free and one-cation models—a three-partner H-bond is formed in the two-cation model, with $(NH_2)_{N155}$ as a donor and two oxygen atoms of the carboxylate groups of D64 and E152 as the acceptors. Thus, in all models, the active site was stabilized by both metal coordination and H-bonding involving catalytic residues. We tried to identify the most probable configuration of D64, E152, and N155 side chains in wild-type IN, by carrying out a statistical analysis of the relative configuration of D, E, and N residues on the basis of reported X-ray structures. We found that the orientation of D64, E152, and N155 in the two-cation models corresponded to the more

populated N–D and N–E distributions, whereas the N–E orientation in cation-free and one-cation models was less probable. These statistical observations are thus consistent with our two-cation model (2LJ) for the structure of the IN active site, supporting the validity of our model. Our models demonstrate that Mg^{2+} cations do not alter the structure of the catalytic core domain. The catalytic loop retained its structure, with the distinctive H-bond pattern of the Ω-shaped hairpin observed for all models generated (Figure 26 d).

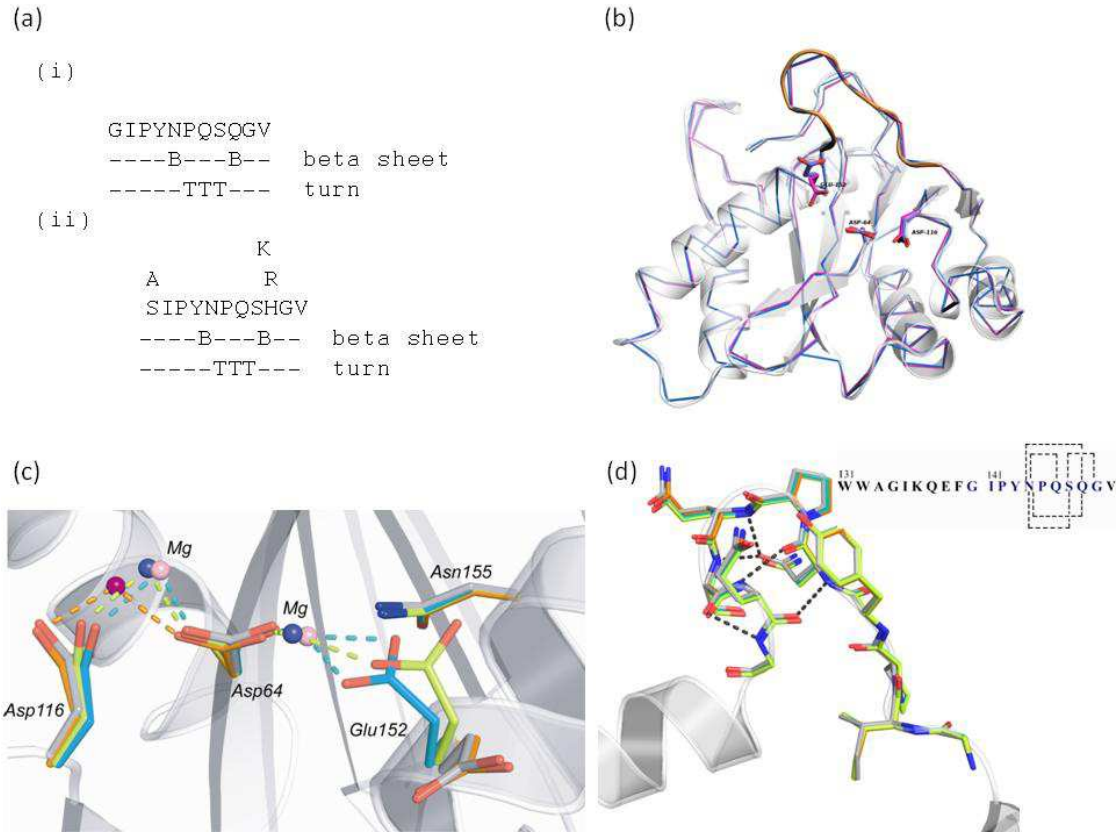

Figure 26. Structure of the HIV-1 IN core domain: (a) 2D prediction of the wild-type (i) and mutated (ii) loop of IN comprising residues 140–149. The first line represents the amino acid sequence; the second line represents the beta sheet stabilized by H-bonding and the third line indicates the turn state per residue. (b) Superimposition of the 0LJ, 1LJ, 2LJ and 4LJ (the wild-type IN) 3D models generated. Ribbon diagram, with the backbone and catalytic amino acid side chains shown as sticks; Mg^{2+} ions are not shown. (c) Active site: side chains of catalytic amino acids and Mg^{2+} cations shown as sticks and balls, respectively; coordination distances shown as dashed lines. Colors: gray (0LJ), orange (1LJ), yellow (2LJ) and green (4LJ). (d) Top: Catalytic loop structure; residues are shown as sticks, H-bonds as dashed lines. Colors: gray (0LJ), orange (1LJ), yellow (2LJ) and green (4LJ). Bottom: H-bonding patterns of the HIV-1 IN 131–149 domain observed in 3-D models. The residues 140–149 are shown in blue. H-bonds between the residues are shown by dashed lines. (Mouscadet *et al*. 2009).

3. Effect of raltegravir-selected mutations on Catalytic Core Domain structure

We then investigated the effect of the mutations selected by RAL and belonging to the independent N155 and Q148 pathways identified in previous studies (Charpentier *et al*., 2008; Cooper *et al*., 2008; Malet *et al*., 2008). The Q148 pathway is characterized by the presence of G140S or E138K secondary mutations. We first investigated the effect on structure of the N155H mutation affecting a residue in the catalytic site. We chose to study the N155H substitution because the imidazole side chain of histidine, if uncharged, may exist in either the $N^{\delta 1}$–H or the $N^{\varepsilon 2}$–H tautomeric form (at pH 7, the $N^{\varepsilon 2}$–H predominates). We generated mutated models for both H-donor orientations, with the protonated N pointing either towards the catalytic site or in the opposite direction. The two tautomeric forms of histidine in both orientations led to local reorganization of the structure of the active site (Figure 27 a-c). Conformations differed most between models with the same tautomers oriented differently, stabilized by different patterns of H-bonding. In one-cation models, the $N^{\varepsilon 2}$–H tautomer with the H-atom pointing toward the active site was stabilized by $N\text{-}H_{H155}...O{=}_{D64}$, with O= corresponding to the oxygen atom of the carboxylate group, as observed in the wild-type structure. However, for stabilization of the active site with the $N^{\varepsilon 2}$–H tautomer in the opposite orientation, O= was the backbone atom. The conformation of $N^{\delta 1}$–H was not influenced by H-bonding in the one-cation model, whereas, in the two-cation model, this tautomer with N–H pointing towards the active site was stabilized by H-bonding with the E152 side chain (Figure 27 b and c).We conclude that the active site structure may be conserved in the N155H mutant at physiological pH and, in this case, the $N^{\varepsilon 2}$–H tautomer of histidine acts as a conformational bioisoster of asparagine. We then studied six representative combinations of mutations including primary and secondary mutations of the Q148 resistance pathway. Three-dimensional models were generated from the ILJ and 2LJ templates. The E138K, G140S/A

and Q148H/K/R mutations only slightly modified the side-chain conformation, and the catalytic loop backbone retained its structure (Figure 27 d).

The H-bond patterns stabilizing the Ω-shaped hairpin in the mutants were similar to that in the wild-type IN. This finding is consistent with our sub-structural motif predictions.

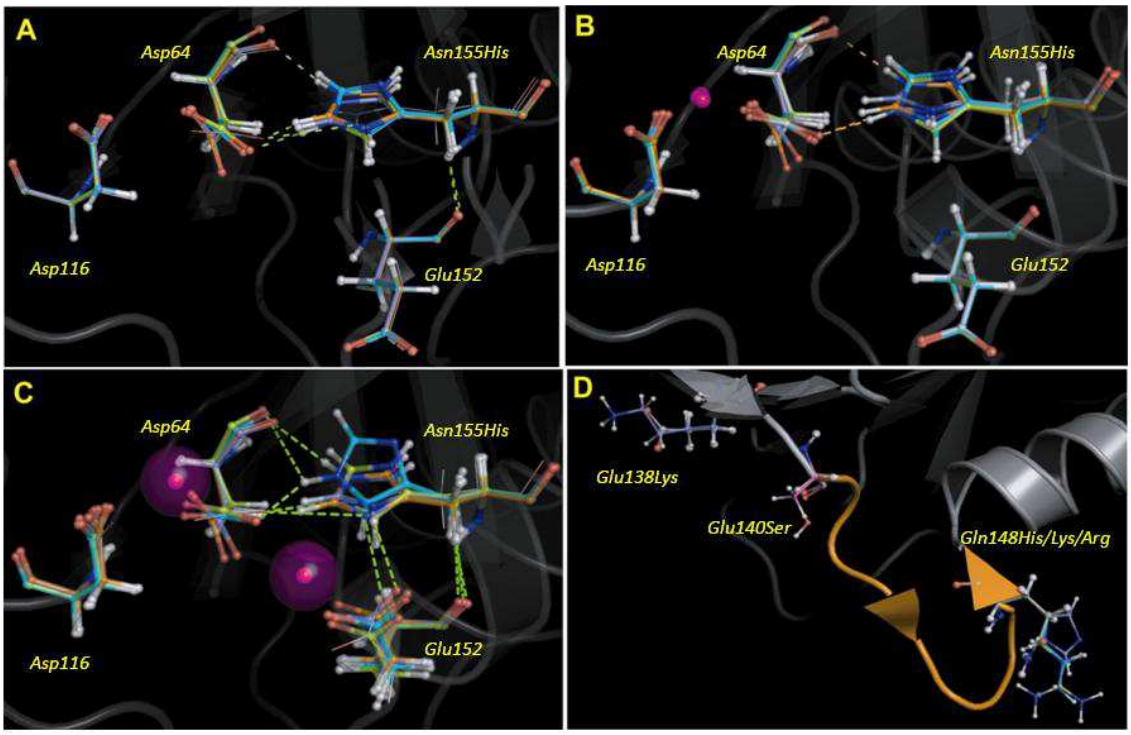

Figure 27. Superimposition of the wild-type and mutated models of the HIV-1 IN in (a) cation-free, (b) one- and (c) two-cation active sites. Molecular display style: enzyme structures shown by ribbons, residues D64, D116, E152 and H155 shown as ball-and-stick representations; the Mg^{2+} cation in (b) and in (c) shown as a ball. The wild-type N155 residue is shown as a wire frame. The mutant H155 is shown as a ball-and-stick representation in the following colors: the $N^{\delta 1}$–H tautomer oriented toward the catalytic site is shown in cyan and that in the opposite direction is shown in sand brown; the $N^{\varepsilon 2}$–H tautomer oriented toward the catalytic site is shown in light blue and that oriented in the opposite direction is shown in yellow. The H-bonds are indicated as dashed lines. (d) Ribbon diagram of the catalytic loop comprising residues 140–149 in the wild-type and mutated models, with residues 140 and 148 presented as ball-and-stick representations. (Mouscadet *et al*. 2009).

Consequently, our results suggest that the two primary pathways implicated in RAL resistance—the N155H substitution or replacement of the Q148 residue by H, R, or K—result in the retention of all the structural features of the catalytic domain of IN, unlike deleterious G140A/G149A mutations, which are thought to cause structural changes (Greenwald *et al*.,

1999). These findings highlight the importance of maintaining the integrity of the catalytic domain structure, consistent with the observation that the virus selects mutations resulting in the maintenance of catalytic activity (Delelis *et al*., 2009). They also suggest that the Ω -shaped hairpin may have a crucial function.

4. Model of the displacement of the Ω-shaped hairpin toward the catalytic site

The stabilization of the Ω -shaped hairpin by the formation of multiple H-bonds suggests that the previously reported flexibility of the 140–149 loop may be limited. We investigated the behavior of the Ω-shaped hairpin through simulations of loop motion in one- (1LJ) and two-cation (2LJ) models. The distance between two centroids—the first of which (C1) describes the center of gravity of the Ω -shaped hairpin and the second (C2), the center of gravity of the active site—gradually decreased, in 2Å steps, from 16 (open form) to 4.5Å A(closed form). Energy minimization was carried out after every step. The conformation of the backbone of the catalytic core domain did not change significantly during this process, but regular movements of the Ω -hairpin loop towards the catalytic site were observed (Figure 28 a). The total energy of all intermediate structures was similar for distances between 16 and 8Å, for both models. Structural fitness, as estimated by the violation values, satisfied constraints for 10<C1…C2<16Å, but showed a weak violation of constraints for 4.5<C1… C2< 8Å in the one-cation model (Figure 28 b). In the two-cation model, the movement of the hairpin satisfied violation criteria for 8<C1…C2<16Å, but further decreases in C1…C2 distance down to 6 or 4.5Å led to strong violation. However, G140A/S mutants displayed lower levels of hairpin mobility than the wild type. The G140S mutant, in particular, had total energy and violation values 10–30% higher than those for the wild type. We have shown that the hairpin can move, as a rigid body, in a gate-like manner toward the active site. Both

extremities of the catalytic loop comprised by residues 140–149 are delimited by glycine residues, conferring conformational flexibility on the polypeptide chain, by acting as a hinge, as previously suggested (Chen *et al*., 2008). However, the steric constraints of the Ω -hairpin in the catalytic loop differed between the left and right sides. On the left, the 140–143 stretch of amino acids forms a random coiled structure with few steric constraints. The C-terminus of the Ω-hairpin is subject to greater constraints due to the a-helix connected to the end of the loop.

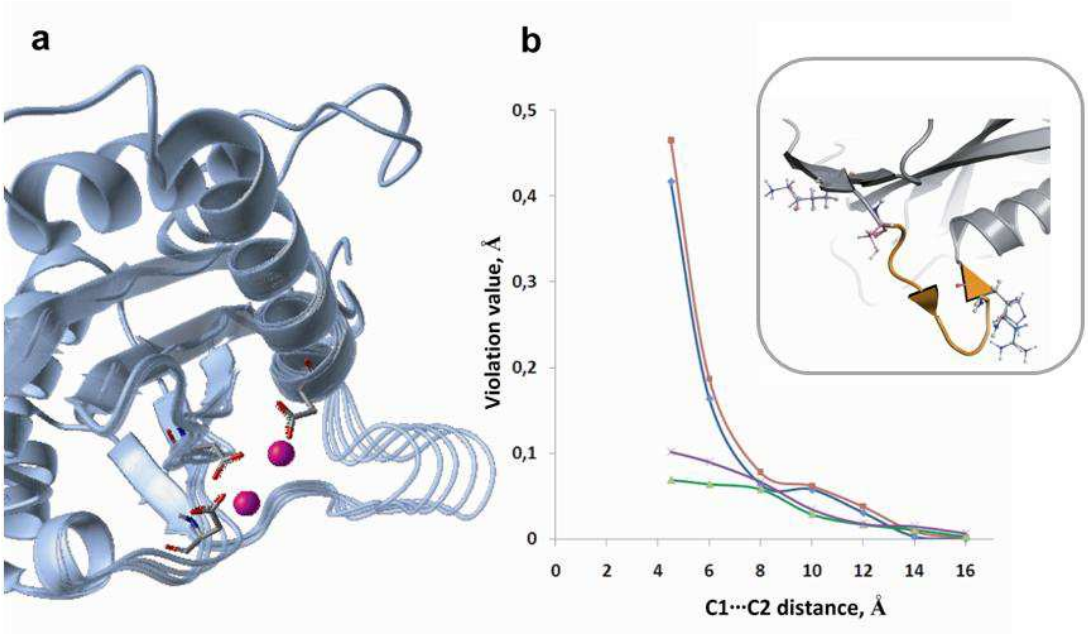

Figure 28. Model of displacement of the Ω-shaped hairpin toward the catalytic site: (a) Superimposition of the HIV-1 IN models (two-cation active site) with the hairpinmoved toward the active site, from16 to 4.5Å, (b) Violation values for distances of 16–4.5 A ° for one-cation models, wild-type (green) and the G140S mutant (violet) and for two cation-model, wild-type (blue), and G140S mutant (red). The Ω-shaped hairpin is shown in the inset. (Mouscadet *et al*. 2009).

5. Intermolecular interactions involving the RAL-selected mutated residues

The modification of both hairpin composition and potential motion associated with these mutations may change the DNA recognition properties of the enzyme. We compared the recognition properties of amino acids in the WT and mutated IN. We focused on the non-

covalent interactions underlying the recognition properties of the residues at positions 155 and 148, corresponding to the primary mutations selected by RAL. Based on the known structures of protein/DNA complexes, we assessed the statistical probability of these residues recognizing DNA bases (see Chapter 4. **MATERIAL AND METHODS**). We found that asparagines (N) and glutamine (Q) residues preferentially recognized adenine, as H-bonds formed with this base represented a significant non-random cluster, whereas the H-bonds formed with cytosine, guanine, and thymine followed a random distribution. The replacement of the N residue in position 155 by an H residue led to the loss of H-bonding with adenine (A), thymine (T), and cytosine (C) (Figure 29).

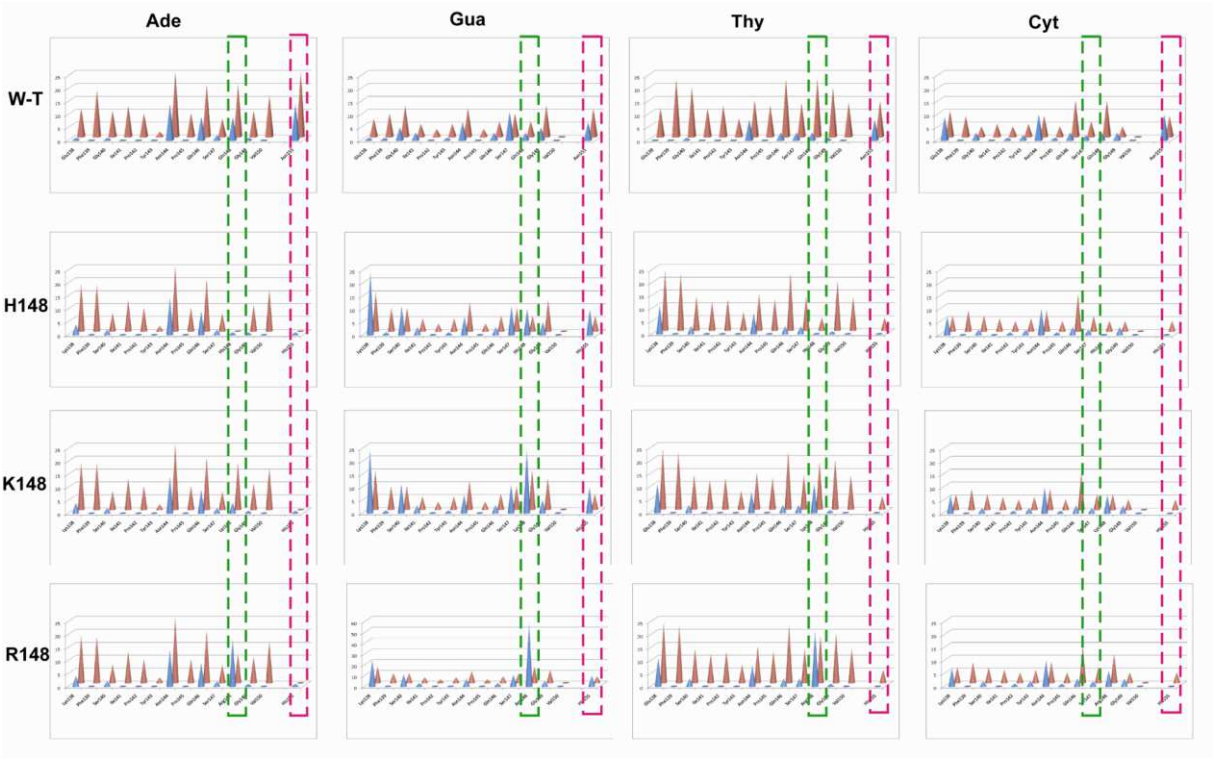

Figure 29. Statistical probability of residues 140–155 recognizing DNA bases based on the known structures of protein/DNA complexes. The H-bond (blue color) and van der Waals (red color) contacts were compiled based on the protein-DNA complexes. Interactions involving residues 148 and 155 are framed by dashed lines, in green and magenta, respectively. (Mouscadet *et al*. 2009)

The replacement of Q148 by a histidine (H) residue had a similar effect, whereas its replacement with a lysine (K) or arginine (R) residue strongly favored interactions with guanine (G), A, and T. Finally, although van der Waals (VdW) contacts are not generally affected by sequence specificity, substitutions resulting in an H residue replacing Q148 or N155 also resulted in a complete loss of VdW contacts with adenine.

6. 3D maps of H-bonding between residues 148 and 155 and DNA bases

We investigated further the DNA recognition properties of the IN residues implicated in RAL resistance, by characterizing in detail the H-bonding between residues 148 and 155 and DNA bases, in particular. We used an IsoStar library, making it possible to construct 3D profiles describing the spatial orientation of non-covalently interacting partners (see Chapter 4. **MATERIALS AND METHODS**). This library provides access to information about the preferences of these amino acids for interaction with particular DNA bases and the geometry of non-covalent interactions.

Despite the lack of one-to-one specificity, proteins have been shown to discriminate between A and G, suggesting that they favor a particular amino acid–base pair (Luscombe, Laskowski, & Thornton, 2001; Luscombe & Thornton, 2002; Cheng *et al*., 2003): for instance, R, K, serine (S), and H interact preferentially with guanine, whereas aspartate (D) and glutamate (E) interact preferentially with adenine. The profiles of single unpaired bases were characterized, to construct 3D profiles of the groups around the DNA base pairs potentially involved in IN/DNA interactions. The 3D distribution and spatial organization of the side-chain fragments surrounding DNA bases were constructed, recapitulating the overall geometry of the DNA bases, and their statistically observed interactions via the major and minor grooves. The potential hydrogen-bonding sites of bases and the 3D profiles of H-

bonding patterns involved in binding between DNA bases and the side chains of Q (Q148), N (N155), and R (Q148R) are shown in Figure 30.

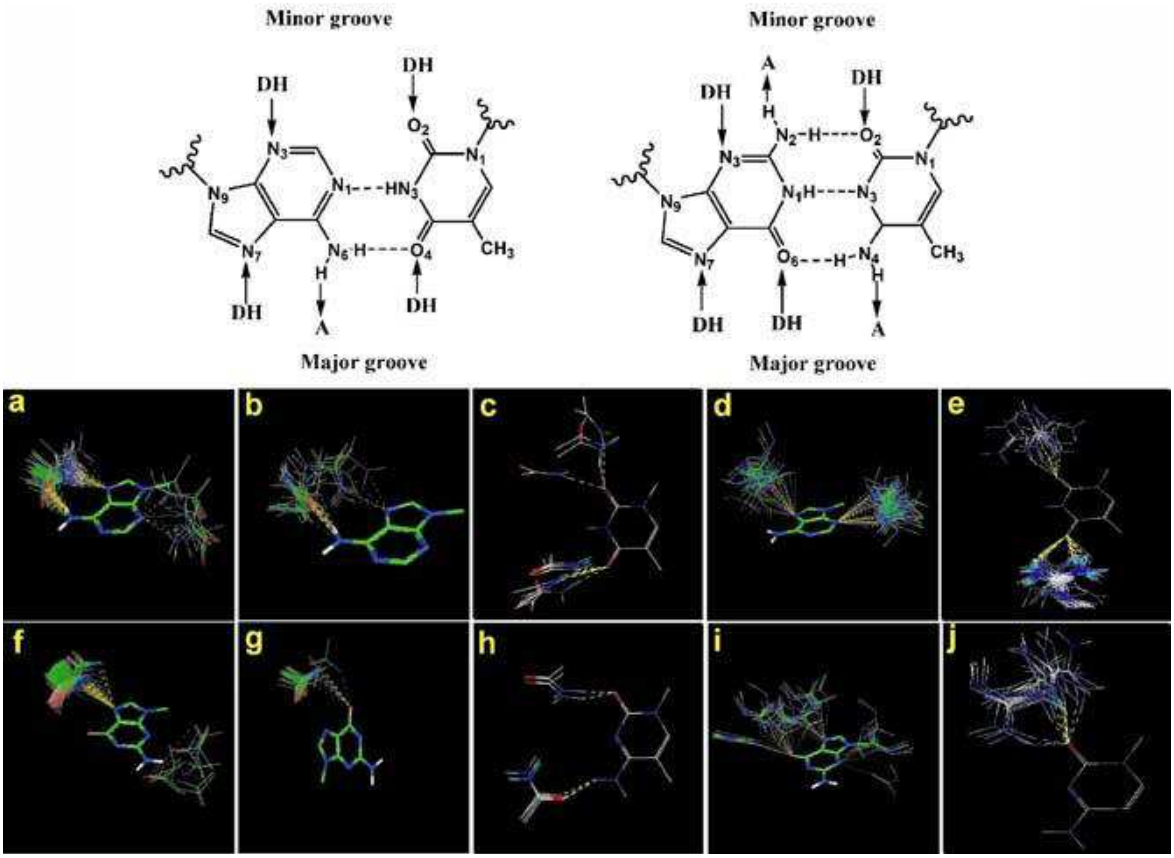

Figure 30. H-bond interactions of DNA bases: Top: diagrams of bases and their pairing in a DNA molecule. Arrows indicate the atoms available for H-bond interactions, oriented towards acceptors and away from donors. Bottom: 3D scatterplots of the side chain distributions around the DNA bases: (a and b) N/Q…A; (c) N/Q…T; (d) R…A; (e) R…T; (f and g) N/Q…G; (h) N/Q…C; (i) R…G; and (j) R …C. H-bonds of purines showing bidentate (a) and monodentate (b)modes of interaction for adenine, withmonodentate interactions involving N7 (f) and O6 (g) binding sites for guanine shown separately. Groups with chemical groups found in natural amino acids were included in the analysis. Carbamoyl is a functional group of N and Q, and guaniduim is afunctional group of R. The main group (DNA bases), contacting groups (Q/N and R) and H-bonds are shown as sticks, wire frames and dashed lines, respectively. (Mouscadet *et al*. 2009).

6.1. The DNA bases recognition by the Wild Type Integrase residues N155 and Q148

Most of the carbamoyl moieties common to N and Q and found in contact with adenine formed a dense, highly populated cluster in the major groove (91% of all interacting groups), whereas a small number of groups interacting with adenine were observed in the

minor groove (Figure 30 a, b). Moreover, most of the carbamoyl groups (67% of all interacting fragments) in the major groove were coplanar with adenine and formed a pair of strong, directional H-bonds with N^7 and N^6H_2 in this base (Figure 38). Other carbamoyl groups formed only one H-bond with adenine, with either N^6-H_2 or N^7 (Figure 30 b). The N/Q side chains in contact with adenine through the minor groove formed moderately strong non-linear H-bonds, $NH_2 \ldots N_3$. Similarly, most of the carbamoyl groups contacting guanine bases (94%) clustered in the major groove (Figure 30 f, g). Nevertheless, all contacts were single H-bonds, with either N^7 or O^6 acceptors, positioned outside the guanine plane, at a dihedral angle of 45^0. Very few occurrences of H-bonded carbamoyl-guanine (N^2H_2 …O=) contacts were observed in the minor groove. In the case of N/Q recognition by pyrimidines, carbamoyl group interactions were observed only rarely (Figure 30 c, h). The positions and mode of interaction of these groups suggested certain common rules. For example, thymine and cytosine binding involves single H-bonds with carbamoyl groups, with no preference for either of the two bases. The binding of the amino acid in position 4 with C or T is characterized by a different orientation of the carbamoyl group, allowing an H-bond to be formed with either O^4 (T) or N^4H_2 (C). All carbamoyl groups interacting with T or C are rotated $30–45^0$ relative to the plane of the base.

6.2. The DNA bases recognition by the mutated Integrase residues N155H and Q148R/H/K

Guanidium fragments (arginine side chain) H-bonded to adenine bases clustered within the major groove (33% of all contacting groups), with a dispersed cloud-like distribution around N^7 (Figure 30 d). The other dense and well grouped cluster (77% of all contacting groups) was localized around the single acceptor site, N^3, in the minor groove. Fragments corresponding to both clusters were rotated relative to the adenine plane and participated in H-

bonding at either one or two NH_2-termini. Guanidium groups forming H-bonds with guanine were grouped into three diffuse clusters. Two of these clusters were positioned within the major groove and the third was positioned in the minor groove (Figure 30 i) and consisted mostly of end-on-oriented guanidium groups H-bonded to O^6, N^7, and N^3, at various angles relative to the guanine plane. Detailed analysis of DNA base recognition by H and K was limited by the small amount of data available (see Appendix, Figure 2). Nevertheless, as for R, the imidazole groups of the H side chain formed separate clusters at the N^7 and N^3 adenine binding sites. The imidazoles interacting with guanine were grouped in the major groove, interacting either with O^6 or N^7. Both adenine and guanine acceptor sites interact preferably with the $N^{\varepsilon 2}$–H tautomer. The numbers of -C-NH_3 groups (terminal moiety of the K side chain) H-bonded to adenine or guanine were similar, but the modes of interaction with these bases were different. The lysine side chains contacting adenine were clustered at the N^7 and N^3 acceptor atoms, whereas all C-NH3 groups were clustered in the major groove of guanine, H-bonded to either the O_6 or N_7 atom. The H-bonds formed between the guanidium fragments of R and pyrimidine bases differed significantly. Thymine binds guanidium at two acceptor sites, O^2 and O^4, whereas interaction with cytosine involves only one acceptor site, O^2 (Figure 30 e, j). The guanidium at the thymine O^4 site displays two orientations, coplanar and orthogonal to the base plane. The coplanar fragments interact through their terminal NH_2 groups, forming a strong bifurcated H-bond with the O^4 atom, whereas guanidium in the orthogonal orientation forms only a single H-bond. The guanidium at the O^2 atom of cytosine displays various orientations, including a rotation by 45^0 allowing the formation of two H-bonds (bifurcated H-bonding). As for purines, the numbers of imidazole and -C-NH_3 groups involved in thymine cytosine recognition were too small to be statistically significant, thus, limiting comparison with purines. Nevertheless, the positions of imidazole and, in particular, -

C-NH_3-contacting groups, and the nature of their interactions with DNA base binding sites were similar to those observed for guanidium.

7. Modeling the ‘‘interacting’’ DNA base pairs

We investigated the recognition pattern for viral DNA base pairs, by combining the 3D scatterplots of individual bases to obtain models of the interacting base pairs, A–T and G–C with N/Q and R (statistically significant). This strategy made it possible to eliminate steric overlaps and to identify new contacts. N/Q interactions with A–T and G–C (Figure 31 a, b) The number of contacting carbamoyl groups and their positions around the A–T and G–C base pairs were generally consistent with their arrangement observed with individual bases. Fragment positions not satisfying steric criteria were eliminated. The dominant bidentate mode of N/Q binding in the major groove of adenine corresponded to specific recognition between the wild-type residues and A–T base pairs. Only a low frequency of moderately strong single H-bonds was observed in the minor groove. By contrast to this marked preference and specificity of WT side chains for A–T base pairs, the interaction of N/Q side chains with G–C base pairs was nonspecific, resulting in the formation of a single H-bond with the N^7 or $=O^6$ acceptor site in guanine.

7.1. Arginine side chain interactions with A–T and G–C

Interactions of guanidium fragments with adenine N^7 or N^3 and thymine O^2 indicated a complete absence of steric overlaps (Figure 31 c, d). However, despite their steric compatibility with A–T geometry, these interactions did not satisfy specific recognition criteria. By contrast, fragments interacting with $=O^4$ through two H-bonds formed a dense cluster in the base-pair plane. Their orientation was not compatible with the adenine NH_2 group, but the steric constraints could be resolved by rotating the guaniduim moieties by 45–

90^0. This rotation did not disrupt the pattern of H-bonding between guanidium and thymidine, revealing a new contact between the deprotonated N atom of the amino acid side chain and the NH_2 group of adenine. Thus, arginine residues behaved like wild-type N/Q residues, binding specifically to A–T base pairs through the major groove, but the sites of R recognition—thymidine O^4 and adenine N^6H_2 groups—were different.

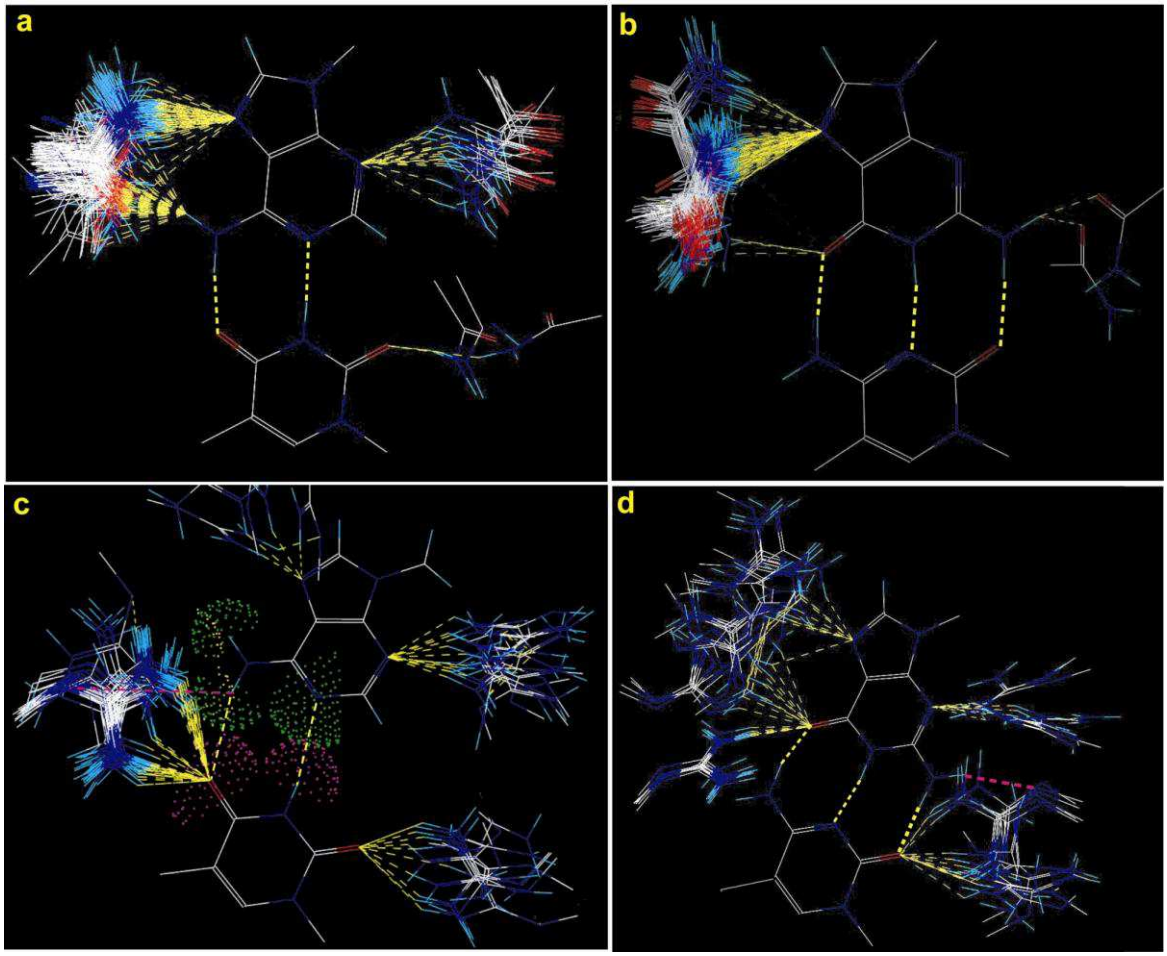

Figure 31. 3D scatterplots of ‘‘interacting’’ base pairs (a) A–T…N/Q; (b) G–C…N/Q; (c) A–T…R; and (d) G–C…R represented in approximately the same orientation, with the purine bases at the top and the major groove at the left. The main group (DNA base pairs) and contacting groups (N/Q and R) are shown as wire frames; H-bonds as yellow dashed lines (including Watson-Crick bonds); additional contacts revealed by the generation of interacting base pairs in magenta, (c) and (d); van der Waals radii (dotted spheres) of groups (N1) and (N6) of adenine in green; (N3) and (O4) of thymine in magenta and arginine in yellow, illustrating conflict between arginine and N1 (A). (Mouscadet *et al*. 2009).

The arginine side-chain distribution around G–C base pairs corresponded exactly to that around the individual DNA bases. Indeed, all side chains avoided steric constraint with

base exocyclic groups. Interestingly, the R fragments H-bonded to the cytosine O^2 binding site were found to be in an appropriate orientation to form a third H-bond with the guanine -N^2H_2group. These chains therefore probably interact with both bases simultaneously, resulting in multi-dentate H-bonding through the minor groove of the G–C base pair.

In conclusion, our results demonstrate that one of the key differences between the wild-type (N/Q) and RAL-selected mutated (R/H/K) residues relates to their DNA base recognition properties. N155 and Q148 clearly interact preferentially with adenine, either as a single base or in the A–T base pair. In both cases, a strong and specific interaction with adenine is ensured by linear and highly directional bidendate H-bonding within the major groove. In contrast, a single, moderately strong and non-linear H-bond is formed with guanine. The DNA base-pair model generated by this strategy identifies new possibilities for H-bonding, demonstrating that the arginine side chain can engage in multiple and directed H-bond interactions, allowing specific R…A–T (major groove) or R…G–C (minor groove) interactions.

8. Discussion

RAL resistance is associated with two genetic pathways defined by the N155H or Q148H/R/K primary mutations (Hazuda *et al*., 2007; Kobayashi *et al*., 2008; Myers & Pillay, 2008). Secondary G140S/A mutation in the Q148H/R/K background compensate for replication defects associated with primary mutations and increases resistance. These substitutions significantly decrease the binding affinity of the integrase inhibitor and allow IN to retain its activity. We performed *in silico* analyses of the structural features and recognition properties of wild-type and mutated INs to gain further insight into the molecular basis of HIV-1 IN resistance. This study focuses on the active site of IN and the catalytic loop-

containing residues in particular, the mutation of which has been selected by RAL in clinical practice.

This study highlighted the importance of a stable Ω-shaped hairpin within the catalytic loop. The importance of this loop has not previously been reported for the HIV-1 IN, although a related subsecondary structure had been described (Maignan *et al.,* 1998; Chen *et al.*, 2008). This hairpin can move toward the active site, defining open and closed conformations. Movements of the hairpin opening the active site lead to the formation of a cleft by the active site and the catalytic loop, which can then accommodate DNA. G140A/S-mutated forms of IN display slightly lower levels of hairpin mobility than the wild-type enzyme. This lower level of mobility is associated with lower levels of G140S mutant enzyme activity *in vitro* (Malet *et al.*, 2008) and slower 3′-processing kinetics for both the G140S and G140S/Q148H mutants (Delelis *et al.*, 2009). Our 3D models of RAL-selected mutants demonstrated that the two primary pathways to RAL resistance, one involving N155H mutations and the other involving the replacement of Q148 by H, R, or K, conserve all the structural features of the IN catalytic domain. They also demonstrated that the specific interactions of RAL-selected amino acids with DNA base pairs differed from those of the wild-type enzyme, accounting for the observed differences in efficacy between mutant and wild-type integrase *in vitro*. Furthermore, the G140S mutation, which occurs after the primary Q148 mutation *in vivo*, changes slightly the mobility of the catalytic loop, thereby possibly modifying the change in base specificity induced by Q148R/H/K mutation. Although this modification appears limited in our study, it may provide a possible basis for the optimizing role of G140S mutation.

Experimental biological data suggest that the core domain interacts with the terminal CAGT bases of LTR ends (Ellison *et al.*, 1995; Heuer & Brown, 1997; Esposito & Craigie, 1998; Heuer & Brown, 1998) required for IN activity. Substitutions introducing nucleotide analogues stabilizing the double strand decrease 3′-processing activity, whereas those

weakening base pairing in the vicinity of the CA dinucleotide increase activity (Agapkina *et al*., 2006). Our data suggest that the A–T pair at the terminus or in the third position is selectively recognized by the WT Q148 or N155 residue. A recent biochemical study (Langley *et al*., 2008) carried out with a different IN inhibitor concluded that the terminal adenosine of the viral LTR controlled the binding of strand transfer inhibitors. This result supports the validity of our model. A recent theoretical prediction for DNA substrate binding sites on HIV-1 IN indicated that amino acids 139–152 constitute a binding site that includes Q148, together with Q137, Q146, and N144 (Chen *et al.*, 2008; Dolan *et al.*, 2009).

Adenine can be specifically recognized in either its paired (A–T) or unpaired form. However, we suggest that Q148/N155 residues interact with the sterically and energetically more favorable terminal unpaired adenine, consistent with previous data showing post-3′-processing contact between Q148 and the 5′-AC overhang (Chiu & Davies, 2004) and the theoretical model of the IN–DNA complex (Dolan *et al.,* 2009). By contrast, the Q148R mutant preferentially established specific interactions by binding the two bases of a pair, either A–T or G–C, simultaneously. This lack of discrimination for base pair binding implies a loss of strict sequence specificity. Thus, Q148R, through its long arginine side chain, may interact either with A–T at the third position, via the major groove edge, or with the next base pair, G–C, across the minor groove. These alternative arrangements are possible due to the flexibility of the catalytic loop, demonstrated by movement of the hairpin.

Strand transfer inhibitors, such as RAL, bind at the interface of the IN-viral DNA complex, by forming a quaternary complex with the catalytic metal in the enzyme active site and the 3′-processed donor DNA. RAL has a very flexible conformation, with multiple H-bonding sites and *E*-, *Z*-conformers of the two pharmacophores, 1,3,4-oxadiazole-2-carboxamide (F1) and *N*-methyl-4-carboxamide-dihydroxy-pyrimidine (F2). The conformers of these two fragments constitute alternative bioisosters of adenine (in *Z-)* or guanine (in *E*-).

RAL may, therefore, act as a base analog, competing with the target DNA for the establishment of specific interactions with IN. We previously reported stabilization of the *β*-ketoenol fragment in the *Z*-conformation by intramolecular H-bonds, suggesting that F2 is a bioisoster of adenine (Tchertanov and Mouscadet, 2007). We have also shown that *β*-ketoenolate is an excellent chelator of divalent metals (Tchertanov and Mouscadet, 2007). Thus, F2 can efficiently coordinate magnesium via the two 1–5 oxygen atoms, orienting RAL such that its "adenine-like" part, adjacent to *β*-ketoenolate, is specifically recognized by N155, which is found close to the Mg^{2+} cation. The F1 fragment can mimic adenine or guanine, depending on its rotational isomer. However, conformational analysis of the isolated compound revealed the adenine bioisoster to be the most stable conformer. Given the specific recognition of adenine by Q148 and N155, the adenine bioisosters of F1 and F2 also constitute targets for these residues.

VI. Molecular Dynamics Simulation of unbound Integrase in the native and mutated forms

The experimental data obtained by our colleagues from the Moscow University (Dr. Marina Gottikh) showed that mutations in the C-terminal domain affect the vDNA binding efficiency and the 3'-processing reaction (Figure 32). Particularly it has been shown that the R228A mutation reduces the 3'-processing efficiency to 5-7% respective to the 100% activity of the WT IN.

Reaction conditions:
Time – 2 h
Concentrations: 100 nM IN, 3 nM DNA-substrate

	3'-processing efficiency, %
wt	100
R228A	5-8
R228C	3-5
D229A	50-60
R231A	100-150
D232A	40-50
K236A	30-35
K236R	70-80
K264A	50-60
K264C	40-50

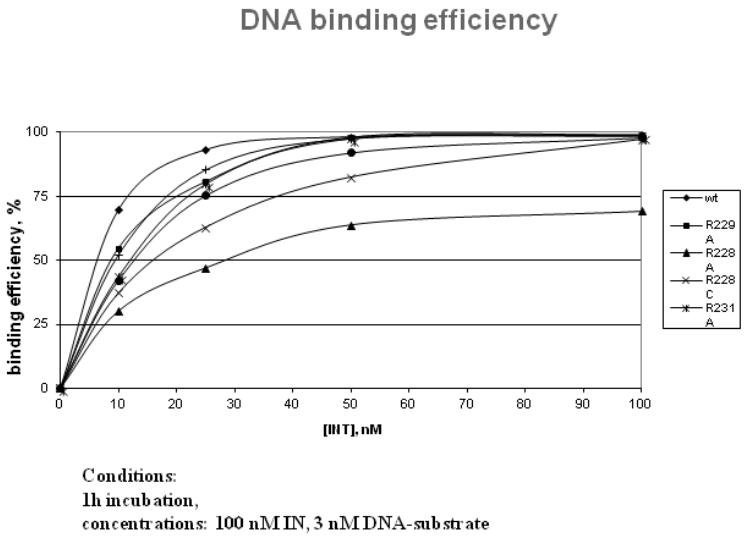

Figure 32. 3'-processing efficiency of the IN C-terminal mutants respective to the wild type enzyme (on the left) and their DNA binding efficiency (on the right) (Marina Gottikh, private communication).

To analyse the mutation effects on the structural and dynamical properties of the HIV-1 IN, Molecular Dynamics (MD) simulations were performed on the WT and R228A models of the unbound IN. Two 50-ns trajectories of MD simulations of the WT and R228A models were obtained. Since the IN models(s) represent a dimer structure, we analysed two monomers (chain A and chain B) separately.

1. Root Mean Squared Deviations (RMSDs) Comparisons

To analyse the global behaviour of the studied systems, the Root Mean Squared Deviations (RMSDs) of the nitrogen and carbon atoms of protein backbone with respect to the initial frames were plotted versus simulation time (Figure 33).

Analysis of Trajectory 1 shows that the RMSD profiles of chain A of both the WT and R228A mutant overlapped for the first 27 ns and display comparable backbone

conformational drift with RMSD mean values in the range 0.20–0.45 nm (Figure 33 a, in the top). Later, after 30 ns, a clear separation of the two RMSD profiles was observed. The RMSDs of the WT model fluctuate in the range 0.40 – 0.65 nm whereas in the R228A mutant these fluctuations are ranged at around 0.40 nm.

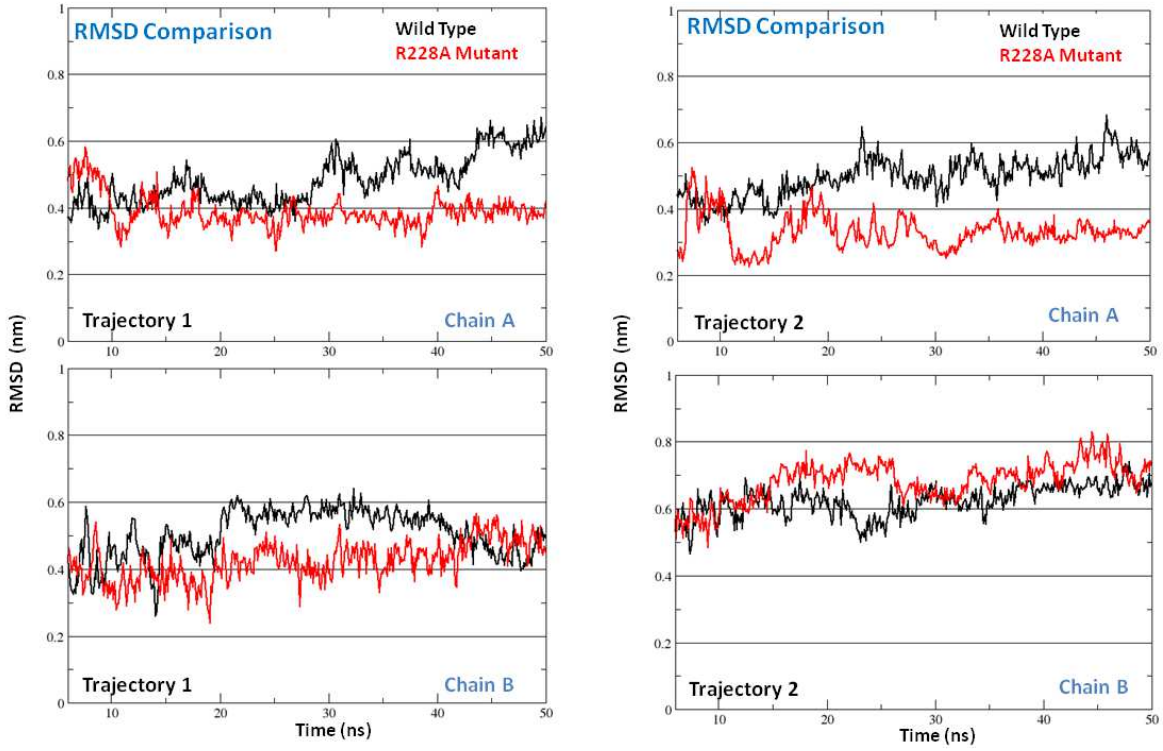

(a) (b)

Figure 33: MD simulations of the unbound Integrase model. Two monomeric chains A and B were analysed separately. The RMSDs (in nm) were calculated from the 50-ns MD simulations for WT (inblack) and R228A mutant (in red). (a) Trajectory 1 and (b) Trajectory 2.

The RMSDs of chain B shows that the WT and R228A mutant profiles are overlapped for the first 15 ns and display comparable backbone conformational drift with RMSD mean values in the range 0.25–0.60 nm. After 15 ns a clear RMSDs profiles separation was observed between the WT and the R228A mutant. The RMSDs of the WT fluctuate in the narrow range with RMSD mean values close to 0.6 nm between 15 and 40 ns time period of

the MD simulations. The last 10 ns simulations evidenced that the RMSDs profiles of chain A and chain B overlap again and fluctuate in the range 0.40–0.55 ns.

Analysis of Trajectory 2 (Figure 33 b) indicated that the RMSDs profiles of chain A from WT and R228A mutant are overlapped for a short time period (the first 10 ns). Starting from 12 ns the RMSDs of the WT fluctuate in the range 0.40–0.65 nm, while the R228A mutant RMSDs are ranged from 0.23 to 0.45 ns. The RMSDs characterising the chain B fluctuations of the WT and R228A mutant overlap for most of the simulation run and their mean values ranged from 0.53 to 0.82 nm, except for the simulation time between 14–27 ns. Within this interval, the RMSDs are in the ranges 0.50–0.60 nm in WT and 0.65–0.75 nm in mutant. At the end of simulation run the RMSDs profiles of the WT and the R228A mutant are superimposed.

2. Root Mean Squared Fluctuations (RMSFs) Analysis

The root mean square fluctuation (RMSF) per residue was computed on the C and N backbone atoms on the last 50-ns of each simulation, referenced to the average structure, and averaged over the two simulation replica of each model (Figure 34). The most fluctuant domains in all models are the CTD and catalytic site loop of CCD. Many regions appear stabilized in both chains of two models.

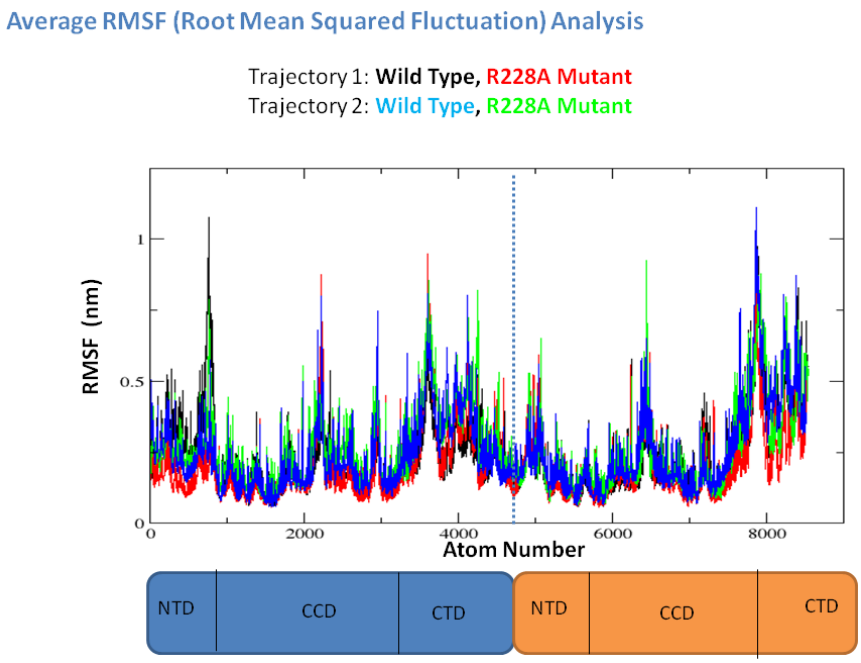

Figure 34. Atomic fluctuations changes per residue in mutants compared to the WT protein. RMSFs are computed on C and N backbone atoms over the total production simulation time of of 50 ns MD simulations (Trajectories 1 and 2) of WT and mutant.

The RMSF values computed either on the WT or on the mutant seems globally quantitatively comparable. The mean RMSF over the whole structure range from 0.24 to 0.27 nm for WT, and from 0.25 to 0.28 for mutant. This allowed us to perform the PCA comparison, on different simulation durations for the different simulated models.

3. Principal Component Analysis (PCA)

To further characterise IN chains motions, principle component analysis (PCA), also called quasi-harmonic analysis or essential dynamics method, of the MD trajectories was performed. The approach is based on the covariance matrix, which provides information on the two-point correlations of the system. The PCA represents a linear transformation that diagonalizes the covariance matrix and thus removes the instantaneous linear correlations among the variables. Ordering the Eigen values of the transformation decreasingly, a large

part of the system's fluctuations can be described in terms of only a few principal components. The PCA was carried out for each of the two trajectories generated by MD simulations of full length WT and R228A IN models taking C-α into consideration.

3.1 Trajectory Analysis

The path of proteins backbone in the WT and R228A mutant were determined by analysing their movements along projections in the eigenvector space (Figure 34).

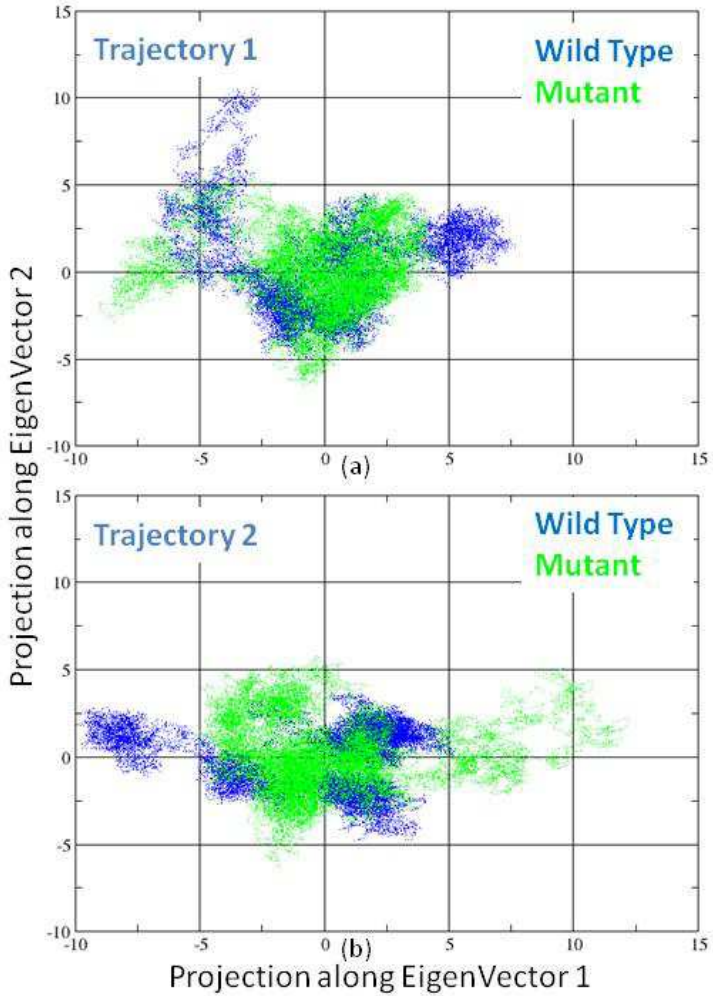

Figure 34. Principle component analysis (PCA) of the IN WT and R228A mutant models. Projection along Eigenvector 1 (X-axis) and Eigenvector 2 (Y-axis) after 50 ns MD simulation for Trajectory 1 (a) and Trajectory 2 (b).

Analysis of Trajectory 1 of the MD simulations evidenced bulk of the protein backbone movements of the WT and mutant that are clustered between -5 and +5 for projection along Eigenvectors 1 and 2 of the principal component space. Whereas, the analysis of Trajectory 2 of the MD simulations indicated that backbone movements of the WT is mainly clustered between -10 and +5 (Eigenvector 1) and -5 and +5 (Eigenvector 2). The backbone movements of the mutant model in this trajectory are clustered between -5 and +10 (Eigenvector 1) and -5 and +5 (Eigenvector 2).

3.2 Eigen RMSFs Analysis

The average atomic mobility of WT and R228A mutant IN atoms where calculated along the eigenvector 1 for two MD trajectories in form of the Eigen RMSFs analysis. We observed that the largest eigenvalue captures the largest fraction of Eigen RMSFs, excepted the sharp rise in the RMSFs of NTD atoms of the WT IN (Trajectory 1) (Figure 35).

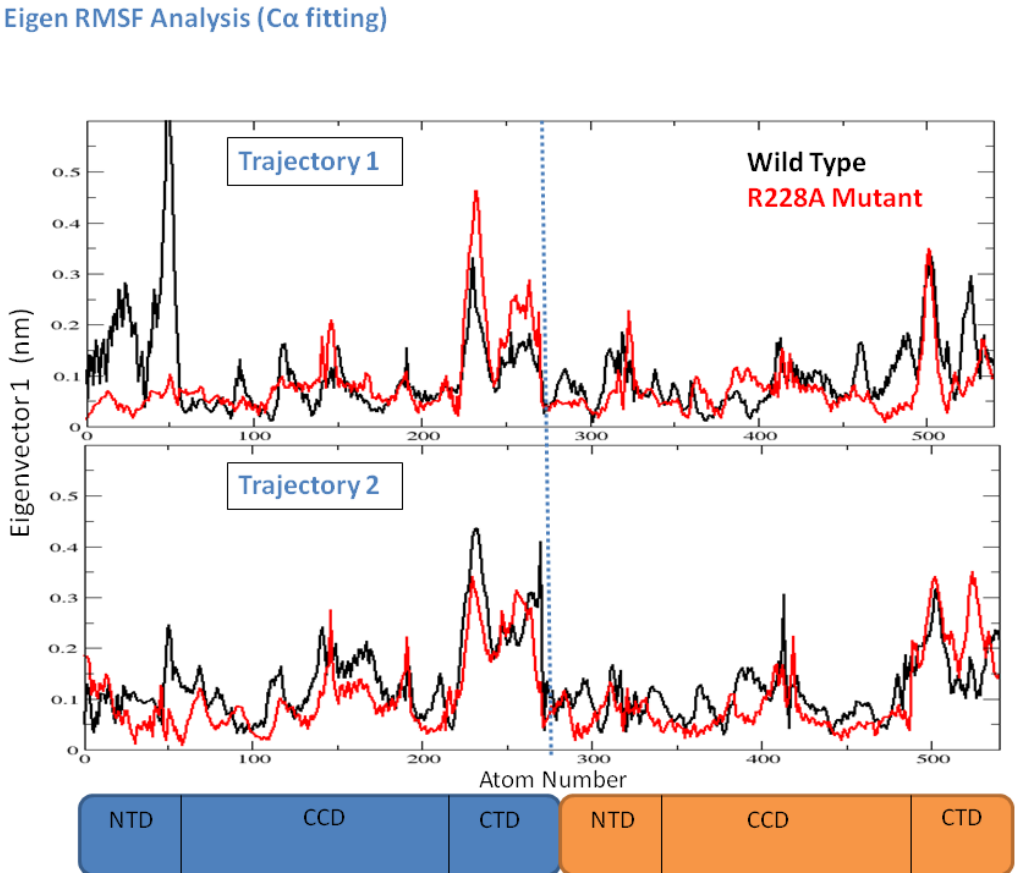

Figure 35. Principle component analysis (PCA) of the IN WT and R228A mutant models. Eigen RMSFs profile projected along Eigenvector 1 for a 50 ns MD simulation of WT and R228A mutant models of the HIV-1 IN along Trajectory 1 and 2.

The highest RMSFs in all the cases was observed in the CTD of WT and R228A mutant. The rise was more prominent and higher in magnitude in the CTD of R228A mutant for the MD trajectories.

4. Structural Analysis

We analysed the MD conformations in details to investigate the mutation effects of R228A on the internal structure and dynamics of the unbound IN and understand the changes induced by this mutation that promote the loss in the binding affinity between IN and DNA.

MD snapshots taken at regular time intervals – 6, 18, 28 and 50 ns – for the WT and R228A mutant were superimposed (Figures 36 and 37).

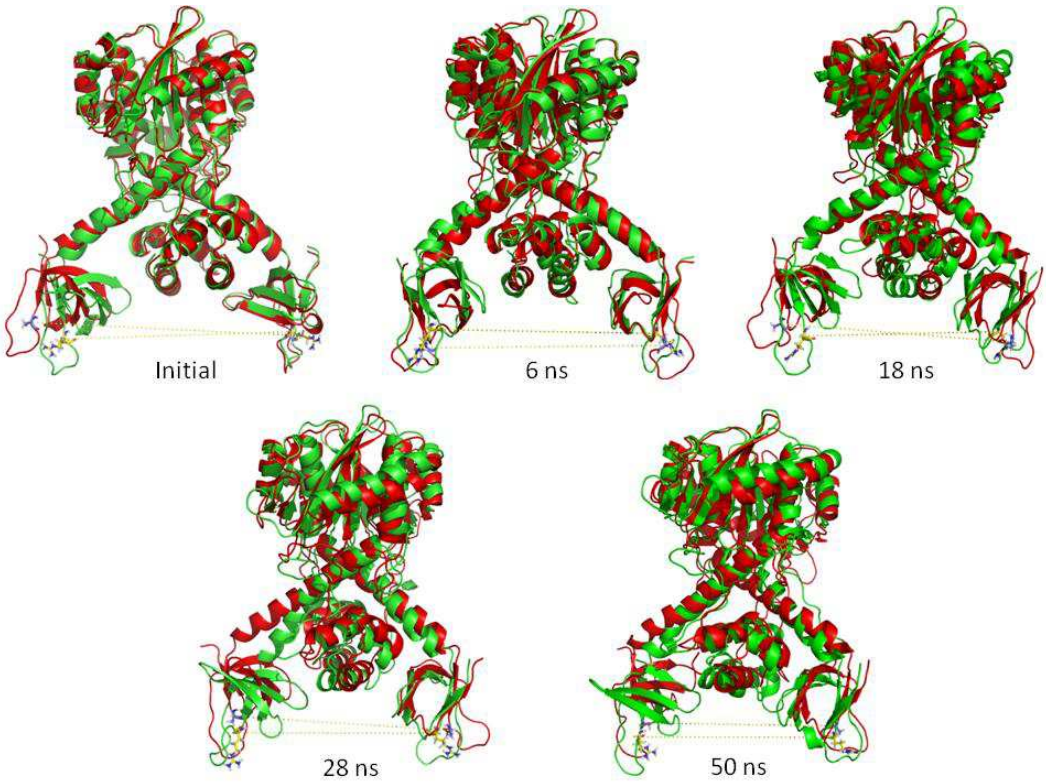

Figure 36: MD conformations of WT (in green) and R228A mutant (in red) were taken at 0.6, 18, 28 and 50 ns (Trajectory 1).

Over Trajectory 1, we observed that structure of the CTD in WT and R228A mutant either relatively close (at 6 and 50 ns) or slightly shifted (18 and 28 ns) (Figure 36). A major shift was observed in chain A of the mutant R228A, whereas it remains nearly undisturbed in chain B. The WT and mutant structures at the end of the simulation (50 ns) are close to its position at 6 ns.

Over Trajectory 2, a large gap involving the CTDs of the chains A and B was observed at 6 ns of simulations of the WT and R228A mutant (Figure 37). The chain A in R228A mutant is shifted, making a shorter inter-chains distance in R228A mutant respectively to that in WT. Both chains of the CTD in WT remain nearly undisturbed.

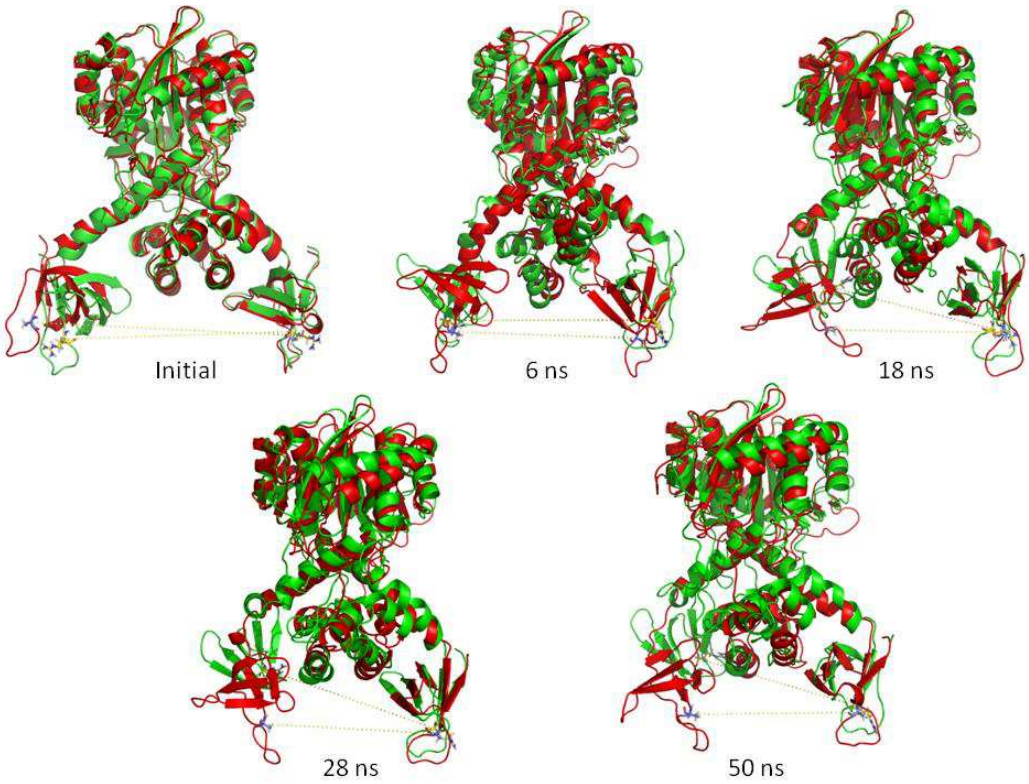

Figure 37: MD conformations of WT (in green) and R228A mutant (in red) were taken at 0.6, 18, 28 and 50 ns (Trajectory 2).

The position of the CTD of chain A in the WT and R228A mutant did not change at 18 and 28 ns of simulation, while the chain B in R228A mutant is shifted towards the chain B of the WT CTD. The chains B of two INs, WT and R228A mutant, appear to almost overlap.

The CTDs positions in WT and R228A mutant (chains A and B) at 50 ns remain to be similar to their positions at 28 ns. Such observation indicates the absence the major inter-chains movement in the CTD as was evidenced by Trajectory 2.

Distance between R228 from the chains A and B in WT and in R228A mutant was monitored over Trajectories 1 and 2. (Figure 38).

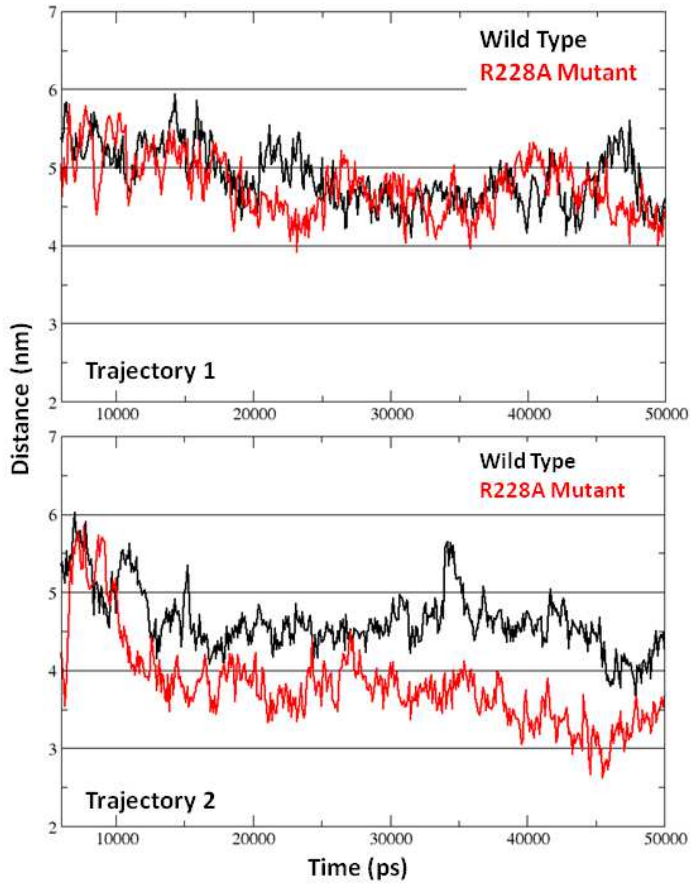

Time	D_{WT} (nm)		D_{mutant} (nm)	
	Traj 1	Traj 2	Traj 1	Traj 2
Initial	5.107	5.107	5.799	5.799
6ns	5.204	5.288	5.127	4.244
18ns	4.630	4.399	5.262	3.977
28ns	4.527	4.370	4.978	3.951
50ns	4.522	4.248	4.587	3.706

$D_{WT} = C\alpha\ (R228_{Chain\ A} - R228_{Chain\ B})$

$D_{Mutant} = C\alpha\ (R228A_{Chain\ A} - R228A_{Chain\ B})$

Figure 38: Distance between R228 from the chains A and B in WT (in black) and in R228A mutant (in red) over Trajectories 1 and 2.The carbon alpha atoms were used for a reference: $C\alpha_{\ R228\ (WT,\ Chain\ A)} - C\alpha_{\ R228\ (WT,\ Chain\ B)}$ and $C\alpha_{\ R228A\ (mutant,\ Chain\ A)} - C\alpha_{\ R228A\ (mutant,\ Chain\ B)}$.

Distance between the Cα atoms of R228 from the chains A and B in WT and in mutant R228A was calculated at 0, 6, 18, 28 and 50 ns over MD simulations. It was observed that this distance between residues in mutant R228A decreases over the simulations, as compared to its WT counterpart. This indicates that the two CTDs of mutant R228A move towards each other over the MD simulations.

5. Secondary Structure Analysis

Secondary structure analysis of WT and R228A mutant was carried out separately for the two trajectories of the MD simulations and only the CTD of the IN was considered. First, a comparison between chain A from the CTD in WT and mutant was performed over Trajectory 1 of the MD simulations. The main difference between WT and R228A mutant was observed in the region from 227 to 235 amino acids. It was observed that in chain A of WT, the average secondary structure represents an approximately 90% of turn, 70% of coil and near 50% of bend (Figure 39). In contrast, the same region in R228A mutant consists mainly of the bend and coil structures with only 10% of turn.

In chain B other region, from 250 to 260 amino acids, shows divergent secondary structures between two integrases. This region in WT consists of the sheets and nearly 50% of the bend and turn (Figure 39). In R228A mutant mainly of the sheet structures were observed similarly to the WT, while the turn portion is increased up to 85% and the bend was at almost 10%.

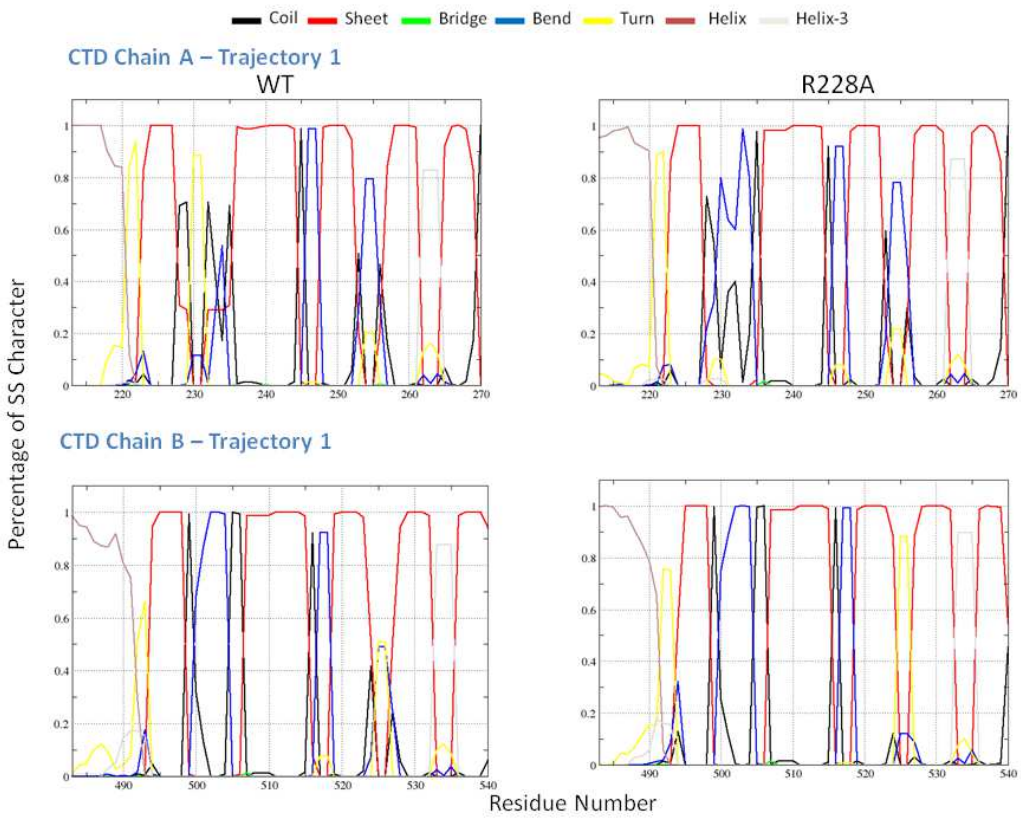

Figure 39: MD simulations (50 ns) of the WT and R228A mutant. Average secondary structure profile of the IN CTD (Chains A and B) over Trajectory 1.

Similar analysis of average secondary structure performed for Trajectory 2 put in evidence that other regions show a difference at the secondary structure level, particularly, the region from 220 to 225 amino acids (aas) in chain A and from 213 to 220 amino acids in B. In WT the 220-225 aas from the chain A is characterised by the turn structures (60%) while the bend and coil are 20% each (Figure 40). In contrast, the same region in R228A mutant shows that the turn is 85%.

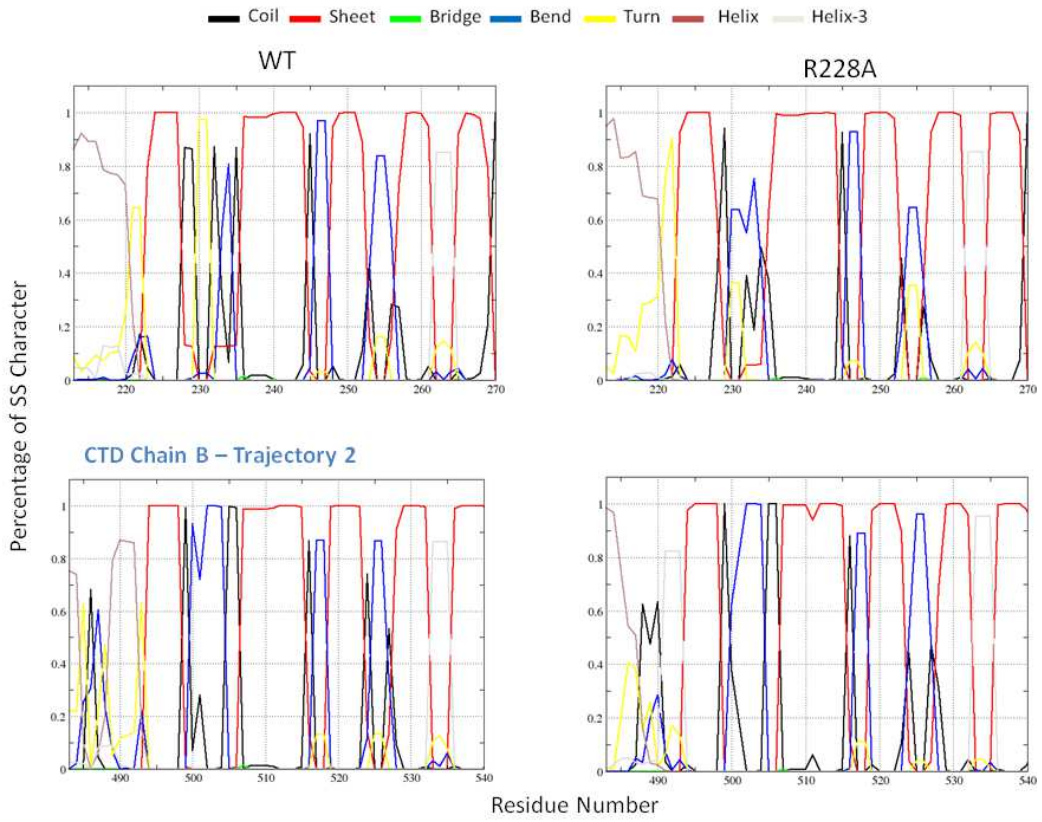

Figure 40: MD simulations (50 ns) of the WT and R228A mutant. Average secondary structure profile of the IN CTD (Chains A and B) over Trajectory 2.

The region 213 - 220 aas in the chain B shows that the bend structures are reduced to 30% in R228A mutant (60% in WT). The coiled structures remain approximately the same in both proteins, but it is spread over more number of residues in the mutant (Figure 40).

As we mentioned above, the CTDs of two chains A and B in WT and R228A mutant exhibit different dynamic properties. To analyse further the mutation impact on dynamic behaviour of IN, we compared the average secondary structure between different chains, A and B, of the same protein over both MD trajectories.

In WT the fragment 225 – 235 aas (chain A) forms the secondary structure of the bend, sheet, turn, and coil types, all varying at different average percentages (Trajectory 1) (Figure 39). The same region in chain B contains high percentages of sheet, coil and bend

secondary structures. In R228A mutant the region 250 – 260 aas (chain A) revealed a significantly higher average percentage of the bend (80%) and coil (60%) secondary structure elements; the turn was much less (20%). In chain B the same sequence sows a high average percentage of the bend structure (80%) while the average percentages of the bend and coil was low (10%). A comparison between chains A and B of WT indicated that the secondary structure of the region 225 -235 aas is similar over Trajectory 1 and 2 (Figure 40).

6. Discussion

The role of CTD in non-specific binding of the vDNA was previously well-documented experimentally. Experimental results have shown a particular mutation R228A decreases the vDNA binding with the IN to 5-8% of its WT value. We contributed to characterisation of this domain by using the molecular dynamics simulations. The MD simulations of the WT and R228A mutated IN (unbound form) were performed.

In silico results evidenced by analysis of RMSDs, RMSFs, secondary structure, 3D structure of the dynamic conformations show the structural and dynamical differences in the CTD (i) between the similar chains in WT and R228A mutant ; and (ii) between the different chains, A and B, of the same protein. Analysis of the distance profile between CTDs of the same protein (WT and R228A mutant) over the MD simulations shows a change in the R228A mutant conformation respectively to the WT.

Chapter 3. GENERAL CONCLUSIONS AND PERSPECTIVES

The structural and recognition properties of the first the HIV-1 Integrase specific drug – Raltegravir were studied. First, we characterised the conformational/configurational properties of RAL, a very flexible molecule displaying the E/Z isomerism. Second, we characterised the RAL recognition by its putative HIV-1 targets – the unbound IN, the viral DNA and the IN•vDNA complex. The docked confirmations we observed represent a spectrum of possible conformational/configurational states. The lower docking scores and RAL poses confirms that the generated structure of the IN•vDNA complex is the biologically relevant target of this inhibitor. The results of the docking are in perfect agreement with the proposed mechanism of action for such type of the inhibitors, INSTIs. The identified RAL pose at the cleaved vDNA shed light on a putative even plausible step of the RAL inhibition mechanism. Based on the docking results we suggested that the inhibition process may include as a first step the RAL recognition by the processed viral DNA bound to a transient intermediate IN state. RAL coupled to vDNA shows an outside orientation of all oxygen atoms, excellent putative chelating agents of Mg^{2+} cations, which could facilitate the insertion of RAL into the active site. The conformational flexibility of RAL further allows the accommodation/adaptation of the inhibitor in a relatively large binding pocket of IN•vDNA pre-integration complex thus producing various RAL docked conformation. We believe that such variety of the RAL conformations contributing alternatively to the enzyme residue recognition may impact the selection of the clinically observed alternative resistance pathways to the drug.

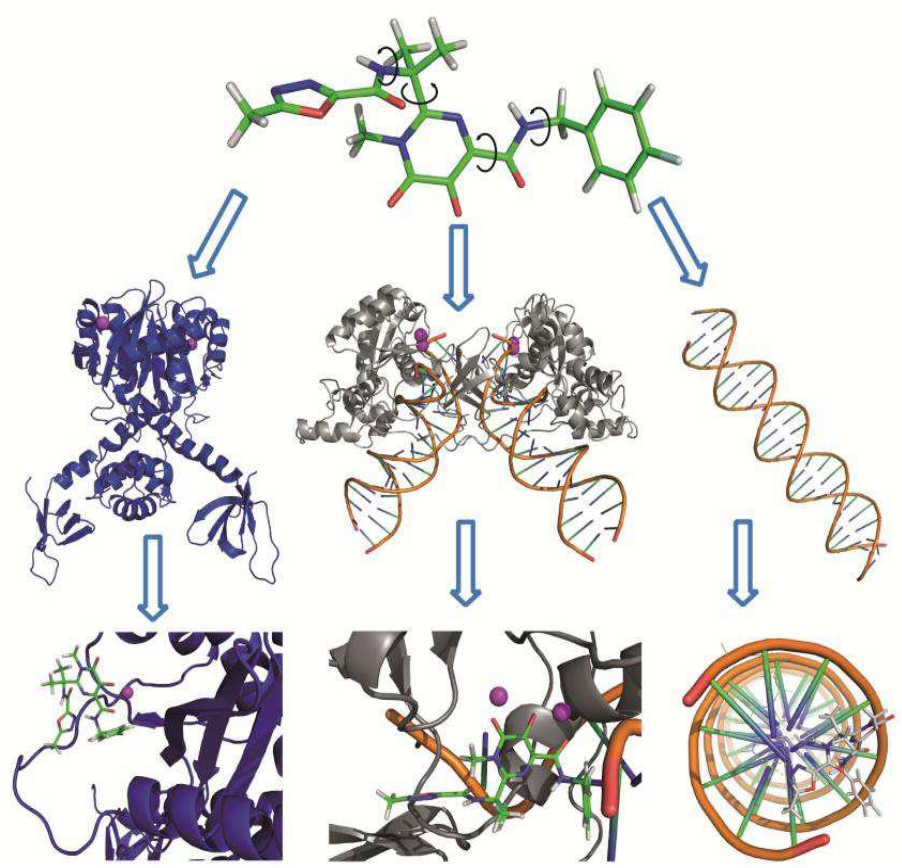

Conformational flexibility in protein-ligand interactions is nothing new; numerous cases have been reported (for example, the oestrogen or tyrosine kinases receptors). Using the model systems presented here, we attempted to estimate the extent of conformational variability, and relate this to the RAL-IN interaction. Clearly, many aspects such a solvation/desolvation or entropic/ethalpic contributions remain open questions. Further studies of the energetic and dynamics of theses process will give us a better understanding of what makes a target attractive for an inhibitor, which in turn will assist in the search for novel candidate drug related with Raltegravir for the AIDS treatment.

We also studied the two of HIV-1 IN strains, B and CRF02_AG. The naturally occurring variations in HIV-1 subtype CRF02_AG IN K14R, V31I, L101I, T112V, T124A, T125A, G134N, I135V, K136T, V201I, T206S, V234I, and S283G, do not affect notably integrase structure, neither *in vitro* enzymatic activity, 3′-processing, nor strand transfer

reaction. Docking results reveal that the modes of binding and docking conformations of three studied molecules are identical for the HIV-1 IN from B and CRF02_AG strains. The proposed mechanism of the integrase inhibition based on considering of different conformational states, unbound IN, and IN•vDNA complex holds for the two studied strains.

We performed a detailed *in silico* study of the structural and molecular recognition of DNA, induced by raltegravir-selected mutations. We demonstrated the topological invariance of the integrase core domain, including the conservation of a recently identified Ω-shaped hairpin in the catalytic loop. By contrast, we showed that the mutations greatly altered the specificity of DNA recognition by integrase. The native residues displayed a clear preference for adenine, whereas the mutants strongly favored pyrimidines. We propose a hypothetical model, in which raltegravir inhibits HIV-1 replication by acting as an adenine mimic and establishing specific interactions with the Q148 and/or N155 residues of the integrase. We also provide a plausible explanation for the decrease in responsiveness to RAL when these residues are replaced by arginine, histidine, or lysine. One of the obvious applications of our models is as a docking guide for the placement of the viral DNA within its binding site in IN. Future studies could focus on the correlation between the spatial orientation of the side chains around the DNA bases and their pairs and the mapping of different frames from a Molecular Dynamics run. Such work might open up new opportunities for the design of HIV-1 IN inhibitors active against emerging HIV-1 mutants.

The novel drugs, targeted the HIV-1 Integrase, outcome primarily due to the rapid emergence of RAL analogues (for example, GS-9137 or elvitegravir, MK-2048 and S/GSK 1349572, currently under clinical trials (Korolev *et al*., 2011). The clinical trials of several RAL analogues (BMS-707035, GSK-364735) were suspended. All these molecules specifically suppress the IN ST reaction. We conceive that the future HIV-1 integrase drug development will be mainly oriented to design of inhibitors with a mechanism of action that

differs from that of RAL and its analogues. Distinct conceptions are potentially conceivable: (i) Design of the allosteric inhibitors, able to recognize specifically the binding sites that differ from the IN active site. Inhibitor V-165, belonging to such type inhibitors, prevents IN binding with the viral DNA such blocking 3'-processing reaction (Pannecouque *et al.,* 2002). (ii) Design of the protein-protein inhibitors (PPIs) acting on interaction interface between either viral components (the IN monomers upon multimerization process or sub-units of the IN•vDNA complex) (Mazumder *et al*. 1996; Tsiang *et al*. 2011) or between viral and cellular proteins (IN/LEDGF) (De Luca *et al.*, 2010; Tsiang *et al*., 2012). These alternative strategies represent rational and prospective directions in the HIV-1 integrase drug development.

Chapter 4. MATERIALS AND METHODS

I. Probing of Raltegravir Structure

1. Conformational analysis

RAL in Z-1/Z-2 configuration was taken from the X-ray structure of the Prototype Foamy Virus (PFV) integrase co-crystallised with RAL (PDB code: 3OYA, 2.65 Å resolution) (Hare *et al*., 2010b). Alternative RAL configurations (or isomers) – Z-1/E-2, E-1/Z-2 and E-1/E-2 (Chart 1) – were generated using the SYBYL package (Tripos Inc. Sybyl-X 1.1.1, 2009) by employing simple carbon-carbon bond rotation to achieve the desired configuration, followed by minimization. Further, the conformational space of each of four RAL isomers was characterized by relaxed scan of molecular fragments around four single bonds using the *Jaguar* program of MAESTRO molecular modeling package (Jaguar, version 7.0, Schrödinger, LLC, New York, NY, 2007). In each case, rotation was performed from 0^0 to 360^0 with an increment step of 30^0 for each particular single bond while the others were kept fixed. All the scans were performed with 6-31g(d) basis set at the Hartree-Fock (HF) level of theory (Friesner & R.A, 1987). Each scan was analyzed and corresponding potential energy plot and the RAL conformations were characterized for each of the four configurations.

2. Molecular Dynamics simulations

The initial molecular geometry of RAL was taken from the crystallographic coordinates file representing RAL co-crystallized with integrase of the Prototype Foamy Virus (PFV) (PDB code: 3OYA, at 2.65 Å resolution) (Hare *et al*., 2010). The initial model was prepared with *pdb2gmx o*f *G*ROMACS 4.0 (van der Spoel *et al*., 2005); The ligand topology was generated by Acpype using a combination of GAFF with Amber 99sb-ILDN force field; The charge on the ligand was -1, generated by Acpype; The hydrogen *a*toms were then added;

*I*n-vacuum minimization of the RAL for 1000 steps was performed using a Steepest-Descent (SD) integrator. The minimized model of RAL was placed in an octahedral TIP3P water box. The charge of the solvated system was neutralized by adding Na^+ counter ions. The system was then heated up to 300° K at a constant volume using a modified Berendsen thermostat (Berendsen, Postma, Vangunsteren, Dinola, & Haak, 1984) while restraining the solute atoms by 1 000 kJ/mol/$nm^{2.}$ The system was then equilibrated for 1 ns under the constant volume and temperature conditions (NVT). The pressure coupling was also turned "on" using *Parrinello-Rahman* barostat (Martonak, Laio, & Parrinello, 2003). Thereafter, three replicas of MD simulations were produced for the equilibrated system during 10 ns. The torsion angles τ1-τ4 were monitored over the MD simulations. The average fraction of distribution expressed as a probability of the occurrence of τ1-τ4 is given by (1):

$$f(x) = \frac{1}{\sigma\sqrt{2\pi}} e^{-(x-\mu)^2/2\sigma^2} \qquad (1)$$

where μ is a mean value and σ is a standard deviation.

The H-bonds formed by RAL with the water molecules were recovered over the MD simulations. The contacts D-H···A, where D and A = O/N, with D···A distances < 3.4 Å and pseudo valent angles ∠D-H···A > 90°, were considered as the H-bonds.

3. Structural fragment-based analysis (Cambridge Structural Database)

Relevant structures were retrieved from the CSD (Release 2011, 541,748 entries) (Allen, 2002). Substructural searches, geometry calculations and data analysis were carried out with the CSD programs ConQuest 1.13 (Bruno *et al*., 1997), Vista v2.1 (CSD, 1994) and Mercury 2.4.5 (Macrae *et al*., 2006). Structures flagged in the database as being erroneous or disordered were rejected from analysis.

We searched CSD for three groups of molecules based on the 1,3,4-oxadiazole-2-carboxamide (**1**), carbonylamino-1-N-alkyl-5-hydroxypyrimidinone (**2**) and fluorobenzyl carbamoyl (**3**) moieties. No structures included moiety (**1**) and a limited number (3 structures) of molecules based on moiety (**2**) was retrieved, therefore the search was performed using the more general fragments − **F1, F2** and **F3** (**Table 2**). The **F1** and **F2** were investigated to characterise the molecular geometry and intramolecular H-bonding (D-H…A, where D and A = O/N). The definition of the parameters characterizing the H-bonds was used as reported early (Tchertanov & Mouscadet, 2007). Molecules based on **F3** with halogen atom F, Cl or Br in the *para* position, were analysed for the torsion and dihedral angles. The coordination geometry in metal complexes was probed for the Mn, Mg and K complexes chelated with **F1** and **F2** as defined in (Tchertanov & Mouscadet, 2007).

A simple and general computational procedure was carried out with all selected crystallographic observations obtained from the CSD. For each instance of every fragment, **F1**, **F2** and **F3**, the related geometric parameters (depicted in **Table 2)** were calculated. The structural relationships in the studied molecular fragments were estimated by carrying out univariate and bivariate analysis. The results obtained for univariate analysis are presented as numerical values, and those for bivariate analyses are presented as scatter plots.

II. Targets modeling

1. The HIV-1 Integrase Models of the B and CRF02_AG strains

3D models of the full-length IN homo-dimer (the *apo* state respectively to DNA) representing one- and two Mg^{+2} cation(s) active sites were generated as follows: (i) The X-Ray structures of the isolated fragmented domains, IN^{1-210} (1K6Y) (Wang, Ling, Yang, & Craigie, 2001) and IN^{56-270} (1EX4) (Chen *et al*., 2000) were chosen as the initial templates.

Both structures were superposed; CCD domain (IN^{56-210}) of 1EX4 determined with lower resolution (2.8 Å) than 1K6Y (2.4 Å) was deleted. Crystal structures represent the multiple mutants, W131D/F139D/F185K in 1K6Y and C56S/W131D/F139/F185K/ C180S in 1EX4; the mutated residues were replaced by the wild type amino acids of the B strain (model 1); the homology modeling produced the model CRF02_AG (model 2) corresponding to followed replacements, K14R/T112V/T125A/G134N/K136T/T206S. Residues 271-288 in 1EX4 and in 1K6Y are disordered and were omitted from the model. The missing loops (47-55 and 140-148) were constructed using Modeller program. The models were exposed to further refinement at the loop regions level (139-149 catalytic site loop and 47-55 CCD and N-terminal linker) using the loop-refining protocol based on DOPE scoring as implemented in Modeller software. Further the models were ranked based on the Discrete Optimized Protein Energy (DOPE) score (Shen & Sali, 2006) and the models of the lowest energy were selected. In the one- and two-cation models, the Mg^{2+} ions were inserted at the catalytic residues D64, D116 and E152, as described for the two-cation structure of 1VSH (Bujacz *et al*., 1997) and minimized using the molecular mechanics under constrains as described in (Mouscadet *et al*., 2009) by using CHARMM program (Brooks *et al*., 2009).

2. IN•DNA Models of the B and CRF02_AG strains

3D models (Model 3 and Model 4) of the full-length IN homo-dimer (*Holo* state respectively to DNA) were generated as follows:

(i) Full length sequence alignment of the HIV-1 (B strain) and PFV INs: In order to favor pertinent superimposition of the residues conserved, the alignment of the sequences was shifted for 1-50 residues (NED domain in PFV IN) and broken down in two steps, allowing for more flexible inspection of the results and easier corrections. First, the sequences were subjected to a pair wise alignment archived with ClustalW. Second, the helices from PFV IN

as defined in the original description of X-ray structure (Hare *et al*., 2010) and the corresponding residues of the INs were examined to verify the correspondence of conserved amino acids. Then each inter-helical alignment was refined separately without altering the rest of superimposition using the selected residue range realignment feature of ClustalW.

(ii) The sequence alignment files were used as input for homology modeling with the X-ray structure of IN•DNA complex of PFV co-crystallized with RAL 3L2T (Hare *et al*., 2010) which were chosen as the template.

(iii) The stereochemical quality of the models was assessed with ProTable Procheck (Laskowski, Macarthur, Moss, & Thornton, 1993), which showed that more than 97% of the non-glycine residues in all models had dihedral angles in the most favorable and allowed regions of the Ramachandram plot, consistent with high model quality. This part of the calculations was carried out using Sybyl package (Tripos Inc., 2007).

3. Secondary structure prediction

Secondary structure assignment for the 1BL3 (Maignan *et al*., 1998), 1B9F (Greenwald *et al*., 1999) – the crystallographic structures of the HIV-1 IN catalytic core domain representing the single F185H mutant and the G140A/G149A/F185K triple mutant respectively, and 3DLR (Valkov *et al*., 2009) and 3OYA (Hare *et al*., 2010) – the crystallographic structures of PFV IN, either isolated or in complex with DNA, respectively, was achieved with the DSSP (Kabsch & Sander, 1983) and Stride (Frishman & Argos, 1995) algorithms.

The secondary structures of the 23 amino acids (aas) polypeptides $IN^{133-155}$ of the HIV-1 IN and $IN^{202-225}$ of the PFV IN were predicted by combining different methods: GOR4 (Garnier, Gibrat, & Robson, 1996); SIMPA96 (Levin, 1997); PSIpred (McGuffin, Bryson, & Jones, 2000); APSSP2 (Raghava, 2002); DSC (King, Saqi, Sayle, & Sternberg, 1997); HNN (NPS@ : CLUSTALW ALIGNMENT); PHD (Rost, Sander, & Schneider, 1994); SORMA

(Deleage, 1995); Jnet (Cuff, Clamp, Siddiqui, Finlay, & Barton, 1998); MLRC (Guermeur, Geourjon, Gallinari, & Deleage, 1999) combining GOR4, SIMPA96 and SOPMA; and SSPRO (Pollastri, Przybylski, Rost, & Baldi, 2002). A score was assigned to each predicted secondary structures (β-strand, α-helix, coil and turns) per amino acid by each method applied, to further derive a consensus prediction. Two types of consensus predictions were computed: the first type was derived from the tools that do not perform alignment before computing predictions (DPM, PREDATOR and GOR4), and the second type was derived from the tools that are based on multiple alignments (SIMPA96, PHD, SOPMA, Jnet, DSC, GORV and PSIPRED). The occurrences of each structural element at a given position were summed over all the predictions for each set resulting as consensus 1 and consensus 2. The confidence rate of a consensus prediction at one position was considered as "high" when at least 75% of the predictions of the set converged.

4. Generation of the models of unbound IN_{HIV}, IN_{HIV}•$vDNA_{PFV}$ complex and $vDNA_{HIV}$

The IN models were constructed using Modeller package 9V8 (Eswar *et al*., 2003) as we reported above. The sequence alignment was performed using ClustalW server (http://www.ebi.ac.uk/Tools/clustalw2/index.html). Briefly, 3D model of the full-length IN homo-dimer, IN^{1-270} (unbound state respectively to DNA) was generated by homology modeling from crystallographic structures of isolated pairs of IN domains, IN^{1-210} (PDB code: 1K6Y) (Wang *et al*., 2001) and IN^{56-270} (PDB code: 1EX4) (Chen *et al*., 2000). The sequence of the native HIV-1 IN was aligned to the templates sequences (non wild-type) using ClustalW (Thompson, Higgins, & Gibson, 1994; Larkin *et al*., 2007). The missing regions, namely the linker from residues 47 to 55 and the catalytic site loop, from residues 140 to 148, were constructed by an *ab initio* approach as we reported in (Mouscadet *et al*., 2009). We shall refer the model with one Mg^{+2} cation inserted into the active site as reported in structure

1BI4 (Maignan *et al*., 1998) as model **1A**, and to the model with two Mg^{+2} cations inserted as reported in (Mouscadet *et al*., 2009) as model **1B**.

The 3D model of the IN•vDNA pre-integration complex was generated by homology modeling from the crystal structure of the PFV IN•vDNA complex (PDB code: 3OYA, resolution of 2.65 Å) (Hare *et al*., 2010b; Hare *et al*., 2010). Despite the low sequence identity between these two INs (22%), a high conservation of key structural elements in the both integrases, allowed us to use the PFV IN structure as a template for the HIV-1 IN model generation. We shall refer to the constructed and optimized model as model **2A.** The stereochemical quality of the models was assessed with ProTable Procheck (Laskowski *et al*., 1993).

A 27 base pair model of the vDNA was constructed using the 3D-DART webserver (van & Bonvin, 2009) according to the following sequence: TAGTCAGTGTGGAAAATCT CTAGCAGT/complement (Hazuda *et al*., 2000) in B-form (model **3A)**. A subsequent model was generated by removing *in silico* the two nucleotides GT from the 3'-end of the modelled vDNA, leaving a CA dinucleotide sequence at the terminal end that is required for integration (model **3B**).

III. Molecular Docking Protocols

1. Integrase Strand Transfer Inhibitors (INSTIs) Binding with IN and IN●vDNA Complex of B and CRF02_AG strains

Docking studies of the studied compounds were performed on the models of IN corresponding to 3-processing and strand transfer pre-integration complex IN•DNA from the B and CRF02_AG strains using the Glide (Friesner *et al*., 2004), incorporated in the Schrödinger suite (Schrödinger Inc.) and the Autodock 4.2 (Morris *et al*., 2009) algorithms.

The initial geometry of the inhibitors was obtained by minimization with the semi-empirical method AM1 (Dewar, 1993) by using Gaussian03 (Gaussian, Inc.) program in vacuum.

The docking results were compared to the *in vitro* enzymatic activity of B and CRF02_AG strains of IN obtained by using steady-state fluorescence anisotropy assay (Ni *et al.,* 2012).

2. Raltegravir docking onto the targets - IN_{HIV}, IN_{HIV}•$vDNA_{PFV}$ complex and $vDNA_{HIV}$

Recorded configurational (isomeric) and conformational states of RAL (see **Conformational analysis**) were used for the inhibitor docking onto the generated models representing the targets with an extended loop in an open conformation, unbound IN (models **1A** and **1B**), and the target with a shortened loop and a well-delimited binding site, IN•vDNA complex (model **2A**). The docking was performed by using four algorithms: GLIDE (Friesner *et al*., 2004) incorporated in the Schrödinger suite (Schrödinger Inc.), AutoDock 4.2 (Morris *et al*., 2009), VINA (Trott & Olson, 2010) and SurFlex (Jain, 2003). The targets were considered as rigid bodies while the inhibitor was treated as wholly flexible. Before the docking, the models were prepared (addition of hydrogen atoms, bond order assignment) according to the given software default requirements.

The conformation of RAL determined by X-ray analysis of PFV IN•DNA complex (PDB code: 3OYA) was optimized and docked onto the vDNA (models **3A** and **3B**) using GLIDE.

AutoDock: AutoDock (Morris *et al*., 2009) is based on a hybrid search method that applies a Lamarckian genetic algorithm. Exploration of the binding site is based on a global search that uses a Genetic Algorithm (GA) followed by an adaptive local search method derived from the optimization algorithm of Solis and Wets which has the advantage of not requiring gradient

computation while it performs torsional angles space search. The graphical user interface (GUI) of AutoDock 4.2 (Morris *et al*., 2009) was used for preparation of ligand and receptor files. Grid maps of interaction energies for various atom types were carried out with a grid box of dimension 25×25×25 $Å^3$ centred on the active site. Calculations were performed with a population size of 150, number of energy evaluations of $5x10^6$, maximum number of generations of 27,000 and crossover rate of 0.02 and 0.8, respectively. The number of runs was set to 100 to explore a large number of poses of the highest affinity and the Solis and Wets algorithm was used to relax the best 10 % of the obtained conformations. The active site coordinates were explicitly defined in the input file.

GLIDE: GLIDE 4.5 (Grid-based Ligand Docking with Energetics) (Friesner *et al*., 2004) program uses a hierarchical series of filters to search for possible locations of the ligand in the binding site region of the receptor. The shape and properties of the receptor are represented on a grid by several sets of fields that provide progressively more accurate scoring of the ligand poses. Conformational flexibility of the ligand is handled by an extensive conformational search. Receptor grids were generated by GLIDE within an enclosing box of size 20 Å centred on the active site. The inhibitor was docked flexibly to these pre-computing grids using standard precision (SP) scoring (Friesner *et al*., 2004).

VINA: VINA (Trott & Olson, 2010) uses a gradient optimization method in its local optimization procedure. It uses an Iterated Local Search global optimizer algorithm where a succession of steps consisting of a mutation in the context of a genetic algorithm, where it is a genetic operator that alters one or more gene values in an algorithm chromosome from its initial state, and a local optimization are taken, with each step being accepted according to the Metropolis criterion. The general functional form of the conformation-dependent part of the scoring function VINA works with the summation over all of the pairs of atoms that can move relative to each other (excluding) 1–4 atoms interactions (Trott & Olson, 2010). The binding

site for each receptor was explicitly defined. Grid maps were generated on a grid box with dimensions 25 Å centered over the binding site of the receptor. The maximum energy difference between the best and the worst binding mode was set to 4 kcal/mol, while the exhaustiveness and the maximum number of binding modes were set to 80 and 100, respectively.

SURFLEX: SurFlex (Jain, 2003) is a relatively new docking algorithm that combines Hammerhead's empirical scoring function (Welch, Ruppert, & Jain, 1996) with a molecular similarity (morphological similarity) to generate putative poses of ligand fragments. It implements an incremental construction search approach, as in Hammerhead (Welch *et al*., 1996) but also implements a new fragment assembly method that is both faster and more accurate. SurFlex employs an idealized active site ligand (a protomol) as a target to generate putative poses of molecular fragments. These putative poses are scored using the Hammerhead function. The protomol was generated with a threshold value of 0.5 and bloat value of 1 Å. The SurFlex package integrated in SYBYL-X 1.1.1 was used for docking.

The scoring functions of GLIDE, AudoDock, VINA and SurFlex, developed in order to rank the solutions, give an estimation of the free binding energy ΔΔG of the protein-ligand interaction. The binding affinity of RAL-IN complexes was expressed in terms of docking scores. For each RAL conformation, the best-scored pose was saved and analyzed.

IV. Molecular Dynamics Simulations of unbound Integrase

The model of WT IN (as prepared above) was used to generate the R228A mutant using MODELLER. The initial models of IN were prepared for GROMACS run with *pdb2gmx* of GROMACS 4.0 (van der Spoel *et al*., 2005); The protein topologies were generated with Amber 99sb-ILDN force field; The hydrogen atoms were then added; In-vacuum minimization of the IN models (WT and mutant) for 1000 steps was performed using

a Steepest-Descent (SD) integrator. The minimized models of WT and mutant were placed in an octahedral TIP3P water box. The charge of the solvated system was neutralized by adding Na^+ counter ions. The system was then heated up to 300° K at a constant volume using a modified Berendsen thermostat (Berendsen *et al*., 1984) while restraining the solute atoms by 1 000 kJ/mol/nm^2. The system was then equilibrated for 1 ns under the constant volume and temperature conditions (NVT). The pressure coupling was also turned "on" using *Parrinello-Rahman* barostat (Martonak *et al*., 2003). Thereafter, two replicas of MD simulations were produced for the equilibrated system during 50 ns, for each system, separately.

V. Molecular modeling

1. Wild-type IN models

3D models of the WT IN core domain representing cation-free, one- and two-Mg^{2+} active sites were generated as follows: (i) X-ray data for 1BI4 and 1BL3 were chosen as the initial templates (Maignan *et al*., 1998); crystal structures represent the F185H mutant; for the WT model, H185 was replaced by F. (ii) In two-cation models, the second Mg^{2+} ion was inserted at the catalytic residues D64 and E152, as described for the two-cation structure of 1VSH (Bujacz *et al*., 1997). In two-cation models, D64 was considered to act as a ligand bridging the two metals, and was referred to as a "μ-bridge" (Cotton and Wilkinson, 1999), whereas D116 and E152 were monodentate, bidentate or mixed. (iii) Coordination spheres of the Mg cations were completed with water molecules to give octahedral coordination, as suggested by structural data for CSD (Allen, 2002). In all the models considered, one water molecule was fixed between two Mg^{2+} cations, forming a second bridge of the μ-aqua type (aqua refers here to the nature of the second bridging group). (iv) Residues 143–148 were deleted from X-ray structures and the 3D structure of the loop was reconstituted with two different modeling

protocols: a loop-generating algorithm based on database searches known as Protein Loop Search (Sybyl), and ab initio loop generation with PEP-FOLD. The candidates identified by Protein Loop Search were compared with the lowest energy solution for peptide structures generated with PEP-FOLD (see Appendix, Figure 3). The loop yielding the best solution with both methods was inserted into the target molecule and the coordinates of the fragment atoms were transformed according to the fragment least-squares fit to anchor regions. (v) H-atoms were added with the Biopolymer and Build/Edit options (SYBYL). The models generated, corresponding to different active site structures, were denoted as **0LJ**, **1LJ**, **2LJ**, **3LJ**, **4LJ**, and **5LJ** (Figure 33).

2. Model minimizations

The Simplex method was used for the initial optimization. Energy minimization of the wild-type and "mutated" promodels was performed with the Powell algorithm and Amber/Kollman atom–atom force field, for 10 000 steps, or if the energy gradient was lower than 0.005 kcal/mol Å. The following parameters were used: a dielectric constant of 1, a minimization step of 0.001, a scaling factor of 1, an H-bond radius scaling of 0.7 and the non-bonded interaction list was set to 8 Å. Constraints were defined between Mg^{2+} ions and the coordinating oxygen atoms, based on the data for CSD data (Allen, 2002). The stereochemical quality of the models was assessed with ProTable Procheck (Laskowski *et al*., 1993), which showed that more than 97% of the non-glycine residues in all models had dihedral angles in the most favored and allowed regions of the Ramachandran plot, consistent with high model quality. The overall folding of the mutant proteins was similar to that of the WT protein and the RMSD coordinate difference between WT and mutant proteins was small (0.6 Å) for the common Cα atoms.

3. Simulations of the movement of the 140–149 loop towards the catalytic site

Simulations of 140–149 loop movement were carried out with the one- (**1LJ**) and two-cation (**2LJ**) models for WT and mutated IN. We compared the total energy and conformation of intermediate states by carrying out energy minimization for the protein structures of the IN models, with different distances between two centroids: C1, describing the center of gravity of the Ω-shaped hairpin and C2, corresponding to the center of gravity of the active site. The movement was simulated in 2 Å steps, extending from 16 (open form) to 4.5 Å (closed form) for models, **1LJ** and **2LJ**.

4. Characterization of the side-chains and DNA base interaction

We investigated two types of molecular complex deposited in the PDB, for analyses of side chain-DNA base interactions: (i) protein/DNA complexes and (ii) protein–ligand complexes with nucleic acid bases as the ligands. The protein/DNA complexes were analyzed for H-bonding and van der Waals contacts, using the "Atlas of Protein Side-Chain Interactions" (Singh and Thornton, 1992). The number of contacts identified between the loop side chains and DNA bases were represented graphically as superimposed diagrams of H-bonds and van der Waals contacts. H-bonding between amino acid 148 or 155 and DNA bases was characterized in details with IsoStar 2.0 (Bruno *et al*., 1997). Data extracted from X-ray structures (resolution > 2.0 Å) of protein–ligand complexes (nucleic acid bases as ligands) are presented as scatterplots, showing the distribution of a contact group (side chain) around a specified central group (DNA base). Groups with chemical functions found in natural amino acids were included in the analysis. Carbamoyl is a functional group of N and Q, guaniduim is a functional group of R, imidazol is a functional group of H, and the cationic —C—

NH_3 group is a functional group of K. The ionization states of acidic and basic groups could not be determined unambiguously from protein structures. These groups were combined for PDB-based plots. The primary IsoStar scatterplots were stored in a modeling format, mol2, and used for further analysis. For these data only, interactions were considered for distances up to 3.4 Å (van der Waals overlaps) and contacting groups involved in π–π interactions were excluded from the analysis. The H-atoms of groups involved in H-bonding were placed in normalized positions. The resulting 3D distributions of side-chain-like fragments around the individual bases were superimposed to represent the A–T and G–C base-pair environment.

REFERENCES

Agapkina, J., Smolov, M., Barbe, S., Zubin, E., Zatsepin, T., Deprez, E. *et al*. (2006). Probing of HIV-1 integrase/DNA interactions using novel analogs of viral DNA. *Journal of Biological Chemistry, 281,* 11530-11540.

Allen, F. H. (2002). The Cambridge Structural Database: a quarter of a million crystal structures and rising. *Acta Crystallogr.B, 58,* 380-388.

Aloy, P., Moont, G., Gabb, H. A., Querol, E., Aviles, F. X., & Sternberg, M. J. (1998). Modeling repressor proteins docking to DNA. *Proteins, 33,* 535-549.

Ammar FF, Abdel-Azeim S, Zargarian L, Hobaika Z, Maroun RG, Fermandjian S. (2012). Unprocessed Viral DNA Could Be the Primary Target of the HIV-1 Integrase Inhibitor Raltegravir. *PLoS One.;7(7)*:e40223.

Arhel, N. J., Souquere-Besse, S., Munier, S., Souque, P., Guadagnini, S., Rutherford, S. *et al*. (2007). HIV-1 DNA Flap formation promotes uncoating of the pre-integration complex at the nuclear pore. *Embo Journal, 26,* 3025-3037.

Arora R. and Tchertanov L. (2012). *The HIV-1 Integrase: Modeling and Beyond*. Chapter in the Book "*An Integrated View of the Molecular Recognition and Toxicology - From Analytical Procedures to Biomedical Applications*". INTECH. ISBN 980-953-307-586-5.

Asante-Appiah, E. & Skalka, A. M. (1999). HIV-1 integrase: structural organization, conformational changes, and catalysis. *Adv.Virus Res., 52,* 351-369.

Ason, B., Knauss, D. J., Balke, A. M., Merkel, G., Skalka, A. M., & Reznikoff, W. S. (2005). Targeting Tn5 transposase identifies human immunodeficiency virus type 1 inhibitors. *Antimicrobial Agents and Chemotherapy, 49,* 2035-2043.

Banitt, I. & Wolfson, H. J. (2011). ParaDock: a flexible non-specific DNA--rigid protein docking algorithm. *Nucleic Acids Res., 39,* e135.

Bar-Magen, T., Sloan, R. D., Faltenbacher, V. H., Donahue, D. A., Kuhl, B. D., Oliveira, M. *et al*. (2009). Comparative biochemical analysis of HIV-1 subtype B and C integrase enzymes. *Retrovirology, 6*. 103.

Barre-Sinoussi, F., Chermann, J. C., Rey, F., Nugeyre, M. T., Chamaret, S., Gruest, J. et al. (1983). Isolation of a T-lymphotropic retrovirus from a patient at risk for acquired immune deficiency syndrome (AIDS). *Science, 220,* 868-871.

Barreca, M. L., De Luca, L., Iraci, N., & Chimirri, A. (2006). Binding mode prediction of strand transfer HIV-1 integrase inhibitors using Tn5 transposase as a plausible surrogate model for HIV-1 integrase. *Journal of Medicinal Chemistry, 49,* 3994-3997.

Barreca, M. L., Ferro, S., Rao, A., De Luca, L., Zappala, M., Monforte, A. M. et al. (2005). Pharmacophore-based design of HIV-1 integrase strand-transfer inhibitors. *Journal of Medicinal Chemistry, 48,* 7084-7088.

Barreca, M. L., Iraci, N., De Luca, L., & Chimirri, A. (2009). Induced-Fit Docking Approach Provides Insight into the Binding Mode and Mechanism of Action of HIV-1 Integrase Inhibitors. *Chemmedchem, 4,* 1446-1456.

Barreca, M. L., Lee, K. W., Chimirri, A., & Briggs, J. M. (2003). Molecular dynamics studies of the wild-type and double mutant HIV-1 integrase complexed with the 5CITEP inhibitor: Mechanism for inhibition and drug resistance. *Biophysical Journal, 84,* 1450-1463.

Beese, L. S. & Steitz, T. A. (1991). Structural Basis for the 3'-5' Exonuclease Activity of Escherichia-Coli Dna-Polymerase-I - A 2 Metal-Ion Mechanism. *Embo Journal, 10,* 25-33.

Berendsen, H. J. C., Postma, J. P. M., Vangunsteren, W. F., Dinola, A., & Haak, J. R. (1984). Molecular-Dynamics with Coupling to An External Bath. *Journal of Chemical Physics, 81,* 3684-3690.

Berger, E. A., Murphy, P. M., & Farber, J. M. (1999). Chemokine receptors as HIV-1 coreceptors: roles in viral entry, tropism, and disease. *Annu.Rev.Immunol., 17,* 657-700.

Berman, H. M., Westbrook, J., Feng, Z., Gilliland, G., Bhat, T. N., Weissig, H. et al. (2000). The Protein Data Bank. *Nucleic Acids Research, 28,* 235-242.

Boeckmann, B., Bairoch, A., Apweiler, R., Blatter, M. C., Estreicher, A., Gasteiger, E. et al. (2003). The SWISS-PROT protein knowledgebase and its supplement TrEMBL in 2003. *Nucleic Acids Res., 31,* 365-370.

Bohm, H. J. (1995). Site-directed structure generation by fragment-joining. *Perspectives in Drug Discovery and Design, 3,* 21-33.

Brendesen, H. J. C. (1984). Molecular dynamics with coupling to an external bath. *J.Chem.Phys, 81,* 3684-3690.

Brigo, A., Lee, K. W., Fogolari, F., Mustata, G. L., & Briggs, J. M. (2005). Comparative molecular dynamics simulations of HIV-1 integrase and the T66I/M154I mutant: Binding modes and drug resistance to a diketo acid inhibitor. *Proteins-Structure Function and Bioinformatics, 59,* 723-741.

Brooks, B. R., Brooks, C. L., Mackerell, A. D., Nilsson, L., Petrella, R. J., Roux, B. et al. (2009). CHARMM: The Biomolecular Simulation Program. *Journal of Computational Chemistry, 30,* 1545-1614.

Brooks, B. R., Bruccoleri, R. E., Olafson, B. D., States, D. J., Swaminathan, S., & Karplus, M. (1983). Charmm - A Program for Macromolecular Energy, Minimization, and Dynamics Calculations 1. *Journal of Computational Chemistry, 4,* 187-217.

Brown, P. O. (1990). Integration of Retroviral DNA. *Current Topics in Microbiology and Immunology, 157,* 19-48.

Bruno, I. J., Cole, J. C., Lommerse, J. P. M., Rowland, R. S., Taylor, R., & Verdonk, M. L. (1997). IsoStar: A library of information about nonbonded interactions. *Journal of Computer-Aided Molecular Design, 11,* 525-537.

Bujacz, G., Alexandratos, J., Wlodawer, A., Merkel, G., Andrake, M., Katz, R. A. et al. (1997). Binding of different divalent cations to the active site of avian sarcoma virus integrase and their effects on enzymatic activity. *J.Biol.Chem., 272,* 18161-18168.

Bujacz, G., Alexandratos, J., ZhouLiu, Q., ClementMella, C., & Wlodawer, A. (1996). The catalytic domain of human immunodeficiency virus integrase: Ordered active site in the F185H mutant. *Febs Letters, 398,* 175-178.

Cai, M., Zheng, R., Caffrey, M., Craigie, R., Clore, G. M., & Gronenborn, A. M. (1997). Solution structure of the N-terminal zinc binding domain of HIV-1 integrase. *Nat.Struct.Biol., 4,* 567-577.

Ceccherini-Silberstein, F. (2010). Primary mutations associated with resistance to raltegravir are not detectable by pyrosequencing in integrase inhibitors-naive patients. Armenia, D, D'Arrigo, R., Vandebroucke, I, Van Marck, H, Rizzardini, G, Narciso, P, Antinori, A., Stuyver, L. J., and Perno, C. F. In: 17th Conference on RetrovirusesandOpportunistic Infections (CROI), San Fransisco, February16–19 (abstract #566).

Ceccherini-Silberstein, F., Malet, I., D'Arrigo, R., Antinori, A., Marcelin, A. G., & Perno, C. F. (2009). Characterization and Structural Analysis of HIV-1 Integrase Conservation. *Aids Reviews, 11,* 17-29.

Centers for Disease Control (1981a). Pneumocystis Pneumonia --- Los Angeles. *MMWR Morb.Mortal.Wkly.Rep., 30,* 1-3.

Centers for Disease Control (1981b). Kaposi's sarcoma and Pneumocystis pneumonia among homosexual men--New York City and California. *MMWR Morb.Mortal.Wkly.Rep., 30,* 305-308.

Centers for Disease Control (1982). Update on acquired immune deficiency syndrome (AIDS)-United States. *MMWR Morb.Mortal.Wkly.Rep., 31*.

Cihlar, T. and Ray, A. S. (2010). Nucleoside and nucleotide HIV reverse transcriptase inhibitors: 25 years after zidovudine. *Antiviral Res. 85(1),* 39-58.

Chakrabarti, L., Guyader, M., Alizon, M., Daniel, M. D., Desrosiers, R. C., Tiollais, P. et al. (1987). Sequence of simian immunodeficiency virus from macaque and its relationship to other human and simian retroviruses. *Nature, 328,* 543-547.

Chalifoux, L. V., Ringler, D. J., King, N. W., Sehgal, P. K., Desrosiers, R. C., Daniel, M. D. et al. (1987). Lymphadenopathy in macaques experimentally infected with the simian immunodeficiency virus (SIV). *Am.J.Pathol., 128,* 104-110.

Charpentier, C., Karmochkine, M., Laureillard, D., Tisserand, P., Belec, L., Weiss, L. et al. (2008). Drug resistance profiles for the HIV integrase gene in patients failing raltegravir salvage therapy. *Hiv Medicine, 9,* 765-770.

Chen, A. P., Weber, I. T., Harrison, R. W., & Leis, J. (2006). Identification of amino acids in HIV-1 and avian sarcoma virus integrase subsites required for specific recognition of the long terminal repeat ends. *Journal of Biological Chemistry, 281,* 4173-4182.

Chen, J. C. H., Krucinski, J., Miercke, L. J. W., Finer-Moore, J. S., Tang, A. H., Leavitt, A. D. et al. (2000). Crystal structure of the HIV-1 integrase catalytic core and C-terminal domains: A model for viral DNA binding. *Proceedings of the National Academy of Sciences of the United States of America, 97,* 8233-8238.

Chen, X., Tsiang, M., Yu, F., Hung, M., Jones, G. S., Zeynalzadegan, A. et al. (2008). Modeling, analysis, and validation of a novel HIV integrase structure provide insights into the binding modes of potent integrase inhibitors. *Journal of Molecular Biology, 380,* 504-519.

Chen, X. H. & Zhang, J. Z. (2004). Theoretical method for full ab initio calculation of DNA/RNA-ligand interaction energy. *J.Chem Phys, 120,* 11386-11391.

Chen, Z., Yan, Y., Munshi, S., Li, Y., Zugay-Murphy, J., Xu, B. et al. (2000). X-ray structure of simian immunodeficiency virus integrase containing the core and C-terminal domain (residues 50-293)--an initial glance of the viral DNA binding platform. *J.Mol.Biol., 296,* 521-533.

Cheng, A. C., Chen, W. W., Fuhrmann, C. N., & Frankel, A. D. (2003). Recognition of nucleic acid bases and base-pairs by hydrogen bonding to amino acid side-chains. *Journal of Molecular Biology, 327,* 781-796.

Chirch, L. M., Morrison, S., & Steigbigel, R. T. (2009). Treatment of HIV infection with raltegravir. *Expert.Opin.Pharmacother., 10,* 1203-1211.

Chiu, T. K. & Davies, D. R. (2004). Structure and function of HIV-1 integrase. *Current Topics in Medicinal Chemistry, 4,* 965-977.

Chothia, C. & Lesk, A. M. (1986). The relation between the divergence of sequence and structure in proteins. *EMBO J., 5,* 823-826.

Clavel, F. & Hance, A. J. (2004). HIV drug resistance. *N.Engl.J.Med., 350,* 1023-1035.

Cooper, D. A., Steigbigel, R. T., Gatell, J. M., Rockstroh, J. K., Katlama, C., Yeni, P. et al. (2008). Subgroup and resistance analyses of raltegravir for resistant HIV-1 infection. *New England Journal of Medicine, 359,* 355-365.

Cortes-Cabrera, A., Gago, F., & Morreale, A. (2012). A reverse combination of structure-based and ligand-based strategies for virtual screening. *J.Comput.Aided Mol.Des, 26,* 319-327.

Croxtall, J. D. & Keam, S. J. (2009). Raltegravir: a review of its use in the management of HIV infection in treatment-experienced patients. *Drugs, 69,* 1059-1075.

Crum, N. F., Riffenburgh, R. H., Wegner, S., Agan, B. K., Tasker, S. A., Spooner, K. M. et al. (2006). Comparisons of causes of death and mortality rates among HIV-infected persons: analysis of the pre-, early, and late HAART (highly active antiretroviral therapy) eras. *J.Acquir.Immune Defic.Syndr., 41,* 194-200.

Costin, J. M. (2007).Cytopathic mechanisms of HIV-1. *Virol.J. 4*, 100.

CSD (1994). Vista - A Program for the Analysis and Display of Data Retrieved from the CSD. [Computer software]. Cambridge Crystallographic Data Centre, 12 Union Road, Cambridge, England.

Cuff, J. A., Clamp, M. E., Siddiqui, A. S., Finlay, M., & Barton, G. J. (1998). JPred: a consensus secondary structure prediction server. *Bioinformatics, 14,* 892-893.

Dalgleish, A. G., Beverley, P. C., Clapham, P. R., Crawford, D. H., Greaves, M. F., & Weiss, R. A. (1984). The CD4 (T4) antigen is an essential component of the receptor for the AIDS retrovirus. *Nature, 312,* 763-767.

Davies, D. R., Goryshin, I. Y., Reznikoff, W. S., & Rayment, I. (2000). Three-dimensional structure of the Tn5 synaptic complex transposition intermediate. *Science, 289,* 77-85.

De Luca, L., Vistoli, G., Pedretti, A., Barreca, M. L., & Chimirri, A. (2005). Molecular dynamics studies of the full-length integrase-DNA complex. *Biochemical and Biophysical Research Communications, 336,* 1010-1016.

De Luca L, Ferro S, Gitto R, Barreca ML, Agnello S, Christ F, et al. Small molecules targeting the interaction between HIV-1 integrase and LEDGF/p75 cofactor. *Bioorg Med Chem.* 2010 Nov 1;18(21):7515-21.

De, L. L., Pedretti, A., Vistoli, G., Barreca, M. L., Villa, L., Monforte, P. et al. (2003). Analysis of the full-length integrase-DNA complex by a modified approach for DNA docking. *Biochem.Biophys.Res.Commun., 310,* 1083-1088.

de Silva, T. I., Cotten, M., and Rowland-Jones, S. L.(2008). HIV-2: the forgotten AIDS virus. *Trends Microbiol. 16(12)*,588-595.

Delelis, O., Malet, I., Na, L., Tchertanov, L., Calvez, V., Marcelin, A. G. et al. (2009). The G140S mutation in HIV integrases from raltegravir-resistant patients rescues catalytic defect due to the resistance Q148H mutation. *Nucleic Acids Research, 37,* 1193-1201.

Delelis, O., Thierry, S., Subra, F., Simon, F., Malet, I., Alloui, C. et al. (2010). Impact of Y143 HIV-1 Integrase Mutations on Resistance to Raltegravir In Vitro and In Vivo. *Antimicrobial Agents and Chemotherapy, 54,* 491-501.

Descamps, D., Apetrei, C., Collin, G., Damond, F., Simon, F., & Brun-Vezinet, F. (1998). Naturally occurring decreased susceptibility of HIV-1 subtype G to protease inhibitors. *AIDS, 12,* 1109-1111.

Descamps, D., Chaix, M. L., Montes, B., Pakianather, S., Charpentier, C., Storto, A. et al. (2010). Increasing prevalence of transmitted drug resistance mutations and non-B subtype circulation in antiretroviral-naive chronically HIV-infected patients from 2001 to 2006/2007 in France. *J.Antimicrob.Chemother., 65,* 2620-2627.

Dewar, M. J. S. (1993). The Semi-Abinitio (Sa) Approach to Chemistry. *Organic Mass Spectrometry, 28,* 305-310.

Dhaked, D. K., Verma, J., Saran, A., & Coutinho, E. C. (2009). Exploring the binding of HIV-1 integrase inhibitors by comparative residue interaction analysis (CoRIA). *Journal of Molecular Modeling, 15,* 233-245.

Dhaked, D. K., Verma, J., Saran, A., & Coutinho, E. C. (2009). Exploring the binding of HIV-1 integrase inhibitors by comparative residue interaction analysis (CoRIA). *Journal of Molecular Modeling, 15,* 233-245.

Dolan, J., Chen, A. P., Weber, I. T., Harrison, R. W., & Leis, J. (2009). Defining the DNA Substrate Binding Sites on HIV-1 Integrase. *Journal of Molecular Biology, 385,* 568-579.

Dybul, M., Fauci, A. S., Bartlett, J. G., Kaplan, J. E., & Pau, A. K. (2002). Guidelines for using antiretroviral agents among HIV-infected adults and adolescents. *Ann.Intern.Med., 137,* 381-433.

Dyda, F., Hickman, A. B., Jenkins, T. M., Engelman, A., Craigie, R., & Davies, D. R. (1994). Crystal structure of the catalytic domain of HIV-1 integrase: similarity to other polynucleotidyl transferases. *Science, 266,* 1981-1986.

Efimov, A. V. (1993a). Patterns of Loop Regions in Proteins. *Current Opinion in Structural Biology, 3,* 379-384.

Efimov, A. V. (1993b). Standard Structures in Proteins. *Progress in Biophysics & Molecular Biology, 60,* 201-239.

Eijkelenboom, A. P., Lutzke, R. A., Boelens, R., Plasterk, R. H., Kaptein, R., & Hard, K. (1995). The DNA-binding domain of HIV-1 integrase has an SH3-like fold. *Nat.Struct.Biol., 2,* 807-810.

Ellison, V., Gerton, J., Vincent, K. A., & Brown, P. O. (1995). An essential interaction between distinct domains of HIV-1 integrase mediates assembly of the active multimer. *J.Biol.Chem., 270,* 3320-3326.

Emiliani, S., Mousnier, A., Busschots, K., Maroun, M., Van Maele, B., Tempe, D. et al. (2005). Integrase mutants defective for interaction with LEDGF/p75 are impaired in chromosome tethering and HIV-1 replication. *Journal of Biological Chemistry, 280,* 25517-25523.

Espeseth, A. S., Felock, P., Wolfe, A., Witmer, M., Grobler, J., Anthony, N. et al. (2000). HIV-1 integrase inhibitors that compete with the target DNA substrate define a unique strand transfer conformation for integrase. *Proceedings of the National Academy of Sciences of the United States of America, 97,* 11244-11249.

Esposito, D. & Craigie, R. (1998). Sequence specificity of viral end DNA binding by HIV-1 integrase reveals critical regions for protein-DNA interaction. *EMBO J., 17,* 5832-5843.

Este, J. A. & Telenti, A. (2007). HIV entry inhibitors. *Lancet, 370,* 81-88.

Eswar, N., John, B., Mirkovic, N., Fiser, A., Ilyin, V. A., Pieper, U. et al. (2003). Tools for comparative protein structure modeling and analysis. *Nucleic Acids Research, 31,* 3375-3380.

Faure, A., Calmels, C., Desjobert, C., Castroviejo, M., Caumont-Sarcos, A., Tarrago-Litvak, L. et al. (2005). HIV-1 integrase crosslinked oligomers are active in vitro. *Nucleic Acids Res., 33,* 977-986.

Feng, M., Patel, D., Dervan, J. J., Ceska, T., Suck, D., Haq, I. et al. (2004). Roles of divalent metal ions in flap endonuclease-substrate interactions. *Nature Structural & Molecular Biology, 11,* 450-456.

Fenollar-Ferrer, C., Carnevale, V., Raugei, S., & Carloni, P. (2008). HIV-1 integrase-DNA interactions investigated by molecular modelling. *Computational and Mathematical Methods in Medicine, 9,* 231-243.

Fetrow, J. S. (1995). Protein Motifs .6. Omega-Loops - Nonregular Secondary Structures Significant in Protein Function and Stability. *FASEB Journal, 9,* 708-717.

Fischetti, L., Opare-Sem, O., Candotti, D., Lee, H., & Allain, J. P. (2004). Higher viral load may explain the dominance of CRF02_AG in the molecular epidemiology of HIV in Ghana. *Aids, 18,* 1208-1210.

Fischetti, L., Opare-Sem, O., Candotti, D., Sarkodie, F., Lee, H., & Allain, J. P. (2004). Molecular epidemiology of HIV in Ghana: dominance of CRF02_AG. *J.Med.Virol., 73,* 158-166.

Friesner & R.A (1987). Solution of the Hartree-Fock equations for polyatomic molecules by a pseudospectral method. *Journal of Chemical Physics, 86,* 3522-3531.

Flexner, C. (1998). HIV-protease inhibitors. *N.Engl.J.Med. 338(18),* 1281-1292.

Friesner, R. A., Banks, J. L., Murphy, R. B., Halgren, T. A., Klicic, J. J., Mainz, D. T. et al. (2004). Glide: A new approach for rapid, accurate docking and scoring. 1. Method and assessment of docking accuracy. *Journal of Medicinal Chemistry, 47,* 1739-1749.

Frishman, D. & Argos, P. (1995). Knowledge-based protein secondary structure assignment. *Proteins-Structure Function and Genetics, 23,* 566-579.

Gallo, R. C., Salahuddin, S. Z., Popovic, M., Shearer, G. M., Kaplan, M., Haynes, B. F. et al. (1984). Frequent detection and isolation of cytopathic retroviruses (HTLV-III) from patients with AIDS and at risk for AIDS. *Science, 224,* 500-503.

Gallo, R. C., Sarin, P. S., Gelmann, E. P., Robert-Guroff, M., Richardson, E., Kalyanaraman, V. S. et al. (1983). Isolation of human T-cell leukemia virus in acquired immune deficiency syndrome (AIDS). *Science, 220,* 865-867.

Gao, K., Butler, S. L., & Bushman, F. (2001). Human immunodeficiency virus type 1 integrase: arrangement of protein domains in active cDNA complexes. *EMBO J., 20,* 3565-3576.

Garnier, J., Gibrat, J. F., & Robson, B. (1996). GOR method for predicting protein secondary structure from amino acid sequence. *Computer Methods for Macromolecular Sequence Analysis, 266,* 540-553.

Ghosn, J., Mazet, A. A., Avettand-Fenoel, V., Peytavin, G., Wirden, M., Delfraissy, J. F. et al. (2009). Rapid selection and archiving of mutation E157Q in HIV-1 DNA during short-term low-level replication on a raltegravir-containing regimen. *J.Antimicrob.Chemother., 64,* 433-434.

Glass, T. R., De, G. S., Hirschel, B., Battegay, M., Furrer, H., Covassini, M. et al. (2008). Self-reported non-adherence to antiretroviral therapy repeatedly assessed by two questions predicts treatment failure in virologically suppressed patients. *Antivir.Ther., 13,* 77-85.

Goethals, O., Clayton, R., Van Ginderen, M., Vereycken, I., Wagemans, E., Geluykens, P. et al. (2008). Resistance Mutations in Human Immunodeficiency Virus Type 1 Integrase Selected with Elvitegravir Confer Reduced Susceptibility to a Wide Range of Integrase Inhibitors. *Journal of Virology, 82,* 10366-10374.

Goldgur, Y., Craigie, R., Cohen, G. H., Fujiwara, T., Yoshinaga, T., Fujishita, T. et al. (1999). Structure of the HIV-1 integrase catalytic domain complexed with an inhibitor: A platform for antiviral drug design. *Proceedings of the National Academy of Sciences of the United States of America, 96,* 13040-13043.

Goldgur, Y., Dyda, F., Hickman, A. B., Jenkins, T. M., Craigie, R., & Davies, D. R. (1998). Three new structures of the core domain of HIV-1 integrase: An active site that binds magnesium. *Proceedings of the National Academy of Sciences of the United States of America, 95,* 9150-9154.

Greenwald, J., Le, V., Butler, S. L., Bushman, F. D., & Choe, S. (1999). The mobility of an HIV-1 integrase active site loop is correlated with catalytic activity. *Biochemistry, 38,* 8892-8898.

Grinsztejn, B., Nguyen, B. Y., Katlama, C., Gatell, J. M., Lazzarin, A., Vittecoq, D. et al. (2007). Safety and efficacy of the HIV-1 integrase inhibitor raltegravir (MK-0518) in treatment-experienced patients with multidrug-resistant virus: a phase II randomised controlled trial. *Lancet, 369,* 1261-1269.

Grobler, J. A., Stillmock, K., Hu, B. H., Witmer, M., Felock, P., Espeseth, A. S. et al. (2002). Diketo acid inhibitor mechanism and HIV-1 integrase: Implications for metal binding in the active site of phosphotransferase enzymes. *Proceedings of the National Academy of Sciences of the United States of America, 99,* 6661-6666.

Gschwend, D. A., Good, A. C., & Kuntz, I. D. (1996). Molecular docking towards drug discovery. *J.Mol.Recognit., 9,* 175-186.

Guermeur, Y., Geourjon, C., Gallinari, P., & Deleage, G. (1999). Improved performance in protein secondary structure prediction by inhomogeneous score combination. *Bioinformatics, 15,* 413-421.

Guiot, E., Carayon, K., Delelis, O., Simon, F., Tauc, P., Zubin, E. et al. (2006). Relationship between the oligomeric status of HIV-1 integrase on DNA and enzymatic activity. *J.Biol.Chem., 281,* 22707-22719.

Hamel, D. J., Sankale, J. L., Eisen, G., Meloni, S. T., Mullins, C., Gueye-Ndiaye, A., Mboup, S., and Kanki, P. J. (2007). Twenty years of prospective molecular epidemiology in Senegal: changes in HIV diversity. *AIDS Res.Hum.Retroviruses 23(10)*, 1189-1196.

Hajduk, P. J. & Greer, J. (2007). A decade of fragment-based drug design: strategic advances and lessons learned. *Nat.Rev.Drug Discov., 6,* 211-219.

Hahn, B. H., Shaw, G. M., Taylor, M. E., Redfield, R. R., Markham, P. D., Salahuddin, S. Z. et al. (1986). Genetic variation in HTLV-III/LAV over time in patients with AIDS or at risk for AIDS. *Science, 232,* 1548-1553.

Hare, S., Gupta, S. S., Valkov, E., Engelman, A., & Cherepanov, P. (2010a). Retroviral intasome assembly and inhibition of DNA strand transfer. *Nature, 464,* 232-236.

Hare, S., Vos, A. M., Clayton, R. F., Thuring, J. W., Cummings, M. D., & Cherepanov, P. (2010b). Molecular mechanisms of retroviral integrase inhibition and the evolution of viral resistance. *Proc.Natl.Acad.Sci.U.S.A, 107,* 20057-20062.

Harrigan, P. R., Hogg, R. S., Dong, W. W., Yip, B., Wynhoven, B., Woodward, J. et al. (2005). Predictors of HIV drug-resistance mutations in a large antiretroviral-naive cohort initiating triple antiretroviral therapy. *J.Infect.Dis., 191,* 339-347.

Harper, M. E., Marselle, L. M., Gallo, R. C., & Wong-Staal, F. (1986). Detection of lymphocytes expressing human T-lymphotropic virus type III in lymph nodes and peripheral blood from infected individuals by in situ hybridization. *Proc.Natl.Acad.Sci.U.S.A, 83,* 772-776.

Hatano, H., Lampiris, H., Fransen, S., Gupta, S., Huang, W., Hoh, R. et al. (2010). Evolution of integrase resistance during failure of integrase inhibitor-based antiretroviral therapy. *J.Acquir.Immune Defic.Syndr., 54,* 389-393.

Hazuda, D. J., Felock, P., Witmer, M., Wolfe, A., Stillmock, K., Grobler, J. A. et al. (2000). Inhibitors of strand transfer that prevent integration and inhibit HIV-1 replication in cells. *Science, 287,* 646-650.

Hazuda, D. J., Miller, M. D., Nguyen, B. Y., & Zhao, J. (2007). Resistance to the HIV-integrase inhibitor raltegravir: analysis of protocol 005, a Phase II study in patients with triple-class resistant HIV-1 infection. *Antiviral Therapy, 12,* S10.

Hazuda, D. J., Young, S. D., Guare, J. P., Anthony, N. J., Gomez, R. P., Wai, J. S. et al. (2004). Integrase inhibitors and cellular immunity suppress retroviral replication in rhesus macaques. *Science, 305,* 528-532.

Heeney, J. L., Dalgleish, A. G., & Weiss, R. A. (2006). Origins of HIV and the evolution of resistance to AIDS. *Science, 313,* 462-466.

Hemelaar, J., Gouws, E., Ghys, P. D., & Osmanov, S. (2011). Global trends in molecular epidemiology of HIV-1 during 2000-2007. *Aids, 25,* 679-689.

Heuer, T. S. & Brown, P. O. (1997). Mapping features of HIV-1 integrase near selected sites on viral and target DNA molecules in an active enzyme-DNA complex by photo-cross-linking. *Biochemistry, 36,* 10655-10665.

Heuer, T. S. & Brown, P. O. (1998). Photo-cross-linking studies suggest a model for the architecture of an active human immunodeficiency virus type 1 integrase-DNA complex. *Biochemistry, 37,* 6667-6678.

Hu, X., Balaz, S., & Shelver, W. H. (2004). A practical approach to docking of zinc metalloproteinase inhibitors. *Journal of Molecular Graphics & Modelling, 22,* 293-307.

Huang, S. Y. & Zou, X. Q. (2010). Advances and Challenges in Protein-Ligand Docking. *International Journal of Molecular Sciences, 11,* 3016-3034.

Humphrey, G. R., Pye, P. J., Zhong, Y. L., Angelaud, R., Askin, D., Belyk, K. M. et al. (2011). Development of a Second-Generation, Highly Efficient Manufacturing Route for the HIV Integrase Inhibitor Raltegravir Potassium. *Organic Process Research & Development, 15,* 73-83.

Hutchinson, E. G. & Thornton, J. M. (1994). A Revised Set of Potentials for Beta-Turn Formation in Proteins. *Protein Science, 3,* 2207-2216.

Iwamoto, M., Wenning, L. A., Petry, A. S., Laethem, M., De, S. M., Kost, J. T. et al. (2008). Safety, tolerability, and pharmacokinetics of raltegravir after single and multiple doses in healthy subjects. *Clin.Pharmacol.Ther., 83,* 293-299.

Jacks, T., Power, M. D., Masiarz, F. R., Luciw, P. A., Barr, P. J., & Varmus, H. E. (1988). Characterization of ribosomal frameshifting in HIV-1 gag-pol expression. *Nature, 331,* 280-283.

Jain, A. N. (2003). Surflex: Fully automatic flexible molecular docking using a molecular similarity-based search engine. *Journal of Medicinal Chemistry, 46,* 499-511.

Jones, G. & Willett, P. (1995). Docking small-molecule ligands into active sites. *Curr.Opin.Biotechnol., 6,* 652-656.

Kabsch, W. & Sander, C. (1983). Dictionary of Protein Secondary Structure - Pattern-Recognition of Hydrogen-Bonded and Geometrical Features. *Biopolymers, 22,* 2577-2637.

Kanki, P. J., Hamel, D. J., Sankale, J. L., Hsieh, C., Thior, I., Barin, F. et al. (1999). Human immunodeficiency virus type 1 subtypes differ in disease progression. *J.Infect.Dis., 179,* 68-73.

Kantor, R., Katzenstein, D. A., Efron, B., Carvalho, A. P., Wynhoven, B., Cane, P. et al. (2005). Impact of HIV-1 subtype and antiretroviral therapy on protease and reverse transcriptase genotype: results of a global collaboration. *PLoS.Med., 2,* e112.

Karki, R. G., Tang, Y., Burke, T. R., & Nicklaus, M. C. (2004). Model of full-length HIV-1 integrase complexed with viral DNA as template for anti-HIV drug design. *Journal of Computer-Aided Molecular Design, 18,* 739-760.

Karplus, M. (2002). Molecular dynamics simulations of biomolecules. *Acc.Chem.Res., 35,* 321-323.

Karplus, M. & Kuriyan, J. (2005). Molecular dynamics and protein function. *Proc.Natl.Acad.Sci.U.S.A, 102,* 6679-6685.

Kawasuji, T., Fuji, M., Yoshinaga, T., Sato, A., Fujiwara, T., & Kiyama, R. (2006a). A platform for designing HIV integrase inhibitors. Part 2: A two-metal binding model as a potential mechanism of HIV integrase inhibitors. *Bioorganic & Medicinal Chemistry, 14,* 8420-8429.

Kawasuji, T., Yoshinaga, T., Sato, A., Yodo, M., Fujiwara, T., & Kiyama, R. (2006). A platform for designing HIV integrase inhibitors. Part 1: 2-hydroxy-3-heteroaryl acrylic acid derivatives as novel HIV integrase inhibitor and modeling of hydrophilic and hydrophobic pharmacophores. *Bioorganic & Medicinal Chemistry, 14,* 8430-8445.

King, R. D., Saqi, M., Sayle, R., & Sternberg, M. J. E. (1997). DSC: public domain protein secondary structure prediction. *Computer Applications in the Biosciences, 13,* 473-474.

Kobayashi, M., Nakahara, K., Seki, T., Miki, S., Kawauchi, S., Suyama, A. et al. (2008). Selection of diverse and clinically relevant integrase inhibitor-resistant human immunodeficiency virus type 1 mutants. *Antiviral Research, 80,* 213-222.

Kohlstaedt, L. A., Wang, J., Friedman, J. M., Rice, P. A., and Steitz, T. A. (1992). Crystal structure at 3.5 A resolution of HIV-1 reverse transcriptase complexed with an inhibitor. *Science 256(5065),* 1783-1790..

Korber, B., Muldoon, M., Theiler, J., Gao, F., Gupta, R., Lapedes, A. et al. (2000). Timing the ancestor of the HIV-1 pandemic strains. *Science, 288,* 1789-1796.

Korolev S, Agapkina Yu, Gottikh M. Clinical Use of Inhibitors of HIV-1 Integration: Problems and Prospects. *Acta Naturae* 2011;3;3:12-28.

Krovat, E. M., Steindl, T., & Langer, T. (2005). Recent Advances in Docking and Scoring. *Current Computer-Aided Drug Design, 1,* 93-102.

Kumar, G. N., Rodrigues, A. D., Buko, A. M., & Denissen, J. F. (1996). Cytochrome P450-mediated metabolism of the HIV-1 protease inhibitor ritonavir (ABT-538) in human liver microsomes. *J.Pharmacol.Exp.Ther., 277,* 423-431.

Lane, H. C. & Fauci, A. S. (1985). Immunologic abnormalities in the acquired immunodeficiency syndrome. *Annu.Rev.Immunol., 3,* 477-500.

Langley, D. R., Samanta, H. K., Lin, Z., Walker, M. A., Krystal, M. R., & Dicker, I. B. (2008). The terminal (catalytic) adenosine of the HIV LTR controls the kinetics of binding and dissociation of HIV integrase strand transfer inhibitors. *Biochemistry, 47,* 13481-13488.

Larkin, M. A., Blackshields, G., Brown, N. P., Chenna, R., McGettigan, P. A., McWilliam, H. et al. (2007). Clustal W and clustal X version 2.0. *Bioinformatics, 23,* 2947-2948.

Laskowski, R. A., Macarthur, M. W., Moss, D. S., & Thornton, J. M. (1993). Procheck - A Program to Check the Stereochemical Quality of Protein Structures. *Journal of Applied Crystallography, 26,* 283-291.

Lataillade, M., Chiarella, J., & Kozal, M. J. (2007). Natural polymorphism of the HIV-1 integrase gene and mutations associated with integrase inhibitor resistance. *Antiviral Therapy, 12,* 563-570.

Lavery, R. (2005). Recognizing DNA. *Q.Rev.Biophys., 38,* 339-344.

Lee, M. C., Deng, J. X., Briggs, J. M., & Duan, Y. (2005). Large-scale conformational dynamics of the HIV-1 integrase core domain and its catalytic loop mutants. *Biophysical Journal, 88,* 3133-3146.

Lee, M. S. & Craigie, R. (1994). Protection of Retroviral Dna from Autointegration - Involvement of A Cellular Factor. *Proceedings of the National Academy of Sciences of the United States of America, 91,* 9823-9827.

Lee, S. P. & Han, M. K. (1996). Zinc stimulates Mg^{2+}-dependent 3'-processing activity of human immunodeficiency virus type 1 integrase in vitro. *Biochemistry, 35,* 3837-3844.

Leh, H., Brodin, P., Bischerour, J., Deprez, E., Tauc, P., Brochon, J. C. et al. (2000). Determinants of Mg^{2+}-dependent activities of recombinant human immunodeficiency virus type 1 integrase. *Biochemistry, 39,* 9285-9294.

Lengauer, T., Sander, O., Sierra, S., Thielen, A., & Kaiser, R. (2007). Bioinformatics prediction of HIV coreceptor usage. *Nat.Biotechnol., 25,* 1407-1410.

Lennox, J. L., DeJesus, E., Lazzarin, A., Pollard, R. B., Madruga, J. V., Berger, D. S. et al. (2009). Safety and efficacy of raltegravir-based versus efavirenz-based combination therapy in treatment-naive patients with HIV-1 infection: a multicentre, double-blind randomised controlled trial. *Lancet, 374,* 796-806.

Leszczynski, J. F. & Rose, G. D. (1986). Loops in Globular-Proteins - A Novel Category of Secondary Structure. *Science, 234,* 849-855.

Levin, J. M. (1997). Exploring the limits of nearest neighbour secondary structure prediction. *Protein Engineering, 10,* 771-776.

Levitt, M. & Warshel, A. (1975). Computer-Simulation of Protein Folding. *Nature, 253,* 694-698.

Lins, R. D., Adesokan, A., Soares, T. A., & Briggs, J. M. (2000). Investigations on human immunodeficiency virus type 1 integrase/DNA binding interactions via molecular dynamics and electrostatics calculations. *Pharmacology & Therapeutics, 85,* 123-131.

Lins, R. D., Briggs, J. M., Straatsma, T. P., Carlson, H. A., Greenwald, J., Choe, S. et al. (1999). Molecular dynamics studies on the HIV-1 integrase catalytic domain. *Biophysical Journal, 76,* 2999-3011.

Lins, R. D., Straatsma, T. P., & Briggs, J. M. (2000). Similarities in the HIV-1 and ASV integrase active sites upon metal cofactor binding. *Biopolymers, 53,* 308-315.

Loizidou, E. Z., Kousiappa, I., Zeinalipour-Yazdi, C. D., Van de Vijver, D. A. M. C., & Kostrikis, L. G. (2009). Implications of HIV-1 M Group Polymorphisms on Integrase Inhibitor Efficacy and Resistance: Genetic and Structural in Silico Analyses. *Biochemistry, 48,* 4-6.

Loizidou, E. Z., Zeinalipour-Yazdi, C. D., Christofides, T., & Kostrikis, L. G. (2009). Analysis of binding parameters of HIV-1 integrase inhibitors: Correlates of drug inhibition and resistance. *Bioorganic & Medicinal Chemistry, 17,* 4806-4818.

Lovell, S., Goryshin, I. Y., Reznikoff, W. R., & Rayment, I. (2002). Two-metal active site binding of a Tn5 transposase synaptic complex. *Nat.Struct.Biol., 9,* 278-281.

Low, A., Prada, N., Topper, M., Vaida, F., Castor, D., Mohri, H. et al. (2009). Natural Polymorphisms of Human Immunodeficiency Virus Type 1 Integrase and Inherent Susceptibilities to a Panel of Integrase Inhibitors. *Antimicrobial Agents and Chemotherapy, 53,* 4275-4282.

Luscombe, N. M., Laskowski, R. A., & Thornton, J. M. (2001). Amino acid-base interactions: a three-dimensional analysis of protein-DNA interactions at an atomic level. *Nucleic Acids Research, 29,* 2860-2874.

Luscombe, N. M. & Thornton, J. M. (2002). Protein-DNA interactions: Amino acid conservation and the effects of mutations on binding specificity. *Journal of Molecular Biology, 320,* 991-1009.

Machado, L. F., Ishak, M. O., Vallinoto, A. C., Lemos, J. A., Azevedo, V. N., Moreira, M. R. et al. (2009). Molecular epidemiology of HIV type 1 in northern Brazil: identification of subtypes C and D and the introduction of CRF02_AG in the Amazon region of Brazil. *AIDS Res.Hum.Retroviruses, 25,* 961-966.

Macrae, C. F., Edgington, P. R., McCabe, P., Pidcock, E., Shields, G. P., Taylor, R. et al. (2006). Mercury: visualization and analysis of crystal structures. *Journal of Applied Crystallography, 39,* 453-457.

Maiga, A. I., Malet, I., Soulie, C., Derache, A., Koita, V., Amellal, B. et al. (2009). Genetic barriers for integrase inhibitor drug resistance in HIV type-1 B and CRF02_AG subtypes. *Antivir.Ther., 14,* 123-129.

Maignan, S., Guilloteau, J. P., Zhou-Liu, Q., Clement-Mella, C., & Mikol, V. (1998). Crystal structures of the catalytic domain of HIV-1 integrase free and complexed with its metal cofactor: High level of similarity of the active site with other viral integrases. *Journal of Molecular Biology, 282,* 359-368.

Malet, I., Delelis, O., Soulie, C., Wirden, M., Tchertanov, L., Mottaz, P. et al. (2009). Quasispecies variant dynamics during emergence of resistance to raltegravir in HIV-1-infected patients. *Journal of Antimicrobial Chemotherapy, 63,* 795-804.

Malet, I., Delelis, O., Valantin, M. A., Montes, B., Soulie, C., Wirden, M. et al. (2008). Mutations associated with failure of raltegravir treatment affect integrase sensitivity to the inhibitor in vitro. *Antimicrobial Agents and Chemotherapy, 52,* 1351-1358.

Malet, I., Soulie, C., Tchertanov, L., Derache, A., Amellal, B., Traore, O. et al. (2008). Structural effects of amino acid variations between B and CRF02-AG HIV-1 integrases. *Journal of Medical Virology, 80,* 754-761.

Marcelin, A. G. (2010). Resistance-associated mutations to integrase inhibitor S/GSK1349572 in HIV-1 integrase inhibitor- naive and raltegravir-experienced patients. Malet, I, Fabeni, L, Armenia, D, Fourati, S, Masquelier, B, Katlama, C., Perno, C. F., Calvez, T., and Ceccherini-Silberstein, F. In: 17th Conference on Retroviruses and Opportunistic Infections (CROI), San Fransisco, February 16–19 (abstract #554).

Martinez-Cajas, J. L., Pant-Pai, N., Klein, M. B., & Wainberg, M. A. (2008). Role of Genetic Diversity amongst HIV-1 Non-B Subtypes in Drug Resistance: A Systematic Review of Virologic and Biochemical Evidence. *Aids Reviews, 10,* 212-223.

Marti-Renom, M. A., Stuart, A. C., Fiser, A., Sanchez, R., Melo, F., & Sali, A. (2000). Comparative protein structure modeling of genes and genomes. *Annu.Rev.Biophys.Biomol.Struct., 29,* 291-325.

Martonak, R., Laio, A., & Parrinello, M. (2003). Predicting crystal structures: the Parrinello-Rahman method revisited. *Phys.Rev.Lett., 90,* 075503.

Matthews, B. W. (1988). Protein-DNA interaction. No code for recognition. *Nature, 335,* 294-295.

Maupetit, J., Tuffery, P., & Derreumaux, P. (2007). A coarse-grained protein force field for folding and structure prediction. *Proteins-Structure Function and Bioinformatics, 69,* 394-408.

Maurin, C., Bailly, F., Buisine, E., Vezin, H., Mbemba, G., Mouscadet, J. F. et al. (2004). Spectroscopic studies of diketoacids-metal interactions. A probing tool for the pharmacophoric intermetallic distance in the HIV-1 integrase active site. *J.Med.Chem., 47,* 5583-5586.

Mazumder A, Wang S, Neamati N, Nicklaus M, Sunder S, Chen J, et al. Antiretroviral agents as inhibitors of both human immunodeficiency virus type 1 integrase and protease. *J Med Chem.* 1996 Jun 21;39(13):2472-81.

McCammon, J. A., Gelin, B. R., & Karplus, M. (1977). Dynamics of folded proteins. *Nature, 267,* 585-590.

Mccoll, D. J., Fransen, S., Gupta, S., Parkin, N., Margot, N., Chuck, S. et al. (2007). Resistance and cross-resistance to first generation integrase inhibitors: insights from a Phase II study of elvitegravir (GS-9137). *Antiviral Therapy, 12,* S11.

McGuffin, L. J., Bryson, K., & Jones, D. T. (2000). The PSIPRED protein structure prediction server. *Bioinformatics, 16,* 404-405.

Metifiot, M., Maddali, K., Naumova, A., Zhang, X., Marchand, C., & Pommier, Y. (2010). Biochemical and pharmacological analyses of HIV-1 integrase flexible loop mutants resistant to raltegravir. *Biochemistry, 49,* 3715-3722.

Michel, F., Crucifix, C., Granger, F., Eiler, S., Mouscadet, J. F., Korolev, S. et al. (2009). Structural basis for HIV-1 DNA integration in the human genome, role of the LEDGF/P75 cofactor. *EMBO J, 28,* 980-991.

Miller, M. D. & Hazuda, D. J. (2004). HIV resistance to the fusion inhibitor enfuvirtide: mechanisms and clinical implications. *Drug Resist.Updat., 7,* 89-95.

Miranker, A. & Karplus, M. (1991). Functionality maps of binding sites: a multiple copy simultaneous search method. *Proteins, 11,* 29-34.

Molteni, V., Greenwald, J., Rhodes, D., Hwang, Y., Kwiatkowski, W., Bushman, F. D. et al. (2001). Identification of a small-molecule binding site at the dimer interface of the HIV integrase catalytic domain. *Acta Crystallographica Section D-Biological Crystallography, 57,* 536-544.

Morgan, D. A., Ruscetti, F. W., & Gallo, R. (1976). Selective in vitro growth of T lymphocytes from normal human bone marrows. *Science, 193,* 1007-1008.

Morris, G. M., Huey, R., Lindstrom, W., Sanner, M. F., Belew, R. K., Goodsell, D. S. et al. (2009). AutoDock4 and AutoDockTools4: Automated Docking with Selective Receptor Flexibility. *Journal of Computational Chemistry, 30,* 2785-2791.

Mouscadet, J. F., Arora, R., Andre, J., Lambry, J. C., Delelis, O., Malet, I. et al. (2009). HIV-1 IN alternative molecular recognition of DNA induced by raltegravir resistance mutations. *J.Mol.Recognit., 22,* 480-494.

Mouscadet, J. F., Delelis, O., Marcelin, A. G., & Tchertanov, L. (2010). Resistance to HIV-1 integrase inhibitors: A structural perspective. *Drug Resist.Updat., 13,* 139-150.

Mouscadet, J. F. & Tchertanov, L. (2009). Raltegravir: molecular basis of its mechanism of action. *Eur.J.Med.Res., 14 Suppl 3,* 5-16.

Myers, R. E. & Pillay, D. (2008). Analysis of natural sequence variation and covariation in human immunodeficiency virus type 1 integrase. *Journal of Virology, 82,* 9228-9235.

Neamati, N., Lin, Z. W., Karki, R. G., Orr, A., Cowansage, M., Strumberg, D. et al. (2002). Metal-dependent inhibition of HIV-1 integrase. *Journal of Medicinal Chemistry, 45,* 5661-5670.

Ni, H. H., Sotriffer, C. A., & McCammon, J. A. (2001). Ordered water and ligand mobility in the HIV-1 integrase-5CITEP complex: A molecular dynamics study. *Journal of Medicinal Chemistry, 44,* 3043-3047.

Ni, X., Abdel-Azeim, S., Laine, E., Arora, R., Osemwota, O., Marcelin, A. G. et al. (2012). In Silico and In Vitro Comparison of HIV-1 Subtypes B and CRF02_AG Integrases Susceptibility to Integrase Strand Transfer Inhibitors. *Adv.Virol., 2012,* 548657.

Nijhuis, M., van Maarseveen, N. M., Lastere, S., Schipper, P., Coakley, E., Glass, B. et al. (2007). A novel substrate-based HIV-1 protease inhibitor drug resistance mechanism. *PLoS.Med., 4,* e36.

Njai, H. F., Gali, Y., Vanham, G., Clybergh, C., Jennes, W., Vidal, N. et al. (2006). The predominance of Human Immunodeficiency Virus type 1 (HIV-1) circulating recombinant form 02 (CRF02_AG) in West Central Africa may be related to its replicative fitness. *Retrovirology, 3,* 40.

Nunthaboot, N., Pianwanit, S., Parasuk, V., Ebalunode, J. O., Briggs, J. M., & Kokpol, S. (2007). Hybrid quantum mechanical/molecular mechanical molecular dynamics simulations of HIV-1 integrase/inhibitor complexes. *Biophysical Journal, 93,* 3613-3626.

Nunthaboot, N., Planwanit, S., Parasuk, V., Kokpol, S., & Wolschann, P. (2007). Theoretical study on the HIV-1 integrase inhibitor 1-(5-chloroindol-3-yl)-3-hydroxy-3-(2H-tetrazol-5-yl)-propenone (5CITEP). *Journal of Molecular Structure, 844,* 208-214.

Pace, P., Di Francesco, M. E., Gardelli, C., Harper, S., Muraglia, E., Nizi, E. et al. (2007). Dihydroxypyrimidine-4-carboxamides as novel potent and selective HIV integrase inhibitors. *Journal of Medicinal Chemistry, 50,* 2225-2239.

Pannecouque, C., Pluymers, W., Van, Maele B., Tetz, V., Cherepanov, P., De, Clercq E., Witvrouw, M., and Debyser, Z. (2002). New class of HIV integrase inhibitors that block viral replication in cell culture. *Curr.Biol. 12(14),* 1169-1177.

Pasquini, S., Mugnaini, C., Tintori, C., Botta, M., Trejos, A., Arvela, R. K. et al. (2008). Investigations on the 4-quinolone-3-carboxylic acid motif. 1. Synthesis-activity relationship of a class of human immunodeficiency virus type 1 integrase inhibitors. *Journal of Medicinal Chemistry, 51,* 5125-5129.

Perryman, A. L., Forli, S., Morris, G. M., Burt, C., Cheng, Y. H., Palmer, M. J. et al. (2010). A Dynamic Model of HIV Integrase Inhibition and Drug Resistance. *Journal of Molecular Biology, 397,* 600-615.

Pettit, S. C., Everitt, L. E., Choudhury, S., Dunn, B. M., & Kaplan, A. H. (2004). Initial cleavage of the human immunodeficiency virus type 1 GagPol precursor by its activated protease occurs by an intramolecular mechanism. *J.Virol., 78,* 8477-8485.

Plantier, J. C., Leoz, M., Dickerson, J. E., De, O. F., Cordonnier, F., Lemee, V. et al. (2009). A new human immunodeficiency virus derived from gorillas. *Nat.Med., 15,* 871-872.

Podtelezhnikov, A. A., Gao, K., Bushman, F. D., & McCammon, J. A. (2003). Modeling HIV-1 integrase complexes based on their hydrodynamic properties. *Biopolymers, 68,* 110-120.

Pollastri, G., Przybylski, D., Rost, B., & Baldi, P. (2002). Improving the prediction of protein secondary structure in three and eight classes using recurrent neural networks and profiles. *Proteins-Structure Function and Genetics, 47,* 228-235.

Pommier, Y., Johnson, A. A., & Marchand, C. (2005). Integrase inhibitors to treat HIV/AIDS. *Nature Reviews Drug Discovery, 4,* 236-248.

Popovic, M., Sarngadharan, M. G., Read, E., & Gallo, R. C. (1984). Detection, isolation, and continuous production of cytopathic retroviruses (HTLV-III) from patients with AIDS and pre-AIDS. *Science, 224,* 497-500.

Raghava, G. P. S. (2002). APSSP2 : A combination method for protein secondary structure prediction based on neural network and example based learning. CASP5. A-132. [Computer software].

Ratner, L., Haseltine, W., Patarca, R., Livak, K. J., Starcich, B., Josephs, S. F. et al. (1985). Complete nucleotide sequence of the AIDS virus, HTLV-III. *Nature, 313,* 277-284.

Ren, G., Gao, K., Bushman, F. D., & Yeager, M. (2007). Single-particle image reconstruction of a tetramer of HIV integrase bound to DNA. *Journal of Molecular Biology, 366,* 286-294.

Rhee, S. Y., Liu, T. F., Kiuchi, M., Zioni, R., Gifford, R. J., Holmes, S. P. et al. (2008). Natural variation of HIV-1 group M integrase: Implications for a new class of antiretroviral inhibitors. *Retrovirology, 5*.

Robertson, D. L., Anderson, J. P., Bradac, J. A., Carr, J. K., Foley, B., Funkhouser, R. K. et al. (2000). HIV-1 nomenclature proposal. *Science, 288,* 55-56.

Roquebert, B., Damond, F., Collin, G., Matheron, S., Peytavin, G., Benard, A. et al. (2008). HIV-2 integrase gene polymorphism and phenotypic susceptibility of HIV-2 clinical isolates to the integrase inhibitors raltegravir and elvitegravir in vitro. *J.Antimicrob.Chemother., 62,* 914-920.

Rost, B., Sander, C., & Schneider, R. (1994). Phd - An Automatic Mail Server for Protein Secondary Structure Prediction. *Computer Applications in the Biosciences, 10,* 53-60.

Rowland-Jones, S. L. and Whittle, H. C. (2007). Out of Africa: what can we learn from HIV-2 about protective immunity to HIV-1? *Nat.Immunol. 8(4)*, 329-331.

Saag, M. S., Hahn, B. H., Gibbons, J., Li, Y., Parks, E. S., Parks, W. P. et al. (1988). Extensive variation of human immunodeficiency virus type-1 in vivo. *Nature, 334,* 440-444.

Sanchez, R. & Sali, A. (1997). Advances in comparative protein-structure modeling. *Curr.Opin.Struct.Biol., 7,* 206-214.

Sanchez-Pescador, R., Power, M. D., Barr, P. J., Steimer, K. S., Stempien, M. M., Brown-Shimer, S. L. et al. (1985). Nucleotide sequence and expression of an AIDS-associated retrovirus (ARV-2). *Science, 227,* 484-492.

Sante-Appiah, E. & Skalka, A. M. (1999). HIV-1 integrase: Structural organization, conformational changes, and catalysis. *Advances in Virus Research, Vol 52, 52,* 351-369.

Sarngadharan, M. G., Popovic, M., Bruch, L., Schupbach, J., & Gallo, R. C. (1984). Antibodies reactive with human T-lymphotropic retroviruses (HTLV-III) in the serum of patients with AIDS. *Science, 224,* 506-508.

Sato, M., Motomura, T., Aramaki, H., Matsuda, T., Yamashita, M., Ito, Y. et al. (2006). Novel HIV-1 integrase inhibitors derived from quinolone antibiotics. *Journal of Medicinal Chemistry, 49,* 1506-1508.

Savarino, A. (2007). In-Silico docking of HIV-1 integrase inhibitors reveals a novel drug type acting on an enzyme/DNA reaction intermediate. *Retrovirology, 4*.

Savarino, A., Pistello, M., D'Ostilio, D., Zabogli, E., Taglia, F., Mancini, F. et al. (2007). Human immunodeficiency virus integrase inhibitors efficiently suppress feline immunodeficiency virus replication in vitro and provide a rationale to redesign antiretroviral treatment for feline AIDS. *Retrovirology, 4*.

Schupbach, J., Popovic, M., Gilden, R. V., Gonda, M. A., Sarngadharan, M. G., & Gallo, R. C. (1984). Serological analysis of a subgroup of human T-lymphotropic retroviruses (HTLV-III) associated with AIDS. *Science, 224,* 503-505.

Schwede, T., Kopp, J., Guex, N., & Peitsch, M. C. (2003). SWISS-MODEL: An automated protein homology-modeling server. *Nucleic Acids Res., 31,* 3381-3385.

Seki, T. (2010). S/GSK1349572 is a potent next generation HIV integrase inhibitor and demonstrates a superior resistance profile substantiated with 60 integrase mutant molecular clones. Kobayashi, M., Wakasa-Morimoto, C., Yoshinaga, T., Sato, A., Fujiwara, T., Underwood, M. R., Garvey, E. P., and Johns, B. A. . In: 17th Conference on Retroviruses and Opportunistic Infections (CROI), San Fransisco, February 16–19 (abstract #555).

Segall, M. D., Payne, M. C., Ellis, S. W., Tucker, G. T., & Boyes, R. N. (1997). Ab initio molecular modeling in the study of drug metabolism. *Eur.J.Drug Metab Pharmacokinet., 22,* 283-289.

Semenova, E. A., Marchand, C., & Pommier, Y. (2008). HIV-1 integrase inhibitors: update and perspectives. *Adv.Pharmacol., 56,* 199-228.

Sension, M. G. (2007). Long-Term suppression of HIV infection: benefits and limitations of current treatment options. *J.Assoc.Nurses AIDS Care 18(1 Suppl)*, S2-10.

Serrao, E., Odde, S., Ramkumar, K., & Neamati, N. (2009). Raltegravir, elvitegravir, and metoogravir: the birth of "me-too" HIV-1 integrase inhibitors. *Retrovirology, 6,* 25.

Setny, P., Bahadur, R. P., & Zacharias, M. (2012). Protein-DNA docking with a coarse-grained force field. *BMC Bioinformatics, 13,* 228.

Shaw, G. M., Hahn, B. H., Arya, S. K., Groopman, J. E., Gallo, R. C., & Wong-Staal, F. (1984). Molecular characterization of human T-cell leukemia (lymphotropic) virus type III in the acquired immune deficiency syndrome. *Science, 226,* 1165-1171.

Shaw, G. M., Harper, M. E., Hahn, B. H., Epstein, L. G., Gajdusek, D. C., Price, R. W. et al. (1985). HTLV-III infection in brains of children and adults with AIDS encephalopathy. *Science, 227,* 177-182.

Shehu-Xhilaga, M., Crowe, S. M., & Mak, J. (2001). Maintenance of the Gag/Gag-Pol ratio is important for human immunodeficiency virus type 1 RNA dimerization and viral infectivity. *J.Virol., 75,* 1834-1841.

Shen, M. Y. & Sali, A. (2006). Statistical potential for assessment and prediction of protein structures. *Protein Science, 15,* 2507-2524.

Shimura, K., Kodama, E., Sakagami, Y., Matsuzaki, Y., Watanabe, W., Yamataka, K. et al. (2008). Broad Antiretroviral activity and resistance profile of the novel human immunodeficiency virus integrase inhibitor elvitegravir (JTK-303/GS-9137). *Journal of Virology, 82,* 764-774.

Shuker, S. B., Hajduk, P. J., Meadows, R. P., & Fesik, S. W. (1996). Discovering high-affinity ligands for proteins: SAR by NMR. *Science, 274,* 1531-1534.

Sichtig, N., Sierra, S., Kaiser, R., Daumer, M., Reuter, S., Schulter, E. et al. (2009). Evolution of raltegravir resistance during therapy. *Journal of Antimicrobial Chemotherapy, 64,* 25-32.

Smolov, M., Gottikh, M., Tashlitskii, V., Korolev, S., Demidyuk, I., Brochon, J. C. et al. (2006). Kinetic study of the HIV-1 DNA 3 '-end processing - Single-turnover property of integrase. *Febs Journal, 273,* 1137-1151.

Steigbigel, R. T., Cooper, D. A., Kumar, P. N., Eron, J. E., Schechter, M., Markowitz, M. et al. (2008). Raltegravir with optimized background therapy for resistant HIV-1 infection. *N.Engl.J.Med., 359,* 339-354.

Street, T. O., Fitzkee, N. C., Perskie, L. L., & Rose, G. D. (2007). Physical-chemical determinants of turn conformations in globular proteins. *Protein Science, 16,* 1720-1727.

Strobel, S. A. & Ryder, S. P. (2001). The hairpin's turn. *Nature, 410,* 761-763.

Summa, V., Petrocchi, A., Bonelli, F., Crescenzi, B., Donghi, M., Ferrara, M. et al. (2008). Discovery of Raltegravir, a potent, selective orally bioavailable HIV-integrase inhibitor for the treatment of HIV-AIDS infection. *Journal of Medicinal Chemistry, 51,* 5843-5855.

Sunderland, C. J., Botta, M., Aime, S., & Raymond, K. N. (2001). 6-carboxamido-5,4-hydroxypyrimidinones: A new class of heterocyclic ligands and their evaluation as gadolinium chelating agents. *Inorganic Chemistry, 40,* 6746-6756.

Taylor, B. S., Sobieszczyk, M. E., McCutchan, F. E., & Hammer, S. M. (2008). Medical progress: The challenge of HIV-1 subtype diversity. *New England Journal of Medicine, 358,* 1590-1602.

Tchertanov, L., Delelis, O., & Mouscadet, J. (2007). Structural and functional insight into molecular recognition of HIV-1 integrase catalytic loop. *Febs Journal, 274,* 260.

Tchertanov, L. & Mouscadet, J. F. (2007). Target recognition by catechols and beta-ketoenols: Potential contribution of hydrogen bonding and Mn/Mg chelation to HIV-1 integrase inhibition. *Journal of Medicinal Chemistry, 50,* 1133-1145.

Thompson, J. D., Higgins, D. G., & Gibson, T. J. (1994). Clustal-W - Improving the Sensitivity of Progressive Multiple Sequence Alignment Through Sequence Weighting, Position-Specific Gap Penalties and Weight Matrix Choice. *Nucleic Acids Research, 22,* 4673-4680.

Thomsen, R. (2003). Flexible ligand docking using evolutionary algorithms: investigating the effects of variation operators and local search hybrids. *Biosystems, 72,* 57-73.

Tilton, J. C. and Doms, R. W. (2010) Entry inhibitors in the treatment of HIV-1 infection. *Antiviral Res. 85(1),* 91-100.

Tripos Inc. (2007). SYBYL 7.2 [Computer software].

Trott, O. & Olson, A. J. (2010). Software News and Update AutoDock Vina: Improving the Speed and Accuracy of Docking with a New Scoring Function, Efficient Optimization, and Multithreading. *Journal of Computational Chemistry, 31,* 455-461.

Tsiang M, Jones GS, Hung M, Samuel D, Novikov N, Mukund S, et al. Dithiothreitol causes HIV-1 integrase dimer dissociation while agents interacting with the integrase dimer interface promote dimer formation. *Biochemistry.* 2011 Mar 15;50(10):1567-81.

Tsiang M, Jones GS, Niedziela-Majka A, Kan E, Lansdon EB, Huang W, Hung M, et al. New Class of HIV-1 Integrase (IN) Inhibitors with a Dual Mode of Action. *Biol Chem.* 2012 Jun 15;287(25):21189-203.

Uchil, P. D. & Mothes, W. (2009). HIV Entry Revisited. *Cell, 137,* 402-404.

Valkov, E., Gupta, S. S., Hare, S., Helander, A., Roversi, P., McClure, M. et al. (2009). Functional and structural characterization of the integrase from the prototype foamy virus. *Nucleic Acids Research, 37,* 243-255.

Van Baelen, K., Van Eygen, V., Rondelez, E., & Stuyver, L. J. (2008). Clade-specific HIV-1 integrase polymorphisms do not reduce raltegravir and elvitegravir phenotypic susceptibility. *Aids, 22,* 1877-1880.

van der Loeff, M. F., Awasana, A. A., Sarge-Njie, R., van der Sande, M., Jaye, A., Sabally, S., Corrah, T., McConkey, S. J., and Whittle, H. C. (2006). Sixteen years of HIV surveillance in a West African research clinic reveals divergent epidemic trends of HIV-1 and HIV-2. *Int.J.Epidemiol. 35(5)*, 1322-1328.

van der Spoel, D., Lindahl, E., Hess, B., Groenhof, G., Mark, A. E., & Berendsen, H. J. (2005). GROMACS: fast, flexible, and free. *J.Comput.Chem., 26,* 1701-1718.

van, D. M. & Bonvin, A. M. (2009). 3D-DART: a DNA structure modelling server. *Nucleic Acids Res., 37,* W235-W239.

van, D. M. & Bonvin, A. M. (2010). Pushing the limits of what is achievable in protein-DNA docking: benchmarking HADDOCK's performance. *Nucleic Acids Res., 38,* 5634-5647.

van, D. M., van Dijk, A. D., Hsu, V., Boelens, R., & Bonvin, A. M. (2006). Information-driven protein-DNA docking using HADDOCK: it is a matter of flexibility. *Nucleic Acids Res., 34,* 3317-3325.

Verdonk, M. L., Cole, J. C., Hartshorn, M. J., Murray, C. W., & Taylor, R. D. (2003). Improved protein-ligand docking using GOLD. *Proteins, 52,* 609-623.

Verkhivker, G. M., Bouzida, D., Gehlhaar, D. K., Rejto, P. A., Arthurs, S., Colson, A. B. et al. (2000). Deciphering common failures in molecular docking of ligand-protein complexes. *J.Comput.Aided Mol.Des, 14,* 731-751.

Wain-Hobson, S., Sonigo, P., Danos, O., Cole, S., & Alizon, M. (1985). Nucleotide sequence of the AIDS virus, LAV. *Cell, 40,* 9-17.

Walker, B. D. & Burton, D. R. (2008). Toward an AIDS vaccine. *Science, 320,* 760-764.

Wang, J. Y., Ling, H., Yang, W., & Craigie, R. (2001). Structure of a two-domain fragment of HIV-1 integrase: implications for domain organization in the intact protein. *EMBO J., 20,* 7333-7343.

Wang, L. D., Liu, C. L., Chen, W. Z., & Wang, C. X. (2005). Constructing HIV-1 integrase tetramer and exploring influences of metal ions on forming integrase-DNA complex. *Biochemical and Biophysical Research Communications, 337,* 313-319.

Wang, W., Donini, O., Reyes, C. M., & Kollman, P. A. (2001). Biomolecular simulations: recent developments in force fields, simulations of enzyme catalysis, protein-ligand, protein-protein, and protein-nucleic acid noncovalent interactions. *Annu.Rev.Biophys.Biomol.Struct., 30,* 211-243.

Weber, W., Demirdjian, H., Lins, R. D., Briggs, J. M., Ferreira, R., & McCammon, J. A. (1998). Brownian and essential dynamics studies of the HIV-1 integrase catalytic domain. *Journal of Biomolecular Structure & Dynamics, 16,* 733-745.

Welch, W., Ruppert, J., & Jain, A. N. (1996). Hammerhead: Fast, fully automated docking of flexible ligands to protein binding sites. *Chemistry & Biology, 3,* 449-462.

Westbrook, J., Feng, Z., Chen, L., Yang, H., & Berman, H. M. (2003). The Protein Data Bank and structural genomics. *Nucleic Acids Res., 31,* 489-491.

Wielens, J., Crosby, I. T., & Chalmers, D. K. (2005). A three-dimensional model of the human immunodeficiency virus type 1 integration complex. *Journal of Computer-Aided Molecular Design, 19,* 301-317.

Wijitkosoom, A., Tonmunphean, S., Truong, T. N., & Hannongbua, S. (2006). Structural and dynamical properties of a full-length HIV-1 integrase: Molecular dynamics simulations. *Journal of Biomolecular Structure & Dynamics, 23,* 613-624.

Williams, S. L. & Essex, J. W. (2009). Study of the Conformational Dynamics of the Catalytic Loop of WT and G140A/G149A HIV-1 Integrase Core Domain Using Reversible Digitally Filtered Molecular Dynamics. *Journal of Chemical Theory and Computation, 5,* 411-421.

Wirden, M., Simon, A., Schneider, L., Tubiana, R., Malet, I., Ait-Mohand, H. et al. (2009). Raltegravir has no residual antiviral activity in vivo against HIV-1 with resistance-associated mutations to this drug. *J.Antimicrob.Chemother., 64,* 1087-1090.

Wong-Staal, F., Shaw, G. M., Hahn, B. H., Salahuddin, S. Z., Popovic, M., Markham, P. et al. (1985). Genomic diversity of human T-lymphotropic virus type III (HTLV-III). *Science, 229,* 759-762.

Xu, J. D., Whisenhunt, D. W., Veeck, A. C., Uhlir, L. C., & Raymond, K. N. (2003). Thorium(IV) complexes of bidentate hydroxypyridinonates. *Inorganic Chemistry, 42,* 2665-2674.

Ye, J. R., Yu, S. Q., Lu, H. Y., Wang, W. S., Xin, R. L., & Zeng, Y. (2012). Genetic diversity of HIV type 1 isolated from newly diagnosed subjects (2006-2007) in Beijing, China. *AIDS Res.Hum.Retroviruses, 28,* 119-123.

Yin, Z. Q. & Craigie, R. (2010). Modeling the HIV-1 Intasome: A Prototype View of the Target of Integrase Inhibitors. *Viruses-Basel, 2,* 2777-2781.

Yoder, K. E. & Bushman, F. D. (2000). Repair of gaps in retroviral DNA integration intermediates. *J.Virol., 74,* 11191-11200.

Zhong, Y. L., Krska, S. W., Zhou, H., Reamer, R. A., Lee, J., Sun, Y. K. et al. (2009). Catalytic Asymmetric Synthesis of an HIV Integrase Inhibitor. *Organic Letters, 11,* 369-372.

Zhu, T., Korber, B. T., Nahmias, A. J., Hooper, E., Sharp, P. M., & Ho, D. D. (1998). An African HIV-1 sequence from 1959 and implications for the origin of the epidemic. *Nature, 391,* 594-597.

Zhuang, L. C., Wai, J. S., Embrey, M. W., Fisher, T. E., Egbertson, M. S., Payne, L. S. et al. (2003). Design and synthesis of 8-hydroxy-[1,6]naphthyridines as novel inhibitors of HIV-1 integrase in vitro and in infected cells. *Journal of Medicinal Chemistry, 46,* 453-456.

APPENDIX

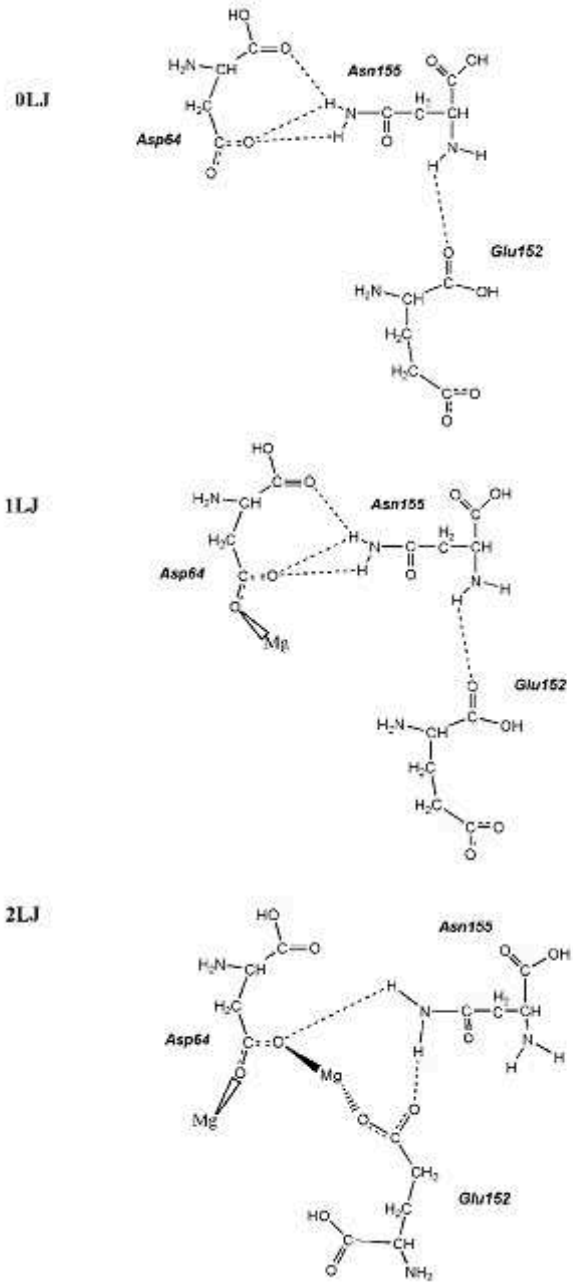

Figure 1: Sketch of N155 H-bonding in 0LJ, 1LJ and 2LJ models.

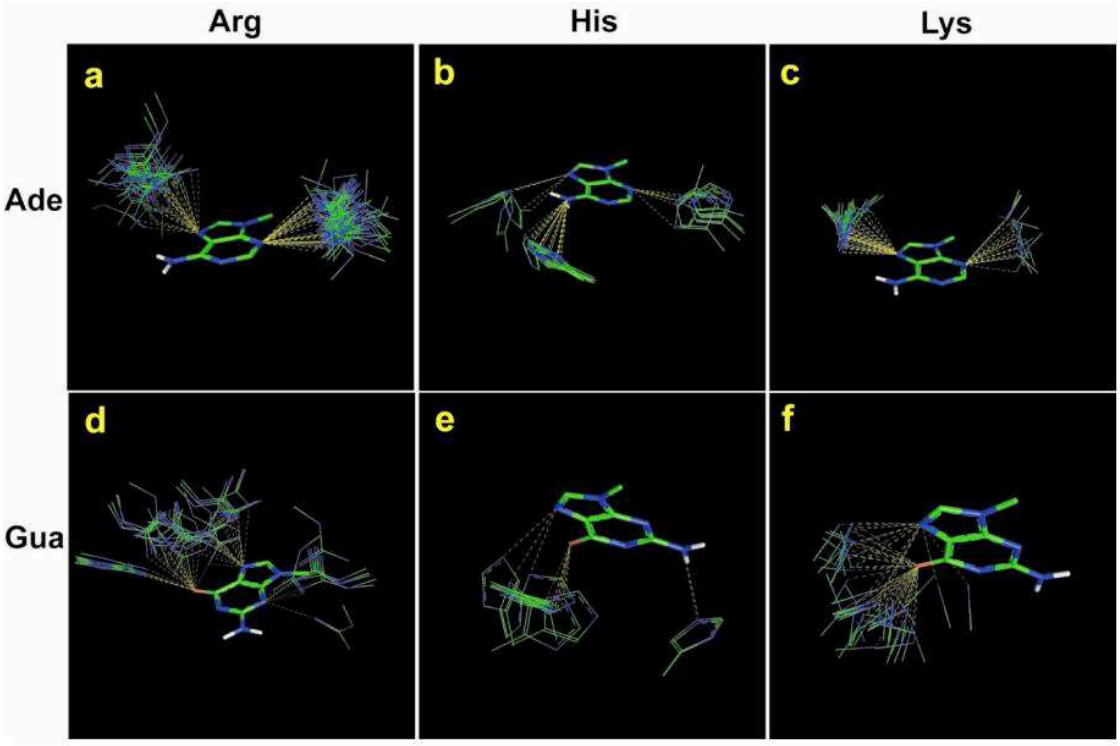

Figure 2: 3D scatterplots of mutated side chains forming H-bonds with DNA bases: (a) R···A; (b) H···A; (c) K···A; (d) R···G; (e) H···G; (f) and K···G. Only groups related to natural amino acids were included in the analysis; guaniduim of R, imidazol of H, and cationic -C-NH3 group of K. The main group (DNA bases), contacting groups (R, H and K) and the H-bonds are shown as sticks, wire frame and dashed lines, respectively.

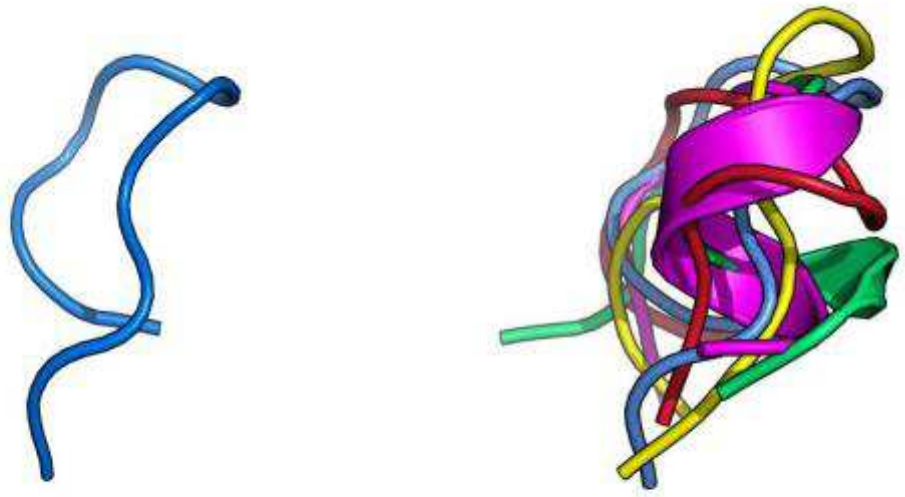

a b

Figure 3: Loop structure modeling with PEP-FOLD (Maupetit, Tuffery, & Derreumaux, 2007). Starting from the amino acid sequence GIPYNPQSQGV the PEP-FOLD runs 50 greedy simulations and gives the lowest energy conformation. A snapshot of all clusters lowest energy solution superimposed to the lowest energy conformation (in blue). This gives an idea of the conformational diversity of analysed polypeptide

Research Article

Journal of Molecular Recognition

Received: 5 February 2009, Revised: 28 May 2009, Accepted: 28 May 2009, Published online in Wiley InterScience: 21 July 2009

(www.interscience.wiley.com) DOI:10.1002/jmr.970

HIV-1 IN alternative molecular recognition of DNA induced by raltegravir resistance mutations

Jean-François Mouscadet[a], Rohit Arora[a], Joseph André[a], Jean-Christophe Lambry[b], Olivier Delelis[a], Isabelle Malet[c], Anne-Geneviève Marcelin[c], Vincent Calvez[c] and Luba Tchertanov[a]*

Virologic failure during treatment with raltegravir, the first effective drug targeting HIV integrase, is associated with two exclusive pathways involving either Q148H/R/K, G140S/A or N155H mutations. We carried out a detailed analysis of the molecular and structural effects of these mutations. We observed no topological change in the integrase core domain, with conservation of a newly identified Ω-shaped hairpin containing the Q148 residue, in particular. In contrast, the mutations greatly altered the specificity of DNA recognition by integrase. The native residues displayed a clear preference for adenine, whereas the mutant residues strongly favored pyrimidines. Raltegravir may bind to N155 and/or Q148 residues as an adenine bioisoster. This may account for the selected mutations impairing raltegravir binding while allowing alternative DNA recognition by integrase. This study opens up new opportunities for the design of integrase inhibitors active against raltegravir-resistant viruses. Copyright © 2009 John Wiley & Sons, Ltd.

Supporting information may be found in the online version of this article.

Keywords: HIV-1 IN; resistance; DNA recognition; modeling; crystallographic database analysis

INTRODUCTION

Integrase (IN) is a key enzyme for HIV-1 replication, catalyzing the integration of reverse transcribed DNA into the host cell genome. This enzyme is therefore an attractive target for antiviral drugs. HIV-1 IN is a 32 kDa protein with three different, independent functional domains (Engelman *et al*., 1993; Katzman and Sudol, 1995). The N-terminal domain (aa 1–49), contains a non-conventional HHCC zinc-finger motif, which promotes the formation of IN tetramers *in vitro* (Cai *et al*., 1997; Eijkelenboom *et al*., 1997), this form being required for strand transfer activity (Heuer and Brown, 1998; Deprez *et al*., 2000; Cherepanov *et al*., 2003). The central core domain (aa 50–212), also known as the catalytic core domain, contains the canonical D,D(35)E motif characteristic of many polynucleotidyl transferases (Engelman *et al*., 1993; Dyda *et al*., 1994). These amino acid residues (Asp64, Asp116, and Glu152) form a divalent metal-binding site, which recognizes cations such as Mg^{2+} and Mn^{2+}. There is considerable experimental evidence to suggest that Mg^{2+} is the more physiologically relevant of these cations, including the much greater specificity of the reaction in the presence of this cation, with IN displaying strong non-specific nuclease activity in the presence of Mn^{2+} (Gao *et al*., 2004). Crystal structures of enzymes containing only one divalent cation have been observed, but, as for other retroviral integrases and according to the proposed mechanism of action of polynucleotidyl transferases, we would expect two metal cations to be required for the formation of an active complex between HIV-1 IN and its DNA target (Wlodawer, 1999). The C-terminal domain (aa 213–288), which displays nonspecific DNA-binding activity, is involved in stabilizing the IN–DNA complex (Lutzke *et al*., 1994; Esposito and Craigie, 1998; Wlodawer, 1999; Gao *et al*., 2001).

IN catalyzes two reactions during retrovirus integration (Brown, 1990; Asante-Appiah and Skalka, 1997; Hindmarsh and Leis, 1999). The first is 3′-processing, during which the terminal GT dinucleotide is cleaved and removed from the 3′-end of each long terminal repeat (LTR), producing a CA 3′-hydroxyl group for nucleophilic attack. This transformation takes place in the cytoplasm of the cell. IN bound to viral DNA (pre-integration complex IN–DNA) is then transported through the nuclear pore into the nucleus, where the second step—strand transfer—occurs. During this second step, IN catalyzes the transfer of both newly exposed 3′ extremities of the vDNA into the host genome. The product of this step is a gapped intermediate in which the 5′-phosphate ends of the vDNA are no longer linked to the 3′-OH ends of the host DNA (hDNA). The integration process is

* *Correspondence to: L. Tchertanov, LBPA, CNRS, Ecole Normale Supérieure de Cachan, 61 Avenue du Président Wilson, 94235 Cachan, France. E-mail: luba.tchertanov@lbpa.ens-cachan.fr*

a *J.-F. Mouscadet, R. Arora, J. André, O. Delelis, L. Tchertanov*
LBPA, CNRS, Ecole Normale Supérieure de Cachan, 61 Avenue du Président Wilson, 94235 Cachan, France

b *J.-C. Lambry*
Laboratoire d'Optique et Biosciences, Ecole Polytechnique, 91128 Palaiseau, France

c *I. Malet, A.-G. Marcelin, V. Calvez*
Laboratoire de Virologie, INSERM U943, Hôpital Pitié-Salpêtrière, Université Pierre et Marie Curie, 75013 Paris, France

Journal of Molecular Recognition

completed by removal of the unpaired dinucleotides from the 5′-ends of the vDNA, filling of the single-strand gaps between viral and target DNA and ligation of the 3′-ends of the vDNA to the 5′-ends of the hDNA (Li *et al*., 2001). Both steps involve the active site of IN, which contains a conserved DDE motif next to the active site flexible loop, comprising residues 140–149. This loop is known to be required for efficient IN function, but its precise role in integration is unknown. The conformational flexibility of the 140–149 loop is thought to be important for the catalytic steps following DNA binding and decreases in loop flexibility have been shown to result in much lower levels of activity (Greenwald *et al*., 1999).

Dimerization is required for the 3′-processing step (Guiot *et al*., 2006; Hayouka *et al*., 2007). By contrast, based on structural considerations, tetrameric IN is thought to be required for the strand transfer step (Faure *et al*., 2005; Wang *et al*., 2005; Li *et al*., 2006). Neither the structure of isolated full-length IN nor that of IN complexed to its DNA substrate have been determined. The available structural data relate to the N-terminal, core, and C-terminal domains separately, or to two-domain fragments, consisting of the catalytic core plus the C-terminal domain or the catalytic core plus the N-terminal domain (reviewed in Chiu and Davies, 2004 and references therein). These data have been used for prediction of the catalytic mechanism, structure-based drug design and the construction of HIV-1 IN models (see Supporting Materials, Table 1**)**. These theoretical models have been used as a platform for the design of antiviral drugs. Several of the reported models represent HIV-1 IN oligomeric structures after 3′-processing and either before or after hDNA binding. Both types of model include a tetrameric IN complex with one or two vDNA fragments (Chen *et al*., 2006; Wang *et al*., 2005) and models including hDNA binding also include IN–vDNA complexed with hDNA (Heuer and Brown, 1998; Gao *et al*., 2001; Podtelezhnikov *et al*., 2003; Karki *et al*., 2004; Wielens *et al*., 2005; Fenollar-Ferrer *et al*., 2008). These models consist of various building blocks (IN units, DNA, cofactor) and represent divergent architectural assemblies constructed with different procedures based on diverse algorithms, with different partial crystallographic structures as templates and the imposition of experimentally observed constraints. Experimental studies of IN–DNA complexes have been hindered by the poor solubility of the protein *in vitro*. One strategy used to overcome this problem involves the assembly of IN derivatives with DNA three-way junction substrates. Electron microscopy (EM) and single-particle image analysis have been used to characterize the 3D structure of IN–DNA complex at ~27 Å resolution (Ren *et al*., 2007). Single-particle image analysis has been used to characterize a stable and functional complex between the wild-type full-length IN and the cellular cofactor LEDGF/p75 in the presence of DNA (Michel *et al*., 2009). In both studies, the complexes were found to be asymmetric, a feature not previously considered in structural models of IN–DNA.

The active site of HIV-1 IN and its role in the catalytic process have been key areas of study in biochemical and structural research. By contrast, little is known about the loop, which encompasses residues 140–149 and forms the boundary of the active site. Only limited, ambiguous structural data are available for this region. The loop has been shown to be highly disordered in most crystallographic structures of IN. A few studies have reported a partially resolved loop, and IN catalytic core domains with a complete loop have been described for only five structures (1BI4, 1BL3 (Maignan *et al*., 1998), 1BIS (Goldgur *et al*., 1998), 2ITG (Bujacz *et al*., 1996), and 1B9F (Greenwald *et al*., 1999)). These structures are those of single mutants (F185H in 1BL3, 1BI4, and 2ITG), double mutants (W131E/F185K in 1BIS) or triple mutants (G140A/G149A/F185K in 1B9F). Major differences have been observed between the conformations of the catalytic loop in structures in which it is ordered.

Structural data relate to the protein in a static state and provide no time-dependent information about conformational flexibility. Molecular dynamics (MD) simulations are therefore required to obtain additional information about protein mobility. It has been demonstrated for the simplest catalytic domain model that the 140–149 loop moves like a gate, opening and closing the catalytic site (Weber *et al*., 1998). A significant conformational change, involving the catalytic site loop and the E152 residue of the DDE motif, has been shown to occur when a second metal ion is included (Lins *et al*., 2000a, b). The dynamic behavior of the HIV-1 IN catalytic domain has been described for the wild-type (WT) enzyme (Lins *et al*., 1999), for the T66I/M154I (Brigo *et al*., 2005) and G140A/G149A (Lee *et al*., 2005) mutants; and for the enzyme alone and complexed with the inhibitor 5CITEP (Nunthaboot *et al*., 2007a, b). These MD studies showed that significant, and apparently important conformational interactions occur in the active site. They also demonstrate the importance of the flexibility of the 140–149 loop for catalysis, but not for substrate recognition. Subsequent studies of the dynamic behavior of the 140–149 loop as a function of the presence/absence of the vDNA demonstrated that interactions with DNA induced an increase in the degree of folding of the protein structure (De Luca *et al*., 2005).

Interest in the catalytic site loop has recently increased, with the emergence of Q148R/K/H and G140S mutations in the loop or of N155H mutations in the catalytic site being linked to the development of resistance to raltegravir (RAL), the first efficient IN inhibitor to be identified in clinical practice (Charpentier *et al*., 2008; Cooper *et al*., 2008; Kobayashi *et al*., 2008; Malet *et al*., 2008; Myers and Pillay, 2008). We investigated the impact of the resistance mutations selected by RAL, by comparing the structural and DNA recognition properties of the WT and RAL-resistant HIV-1 IN catalytic core domain. We carried out an exhaustive *in silico* study of the impact of RAL-selected mutations on IN structure. Secondary structure and substructure folding predictions, 3D modeling of the catalytic core domain architecture and comparisons of the DNA base recognition properties of WT and mutant proteins provided insight into the potential mechanisms of action of raltegravir against integrase and a possible explanation for the two alternative pathways of RAL-selected mutations.

METHODS

All calculations were carried out on a PC running RedHat Enterprise Linux5. The PDB (Berman *et al*., 2000) and IsoStar (v2.0) (Bruno *et al*., 1997) databases were used. Modeling was performed with SYBYL (version 7.3) software (Tripos Inc., 2007). The *ab initio* 3D structure of the 10-residue GIPYNPQSQGV polypeptide was generated with the PEP-FOLD approach (Maupetit *et al*., 2007). Figures were produced with Benchware 3D Explorer (Tripos Inc., 2008) and PyMol (DeLano, 2002).

Secondary structure analysis

Secondary structure assignment for the 1BL3 (Maignan *et al*., 1998) (chain C) structure was achieved with the DSSP (Kabsch and Sander, 1983) and Stride (Frishman and Argos, 1995) approaches

(see Supporting Materials, Figure S1). The secondary structures of the WT and mutated HIV-1 IN were predicted with GORV (Garnier *et al.*, 1996; Sen *et al.*, 2005), on the basis of a combination of amino acid frequencies with information theory and Bayesian statistics, and JPRED (Sen *et al.*, 2005; Cole *et al.*, 2008), a method combining multiple neutral networks. The Thornton method was used to predict tight turns as supersecondary structures of the loop (Thornton *et al.*, 1988; De la Cruz *et al.*, 2002).

Molecular modeling

Wild-type IN models

3D models of the WT IN core domain representing cation-free, one- and two-Mg^{2+} active sites were generated as follows: (i) X-ray data for 1BI4 and 1BL3 were chosen as the initial templates (Maignan *et al.*, 1998); crystal structures represent the F185H mutant; for the WT model, H185 was replaced by F. (ii) In two-cation models, the second Mg^{2+} ion was inserted at the catalytic residues D64 and E152, as described for the two-cation structure of 1VSH (Bujacz *et al.*, 1997). In two-cation models, D64 was considered to act as a ligand bridging the two metals, and was referred to as a "μ-bridge" (Cotton and Wilkinson, 1999), whereas D116 and E152 were monodentate, bidentate or mixed. (iii) Coordination spheres of the Mg cations were completed with water molecules to give octahedral coordination, as suggested by structural data for CSD (Allen, 2002). In all the models considered, one water molecule was fixed between two Mg^{2+} cations, forming a second bridge of the μ-aqua type (aqua referring here to the nature of the second bridging group). (iv) Residues 143–148 were deleted from X-ray structures and the 3D structure of the loop was reconstituted with two different modeling protocols: a loop-generating algorithm based on database searches known as Protein Loop Search (Sybyl), and *ab initio* loop generation with PEP-FOLD. The candidates identified by Protein Loop Search were compared with the lowest energy solution for peptide structures generated with PEP-FOLD (see Supporting Materials, Figure S2). The loop yielding the best solution with both methods was inserted into the target molecule and the coordinates of the fragment atoms were transformed according to the fragment least-squares fit to anchor regions. (v) H-atoms were added with the Biopolymer and Build/Edit options (SYBYL). The models generated, corresponding to different active site structures, were denoted as **0LJ**, **1LJ**, **2LJ**, **3LJ**, **4LJ**, and **5LJ** (Figure 1).

Mutated IN models

3D models of raltegravir-selected mutants were built by individual amino acid substitutions, using models **1LJ** and **2LJ**. We considered the single amino acid substitutions resulting from the E138K and N155H point mutations, and the multiple substitutions for the catalytic loop residues, giving the following combinations: **R0** (N155H/Q148/G140/E138), **R1** (N155/Q148H/G140S/E138K), **R2** (N155/Q148K/ G140S/E138K), **R3** (N155/Q148R/G140S/E138K), **R4**(N155/Q148H/G140A/E138K), **R5** (N155/Q148K/G140A/E138K), and **R6** (N155/Q148R/G140A/E138K). N155H and Q148H mutant models were generated taking into account the annular tautomerism of histidine ($N^{\delta 1}$–H and $N^{\varepsilon 2}$–H tautomeric forms) and their different orientations, with protonated nitrogen (H-donor nitrogen) directed toward the catalytic site or in the opposite direction.

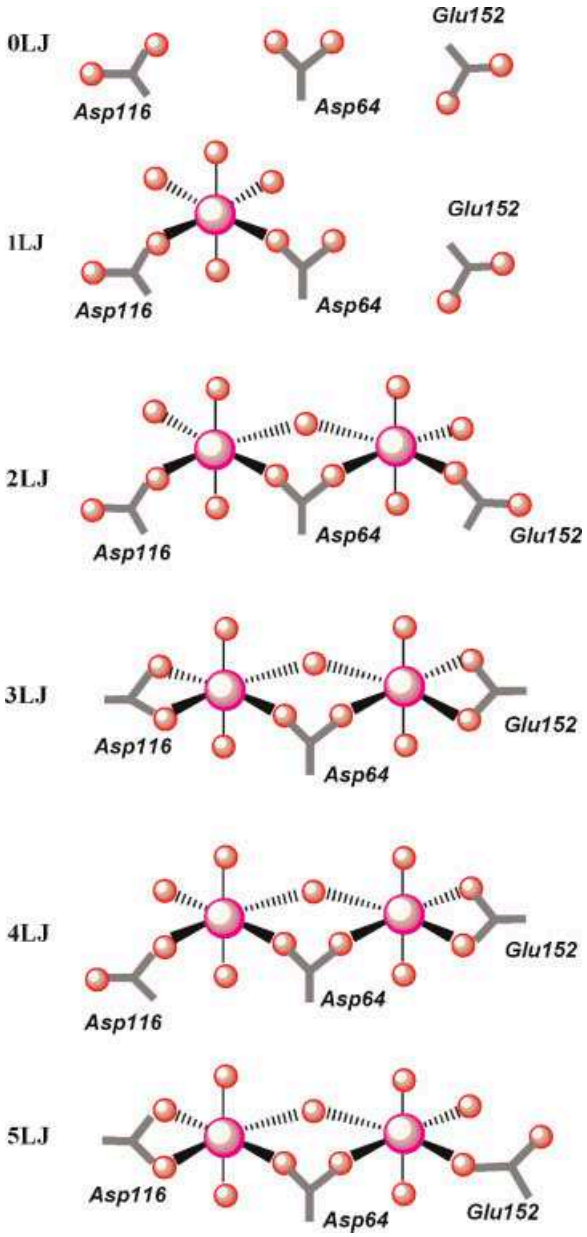

Figure 1. Constructed models of the core domain of IN with no cation (**0LJ**), one (**1LJ**), or two Mg^{2+} cations (**2LJ**–**5LJ**). In **2LJ** and **3LJ**, the binuclear Mg^{2+} cluster was symmetric, with each Mg^{2+} coordinated with D116 and E152 in either the monodentate (**2LJ**) or the bidendate (**3LJ**) mode. In **4LJ** and **5LJ**, the binuclear Mg^{2+} cluster was asymmetric; each Mg^{2+} cation was coordinated with D116 and E152 in either mono- or bidentate mode.

Model minimizations

The Simplex method was used for the initial optimization. Energy minimization of the wild-type and "mutated" promodels was performed with the Powell algorithm and Amber/Kollman atom–atom force field, for 10 000 steps, or if the energy gradient was lower than 0.005 kcal/mol Å. The following parameters were used: a dielectric constant of 1, a minimization step of 0.001, a scaling factor of 1, an H-bond radius scaling of 0.7 and the non-bonded interaction list was set to 8 Å. Constraints were defined between Mg^{2+} ions and the coordinating oxygen atoms,

based on the data for CSD data (Allen, 2002). The stereochemical quality of the models was assessed with ProTable Procheck (Laskowski *et al*., 1993), which showed that more than 97% of the non-glycine residues in all models had dihedral angles in the most favored and allowed regions of the Ramachandran plot, consistent with high model quality. The overall folding of the mutant proteins was similar to that of the WT protein and the RMSD coordinate difference between WT and mutant proteins was small (0.6 Å) for the common C_α atoms.

Simulations of the movement of the 140–149 loop towards the catalytic site

Simulations of 140–149 loop movement were carried out with the one- (**1LJ**) and two-cation (**2LJ**) models for WT and mutated IN. We compared the total energy and conformation of intermediate states by carrying out energy minimization for the protein structures of the IN models, with different distances between two centroids: C1, describing the center of gravity of the Ω-shaped hairpin and C2, corresponding to the center of gravity of the active site. The movement was simulated in 2 Å steps, extending from 16 (open form) to 4.5 Å (closed form) for both models, **1LJ** and **2LJ**.

Characterization of the interaction of the side-chain and DNA base

We investigated two types of molecular complex deposited in the PDB, for analyses of side chain-DNA base interactions: (i) protein/DNA complexes and (ii) protein–ligand complexes with nucleic acid bases as the ligands. The protein/DNA complexes were analyzed for H-bonding and van der Waals contacts, using the "Atlas of Protein Side-Chain Interactions" (Singh and Thornton, 1992). The number of contacts identified between the loop side chains and DNA bases were represented graphically as superimposed diagrams of H-bonds and van der Waals contacts. H-bonding between amino acid 148 or 155 and DNA bases was characterized in details with IsoStar 2.0 (Bruno *et al*., 1997). Data extracted from X-ray structures (resolution $>$ 2.0 Å) of protein–ligand complexes (nucleic acid bases as ligands) are presented as scatterplots, showing the distribution of a contact group (side chain) around a specified central group (DNA base). Groups with chemical functions found in natural amino acids were included in the analysis. Carbamoyl is a functional group of N and Q, guaniduim is a functional group of R, imidazol is a functional group of H, and the cationic $-C-NH_3$ group is a functional group of K. The ionization states of acidic and basic groups could not be determined unambiguously from protein structures. These groups were combined for PDB-based plots. The primary IsoStar scatterplots were stored in a modeling format, *mol2*, and used for further analysis. For these data only, interactions were considered for distances up to 3.4 Å (van der Waals overlaps) and contacting groups involved in π–π interactions were excluded from the analysis. The H-atoms of groups involved in H-bonding were placed in normalized positions. The resulting 3D distributions of side-chain-like fragments around the individual bases were superimposed to represent the A–T and G–C base-pair environment.

RESULTS

Evidence for a stable hairpin in the catalytic loop

We began by carrying out secondary structure assignment for the 1BL3 (chain C) structure with SCOP and DSSP, comparing the results obtained with previous interpretations (see Supporting Materials, Figure S1). The two methods predicted a similar fold for residues 140–149, but this fold was different from that previously reported (Maignan *et al*., 1998). We then used the complete (47–212 aa) and partial sequences (140–151 aa) of WT and mutant IN to predict the 2D structure (helix, strand, and coil) and substructural motifs (γ-, β-, α-, π-turns and hairpins; see the Methods section). Secondary structure prediction confirmed the presence of a coil domain extending from residue 140 to residue 149. Substructural motifs within the loop were indicative of a hairpin with a three-residue turn stabilized twice by $i \rightarrow i \pm 4$ H-bonding involving the N144 and Q148 backbone (Figure 2a(i)). This turn, connecting the helix to the β-sheet, corresponds to the "α–β-arch" described by Efimov (Efimov, 1993a, b) as a standard structure in proteins. Thus, structure-based assignment and sequence-based 2D prediction both suggested that the catalytic active site loop contained two distinct structures: a random coil formed by the highly hydrophobic residues in positions 140–143 and a hairpin composed mostly of the hydrophilic amino acids in positions 144–148, stabilized by double across-loop backbone–backbone H-bonds. The G140A/S and Q148H/R/K mutations did not affect this structure (Figure 2a(ii)). The 3D structure of the loop was built with two independent algorithms: a loop search based on structural data from PDB (a knowledge-based method) and *ab initio* loop generation (conformational search). Both methods identified a loop with a similar supersecondary local structural motif: a hairpin with an Ω-shaped body stabilized by the pair of backbone–backbone and three backbone–sidechain H-bond interactions, shaped like a doughnut and covering an area of 40–44 Å (Figure 2d) (Tchertanov *et al*., 2007). This loop was recently identified in the IN/DNA complex structure, but no specific structure was discussed (Chen *et al*., 2008).

The formation of this hairpin is due to the presence of N, Q, S, G, and P, matching statistical preferences for amino acid type within particular turns (Levitt and Warshel, 1975; Hutchinson and Thornton, 1994). G and P are characteristic of reverse turns, as they confer conformational flexibility and cannot form hydrogen bonds. The importance of loops has been confirmed experimentally. Many enzymes use flexible loops that change conformation upon substrate binding to form a catalytically competent active site. Indeed, 57% of catalytic residues are located in or close to such loops (Dr P. Aloy, personal communication). Ω–loops constitute a relatively new category of secondary structures (Leszczynski and Rose, 1986; Fetrow, 1995; Street *et al*., 2007) and appear to be important for substrate or inhibitor binding and/or protein–protein recognition (Strobel and Ryder, 2001).

Modeling of the catalytic site structure of the HIV-1 integrase

According to X-ray structure data, Mg^{2+}, coordinated by D64 and D116, does not affect the conformation of the catalytic loop (Maignan *et al*., 1998). A second Mg^{2+} ion would be likely to enter the site upon movement of the E152 side chain toward the active site. However, this does not appear to alter the conformation of the loop (Savarino, 2007). Conversely, MD simulation demonstrated a significant conformational change involving the catalytic loop and E152 of the DDE motif in the presence of the second cation (Lins *et al*., 2000b). This conformational change occurred earlier in the simulation, when hydrogen phosphate was included to mimic DNA, suggesting that the binding of

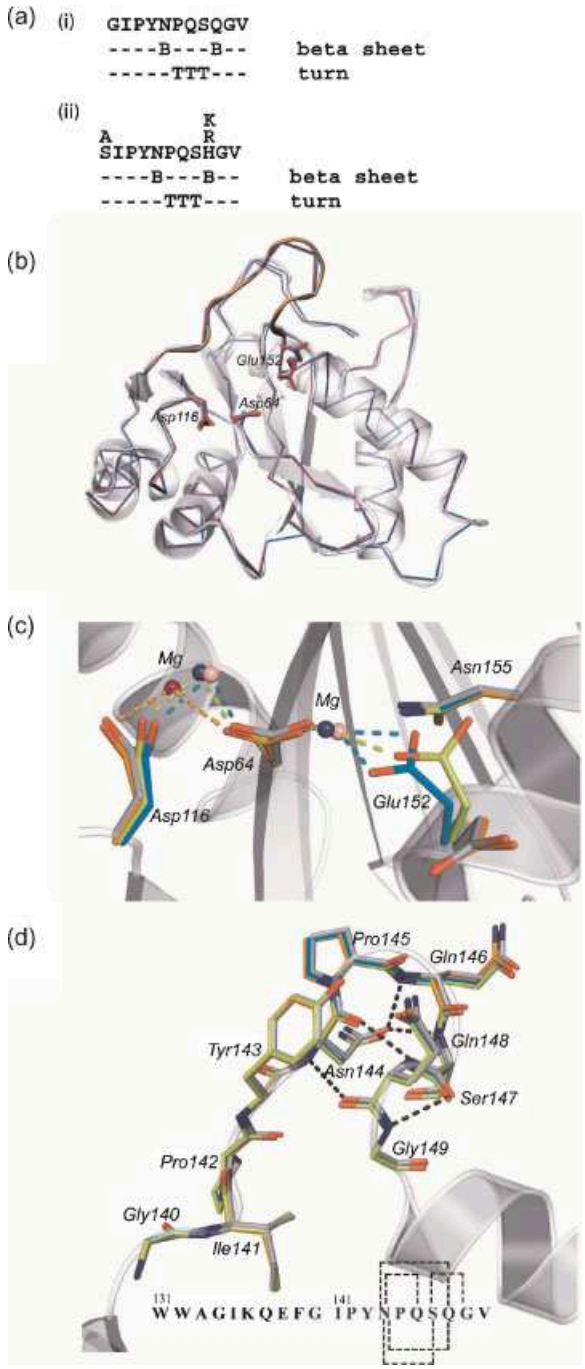

Figure 2. Structure of the HIV-1 IN core domain: (a) 2D prediction of the wild-type (i) and mutated (ii) loop of IN comprising residues 140–149. The first line represents the amino acid sequence; the second line represents the beta sheet stabilized by H-bonding and the third line indicates the turn state per residue. (b) Superimposition of the **0LJ**, **1LJ**, **2LJ** and **4LJ** (the wild-type IN) 3D models generated. Ribbon diagram, with the backbone and catalytic amino acid side chains shown as sticks; Mg^{2+} ions are not shown. (c) Active site: side chains of catalytic amino acids and Mg^{2+} cations shown as sticks and balls, respectively; coordination distances shown as dashed lines. Colors: gray (**0LJ**), orange (**1LJ**), yellow (**2LJ**) and green (**4LJ**). (d) Top: Catalytic loop structure; residues are shown as sticks, H-bonds as dashed lines. Colors: gray (**0LJ**), orange (**1LJ**), yellow (**2LJ**) and green (**4LJ**). Bottom: H-bonding patterns of the HIV-1 IN 131–149 domain observed in 3-D models. The residues 140–149 are shown in blue. H-bonds between the residues are shown by dashed lines.

the second cation and the resulting conformational change occurred upon DNA binding. We investigated the effect of the metal cofactor further, by constructing models of the core domain with no cation (**0LJ**), one (**1LJ**) or two Mg^{2+} cations (**2LJ**–**5LJ**), starting from the 1BI4 and 1BL3 templates, as described in the Methods section (Figure 1). In the **2LJ** and **3LJ** models, the binuclear Mg^{2+} cluster was symmetric, with each Mg^{2+} ion coordinated by the D116 and E152 residues in either a monodentate (**2LJ**) or a bidentate (**3LJ**) mode. In the **4LJ** and **5LJ** models, the binuclear Mg^{2+} cluster was asymmetric, with each Mg^{2+} cation coordinated by D116 and E152 in either a mono- or bidentate mode. All the 3D models had similar topologies (Figure 2b). The first two models, **0LJ** and **1LJ**, did not differ from their templates: Mg^{2+} was coordinated by D64 and D116 and the other positions were occupied by water molecules, constituting *pseudo*-octahedral Mg coordination. The other models had a binuclear Mg^{2+} core with two non-identical bridges, the D64, and the μ-aqua bridge, with the water molecule bridging the gap between the two coordination centers. These binuclear models differed in the mode of chelation of D116 and E152. Based on the total energy values of the complexes modeled, the **3LJ** and **5LJ** models were excluded from further analysis due to their low probability.

D64 and water stabilize the binuclear complex, with a Mg ··· Mg distance of 4.2 Å for both the **2LJ** and **4LJ** models. This distance is slightly smaller than the equivalent distance in the 1SA model (4.5 Å)(Savarino, 2007) and greater than that in the 1WKN model (3.9 Å)(De Luca *et al.*, 2005). All side chains of the catalytic amino acids involved in coordination are in a *cis*-position relative to the Mg ··· Mg axis, with E152 arranged in the equatorial and D116 in the axial position (Figure 2c). In two-cation models, the D64 carboxylate group was rotated by about 30° relative to the Mg ··· O ··· Mg plane, corresponding to the D64 configuration in the cation-free and one-cation models. Thus, the conformation of bridged D64 was not affected by the second Mg^{2+}. By contrast, the binding of the second Mg^{2+} ion required a major change in the conformation of the E152 side chains: the Chi1, Chi2, and Chi3 angles were −167, 169, and −3° in 1LJ and −174, 58, and 56° in 2LJ models. The binding of the second cation also required a slight alteration to both the D116 side chain and the first Mg^{2+} ion relative to its position in the one-cation model. Two modes of Mg coordination by E152 were possible (monodentate for **2LJ** and mixed for **4LJ**), but the type of coordination had no significant effect on the two-cation model. Finally, the Mg^{2+} ··· O distances corresponded to typical coordination bonds in Mg-containing complexes. Based on the covalent and ionic radii of the Mg and O atoms, the chelation of Mg^{2+} was essentially ionic.

The N155 residue, in the α4 helix, is a primary site of mutation leading to raltegravir resistance. The position and orientation of N155 relative to D64 favors $-(NH_2)_{N155} \cdots O{=}_{D64}$ H-bonding (see Supporting Materials, Figure S3). In cation-free and one-cation models, this H-bond was bifurcated and involved both H atoms of the 155 NH_2 group, which was also H-bonded to a carbonyl oxygen atom of the D64 backbone. Only the $N{-}H_{N155} \cdots O{=}_{E152}$ backbone–backbone interaction was involved in stabilizing the α4 helix, the distances between the N155 and E152 side chains being greater than for van der Waals (VdW) contacts. In the two-cation model, the E152 residue complexed with Mg^{2+} is oriented in a position favoring H-bonding with N155. Consequently—unlike the H-bonding involving two partners in cation-free and one-cation models—a three-partner H-bond is

Journal of Molecular Recognition

formed in the two-cation model, with $(NH_2)_{N155}$ as a donor and two oxygen atoms of the carboxylate groups of D64 and E152 as the acceptors.

Thus, in all models, the active site was stabilized by both metal coordination and H-bonding involving catalytic residues. We tried to identify the most probable configuration of D64, E152, and N155 side chains in wild-type IN, by carrying out a statistical analysis of the relative configuration of D, E, and N residues on the basis of reported X-ray structures. We found that the orientation of D64, E152, and N155 in the two-cation models corresponded to the more populated N–D and N–E distributions, whereas the N–E orientation in cation-free and one-cation models was less probable (see Supporting Materials, Figure S4). These statistical observations are thus consistent with our two-cation model (**2JL**) for the structure of the IN active site, supporting the validity of our model. Our models demonstrate that Mg^{2+} cations do not alter the structure of the catalytic core domain. The catalytic loop retained its structure, with the distinctive H-bond pattern of the Ω-shaped hairpin observed for all models generated (Figure 2d).

Effect of raltegravir-selected mutations on core domain structure

We then investigated the effect of the mutations selected by RAL and belonging to the independent N155 and Q148 pathways identified in previous studies (Charpentier *et al*., 2008; Cooper *et al*., 2008; Malet *et al*., 2008). The Q148 pathway is characterized by the presence of G140S or E138K secondary mutations.

We first investigated the effect on structure of the N155H mutation affecting a residue in the catalytic site. We chose to study the N155H substitution because the imidazole side chain of histidine, if uncharged, may exist in either the $N^{\delta1}$–H or the $N^{\varepsilon2}$–H tautomeric form (at pH 7, the $N^{\varepsilon2}$–H predominates). We generated mutated models for both H-donor orientations, with the protonated N pointing either towards the catalytic site or in the opposite direction. The two tautomeric forms of histidine in both orientations led to local reorganization of the structure of the active site (Figure 3a–c). Conformations differed most between models with the same tautomers oriented differently, stabilized by different patterns of H-bonding. In one-cation models, the $N^{\varepsilon2}$–H tautomer with the H-atom pointing toward the active site was stabilized by $N{-}H_{H155} \cdots O{=}_{D64}$, with O= corresponding to the oxygen atom of the carboxylate group, as observed in the wild-type structure. However, for stabilization of the active site with the $N^{\varepsilon2}$–H tautomer in the opposite orientation, O= was the backbone atom. The conformation of $N^{\delta1}$–H was not influenced by H-bonding in the one-cation model, whereas, in the two-cation model, this tautomer with N–H pointing towards the active site was stabilized by H-bonding with the E152 side chain (Figure 3b and c). We conclude that the active

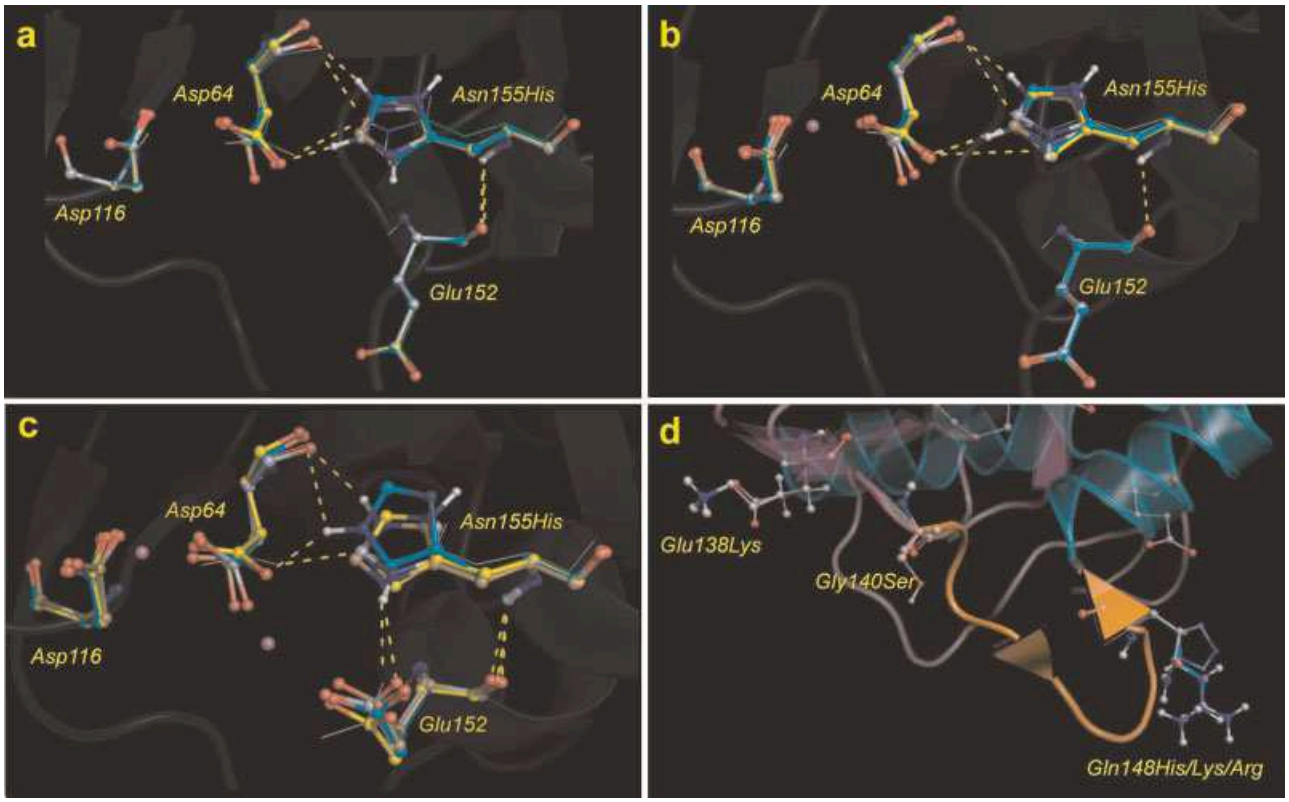

Figure 3. Superimposition of the wild-type and mutated models of the HIV-1 IN in (a) cation-free, (b) one- and (c) two-cation active sites. Molecular display style: enzyme structures shown by ribbons, residues D64, D116, E152 and H155 shown as ball-and-stick representations; the Mg^{2+} cation in (b) and in (c) shown as a ball. The wild-type N155 residue is shown as a wire frame. The mutant H155 is shown as a ball-and-stick representation in the following colors: the $N^{\delta1}$–H tautomer oriented toward the catalytic site is shown in cyan and that in the opposite direction is shown in sand brown; the $N^{\varepsilon2}$–H tautomer oriented toward the catalytic site is shown in light blue and that oriented in the opposite direction is shown in yellow. The H-bonds are indicated as dashed lines. (d) Ribbon diagram of the catalytic loop comprising residues 140–149 in the wild-type and mutated models, with residues 140 and 148 presented as ball-and-stick representations. Non-polar H atoms have been omitted.

site structure may be conserved in the N155H mutant at physiological pH and, in this case, the $N^{\varepsilon 2}$–H tautomer of histidine acts as a conformational bioisoster of asparagine.

We then studied six representative combinations of mutations including primary and secondary mutations of the Q148 resistance pathway. Three-dimensional models were generated from the **1LJ** and **2LJ** templates (see the Methods section). The E138K, G140S/A and Q148H/K/R mutations only slightly modified the side-chain conformation, and the catalytic loop backbone retained its structure (Figure 3d). The H-bond patterns stabilizing the Ω-shaped hairpin in the mutants were similar to that in the wild-type IN. This finding is consistent with our substructural motif predictions.

Consequently, our results suggest that the two primary pathways implicated in raltegravir resistance—the N155H substitution or replacement of the Q148 residue by H, R, or K—result in the retention of all the structural features of the catalytic domain of IN, unlike deleterious G140A/G149A mutations, which are thought to cause structural changes (Greenwald *et al*., 1999). These findings highlight the importance of maintaining the integrity of the catalytic domain structure, consistent with the observation that the virus selects mutations resulting in the maintenance of catalytic activity (Delelis *et al*., 2009). They also suggest that the Ω-shaped hairpin may have a crucial function.

Model of the displacement of the Ω-shaped hairpin toward the catalytic site

The stabilization of the Ω-shaped hairpin by the formation of multiple H-bonds suggests that the previously reported flexibility of the 140–149 loop may be limited. We investigated the behavior of the Ω-shaped hairpin through simulations of loop motion in one- (**1LJ**) and two-cation (**2LJ**) models. The distance between two centroids—the first of which (C1) describes the center of gravity of the Ω-shaped hairpin and the second (C2), the center of gravity of the active site—gradually decreased, in 2 Å steps, from 16 (open form) to 4.5 Å (closed form). Energy minimization was carried out after every step. The conformation of the backbone of the catalytic core domain did not change significantly during this process, but regular movements of the Ω-hairpin loop towards the catalytic site were observed (Figure 4a). The total energy of all intermediate structures was similar for distances between 16 and 8 Å, for both models. Structural fitness, as estimated by the violation values, satisfied constraints for $10 < C1 \cdots C2 < 16$ Å, but showed a weak violation of constraints for $4.5 < C1 \cdots C2 < 8$ Å in the one-cation model (Figure 4b). In the two-cation model, the movement of the hairpin satisfied violation criteria for $8 < C1 \cdots C2 < 16$ Å, but further decreases in $C1 \cdots C2$ distance down to 6 or 4.5 Å led to strong violation. However, G140A/S mutants displayed lower levels of hairpin mobility than the wild type. The G140S mutant, in particular, had total energy and violation values 10–30% higher than those for the wild type.

We have shown that the hairpin can move, as a rigid body, in a gate-like manner toward the active site. Both extremities of the catalytic loop comprised by residues 140–149 are delimited by glycine residues, conferring conformational flexibility on the polypeptide chain, by acting as a hinge, as previously suggested (Chen *et al*., 2008). However, the steric constraints of the Ω-hairpin in the catalytic loop differed between the left and right

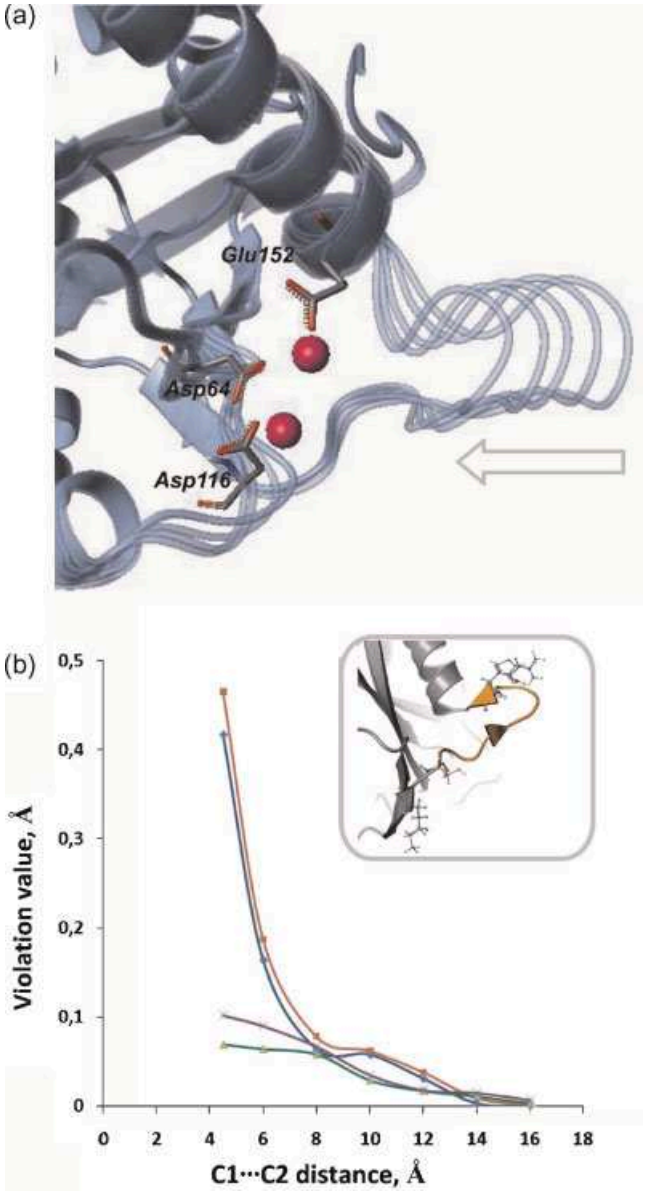

Figure 4. Model of displacement of the Ω-shaped hairpin toward the catalytic site: (a) Superimposition of the HIV-1 IN models (two-cation active site) with the hairpin moved toward the active site, from 16 to 4.5 Å. (b) Violation values for distances of 16–4.5 Å for one-cation models, wild-type (green) and the G140S mutant (violet) and for two cation-model, wild-type (blue), and G140S mutant (red). The Ω-shaped hairpin is shown in the inset.

sides. On the left, the 140–143 stretch of amino acids forms a random coiled structure with few steric constraints. The C-terminus of the Ω-hairpin is subject to greater constraints due to the α-helix connected to the end of the loop.

Intermolecular interactions involving the raltegravir-selected mutated residues

The modification of both hairpin composition and potential motion associated with these mutations may change the DNA recognition properties of the enzyme. We compared the recognition properties of amino acids in the WT and mutated

Journal of Molecular Recognition

IN. We focused on the non-covalent interactions underlying the recognition properties of the residues at positions 155 and 148, corresponding to the primary mutations selected by raltegravir. Based on the known structures of protein/DNA complexes, we assessed the statistical probability of these residues recognizing DNA bases (see the Methods section). We found that asparagine (N) and glutamine (Q) residues preferentially recognized adenine, as H-bonds formed with this base represented a significant non-random cluster, whereas the H-bonds formed with cytosine, guanine, and thymine followed a random distribution. The replacement of the N residue in position 155 by an H residue led to the loss of H-bonding with adenine (A), thymine (T), and cytosine (C) (Figure 5). The replacement of Q148 by a histidine (H) residue had a similar effect, whereas its replacement with a lysine (K) or arginine (R) residue strongly favored interactions with guanine (G), A, and T. Finally, although van der Waals (VdW) contacts are not generally affected by sequence specificity, substitutions resulting in an H residue replacing Q148 or N155 also resulted in a complete loss of VdW contacts with adenine.

3D maps of H-bonding between residues 148 and 155 and DNA bases

We investigated further the DNA recognition properties of the IN residues implicated in RAL resistance, by characterizing in detail the H-bonding between residues 148 and 155 and DNA bases, in particular. We used an IsoStar library, making it possible to construct 3D profiles describing the spatial orientation of non-covalently interacting partners (see the Methods section). This library provides access to information about the preferences of these amino acids for interaction with particular DNA bases and the geometry of non-covalent interactions. Despite the lack of one-to-one specificity, proteins have been shown to discriminate between A and G, suggesting that they favor a particular amino acid–base pair (Luscombe *et al*., 2001; Luscombe and Thornton, 2002; Cheng *et al*., 2003): for instance, R, K, serine (S), and H interact preferentially with guanine, whereas aspartate (D) and glutamate (E) interact preferentially with adenine.

The profiles of single unpaired bases were characterized, to construct 3D profiles of the groups around the DNA base pairs potentially involved in IN/DNA interactions. The 3D distribution and spatial organization of the side-chain fragments surrounding DNA bases were constructed, recapitulating the overall geometry of the DNA bases, and their statistically observed interactions via the major and minor grooves. The potential hydrogen-bonding sites of bases and the 3D profiles of H-bonding patterns involved in binding between DNA bases and the side chains of Q (Q148), N (N155), and R (Q148R) are shown in Figure 6.

N155 and Q148

Most of the carbamoyl moieties common to N and Q and found in contact with adenine formed a dense, highly populated cluster in the major groove (91% of all interacting groups), whereas a small number of groups interacting with adenine were observed in the minor groove (Figure 6a and b). Moreover, most of the carbamoyl groups (67% of all interacting fragments) in the major groove were coplanar with adenine and formed a pair of strong, directional H-bonds with N^7 and N^6H_2 in this base (Figure 6a). Other carbamoyl groups formed only one H-bond with adenine, with either $N^6{-}H_2$ or N^7 (Figure 6b). The N/Q side chains in contact with adenine through the minor groove formed moderately strong non-linear H-bonds, $NH_2 \cdots N^3$. Similarly, most of the carbamoyl groups contacting guanine bases (94%) clustered in the major groove (Figure 6f and g). Nevertheless, all contacts were single H-bonds, with either N^7 or O^6 acceptors, positioned outside the guanine plane, at a dihedral angle of 45°. Very few occurrences of H-bonded carbamoyl-guanine ($N^2H_2 \cdots O{=}$) contacts were observed in the minor groove.

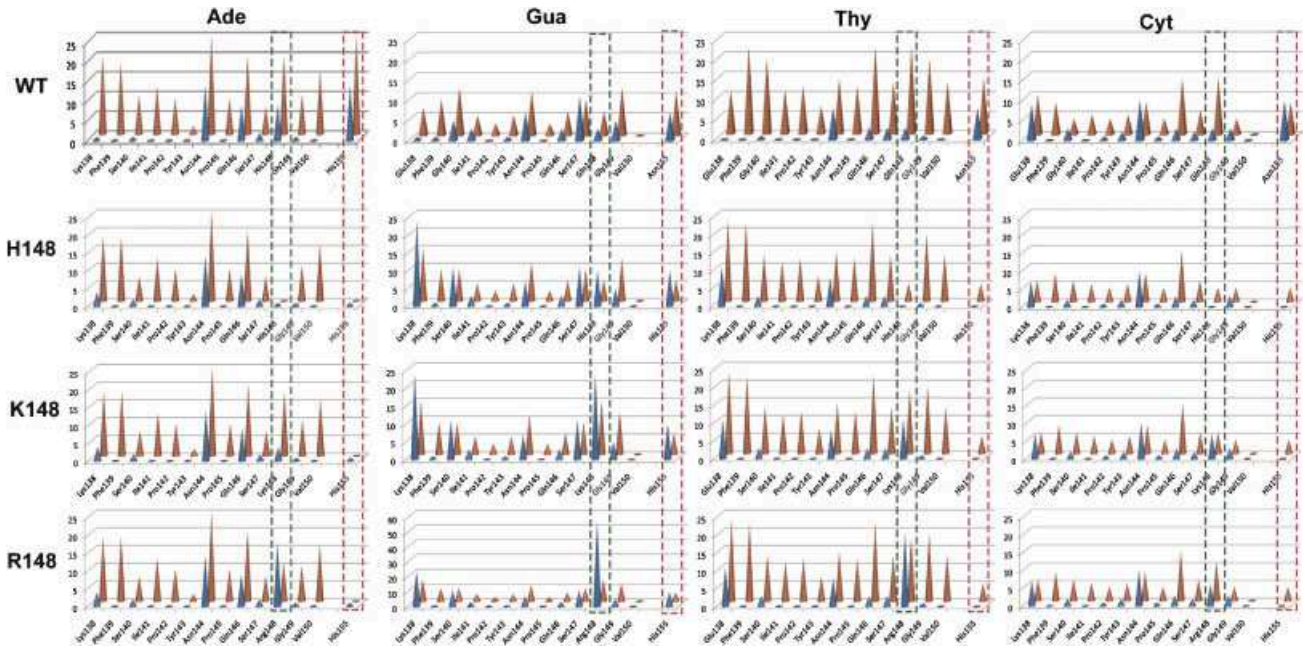

Figure 5. Statistical probability of residues 140–155 recognizing DNA bases based on the known structures of protein/DNA complexes. The H-bond (blue color) and van der Waals (red color) contacts were compiled based on the protein-DNA complexes. Interactions involving residues 148 and 155 are framed by dashed lines, in green and magenta, respectively.

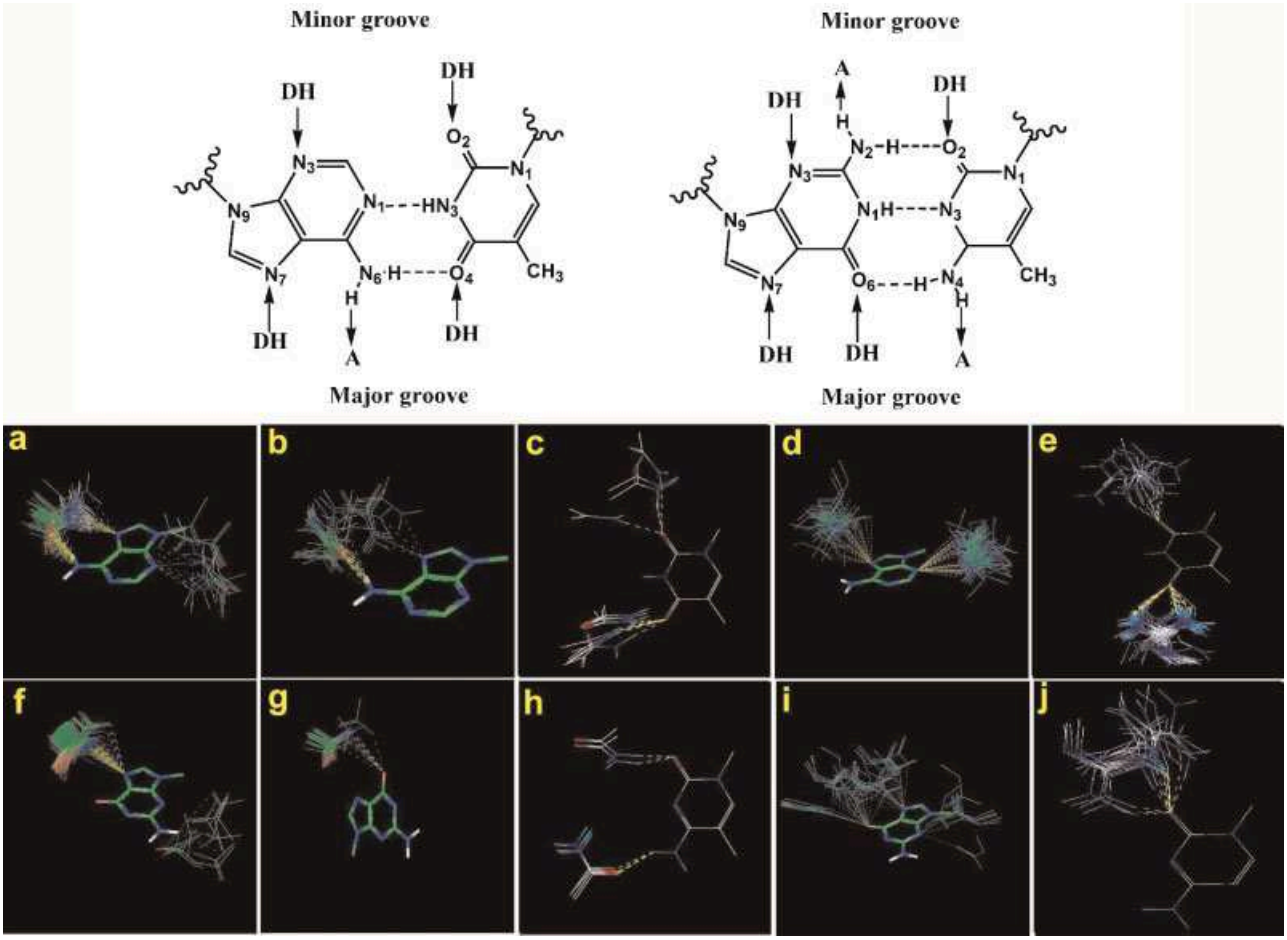

Figure 6. H-bond interactions of DNA bases: Top: diagrams of bases and their pairing in a DNA molecule. Arrows indicate the atoms available for H-bond interactions, oriented towards acceptors and away from donors. Bottom: 3D scatterplots of the side chain distributions around the DNA bases: (a and b) N/Q ··· A; (c) N/Q ··· T; (d) R ··· A; (e) R ··· T; (f and g) N/Q ··· G; (h) N/Q ··· C; (i) R ··· G; and (j) R ··· C. H-bonds of purines showing bidentate (a) and monodentate (b) modes of interaction for adenine, with monodentate interactions involving N^7 (f) and O^6 (g) binding sites for guanine shown separately. Groups with chemical groups found in natural amino acids were included in the analysis. Carbamoyl is a functional group of N and Q, and guanidium is a functional group of R. The main group (DNA bases), contacting groups (Q/N and R) and H-bonds are shown as sticks, wire frames and dashed lines, respectively.

In the case of N/Q recognition by pyrimidines, carbamoyl group interactions were observed only rarely (Figure 6c and h). The positions and mode of interaction of these groups suggested certain common rules. For example, thymine and cytosine binding involves single H-bonds with carbamoyl groups, with no preference for either of the two bases. The binding of the amino acid in position 4 with C or T is characterized by a different orientation of the carbamoyl group, allowing an H-bond to be formed with either O^4 (T) or N^4H_2 (C). All carbamoyl groups interacting with T or C are rotated 30–45° relative to the plane of the base.

R/H/K residues

Guanidium fragments (arginine side chain) H-bonded to adenine bases clustered within the major groove (33% of all contacting groups), with a dispersed cloud-like distribution around N^7 (Figure 6d). The other dense and well grouped cluster (77% of all contacting groups) was localized around the single acceptor site, N^3, in the minor groove. Fragments corresponding to both clusters were rotated relative to the adenine plane and participated in H-bonding at either one or two NH_2-termini. Guanidium groups forming H-bonds with guanine were grouped into three diffuse clusters. Two of these clusters were positioned within the major groove and the third was positioned in the minor groove (Figure 6i) and consisted mostly of end-on-oriented guanidium groups H-bonded to O^6, N^7, and N3, at various angles relative to the guanine plane.

Detailed analysis of DNA base recognition by H and K was limited by the small amount of data available (see Supporting Materials, Figure S5). Nevertheless, as for R, the imidazole groups of the H side chain formed separate clusters at the N^7 and N^3 adenine binding sites. The imidazoles interacting with guanine were grouped in the major groove, interacting either with O^6 or N^7. Both adenine and guanine acceptor sites interact preferably with the $N^{\varepsilon 2}$–H tautomer. The numbers of $-C-NH_3$ groups (terminal moiety of the K side chain) H-bonded to adenine or guanine were similar, but the modes of interaction with these bases were different. The lysine side chains contacting adenine were clustered at the N^7 and N^3 acceptor atoms, whereas all $-C-NH_3$ groups were clustered in the major groove of guanine, H-bonded to either the O_6 or N_7 atom.

Journal of Molecular Recognition

The H-bonds formed between the guanidium fragments of R and pyrimidine bases differed significantly. Thymine binds guanidium at two acceptor sites, O^2 and O^4, whereas interaction with cytosine involves only one acceptor site, O^2 (Figure 6e and j). The guanidium at the thymine O^4 site displays two orientations, coplanar and orthogonal to the base plane. The coplanar fragments interact through their terminal NH_2 groups, forming a strong bifurcated H-bond with the O^4 atom, whereas guanidium in the orthogonal orientation forms only a single H-bond. The guanidium at the O^2 atom of cytosine displays various orientations, including a rotation by 45° allowing the formation of two H-bonds (bifurcated H-bonding). As for purines, the numbers of imidazole and $-C-NH_3$ groups involved in thymine cytosine recognition were too small to be statistically significant, thus, limiting comparison with purines. Nevertheless, the positions of imidazole and, in particular, $-C-NH_3$-contacting groups, and the nature of their interactions with DNA base binding sites were similar to those observed for guanidium.

Modeling the "interacting" DNA base pairs

We investigated the recognition pattern for viral DNA base pairs, by combining the 3D scatterplots of individual bases to obtain models of the interacting base pairs, A–T and G–C with N/Q and R (statistically significant). This strategy made it possible to eliminate steric overlaps and to identify new contacts.

N/Q interactions with A–T and G–C (Figure 7a and b)

The number of contacting carbamoyl groups and their positions around the A–T and G–C base pairs were generally consistent with their arrangement observed with individual bases. Fragment positions not satisfying steric criteria were eliminated. The dominant bidentate mode of N/Q binding in the major groove of adenine corresponded to specific recognition between the wild-type residues and A–T base pairs. Only a low frequency of moderately strong single H-bonds was observed in the minor

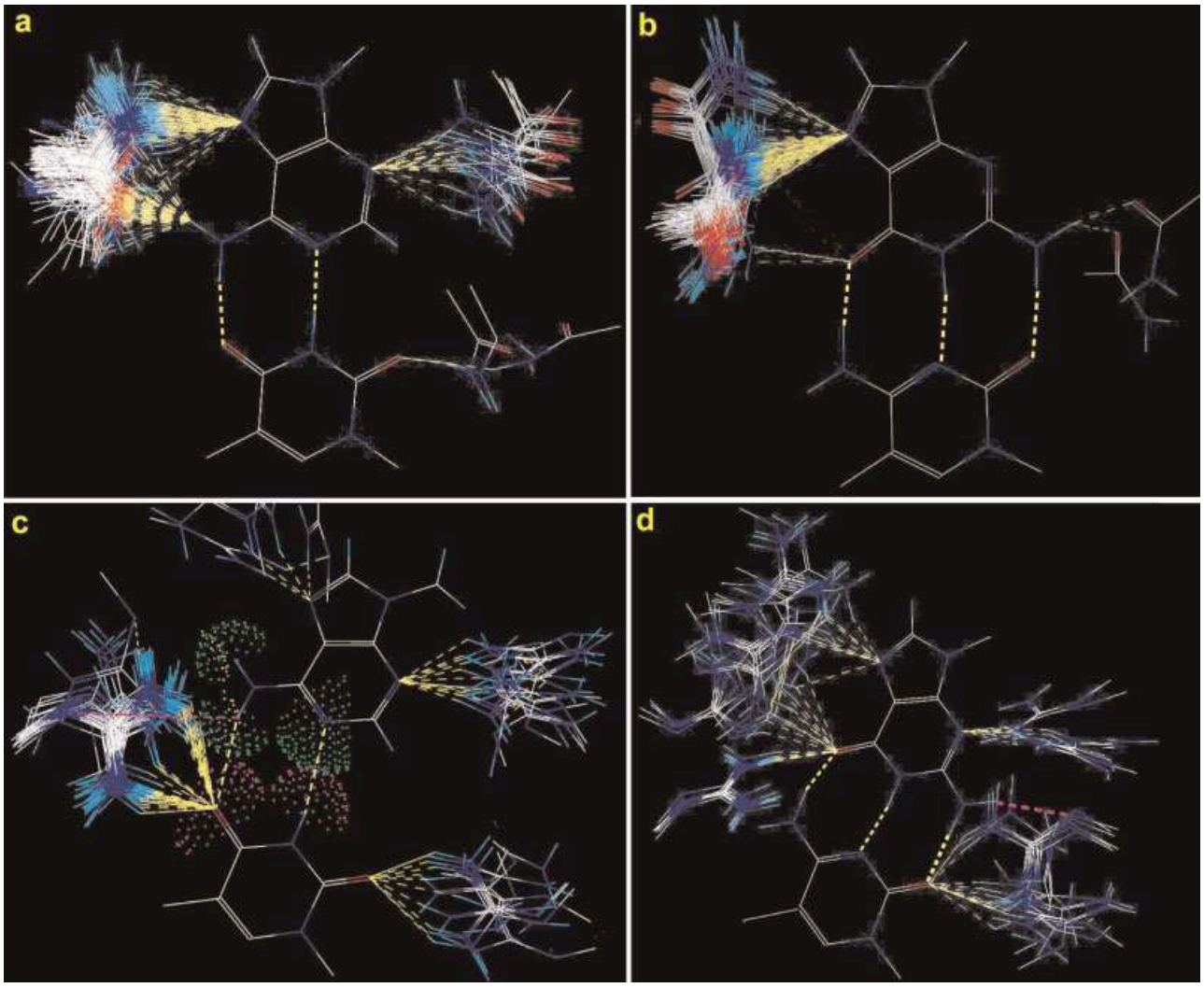

Figure 7. 3D scatterplots of "interacting" base pairs (a) A–T ··· N/Q; (b) G–C ··· N/Q; (c) A–T ··· R; and (d) G–C ··· R represented in approximately the same orientation, with the purine bases at the top and the major groove at the left. The main group (DNA base pairs) and contacting groups (N/Q and R) are shown as wire frames; H-bonds as yellow dashed lines (including Watson-Crick bonds); additional contacts revealed by the generation of interacting base pairs in magenta, (c) and (d); van der Waals radii (dotted spheres) of groups (N1) and (N6) of adenine in green; (N3) and (O4) of thymine in magenta and arginine in yellow, illustrating conflict between arginine and N1 (A).

groove. By contrast to this marked preference and specificity of WT side chains for A–T base pairs, the interaction of N/Q side chains with G–C base pairs was nonspecific, resulting in the formation of a single H-bond with the N^7 or $=O^6$ acceptor site in guanine.

Arginine side chain interactions with A–T and G–C (Figure 7c and d)

Interactions of guanidium fragments with adenine N^7 or N^3 and thymine O^2 indicated a complete absence of steric overlaps. However, despite their steric compatibility with A–T geometry, these interactions did not satisfy specific recognition criteria. By contrast, fragments interacting with $=O^4$ through two H-bonds formed a dense cluster in the base-pair plane. Their orientation was not compatible with the adenine NH_2 group, but the steric constraints could be resolved by rotating the guaniduim moieties by 45–90°. This rotation did not disrupt the pattern of H-bonding between guanidium and thymidine, revealing a new contact between the deprotonated N atom of the amino acid side chain and the NH_2 group of adenine. Thus, arginine residues behaved like wild-type N/Q residues, binding specifically to A–T base pairs through the major groove, but the sites of R recognition—thymidine O^4 and adenine N^6H_2 groups—were different.

The arginine side-chain distribution around G–C base pairs corresponded exactly to that around the individual DNA bases. Indeed, all side chains avoided steric constraint with base exocyclic groups. Interestingly, the R fragments H-bonded to the cytosine O^2 binding site were found to be in an appropriate orientation to form a third H-bond with the guanine $-N^2H_2$ group. These chains therefore probably interact with both bases simultaneously, resulting in multidentate H-bonding through the minor groove of the G–C base pair.

In conclusion, our results demonstrate that one of the key differences between the wild-type (N/Q) and raltegravir-selected mutated (R/H/K) residues relates to their DNA base recognition properties. N155 and Q148 clearly interact preferentially with adenine, either as a single base or in the A–T base pair. In both cases, a strong and specific interaction with adenine is ensured by linear and highly directional bidendate H-bonding within the major groove. In contrast, a single, moderately strong and non-linear H-bond is formed with guanine. The DNA base-pair model generated by this strategy identifies new possibilities for H-bonding, demonstrating that the arginine side chain can engage in multiple and directed H-bond interactions, allowing specific R⋯A–T (major groove) or R⋯G–C (minor groove) interactions.

DISCUSSION

Raltegravir resistance is associated with two genetic pathways defined by the N155H or Q148H/R/K primary mutations (Hazuda *et al*., 2007; Kobayashi *et al*., 2008; Malet *et al*., 2008; Myers and Pillay, 2008). Secondary G140S/A mutation in the Q148H/R/K background compensates for replication defects associated with primary mutations and increases resistance. These substitutions significantly decrease the binding affinity of the integrase inhibitor and allow IN to retain its activity. We performed *in silico* analyses of the structural features and recognition properties of wild-type and mutated INs to gain further insight into the molecular basis of HIV-1 IN resistance. This study focuses on the active site of IN and the catalytic loop-containing residues in particular, the mutation of which has been selected by raltegravir in clinical practice.

This study highlighted the importance of a stable Ω-shaped hairpin within the catalytic loop. The importance of this loop has not previously been reported for the HIV-1 IN, although a related subsecondary structure had been described (Maignan *et al*., 1998; Chen *et al*., 2008). This hairpin can move toward the active site, defining open and closed conformations. Movements of the hairpin opening the active site lead to the formation of a cleft by the active site and the catalytic loop, which can then accommodate DNA. G140A/S-mutated forms of IN display slightly lower levels of hairpin mobility than the wild-type enzyme. This lower level of mobility is associated with lower levels of G140S mutant enzyme activity *in vitro* (Malet *et al*., 2008) and slower 3′-processing kinetics for both the G140S and G140S/Q148H mutants (Delelis *et al*., 2009). Our 3D models of RAL-selected mutants demonstrated that the two primary pathways to raltegravir resistance, one involving N155H mutations and the other involving the replacement of Q148 by H, R, or K, conserve all the structural features of the IN catalytic domain. They also demonstrated that the specific interactions of raltegravir-selected amino acids with DNA base pairs differed from those of the wild-type enzyme, accounting for the observed differences in efficacy between mutant and wild-type integrase *in vitro*. Furthermore, the G140S mutation, which occurs after the primary Q148 mutation *in vivo*, changes slightly the mobility of the catalytic loop, thereby possibly modifying the change in base specificity induced by Q148R/H/K mutation. Although this modification appears limited in our study, it may provide a possible basis for the optimizing role of G140S mutation.

Experimental biological data suggest that the core domain interacts with the terminal CAGT bases of LTR ends (Ellison *et al*., 1995; Heuer and Brown, 1997; Esposito and Craigie, 1998; Heuer and Brown, 1998) required for IN activity. Substitutions introducing nucleotide analogs stabilizing the double strand decrease 3′-processing activity, whereas those weakening base pairing in the vicinity of the CA dinucleotide increase activity (Agapkina *et al*., 2006). Our data suggest that the A–T pair at the terminus or in the third position is selectively recognized by the WT Q148 or N155 residue. A recent biochemical study (Langley *et al*., 2008) carried out with a different IN inhibitor concluded that the terminal adenosine of the viral LTR controlled the binding of strand transfer inhibitors. This result supports the validity of our model. A recent theoretical prediction for DNA substrate binding sites on HIV-1 IN indicated that amino acids 139–152 constitute a binding site that includes Q148, together with Q137, Q146, and N144 (Chen *et al*., 2008; Dolan *et al*., 2009).

Adenine can be specifically recognized in either its paired (A–T) or unpaired form. However, we suggest that Q148/N155 residues interact with the sterically and energetically more favorable terminal unpaired adenine, consistent with previous data showing post-3′-processing contact between Q148 and the 5′-AC overhang (Chiu and Davies, 2004; Esposito and Craigie, 1998) and the theoretical model of the IN–DNA complex (Dolan *et al*., 2009). By contrast, the Q148R mutant preferentially established specific interactions by binding the two bases of a pair, either A–T or G–C, simultaneously. This lack of discrimination for base pair binding implies a loss of strict sequence specificity.

Thus, Q148R, through its long arginine side chain, may interact either with A–T at the third position, via the major groove edge, or with the next base pair, G–C, across the minor groove. These

Journal of Molecular Recognition

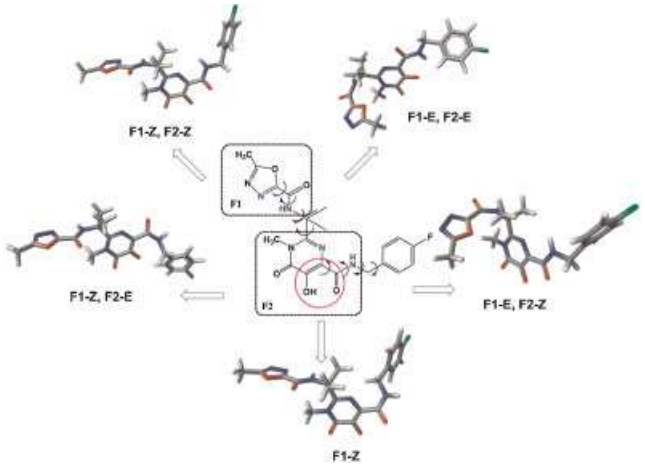

Figure 8. Conformational diversity of raltegravir: The *E-*, *Z-* conformers of the two pharmacophores, 1,3,4-oxadiazole-2-carboxamide (F1) and *N*-methyl-4-carboxamide-dihydroxy-pyrimidine (F2) represent alternative bioisosters of adenine (in *Z-)* or guanine (in *E-*).

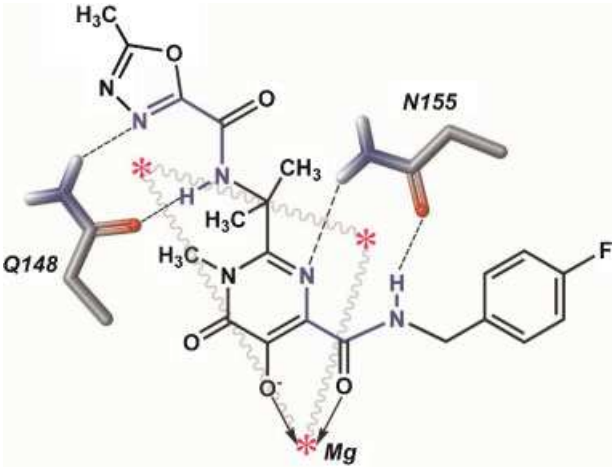

Figure 9. Schematic model of raltegravir interaction with the wild-type IN, involving Mg^{2+} coordination (arrows) and H-bonding (dashed lines) to N155 and Q148. Raltegravir shows two "adenine-like" fragments (blue) and one Mg^{2+}-binding site, forming three pharmacophore sites (asterisks) connected by jagged lines.

alternative arrangements are possible due to the flexibility of the catalytic loop, demonstrated by movement of the hairpin.

Strand transfer inhibitors, such as raltegravir, bind at the interface of the IN-viral DNA complex, by forming a quaternary complex with the catalytic metal in the enzyme active site and the 3′-processed donor DNA. Raltegravir has a very flexible conformation, with multiple H-bonding sites and *E-*, *Z-*conformers of the two pharmacophores, 1,3,4-oxadiazole-2-carboxamide (F1) and *N*-methyl-4-carboxamide-dihydroxy-pyrimidine (F2) (Figure 8). The conformers of these two fragments constitute alternative bioisosters of adenine (in *Z-)* or guanine (in *E-*). Raltegravir may, therefore, act as a base analog, competing with the target DNA for the establishment of specific interactions with IN. We previously reported stabilization of the β-ketoenol fragment in the *Z*-conformation by intramolecular H-bonds, suggesting that F2 is a bioisoster of adenine (Tchertanov and Mouscadet, 2007). We have also shown that β-ketoenolate is an excellent chelator of divalent metals (Tchertanov and Mouscadet, 2007). Thus, F2 can efficiently coordinate magnesium via the two 1–5 oxygen atoms, orienting RAL such that its "adenine-like" part, adjacent to β-ketoenolate, is specifically recognized by N155, which is found close to the Mg^{2+} cation. The F1 fragment can mimic adenine or guanine, depending on its rotational isomer. However, conformational analysis of the isolated compound revealed the adenine bioisoster to be the most stable conformer. Given the specific recognition of adenine by Q148 and N155, the adenine bioisosters of F1 and F2 also constitute targets for these residues.

The three characteristic pharmacophores of RAL—the two "adenine-like" fragments of F1 and F2 and the chelating center of F2—delineate three distances strikingly similar to those defined by binding sites in IN: Q148, N155 and the position of the second Mg^{2+} cation (Figure 9). Thus, the pharmacophore constituents of the inhibitor and the binding sites formed by Q148, N155, and the Mg^{2+} cation are topologicaly equivalent. Overall, these findings suggest that the IN-bound raltegravir can be specifically recognized by either Q148, in the mobile catalytic loop, or N155 in the catalytic site, through one or both of the "adenine-like" pharmacophores. These alternative modes of recognition may underlie the two different pathways of raltegravir-selected

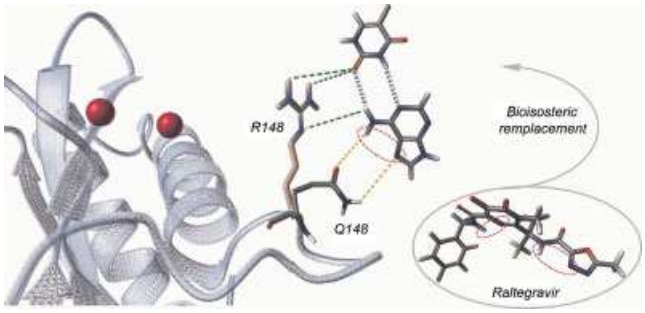

Figure 10. Model representing the alternative molecular recognition of the A–T base pair by HIV-1 IN induced by raltegravir resistance mutations. Molecular display style: the enzyme structure is shown by the ribbon, Mg^{2+} cations are shown as balls; the wild-type Q148 and mutated R148 residues, the A–T base pair of DNA and raltegravir are shown as sticks; H-bonds are shown as green dashed lines and Watson–Crick bonds are shown as blue dashed cylinders.

resistance. They also justify the nature of the selected mutation. Indeed, our model indicates that IN is blocked by the adenine bioisoster competing with the terminal bases of the viral DNA recognized by IN. If they are to block this inhibitory effect, the selected mutations must allow alternative possibilities for DNA recognition, while maintaining the integrity of the IN structure and impairing inhibitor binding (Figure 10). Our findings demonstrate that the R, K, and H residues were probably selected because they are the only residues meeting these criteria.

CONCLUSIONS

We performed a detailed *in silico* study of the structural and molecular recognition effects induced by raltegravir-selected

mutations. We demonstrated the topological invariance of the integrase core domain, including the conservation of a recently identified Ω-shaped hairpin in the catalytic loop. By contrast, we showed that the mutations greatly altered the specificity of DNA recognition by integrase. The native residues displayed a clear preference for adenine, whereas the mutants strongly favored pyrimidines.

We propose a hypothetical model, in which raltegravir inhibits HIV-1 replication by acting as an adenine mimic and establishing specific interactions with the Q148 and/or N155 residues of the integrase. We also provide a possible explanation for the decrease in responsiveness to rategravir when these residues are replaced by arginine, histidine, or lysine.

One of the obvious applications of our models is as a docking guide for the placement of the viral DNA within its binding site in IN. Future studies could focus on the correlation between the spatial orientation of the side chains around the DNA bases and their pairs and the mapping of different frames from a Molecular Dynamics run. Such work might open up new opportunities for the design of HIV-1 IN inhibitors active against emerging HIV-1 mutants.

Acknowledgements

The authors thank Professor Phillipe Cotelle and Dr Sylvie Rimsky for helpful scientific discussions, Tripos and CSDC for providing licences, and Ahmad Fliti for excellent technical assistance. The LBPA laboratory is funded by the French National Centre for Scientific Research (CNRS). This work was supported by the TRIoH European project (FP6 grant 503480), Sidaction and the ANR IMFOVIR (PCV-0015) program.

REFERENCES

Agapkina J, Smolov M, Barbe S, Zubin E, Zatsepin T, Deprez E, Le Bret M, Mouscadet JF, Gottikh M. 2006. Probing of HIV-1 integrase/DNA interactions using novel analogs of viral DNA. *J. Biol. Chem.* **281**: 11530–11540.

Allen FH. 2002. The Cambridge Structural Database: a quarter of a million crystal structures and rising. *Acta Crystallogr. B* **58**: 380–388.

Asante-Appiah E, Skalka AM. 1997. Molecular mechanisms in retrovirus DNA integration. *Antivir. Res.* **36**: 139–156.

Berman HM, Westbrook J, Feng Z, Gilliland G, Bhat TN, Weissig H, Shindyalov IN, Bourne PE. 2000. The Protein Data Bank. *Nucleic Acids Res.* **28**: 235–242.

Brigo A, Lee KW, Mustata GI, Briggs JM. 2005. Comparison of multiple molecular dynamics trajectories calculated for the drug-resistant HIV-1 integrase T66I/M154I catalytic domain. *Biophys. J.* **88**: 3072–3082. DOI:10.1529/biophysj.104.050286

Brown PO. 1990. Integration of retroviral DNA. *Curr. Top. Microbiol. Immunol.* **157**: 19–48.

Bruno IJ, Cole JC, Lommerse JPM, Rowland RS, Taylor R, Verdonk ML. 1997. IsoStar: a library of information about nonbonded interactions. *J. Comput. Aided Mol. Des.* **11**: 525–537.

Bujacz G, Alexandratos J, Wlodawer A. 1997. Binding of different divalent cations to the active site of avian sarcoma virus integrase and their effects on enzymatic activity. *J. Biol. Chem.* **272**: 18161–18168.

Bujacz G, Alexandratos J, ZhouLiu Q, ClementMella C, Wlodawer A. 1996. The catalytic domain of human immunodeficiency virus integrase: ordered active site in the F185H mutant. *FEBS Lett.* **398**: 175–178.

Cai ML, Zheng RL, Caffrey M, Craigie R, Clore GM, Gronenborn AM. 1997. Solution structure of the N-terminal zinc binding domain of HIV-1 integrase. *Nat. Struct. Biol.* **4**: 567–577.

Charpentier C, Karmochkine M, Laureillard D, Tisserand P, Belec L, Weiss L, Si-Mohamed A, Piketty C. 2008. Drug resistance profiles for the HIV integrase gene in patients failing raltegravir salvage therapy. *HIV Med.* **9**: 765–770. DOI: 10.1111/j.1468-1293.2008.00628.x

Chen AP, Weber IT, Harrison RW, Leis J. 2006. Identification of amino acids in HIV-1 and avian sarcoma virus integrase subsites required for specific recognition of the long terminal repeat ends. *J. Biol. Chem.* **281**: 4173–4182.

Chen X, Tsiang M, Yu F, Hung M, Jones GS, Zeynalzadegan A, Qi X, Jin H, Kim CU, Swaminathan S, Chen JM. 2008. Modeling, analysis, and validation of a novel HIV integrase structure provide insights into the binding modes of potent integrase inhibitors. *J. Mol. Biol.* **380**: 504–519. doi:10.1016/j.jmb.2008.04.054.

Cheng AC, Chen WW, Fuhrmann CN, Frankel AD. 2003. Recognition of nucleic acid bases and base-pairs by hydrogen bonding to amino acid side-chains. *J. Mol. Biol.* **327**: 781–796.

Cherepanov P, Maertens G, Proost P, Devreese B, Van Beeumen J, Engelborghs Y, De Clercq E, Debyser Z. 2003. HIV-1 integrase forms stable tetramers and associates with LEDGF/p75 protein in human cells. *J. Biol. Chem.* **278**: 372–381. DOI:10.1074/jbc.M209278200

Chiu TK, Davies DR. 2004. Structure and function of HIV-1 integrase. *Curr. Top. Med. Chem.* **4**: 965–977.

Cole C, Barber JD, Barton GJ. 2008. The Jpred 3 secondary structure prediction server. *Nucleic Acids Res.* **36**: W197–W201. DOI:10.1093/nar/gkn238

Cooper DA, Steigbigel RT, Gatell JM, Rockstroh JK, Katlama C, Yeni P, Lazzarin A, Clotet B, Kumar PN, Eron JE, Schechter M, Markowitz M, Loutfy MR, Lennox JL, Zhao J, Chen J, Ryan DM, Rhodes RR, Killar JA, Gilde LR, Strohmaier KM, Meibohm AR, Miller MD, Hazuda DJ, Nessly ML, DiNubile MJ, Isaacs RD, Teppler H, Nguyen BY. 2008. Subgroup and resistance analyses of raltegravir for resistant HIV-1 infection. *New Engl. J. Med.* **359**: 355–365.

Cotton FA, Wilkinson G. 1999. Advanced Inorganic Chemistry. 6th edition. Wiley: New York.

De Luca L, Vistoli G, Pedretti A, Barreca ML, Chimirri A. 2005. Molecular dynamics studies of the full-length integrase-DNA complex. *Biochem. Biophys. Res. Commun.* **336**: 1010–1016.

De la Cruz X, Hutchinson EG, Shepherd A, Thornton JM. 2002. Toward predicting protein topology: an approach to identifying beta hairpins. *Proc. Natl. Acad. Sci. U.S.A.* **99**: 11157–111162. DOI:10.1073/pnas.162376199. [doi];162376199 [pii]

DeLano WL. 2002. The PyMOL Molecular Grapics System.

Delelis O, Malet I, Na L, Tchertanov L, Calvez V, Marcelin AG, Subra F, Deprez E, Mouscadet JF. 2009. The G140S mutation in HIV integrases from raltegravir-resistant patients rescues catalytic defect due to the resistance Q148H mutation. *Nucleic Acids Res.* **37**: 1193–1201. DOI:10.1093/nar/gkn1050

Deprez E, Tauc P, Leh H, Mouscadet JF, Auclair C, Brochon JC. 2000. Oligomeric states of the HIV-1 integrase as measured by time-resolved fluorescence anisotropy. *Biochemistry* **39**: 9275–9284.

Dolan J, Chen A, Weber IT, Harrison RW, Leis J. 2009. Defining the DNA substrate binding sites on HIV-1 integrase. *J. Mol. Biol.* **385**: 568–579. DOI:S0022-2836(08)01396-X. [pii];10.1016/j.jmb.2008.10.083 [doi]

Dyda F, Hickman AB, Jenkins TM, Engelman A, Craigie R, Davies DR. 1994. Crystal-structure of the catalytic domain of HIV-1 integrase—similarity to other polynucleotidyl transferases. *Science* **266**: 1981–1986.

Efimov AV. 1993a. Patterns of loop regions in proteins. *Curr. Opin. Struct. Biol.* **3**: 379–384.

Efimov AV. 1993b. Standard structures in proteins. *Prog. Biophys. Mol. Biol.* **60**: 201–239.

Eijkelenboom APAM, vandenEnt FMI, Vos A, Doreleijers JF, Hard K, Tullius TD, Plasterk RHA, Kaptein R, Boelens R. 1997. The solution structure of the amino-terminal HHCC domain of HIV-2 integrase: a three-helix bundle stabilized by zinc. *Curr. Biol.* **7**: 739–746.

Ellison V, Gerton J, Vincent KA, Brown PO. 1995. An essential interaction between distinct domains of hiv-1 integrase mediates assembly of the active multimer. *J. Biol. Chem.* **270**: 3320–3326.

Engelman A, Bushman FD, Craigie R. 1993. Identification of discrete functional domains of hiv-1 integrase and their organization within an active multimeric complex. *EMBO J.* **12**: 3269–3275.

Esposito D, Craigie R. 1998. Sequence specificity of viral end DNA binding by HIV-1 integrase reveals critical regions for protein-DNA interaction. *EMBO J.* **17**: 5832–5843.

Faure A, Calmels C, Desjobert C, Castroviejo M, Caumont-Sarcos A, Tarrago-Litvak L, Litvak S, Parissi V. 2005. HIV-1 integrase crosslinked oligomers are active *in vitro*. *Nucleic Acids Res.* **33**: 977–986. DOI:10.1093/nar/gki241

Fenollar-Ferrer C, Carnevale V, Raugei S, Carloni P. 2008. HIV-1 integrase-DNA interactions investigated by molecular modelling. *Comput. Math. Method. Med.* **9**: 231–243. DOI:10.1080/17486700802167918

Fetrow JS. 1995. Protein motifs .6. omega-loops—nonregular secondary structures significant in protein function and stability. *FASEB J.* **9**: 708–717.

Frishman D, Argos P. 1995. Knowledge-based protein secondary structure assignment. *Proteins Struct. Funct. Genet.* **23**: 566–579.

Gao K, Butler SL, Bushman F. 2001. Human immunodeficiency virus type 1 integrase: arrangement of protein domains in active cDNA complexes. *EMBO J.* **20**: 3565–3576.

Gao K, Wong S, Bushman F. 2004. Metal binding by the D,DX35E motif of human immunodeficiency virus type I integrase: selective rescue of Cys substitutions by Mn-2 *in vitro*. *J. Virol.* **78**: 6715–6722 . DOI:10.1128/JVI.78.13.6715-6722.2004

Garnier J, Gibrat JF, Robson B. 1996. GOR method for predicting protein secondary structure from amino acid sequence. *Comput. Method. Macromol. Sequence Anal.* **266**: 540–553.

Goldgur Y, Dyda F, Hickman AB, Jenkins TM, Craigie R, Davies DR. 1998. Three new structures of the core domain of HIV-1 integrase: an active site that binds magnesium. *Proc. Natl. Acad. Sci. U.S.A.* **95**: 9150–9154.

Greenwald J, Le V, Butler SL, Bushman FD, Choe S. 1999. The mobility of an HIV-1 integrase active site loop is correlated with catalytic activity. *Biochemistry* **38**: 8892–8898.

Guiot E, Carayon K, Delelis O, Simon F, Tauc P, Zubin E, Gottikh M, Mouscadet JF, Brochon JC, Deprez E. 2006. Relationship between the oligomeric status of HIV-1 integrase on DNA and enzymatic activity. *J. Biol. Chem.* **281**: 22707–222719. DOI:10.1074/jbc.M602198200

Hayouka Z, Rosenbluh J, Levin A, Loya S, Lebendiker M, Veprintsev D, Kotler M, Hizi A, Loyter A, Friedler A. 2007. Inhibiting HIV-1 integrase by shifting its oligomerization equilibrium. *Proc. Natl. Acad. Sci. U.S.A.* **104**: 8316–8321 . DOI:10.1073/pnas.0700781104

Hazuda DJ, Miller MD, Nguyen BY, Zhao J. 2007. Resistance to the HIV-integrase inhibitor raltegravir: analysis of protocol 005, a Phase II study in patients with triple-class resistant HIV-1 infection. *Antivir. Ther.* **12**: S10.

Heuer TS, Brown PO. 1997. Mapping features of HIV-1 integrase near selected sites on viral and target DNA molecules in an active enzyme-DNA complex by photo-cross-linking. *Biochemistry* **36**: 10655–10665.

Heuer TS, Brown PO. 1998. Photo-cross-linking studies suggest a model for the architecture of an active human immunodeficiency virus type 1 integrase-DNA complex. *Biochemistry* **37**: 6667–6678.

Hindmarsh P, Leis J. 1999. Retroviral DNA integration. *Microbiol. Mol. Biol. Rev.* **63**: 836–843.

Hutchinson EG, Thornton JM. 1994. A revised set of potentials for beta-turn formation in proteins. *Protein Sci.* **3**: 2207–2216 . DOI:10.1002/pro.5560031206 [doi]

Kabsch W, Sander C. 1983. Dictionary of protein secondary structure—pattern-recognition of hydrogen-bonded and geometrical features. *Biopolymers* **22**: 2577–2637.

Karki RG, Tang Y, Burke TR, Nicklaus MC. 2004. Model of full-length HIV-1 integrase complexed with viral DNA as template for anti-HIV drug design. *J. Comput. Aided Mol. Des.* **18**: 739–760. DOI:10.1007/s10822-005-0365-5

Katzman M, Sudol M. 1995. Mapping domains of retroviral integrase responsible for viral-DNA specificity and target site selection by analysis of chimeras between human-immunodeficiency-virus type-1 and visna virus integrases. *J. Virol.* **69**: 5687–5696.

Kobayashi M, Nakahara K, Seki T, Miki S, Kawauchi S, Suyama A, Wakasa-Morimoto C, Kodama M, Endoh T, Oosugi E, Matsushita Y, Murai H, Fujishita T, Yoshinaga T, Garvey E, Foster S, Underwood M, Johns B, Sato A, Fujiwara T. 2008. Selection of diverse and clinically relevant integrase inhibitor-resistant human immunodeficiency virus type 1 mutants. *Antivir. Res.* **80**: 213–222. DOI:10.1016/j.antiviral.2008.06.012

Langley D, Samanta HK, Li ZF, Walker MA, Krystal M, Dicker IB. 2008. The terminal (catalytic) adenosine of the HIV LTR controls the kinetics of binding and dissociation of hiv integrase strand transfer inhibitors. *Biochemistry* **47**(51): 13481–13488.

Laskowski RA, Macarthur MW, Moss DS, Thornton JM. 1993. Procheck—a program to check the stereochemical quality of protein structures. *J. Appl. Crystallogr.* **26**: 283–291.

Lee MC, Deng JX, Briggs JM, Duan Y. 2005. Large-scale conformational dynamics of the HIV-1 integrase core domain and its catalytic loop mutants. *Biophys. J.* **88**: 3133–3146.

Leszczynski JF, Rose GD. 1986. Loops in globular-proteins—a novel category of secondary structure. *Science* **234**: 849–855.

Levitt M, Warshel A. 1975. Computer-simulation of protein folding. *Nature* **253**: 694–698.

Li L, Olvera JM, Yoder KE, Mitchell RS, Butler SL, Lieber M, Martin SL, Bushman FD. 2001. Role of the non-homologous DNA end joining pathway in the early steps of retroviral infection. *EMBO J.* **20**: 3272–3281.

Li M, Mizuuchi M, Burke TR, Craigie R. 2006. Retroviral DNA integration: reaction pathway and critical intermediates. *EMBO J.* **25**: 1295–1304 . DOI:10.1038/sj.emboj.7601005

Lins RD, Adesokan A, Soares TA, Briggs JM. 2000a. Investigations on human immunodeficiency virus type 1 integrase/DNA binding interactions via molecular dynamics and electrostatics calculations. *Pharmacol. Therapeut.* **85**: 123–131.

Lins RD, Briggs JM, Straatsma TP, Carlson HA, Greenwald J, Choe S, McCammon JA. 1999. Molecular dynamics studies on the HIV-1 integrase catalytic domain. *Biophys. J.* **76**: 2999–3011.

Lins RD, Straatsma TP, Briggs JM. 2000b. Similarities in the HIV-1 and ASV integrase active sites upon metal cofactor binding. *Biopolymers* **53**: 308–315.

Luscombe NM, Laskowski RA, Thornton JM. 2001. Amino acid-base interactions: a three-dimensional analysis of protein-DNA interactions at an atomic level. *Nucleic Acids Res.* **29**: 2860–2874.

Luscombe NM, Thornton JM. 2002. Protein-DNA interactions: amino acid conservation and the effects of mutations on binding specificity. *J. Mol. Biol.* **320**: 991–1009.

Lutzke RAP, Vink C, Plasterk RHA. 1994. Characterization of the minimal dna-binding domain of the hiv integrase protein. *Nucleic Acids Res.* **22**: 4125–4131.

Maignan S, Guilloteau JP, Zhou-Liu Q, Clement-Mella C, Mikol V. 1998. Crystal structures of the catalytic domain of HIV-1 integrase free and complexed with its metal cofactor: high level of similarity of the active site with other viral integrases. *J. Mol. Biol.* **282**: 359–368.

Malet I, Delelis O, Valantin MA, Montes B, Soulie C, Wirden M, Tchertanov L, Peytavin G, Reynes J, Mouscadet JF, Katlama C, Calvez V, Marcelin AG. 2008. Mutations associated with failure of raltegravir treatment affect integrase sensitivity to the inhibitor *in vitro*. *Antimicrob. Agents Chemother.* **52**: 1351–1358. DOI:10.1128/AAC.01228-07

Maupetit J, Tuffery P, Derreumaux P. 2007. A coarse-grained protein force field for folding and structure prediction. *Proteins-Struct. Funct. Bioinformatics* **69**: 394–408. DOI:10.1002/prot.21505

Michel F, Crucifix C, Granger F, Eiler S, Mouscadet JF, Korolev S, Agapkina J, Ziganshin R, Gottikh M, Nazabal A, Emiliani S, Benarous R, Moras D, Schultz P, Ruff M. 2009. Structural basis for HIV-1 DNA integration in the human genome, role of the LEDGF/P75 cofactor. *EMBO J.* **28**: 980–991. DOI:emboj200941. [pii];10.1038/emboj.2009.41 [doi]

Myers RE, Pillay D. 2008. Analysis of natural sequence variation and covariation in human immunodeficiency virus type 1 integrase. *J. Virol.* **82**: 9228–9235 . DOI:10.1128/JVI.01535-07

Nunthaboot N, Pianwanit S, Parasuk V, Ebalunode JO, Briggs JM, Kokpol S. 2007a. Hybrid quantum mechanical/molecular mechanical molecular dynamics simulations of HIV-1 integrase/inhibitor complexes. *Biophys. J.* **93**: 3613–3626 . DOI:10.1529/biophysj.107.108464

Nunthaboot N, Planwanit S, Parasuk V, Kokpol S, Wolschann P. 2007b. Theoretical study on the HIV-1 integrase inhibitor 1-(5-chloroindol-3-yl)-3-hydroxy-3-(2H-tetrazol-5-yl)-propenone (5CITEP). *J. Mol. Struct.* **844**: 208–214. DOI:10.1016/j.molstruc.2007.06.026

Podtelezhnikov AA, Gao K, Bushman FD, McCammon JA. 2003. Modeling HIV-1 integrase complexes based on their hydrodynamic properties. *Biopolymers* **68**: 110–120. DOI:10.1002/bip.10217

Ren G, Gao K, Bushman FD, Yeager M. 2007. Single-Particle image reconstruction of a tetramer of HIV integrase bound to DNA. *J. Mol. Biol.* **366**: 286–294.
Savarino A. 2007. *In silico* docking of HIV-1 integrase inhibitors reveals a novel drug type acting on an enzyme/DNA reaction intermediate. *Retrovirology* **4**(21): DOI:10.1186/1742-4690-4-21
Sen TZ, Jernigan RL, Garnier J, Kloczkowski A. 2005. GOR V server for protein secondary structure prediction. *Bioinformatics* **21**: 2787–2788.
Singh J, Thornton JM. 1992. Atlas of Protein Side-Chain Interactions. IRL Press: Oxford.
Street TO, Fitzkee NC, Perskie LL, Rose GD. 2007. Physical-chemical determinants of turn conformations in globular proteins. *Protein Sci.* **16**: 1720–1727. DOI:10.1110/ps.072898507
Strobel SA, Ryder SP. 2001. The hairpin's turn. *Nature* **410**: 761–763.
Tchertanov L, Delelis O, Mouscadet J. 2007. Structural and functional insight into molecular recognition of HIV-1 integrase catalytic loop. *FEBS J.* **274**: 260.
Tchertanov L, Mouscadet JF. 2007. Target recognition by catechols and beta-ketoenols: potential contribution of hydrogen bonding and Mn/Mg chelation to HIV-1 integrase inhibition. *J. Med. Chem.* **50**: 1133–1145.
Thornton JM, Singh J, Campbell S, Blundell TL. 1988. Protein protein recognition via side-chain interactions. *Biochem. Soc. Trans.* **16**: 927–930.
Tripos Inc. 2007. SYBYL 7.2.
Tripos Inc. 2008. Benchware 3D Explorer.
Wang Y, Klock H, Yin H, Wolff K, Bieza K, Niswonger K, Matzen J, Gunderson D, Hale J, Lesley S, Kuhen K, Caldwell J, Brinker A. 2005. Homogeneous high-throughput screening assays for HIV-1 integrase 3 '-processing and strand transfer activities. *J. Biomol. Screen.* **10**: 456–462. DOI:10.1177/108705710275212
Weber W, Demirdjian H, Lins RD, Briggs JM, Ferreira R, McCammon JA. 1998. Brownian and essential dynamics studies of the HIV-1 integrase catalytic domain. *J. Biomol. Struct. Dynam.* **16**: 733–745.
Wielens J, Crosby IT, Chalmers DK. 2005. A three-dimensional model of the human immunodeficiency virus type 1 integration complex. *J. Comput. Aided Mol. Des.* **19**: 301–317.
Wlodawer A. 1999. Crystal structures of catalytic core domains of retroviral integrases and role of divalent cations in enzymatic activity. *Advances in Virus Research* **52**: 335–350.

Hindawi Publishing Corporation
Advances in Virology
Volume 2012, Article ID 548657, 13 pages
doi:10.1155/2012/548657

Research Article

In Silico and *In Vitro* Comparison of HIV-1 Subtypes B and CRF02_AG Integrases Susceptibility to Integrase Strand Transfer Inhibitors

Xiaoju Ni,[1,2] Safwat Abdel-Azeim,[1] Elodie Laine,[1] Rohit Arora,[1] Osamuede Osemwota,[1] Anne-Geneviève Marcelin,[3] Vincent Calvez,[3] Jean-François Mouscadet,[1] and Luba Tchertanov[1]

[1] *LBPA, CNRS, LabEx LERMIT, Ecole Normale Supérieure de Cachan, 61 Avenue du Président Wilson, 94235 Cachan, France*
[2] *School of Life Science, East China Normal University, Shanghai 200062, China*
[3] *Laboratoire de Virologie, AP-HP, Hôpital Pitié-Salpêtrière, EA 2387, UPMC Université Paris VI, 75013 Paris, France*

Correspondence should be addressed to Luba Tchertanov, luba.tchertanov@lbpa.ens-cachan.fr

Received 3 January 2012; Revised 16 April 2012; Accepted 30 April 2012

Academic Editor: Domenico Genovese

Most antiretroviral medical treatments were developed and tested principally on HIV-1 B nonrecombinant strain, which represents less than 10% of the worldwide HIV-1-infected population. HIV-1 circulating recombinant form CRF02_AG is prevalent in West Africa and is becoming more frequent in other countries. Previous studies suggested that the HIV-1 polymorphisms might be associated to variable susceptibility to antiretrovirals. This study is pointed to compare the susceptibility to integrase (IN) inhibitors of HIV-1 subtype CRF02_AG IN respectively to HIV-1 B. Structural models of B and CRF02_AG HIV-1 INs as unbound enzymes and in complex with the DNA substrate were built by homology modeling. IN inhibitors—raltegravir (RAL), elvitegravir (ELV) and L731,988—were docked onto the models, and their binding affinity for both HIV-1 B and CRF02_AG INs was compared. CRF02_AG INs were cloned and expressed from plasma of integrase strand transfer inhibitor (INSTI)-naïve infected patients. Our *in silico* and *in vitro* studies showed that the sequence variations between the INs of CRF02_AG and B strains did not lead to any notable difference in the structural features of the enzyme and did not impact the susceptibility to the IN inhibitors. The binding modes and affinities of INSTI inhibitors to B and CRF02_AG INs were found to be similar. Although previous studies suggested that several naturally occurring variations of CRF02_AG IN might alter either IN/vDNA interactions or INSTIs binding, our study demonstrate that these variations do affect neither IN activity nor its susceptibility to INSTIs.

1. Introduction

The *pol*-encoded HIV-1 integrase (IN) is a key enzyme in the replication mechanism of retroviruses. It catalyses the covalent insertion of the viral cDNA into the chromosomes of the infected cells [1]. Two reactions are required for covalent integration of viral DNA. First, IN binds to a short sequence located at either end of the long terminal repeat (LTR) of the vDNA and catalyzes an endonucleotide cleavage, 3′-processing reaction, resulting in the removal of two nucleotides from each of the 3′-ends of LTR and the delivery of hydroxy groups for nucleophilic attacks. The trimmed DNA is then used as a substrate for strand transfer (ST) reaction, leading to the covalent insertion of the DNA into the host genome [1]. Inhibitors of the strand transfer reaction—INSTIs—constitute a novel family of antiretroviral (ARV) drugs, with raltegravir (RAL) at the cape, which is a first INSTI approved for AIDS treatment. Other inhibitors in advanced phase of development are elvitegravir (ELV) and GSK572.

Human immunodeficiency virus type one (HIV-1) exhibits an exceptional level of genetic variability, which may influence the viral properties such as infectivity, transmissibility, or response to antiviral treatment [2]. The most prevalent HIV-1 group M genetic forms are subtypes A, B, C and circulating recombinant form CRF02_AG.

Analysis of the global distribution of HIV-1 subtypes and recombinants in the two followed three-year periods,

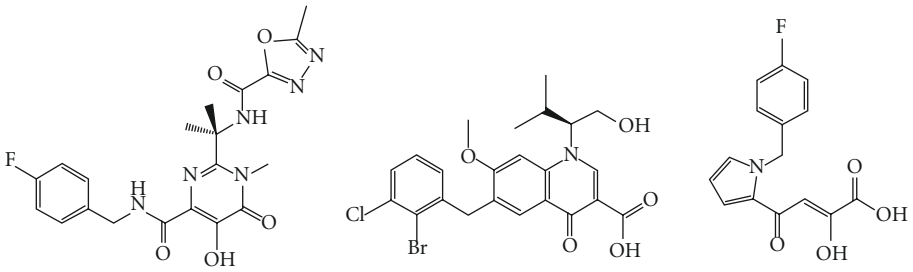

RAL ELV L731,988

Scheme 1

2000–2003 and 2004–2007, indicated a broadly stable distribution of HIV-1 subtypes worldwide with a notable increase in the proportion of circulating recombinant forms (CRFs), a decrease in unique recombinant forms (URFs), and an overall increase in recombinants [3]. Particularly, in 2004–2007, CRF02_AG accounted for 8% of all global infections, following subtypes C (48%), A (12%), and B (11%). CRF02_AG is the predominant HIV strain circulating in West and West Central Africa [4–6]. Recently the recombinant CRF02_AG form was identified in the Amazon region of Brazil [7] and in China [8].

In France the frequency of antiretroviral-naive chronically HIV-infected patients infected with a non-B subtype reached 42% in 2006/2007, having increased significantly since 1998 (10%) and 2001 (33%). This evolution in subtype distribution was mainly due to a higher proportion of patients originating from sub-Saharan countries. Among these non-B subtypes, the most prevalent was CRF02_AG with a stable proportion around 20% between 2001 and 2006/2007 [9].

Enzymatic and virological data support the concept that naturally occurring polymorphisms in different non-B subtypes can affect the susceptibility of HIV-1 to different antiretroviral drugs, the magnitude of resistance conferred by major mutations, and the propensity to acquire some resistance mutations [10]. The genetic variation between viral isolates retroviral enzymes is estimated up to 25–35%; particularly the *pol* gene exhibits high variation, about 10–15% for reverse transcriptase (RT) and 8–12% for integrase (IN) [11]. Integrase inhibitors are active *in vivo* against B and non-B subtypes. Furthermore, *in vitro* studies suggested that subtype C integrase is equally susceptible to INSTIs [12]. Similarly, the analysis of *pol* gene in infected patients showed that highly prevalent polymorphisms have little effect on INSTIs susceptibility [13]. Nevertheless, the comparison of IN sequences of B and CRF02_AG strains showed that CRF02_AG sequence differs from the B sequence by 13 residues (K/R14, V/I31, L/I101, T/V112, T/A124, T/A125, G/N134, I/V135, K/T136, V/I201, T/S206, L/I234 and S/G283) [14]. Based on a model of the B HIV-1 integrase/DNA complex [15], it was suggested that several of these variations K/R14, T/V112, T/A125, G/N134, K/T136, and T/S206 may impact IN interaction with DNA or IN susceptibility to INSTIs. Later we compared the genetic barriers between B and CRF02_AG strains; we found that the variability between subtypes impacted the genetic barrier for G140C/S and V151I with a higher genetic barrier being calculated for subtype CRF02_AG suggesting a great difficulty in selecting these mutations for CR02_AG compared to subtype B [16].

Integrase is a 288 amino acids enzyme, which consists in three structurally distinct functional domains [17]. Structures reporting HIV-1 IN single- or two-domain data allow the generation of biologically relevant models, representing either unbound dimeric enzyme or IN complexes with viral (vDNA) and/or host DNA (hDNA) [18]. The X-ray structures of full-length prototype foamy virus (PFV) IN complex with its cognate DNA and integrase strand transfer inhibitors (INSTIs; RAL, ELV, and others first- and second-generation INSTIs) were recently solved [19, 20]. The reported structures were used for homology modeling of the unbound IN and IN bound to vDNA from CRF02_AG and B strains. Further, the constructed models were used to estimate the susceptibility of both INs to strand transfer inhibitors, RAL, ELV and L731,988 (Scheme 1). Results from molecular modeling were compared to experimental data obtained with B and CRF02_AG INs which were isolated from plasma samples of HIV-1-infected patients and then cloned and expressed *in vitro*.

2. Results and Discussion

2.1. Analysis of CRF02_AG IN Sequences from INSTI-Naive Infected Patients. The complete sequence of the IN coding region of the *pol* gene was amplified and cloned from the plasma samples of CRF02_AG HIV-1-infected patients. Four IN sequences, N^1 to N^4, harbored several variations among the thirteen residues that were shown to be subjected to polymorphic substitutions between CRF02_AG and B HIV-1 sequences (K/R14, V/I31, L/I101, T/V112, T/A124, T/A125, G/N134, I/V135, K/T136, V/I201, T/S206, L/I234 and S/G283; Table 1) [14]. Sequence N_1 (CRF02_AG 33CR) displayed the seven variations K14R, T112V, T125A, G134N, K136T, T206S, S283G; N_2CRF02_AG 49CR the five variations T112V, T125A, G134N, K136T, S283G; N_3 (CRF02_AG 68CR) the five variations K14R, T112V, T125A, K136T, T206S; N_4 (CRF02_AG 52CR Q148K) the two variations T125A and T206S, along with the INSTI resistance mutation Q148K. Although Q148K is involved in INSTIs resistance, the patient from whom the IN coding DNA was derived was

Table 1: Amino acid variations at the positions putatively affecting the susceptibility to INSTI in 4 isolated HIV-1 subtype CRF02_AG IN coding sequences.

Position	B consensus	Subtype CRF02_AG			
		N_1 (33CR)	N_2 (49CR)	N_4 (52CR Q148K)	N_3 (68CR)
14	K	R	K	K	R
112	T	V	V	R	V
125	T	A	A	A	A
134	G	N	N	G	G
136	K	T	T	K	T
206	T	S	T	S	S
283	S	G	G	S	S

Compared with HIV-1 subtype B IN, seven variations present at positions 14, 112, 125, 134, 136, 206, and 283 of CRF02_AG 33CR IN; five variations at positions 112, 125, 134, 136, and 283 of CRF02_AG 49CR IN; five variations at positions 14, 112, 125, 136, and 206 of CRF02_AG 68CR IN; CRF02_AG 52CR Q148K has two variations at positions 125 and 206, and an INSTI-resistant mutation Q148K, the R112 was not considered.

not exposed to the INSTI-containing treatment. Thereby we presume that Q148K may be a naturally occurring amino acid substitution.

2.2. Structural Comparison of HIV-1 B and CRF02_AG Integrases. In order to determine the potential impact of the natural variations on the protein activity and susceptibility to INSTIs, we built models of the IN structures corresponding to the consensus B sequence and the CRF02_AG variant differing from B subtype by twelve residues. The 18-aas C-terminal end containing the S283G was omitted since the structure of this domain was not resolved by X-ray analysis and the folding of this part of protein is extremely difficult to predict in the apo state, due to its essential length and its highly solvent-exposed position.

Comparative structural analysis were performed considering 6 IN models generated by homology modeling (Figure 1). Models 1(B) and 2 (CRF02_AG) (Figure 1(a)) represent the unbound homodimer of integrase (IN^{1-270}), which depicts the conformational state of the enzyme just before the 3′-processing of vDNA (apo state); models 3′(B) and 4 (CRF02_AG) (Figure 1(b)) represent the IN dimer in complex with vDNA (holo state), which depicts the active unit of the IN·vDNA strand transfer intasome; models 5 (B) and 6 (CRF02_AG) (not shown) were derived from models 3 and 4 by removing vDNA.

Models 1 and 2 were constructed from the crystallographic structures of HIV-1 IN-isolated domains or pairs of domains. Overall, the analysis of the models representing the HIV-1 IN conformational state before 3′-processing (apo state) did not show any significant structural change between the two subtypes (Figures 1(a) and 1(c)).

Models 3 and 4 were constructed from the crystallographic structure of the IN·vDNA complex of the PFV intasome [19, 20]. Although the sequence identity between HIV-1 and PFV INs is low (22%), the structure-based alignment of the two proteins demonstrates high conservation of key secondary structural elements and the three PFV IN domains shared with HIV-1 IN have essentially the same structure as the isolated HIV-1 domains. Moreover, the structure of the PFV intasome displays a distance between the reactive 3′ ends of vDNA that corresponds to the expected distance between the integration sites of HIV-1 IN target DNA (4 base pairs). Consequently, we are confident that the PFV IN X-ray structure represents a good template for the HIV-1 IN model generation [21]. To obtain a robust alignment, we adjusted the targets (HIV-1 INs from B and CRF02_AG subtypes) and template (PFV IN) sequences manually, considering each structural domain separately, in order to take into account the conservation of the secondary structure (see Section 4).

Again, models 3 and 4, representing the IN·vDNA intasomes of both strains, superimposed perfectly and no structural dissimilarity was observed (Figures 1(b) and 1(d)). Most of the variations are located far from the active sites, and the nearest two mutated residues to the active site, at positions 134 and 136, are exposed to the solvent and apparently did not affect significantly the structure. Similarly for 3′-processing, strand transfer activities of B and CRF02_AG recombinant proteins were assayed and compared. In agreement with the modeling results, activities of both INs were comparable (Figure 2(c)).

It is worth noting that large structural and conformational changes are observed between the apo (models 1 and 2) and holo (3 and 4) states regarding the relative positions of the IN domains (RMSD, root mean square deviation, of 31 Å, based on C_α) (Figure 1(e)). These structural modifications result in different contacts between IN domains, N-terminal domain (NTD), catalytic core domain (CCD), and C-terminal domain (CDD). As such, in models 1 and 2 (apo state) no interaction was detected between CTD and CCD, whereas the two domains interact tightly in models 3 and 4 (holo state). The NTD-CCD interface also exhibits substantial changes: in the apo form the NTD-CCD interface belongs to the same monomer subunit whereas in the holo form the interface is from two different subunits. Moreover, IN undergoes important structural transformation leading to structural reorganization of the catalytic site loop upon vDNA binding; the coiled portion of the loop reduces from 10 residues (140–149 aas) in the apo form to 5 residues (140–144 aas) in the holo form (Figure 1(f)). This partial folding of the catalytic loop is probably stabilized through intra-IN domain-domain interactions and interactions with vDNA which contribute in the helix $\alpha 4$ elongation.

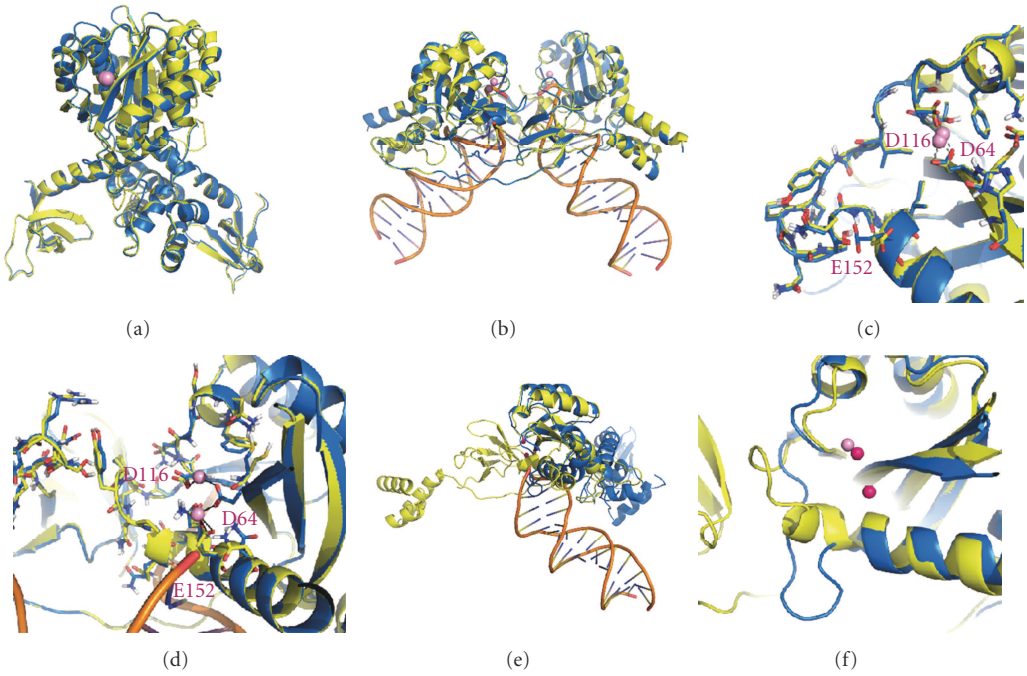

Figure 1: Structural models of the HIV-1 INs from B and CRF02_AG strains. (a) Superimposition of models 1 and 2, representing the enzyme before the 3′ processing from B (in blue) and CRF02_AG (in yellow) strains; (b) Superimposition of models 3 and 4, representing the IN·DNA pre-integration complex from B (in blue) and CRF02_AG (in yellow) strains; (c) and (d) Comparison of the catalytic site and loop 140–149 structure in models 1/3 (in blue) and 2/4 (in yellow) respectively. The proteins are shown as cartoons, Mg^{+2} ions as spheres (in pink). (e and f) superimposition of the structural subunits from models 1 (in blue) and 3 (in yellow) and the structural details of the active site and loop 140–149.

2.3. In Vitro Enzymatic Comparison of Recombinant HIV-1 B IN and CRF02_AG IN. To confirm experimentally the absence of divergence between INs from both strains CRF02_AG and B, N_1 to N_4 sequences were expressed and purified (Figure 2(a)) and their enzymatic activities were compared to the one of HxB2 B IN. First, the DNA binding activities of recombinant INs were compared using a steady-state fluorescence anisotropy assay (Figure 2(b)) [22]. In this assay, the binding of IN to a fluorophore-labeled dsODN substrate mimicking one end of the viral DNA is monitored by the increase of the steady-state anisotropy value, resulting from the restriction of the substrate movements. As shown in Figure 2(b), no significant difference in DNA binding activity of recombinant subtype B IN and the CRF02_AG INs was observed within a range of IN concentrations of 100 to 250 nM, thereby indicating that the variations in IN sequence did not affect the binding affinity of the enzyme. Then, 3′- processing of HIV-1 B IN and CRF02_AG INs was compared *in vitro*. No significant difference of 3′-processing activity of recombinant HIV-1 B IN and CRF02_AG INs was found within a range of IN concentrations of 50 to 400 nM (Figure 2(c)). Impaired 3′-processing and strand transfer activity, but conserved DNA binding ability of CRF02_AG 52CR Q148K were observed, in agreement with previous study [23]. Finally we decided to analyze 3′-processing kinetics of recombinant HIV-1 B IN and CRF02_AG 33CR IN in the presence of increasing concentrations of IN 50 nM to 200 nM recombinant IN proteins with an increasing incubation time, using both *in vitro* 3′-processing activity assay and steady-state fluorescence anisotropy-based assay (Figure 3). Again, no difference could be detected. This result was further confirmed by steady-state fluorescence anisotropy assay (data not shown).

In agreement of the modeling result, *in vitro* study confirmed that the enzymatic activities of both INs were comparable.

2.4. Docking of INSTIs. Although B and CRF02_AG INs are structurally similar, residue variations may impact the interaction and subsequent activity of the inhibitors. To address this hypothesis, the three inhibitors RAL, ELV, and L731,988 (Scheme 1) were docked onto INs by using two different docking algorithms, Glide and AutoDock. RAL and ELV coordinates were taken from the crystallographic structures of PFV intasome cocomplexes [19, 20], L731,988 was built from scratch (see Section 4). The three compounds were considered in their deprotonated form, as it has been clearly established that diketo acids (DKAs) mainly exist in this form in solution [24]. The binding energies obtained by Glide and Autodock scoring functions are reported in Table 2.

The inhibitors were first docked onto the unbound IN, models 1 and 2 (apo state), with a single Mg^{2+} ion within the catalytic site. All three inhibitors are positioned at the catalytic site far from the catalytic site flexible loop. For subtype B, values of binding energies obtained with Glide range in a relatively narrow interval from −8.49 to

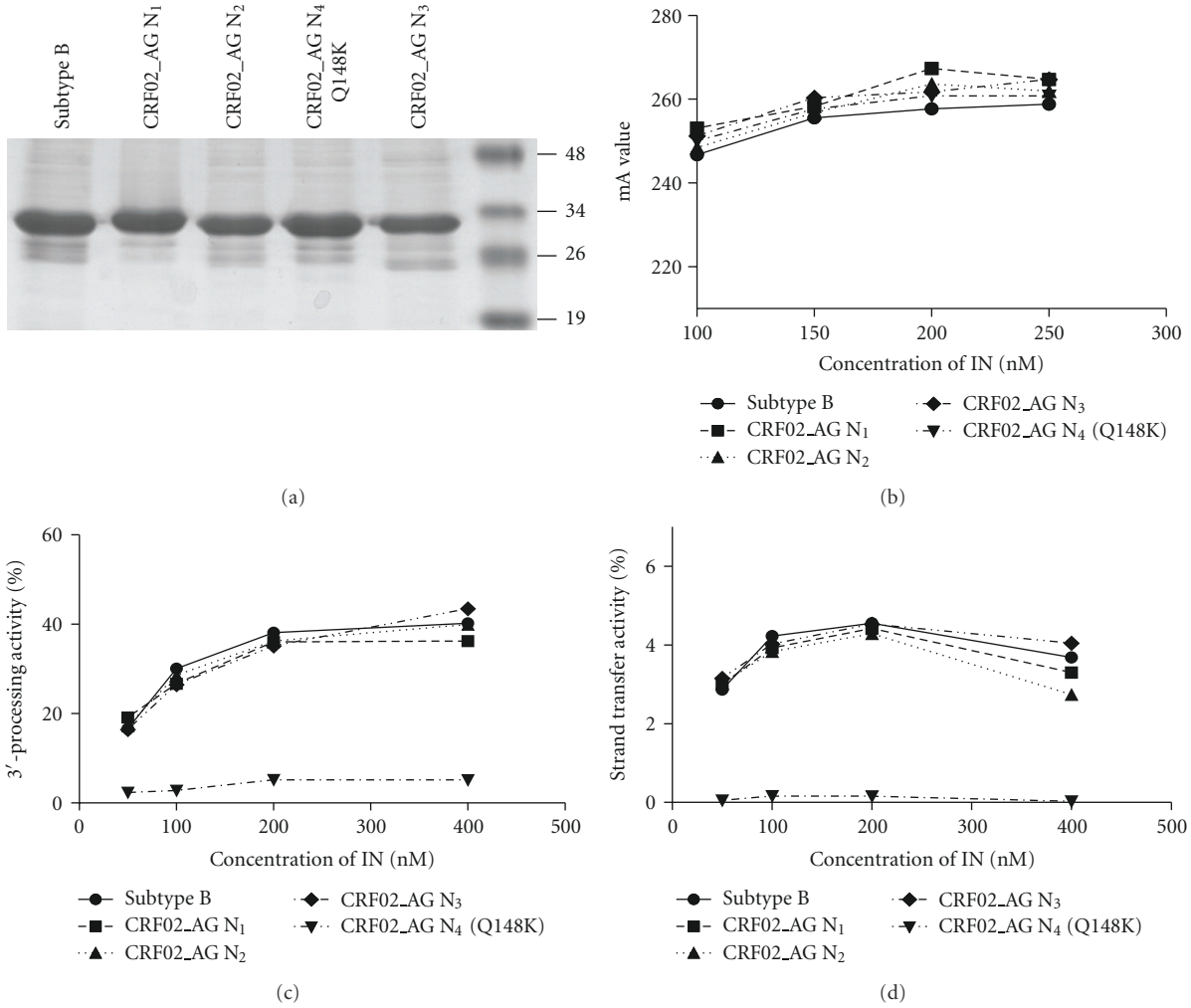

Figure 2: Purification of recombinant HIV-1 INs from B and CRF02_AG subtypes and comparison of their activities. (a) Purification products N_1, N_2, N_3 and N_4 of recombinant HIV-1 INs from B and CRF02_AG subtypes. (b)–(d) Comparison of DNA binding, 3′-processing and strand transfer activities, respectively, of the HIV-1 IN from B and CRF02_AG as a function of IN concentration.

−7.42 kcal/mol while those obtained with AutoDock range from −8.72 to −6.65 kcal/mol. Scores obtained for a given inhibitor display some variations from one strain to another and between the two docking programs. ELV best pose in model 1 (B subtype) predicted by Glide is very close to that in model 2 (CRF02_AG subtype). Small differences relate to an improved affinity of ELV to model 2 evidenced by a better score (−8.20 kcal/mol) and by the formation of an additional H-bond between the hydroxy group of ELV and E152 side chain (Figures 4(a) and 4(b)). RAL poses in models 1 and 2 differ strongly. In both cases RAL coordinates similarly the Mg^{2+} cations by its ketoenolate functionality, but the inhibitor adopts opposite positions, more specifically in model 1 its fluorobenzyl ring is oriented towards Y143, while in 2 towards Q148. L731,988 poses are also different in models 1 and 2, characterized by distinct pyrrole ring positions, close to E152 in 1 and to Y143 in 2. Such presence of alternative poses is likely due to a large pocket formed by the accessible active site and the open conformation of the folded loop which allow a large number of conformations and orientations with equivalent binding affinity for the flexible RAL and L731,988 molecules. Consequently no significant difference can be assessed between the binding of the three studied inhibitors to the unbound IN from strains B and CRF02_AG.

Further the inhibitors were docked onto models 3 and 4 representing preintegration complexes, $IN{\cdot}2Mg^{2+}{\cdot}DNA$, from B and CRF02_AG subtypes, respectively. Docking resulted in a binding for the three inhibitors with significantly higher scores than those found for the apo IN. This finding agrees well with the previously published experimental data that showed a high affinity of L-731,988 only to the IN conformations adopted after assembly with the viral DNA [25]. Glide scores ranked in a range from −10.22 to −8.73 kcal/mol, while AutoDock scores range from −13.45 to −11.11 kcal/mol. Comparisons of the poses produced by the two docking software were found similar, and consequently we focus here on the analysis of Glide results.

The three compounds are positioned in the catalytic site and chelate the Mg^{2+} cations in agreement with the mechanism of action of these molecules, which are strand transfer

Table 2: Docking binding energies of RAL, ELV and L731,988 on the HIV-1 IN from B and CRF02_AG strains predicted by Autodock and Glide. The targets are the IN model with one Mg^{2+} cation in the active site (apo state, models 1 and 2) and IN·DNA model with two Mg^{2+} cations (holo state, models 3 and 4).

Target	Inhibitor	The free binding energies (kcal/mol)	
		Autodock	Glide
IN B (apo)	RAL	−6.83	−8.05
	ELV	−8.22	−7.42
	L731,988	−7.81	−8.49
IN CRF02_AG (apo)	RAL	−6.65	−7.68
	ELV	−8.72	−8.20
	L731,988	−8.31	−7.85
IN·DNA_B (holo)	RAL	−11.43	−10.22
	ELV	−12.45	−9.17
	L731,988	−11.50	−8.73
IN·DNA CRF02_AG (holo)	RAL	−11.11	−9.98
	ELV	−13.45	−9.16
	L731,988	−11.93	−8.82
IN* B (holo)	RAL	−8.29	−8.36
	ELV	−11.62	−8.92
	L731,988	−12.19	−8.96
IN* CRF02_AG (holo)	RAL	−7.98	−8.46
	ELV	−11.80	−8.93
	L731,988	−11.58	−8.82

inhibitors [26]. RAL binding mode is characterized by higher scores in both models 3 (B subtype) and 4 (CRF02_AG subtype), respectively, to the other two inhibitors. RAL predicted poses are identical in models 3 and 4 (Figures 4(a), 4(b), 4(c) and 4(d)). It binds bidentaetly both metal cofactors of the active site acting as a 1–5, and 1–4-type ligand, with the enolic oxygen atom as an oxo-bridge between two Mg^{2+} cations. Additional stabilization of inhibitor RAL is achieved by π-staking of fluorobenzyl ring upon Cyt16 of DNA substrate. Similar to RAL, ELV coordinates the Mg^{2+} cofactors bidentantly through the 1–5 type β-ketoenolate moiety and 1–3 geminal carboxylic oxygen atoms, with a carboxylic oxygen atom as an oxo-bridge at the bicationic cluster. A few differences of ELV binding in models 3 and 4 refer to slightly different conformation of the chlorofluorobenzyl moiety. L731,988 molecule shows different binding poses in models 3 and 4. In model 3 (B subtype) L731,988 coordinates bidentately one Mg^{2+} cation by the oxygen atoms from keto functionality of ketoenolate and carboxylate groups, acting as a ligand of 1-6 type. The second Mg^{2+} cation is coordinated only by the carboxylate oxygen atom. In model 4 (CRF02_AG) L731,988 inhibitor shows exclusively one coordination to the one Mg^{2+} cation (Figures 4(e) and 4(f)).

The predicted binding poses of RAL correlate well with those observed in the X-ray structure of the PFV intasome complex [19, 20]. Undoubtedly, the presence of the second catalytic Mg^{2+} cation, the partial loop folding, and the DNA substrate bearing are presumably the driving determinants for the tight binding of ST inhibitors in the catalytic site. It was perfectly evidenced by Cherepanov that a series of INSTIs fixed similarly to the PFV intasome [19]. Apparently the crystallographic data or static models derived from these data are not suitable means to explain the specificity of inhibitor recognition by a target. Consequently, considering the similar scoring values for a given inhibitor and closed poses, no significant dissimilarity can be assessed between the binding of studied inhibitors to the IN·2Mg^{2+}·DNA complex from strains B and CRF02_AG.

To validate the *in silico* predictions regarding the susceptibility of subtypes B and CRF02_AG INs, the efficiency of INSTIs (RAL, ELV, and L731,988) on recombinant INs proteins was determined by *in vitro* strand transfer assay in the presence of increasing concentration of INSTI (see Section 4). As to all of the three studied INSTIs, no significant difference in IC_{50} values against recombinant HIV-1 INs from B and CRF02_AG strains was observed (Table 3). IC_{50} of RAL, ELV, and L731,988 against HIV-1 INs from B and CRF02_AG strains are 41.8, 93.4, 855 nM and 13.7–25.9, 48.9–66.8, 193–291 nM, respectively. The experimental ranking of the three compounds was predicted correctly by Glide scoring function.

The docking calculations evidenced that (i) the IN·DNA complex represents the best target for the studied inhibitors and (ii) the co-complexed vDNA partially shapes the inhibitors binding site. To further explore the role of vDNA, substrate was removed from the IN·vDNA complex and inhibitors were docked again on unbound IN with a fold corresponding to the holo state, models 5 and 6. The binding energies of RAL are depreciated upon vDNA removal in B and CR02_AG subtypes while ELV and L731,988 binding scores are less affected.

Docking scores are nearly similar between the two strains while poses display some variations, as already observed on the apo form. Surprisingly, the AutoDock results show

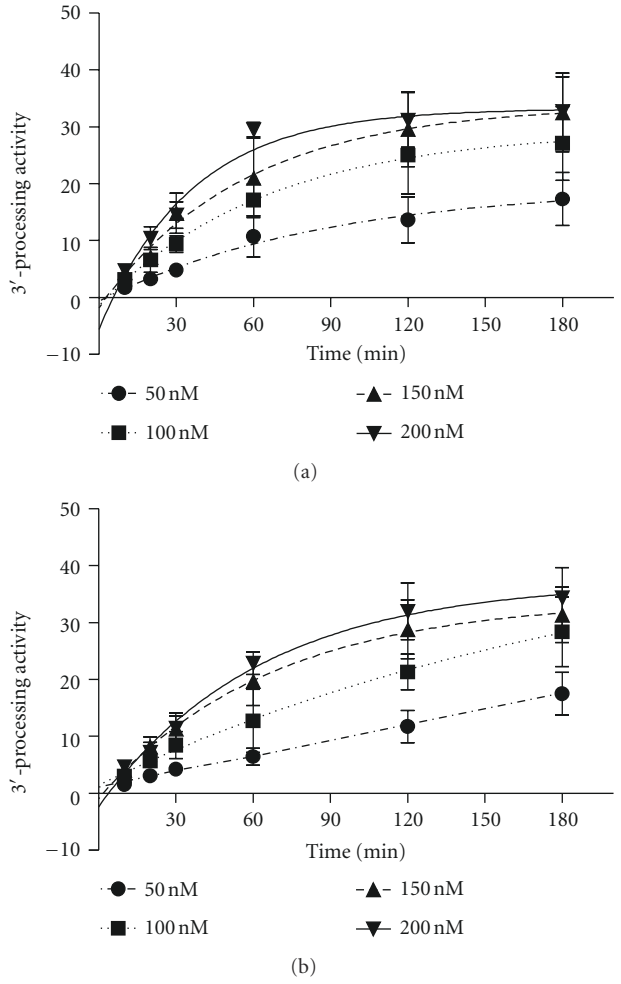

Figure 3: Kinetic comparison of HIV-1 B and CRF02_AG 33CR IN. (A) The kinetic features of recombinant HIV-1 B IN and (B) CRF02_AG IN (N_1) were determined *in vitro* using 3′-processing activity assay, in the presence of 50, 100, 150, and 200 nM recombinant IN proteins with an incubation time of 10, 20, 30, 60, 90, 120, and 180 min, respectively.

the lower score for RAL binding to both models 5 and 6, while the binding of the two other inhibitors are characterized by better scores, closer to those obtained with models 3 and 4. In contrast the scores produced by Glide are identical between the inhibitors and the subtypes. Chelation of the Mg^{2+} ions by the inhibitors is still maintained but the interaction patterns differ from those predicted in models 3 and 4. Indeed, in model 5 (B subtype) RAL chelates the first Mg^{2+} cation through the nitrogen atom of the oxadiazole ring, and the oxygen atom of the carboxamide moiety; the second Mg^{2+} is coordinated by 1–4 oxygen atoms of pyrimidinone fragment. In model 6 RAL mode of coordination resembles that observed in model 4; however, stabilizing π-stacking interactions were vanished. Again, the large volume of the binding pocket and the lack of stabilizing protein-ligand and DNA–ligand interactions can explain such variety. Consequently, unbound IN in the holo conformation, as unbound IN in the apo conformation, does not appear as a suitable target for the inhibitors RAL and

Table 3: IC_{50} of 3 INSTIs against recombinant HIV-1 B IN and CRF02_AG IN.

	IC_{50} (M)		
	RAL	ELV	L731,988
Subtype B	$4.185e-008$	$9.340e-008$	$8.554e-007$
CRF02_AG N_1	$1.373e-008$	$5.562e-008$	$2.115e-007$

ELV. L731,988 appears as a weaker binder, as confirmed by the experimental IC_{50} values.

Molecular modeling approaches were used to investigate the effect of the natural variations showed by CRF02_AG strain on the *in vitro* activities of the enzyme and its susceptibility to INSTIs as compared to the ones of the consensus B integrase. We found that the structural models of unbound (apo state) and viral DNA-bound (holo state) integrase showed very similar folding and tertiary structure for the two studied strains. The structural models of the IN·vDNA complex superimposed perfectly. This similarity was confirmed by comparable strand transfer activity for IN variants in 14, 112, 125, 134, 136, 206, and 283 positions. Consequently, the naturally occurring variations in the HIV-1 IN subtype CRF02_AG – K14R, V31I, L101I, T112V, T124A, T125A, G134N, I135V, K136T, V201I, T206S, V234I, and S283G, which were suggested to modify IN structure, do not affect significantly *in vitro* DNA binding activity, either 3′-processing or strand transfer reaction. Furthermore, docking results revealed that the modes of binding and docking conformations of three studied inhibitors are comparable for B and CRF02_AG strains and these INSTIs possessed similar IN inhibitory activity against B and CRF02_AG HIV-1 strains. Altogether these results demonstrate the absence of difference in susceptibility and confirm previously reported observations for subtype B and C HIV-1 INs [12]. Thus, in contrast to the lower baseline susceptibilities of recombinant A/G subtype virus to protease inhibitors (PIs) and reduced susceptibility of some A/G isolates to abacavir, INSTIs potentially provide an excellent therapeutic options for the treatment of HIV-1 subtype CRF02_AG-infected patients [10].

In the targets all three molecules are positioned similarly with keto-enol moiety in an orientation encouraging coordination of the two metal cofactors in the active site. Furthermore, independently of the method, the three INSTIs displayed a more favorable binding onto the IN·vDNA complex (holo state) than on the unbound enzyme (apo state), in good agreement with their mechanism of action [26]. Same difference in theoretically predicted modes of RAL binding was reported early by Loizidou [27]. The observed conformational and structural transformation of IN upon DNA binding led to an important change in the folding and conformation of the catalytic site loop which in turn favors a formation of the binding pocket accommodating the INSTIs. The binding modes of ELV and L731,988 were practically not altered by the removal of the viral DNA. Conversely removing vDNA had a significant effect on the docking results RAL, thereby highlighting the role of vDNA for RAL recognition most likely due to the halogenated benzyl moiety

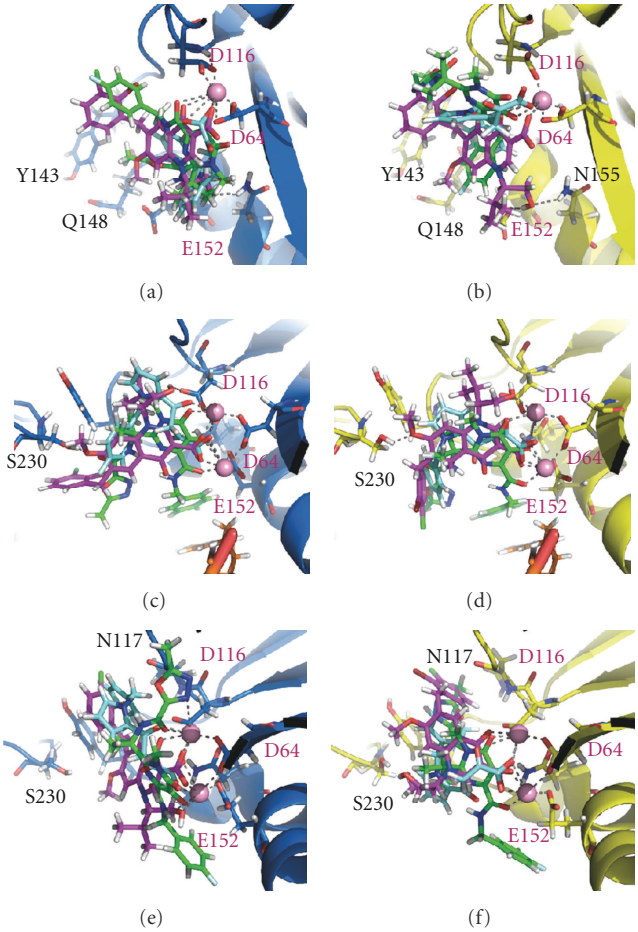

Figure 4: RAL (green), ELV (magenta), and L731,988 (cyan) best poses predicted by Glide. The inhibitors were docked into the active site of unbound IN (top) and IN·DNA complex (middle) and IN in holo conformation without DNA (bottom) from of the B (in blue) and CRF02_AG (in yellow). Proteins and DNA are shown as cartoons, inhibitors as sticks, and Mg^{+2} cations as balls.

that displaces the unpaired 5′-adenine and stacking with the Cyt16 through π-π interactions. Although such interaction is thought to be involved in all the IN strand transfer inhibitors examined [19], our results suggest that ELV and L731,988 binding determinants differed in part from the ones of RAL.

It should be noted that slight differences were observed between the results obtained with Glide and AutoDock scores, which can be ascribed to the impact of electrostatic interactions in the studied molecular systems. Indeed Glide uses higher negative charge localized on the two oxygen atoms of the hydroxypyrimidinone of RAL than AutoDock (-1.22 and $-0.5e$ versus -0.183 and $-0.265e$). Also, within the AutoDock scoring function, the carboxylate charges used for ELV ($2 \times -0.64e$) and L731,988 ($2 \times -0.62e$) are more than two oxygen atoms attached to the pyrimidine cycle of RAL. To verify this hypothesis, we repeated the docking calculations of ELV and L731,988 using the charges of two oxygen atoms attached to the pyrimidine ring of RAL instead of those assigned by Gasteiger charges. The new binding energies of both inhibitors increased from -12.45 and -11.50 to -7.95 and -7.80 kcal/mol for ELV and L731,988, respectively. Since these atomic charges contribute highly in the binding energy as the atoms coordinate Mg^{2+} ions, they are likely responsible for the discrepancies found between the theoretical binding energies and the experimental IC_{50} values. The experimental ranking of the three inhibitors based on IC_{50} is RAL > ELV > L731,988, as predicted by Glide while the ranking predicted by the AutoDock is ELV > L731,988 ≥ RAL. The high negative charges of the carboxylate oxygen atoms of ELV and L731,988 may be the obstacle to have inhibitory actions on integrase, as efficient as RAL, since these charges increase the desolvation free energy and so increase the binding penalty for these inhibitors.

Studies investigating the presence and frequency of polymorphisms in the HIV-1 gene of treatment-native patients are extremely important for tracing the virus evolution and the epidemiology of HIV infections worldwide. Associated crucial questions concern the effect of polymorphisms on viral enzymatic activities, susceptibility towards inhibitors, and inhibitor resistance pathways. The absence of accurate experimental data characterising the IN and/or IN·vDNA complex structures essentially perplexes an exploration of these essential topics. Since the beginning of clinical AIDS treatment with RAL in 2007, only a few attempts to probe RAL binding to integrase from different retroviral strains have been reported. Particularly, molecular docking of RAL into the IN catalytic core domain structure with the inhibitor 5CITEP as a viral DNA mimic has depicted different

binding modes and affinities of RAL to IN from B and C subtypes [27]. Differences between the binding modes of several compounds to IN from B and C subtypes were also communicated [28].

In this context, our combined theoretical (structural modeling) and experimental (biochemical) evaluation of subtype CRF02_AG variation impact/effect on IN interaction with DNA or IN susceptibility to INSTIs contribute to the understanding of polymorphism effects at the molecular and structural level. Our experiments have revealed that IN from subtype CRF02_AG has similar enzymatic activity to IN from subtype B, and the susceptibility of the two INs to strand transfer inhibitors is comparable. Results from molecular modeling and inhibitor docking were found in agreement with *in vitro* observations.

Biochemical studies have revealed the impact of HIV-1 natural polymorphism on the susceptibility of protease (PR)—the other retroviral enzyme—to inhibitors [29]. Recent structural and biophysical studies have also shown that sequence polymorphisms of B and CRF01_AE strains can alter protease activity and PR inhibitors binding [30]. In this protein, the variations between the two strains directly impact the conformation of the flap hinge region and the protease core region that play crucial roles for the enzyme functions.

By contrast, the residues showing natural variations in the HIV-1 integrases from B and CRF02_AG strains are located outside the catalytic region and outer to the binding site of the strand transfer inhibitors. Such type of polymorphism may allow the virus to preserve the integrase structural and functional properties as observed in this study.

The methods we applied could be used for the study of other retroviral substrains emerging at the moment or to appear in the future in order to evaluate and optimize the efficiency of novel specific antiretrovirals. Consequently, our study contributes particularly to this topic and closely relates to a clinically and therapeutically—significant question—does the HIV-1 integrase polymorphisms influence the susceptibility towards integrase inhibitors?

3. Conclusions

The naturally occurring variations in HIV-1 subtype CRF02_AG IN, such as K14R, V31I, L101I, T112V, T124A, T125A, G134N, I135V, K136T, V201I, T206S, V234I, and S283G, do not affect notably integrase structure, neither *in vitro* enzymatic activity, 3′-processing, nor strand transfer reaction. Docking results of all the considered inhibitors into the unbound IN model show the considerably low scores respectively, to docking into the pre integration IN·DNA complex. The docking scores and inhibitor poses confirm that the generated structure of the HIV IN·DNA complex is the appropriate biologically relevant model used to explain the inhibition mechanism of the strand transfer inhibitors. All the three studied molecules are polydentate ligands able to wrap around the metal cations in the active site. The results of the docking are in perfect agreement with the proposed mechanism of action for INSTIs. Docking results reveal that the modes of binding and docking conformations of three studied molecules are identical for the HIV-1 IN from B and CRF02_AG strains. The proposed mechanism of the integrase inhibition based on considering of different conformational states, unbound IN, and IN·vDNA complex holds for the two studied strains.

4. Methods

4.1. Molecular Modeling. All calculations were carried out on a Linux station (4×2 cores) running Centos 5.4. The IN models were constructed using Modeller package 9V8 [31]. The sequence alignment was performed using ClustalW server [32, 33] (http://www.ebi.ac.uk/Tools/clustalw2/index.html). The docking of ST inhibitors, RAL, ELV and L731,988 (Scheme 1), onto the IN models 1–6 was performed using two algorithms, GLIDE [34] incorporated in the Schrödinger suite (Schrödinger Inc.) and Autodock 4.2 [35]. Figures were produced with PyMol [36].

4.2. Models of the HIV-1 IN from B and CRF02_AG Strains. 3D models of the full-length IN homodimer, IN^{1-270} (unbound IN, or *apo* state, resp. to DNA) containing one Mg^{2+} cation in each active site were generated by homology modeling from crystallographic structures of isolated pairs of IN domains. Two structures of the HIV-1 IN, one containing the N-terminal domain (NTD) and the catalytic core domain (CCD) (IN^{1-210}, PDB code: 1K6Y) [37] and the other containing the CCD and the C-terminal domain (CTD) (IN^{56-270}, PDB code: 1EX4) [38], were chosen as the initial templates. These structures represent multiple mutants of the HIV-1 subtype B IN, the mutations being W131D/F139D/F185K in 1K6Y and C56S/W131D/F139/F185K/C180S in 1EX4. Both structures were superimposed and CCD domain (IN^{56-210}) of 1EX4, determined at lower resolution (2.8 Å) than 1K6Y (2.4 Å), was deleted. The disordered residues 271–288 were also omitted. Sequences of the WT HIV-1 INs from B and CRF02_AG strains, which differ by 13 amino acids (K/R14, V/I31, L/I101, T/V112, T/A124, T/A125, G/N134, I/V135, K/T136, V/I201, T/S206, V/I234 and S/G283), were aligned to the templates sequences using ClustalW. The missing CCD-NTD linker (47–55 aas) was constructed by an *ab initio* approach with Modeller 9V8, based on, discrete optimized protein energy (DOPE) scoring function [39]. 100 models were generated for each IN, from B and CRF02_AG strains. The conformation of the folded loop $IN^{140-149}$ with a well-shaped hairpin structure [40] was reconstructed by a loop-generating algorithm based on database searches (Protein Loop Search). Mg^{2+} cation was inserted into the active site (D64, D116, and E152) as reported in structure 1BI4 [41] and minimized by molecular mechanics (MM) under constrains using CHARMM [42]. We shall refer to these generated models as model 1 (B strain) and model 2 (CRF02_AG strain).

4.3. Models of the HIV-1 IN from B and CRF0_AG Strains in Complex with vDNA. 3D models of the IN·vDNA pre integration complex (*holo* state respectively to DNA) from B and CRF02_AG strains were generated by homology

modeling following a two-step procedure. The coordinates of the recently published crystal structure of the PFV IN·vDNA complex cocrystallized with RAL (PDB code: 3OYA, resolution of 2.65 Å) [19, 20] was used as template. The sequence alignment of the HIV-1 IN dimer (B strain) and the PFV IN was performed using ClustalW. The sequence identity between these two INs is 22%. Nevertheless, structure-based alignment of INs from the PFV and HIV-1 demonstrates high conservation of key structural elements and consequently, the PFV IN X-ray structure provides a good template for the HIV-1 IN model generation. In order to increase the quality of our model, the NED domain (residues 1 to 50), only present in PFV IN, was removed from the corresponding sequence. Then, the sequences of the structural domains of HIV-1 and PFV INs were aligned separately, taking into account the conservation of the secondary structure. The obtained sequence alignment was used for homology modeling of the HIV-1 intasome. The interdomains linker were constructed using the *ab initio* LOOP module in Modeller [43]. For both subtypes B and CRF02_AG models, distance restraints were applied to reproduce key interactions reported in earlier experimental studies [37, 44–46]. 100 models were generated for each IN, from B and CRF02_AG strains, and those with the lowest energy were retained. We shall refer to these models as model 3 (B strain) and model 4 (CRF02_AG strain). Two additional models 5 and 6 were generated by removing vDNA from models 3 and 4.

4.4. Refinement of Models 1–6 and Quality Check out. Hydrogen atoms were added by the HBUILD facility in CHARMM [42]. The resulting models were slightly minimized while constraining carbon-α to remove clashes. The stereochemical quality of the models was assessed with Portable ProCheck [47], which showed that more than 97% of the residues in all models had dihedral angles in the most favorable and allowed regions of the Ramachandran plot, indicating high model quality.

4.5. Molecular Docking. Initial molecular geometries of ELV and RAL were taken from the X-ray structures 30YA (RAL) and 3L2U (ELV) of PFV IN·vDNA complexes [19, 20]. The 3D structure of the compound L731,988 was generated by ChemBioOffice 2010 [48]. The models of all inhibitors (Scheme 1) in deprotonated form were minimized with density functional theory (DFT) B3LYP 6-31G* method implemented in *Gaussian03* program [49]. Inhibitors RAL, ELV, and L731,988 were docked onto models 1–6 using two algorithms, GLIDE [34] and AutoDock 4.2 [35]. The receptor is considered as a rigid body while the ligand is treated fully flexible.

In AutoDock 4.2, the graphical user interface (GUI) was used for the preparation of the inhibitor and receptor files. Grid maps of interaction energies for various atom types were constructed with a grid box of dimension $25\times25\times25$ Å^3 centered on the active site. Calculations were performed with a population size of 150, number of energy evaluations of 5×10^6, maximum number of generations of 27,000, mutation and crossover rate of 0.02 and 0.8 respectively. The number of runs was set to 100 to explore a large number of poses of the highest affinity and the Solis and Wets algorithm was used to relax the best 10% of the obtained conformations.

In the Schrödinger suite receptor grids were generated by Glide 4.5 within an enclosing box of size 20 Å centered on the active site. Inhibitors were docked flexibly to these pre-computing grids using standard precision (SP) scoring function. For each compounds, the best-scored pose was saved and analyzed.

4.6. Cloning of IN Gene. IN cDNA was derived from naïve HIV-1 subtype CRF02_AG infected patients. Plasmid pET15b- HIV-1subtype B IN (HBX2) was our lab's conservation [50]. Amplification of IN coding sequence was carried out with specific primers at 94°C for 10 min, then 28 repeat cycles (94°C for 30 s, 55°C for 45 s, and 72°C for 1 min) followed by incubation at 72°C for 10 min. PCR products corresponding to the entire IN sequences were purified and ligated into pGEM-T Easy vector (Promega) and sequenced (Eurofins MWG operon). Then IN gene was inserted into expression vector pET-15b (Novagen) after digested with Nde I and BamH I and verified by sequencing. Forward primer: 5′-CATATGTTTTTAGATGGCATAGATAAAGCC-3′; backward primer for CRF02_AG 33CR, 49CR: 5′ -GATCCTAATCCTCATCCTGTCTACCTGC-3′; backward primer for CRF02_AG 52CR Q148K: 5′-GATCCTAATCCTCATCCTGTCCACTTGC-3′; backward primer for CRF02_AG 68CR: 5′-GGATCCTAATCTTCATCCTGTCTACTTGC-3′.

4.7. Expression and Purification of IN. His-tagged INs were produced in *Escherichia coli* BL21-CodonPlus (DE3)-RIPL (Agilent) and purified under nondenaturing conditions as previously described [50, 51].

4.8. Steady-State Fluorescence Anisotropy-Based Assay. Steady-state fluorescence anisotropy values were recorded on a Beacon 2000 Instrument (Panvera, Madison, WI, USA), in a cell maintained at 25°C or 37°C under thermostatic control. The principle underlying the anisotropy-based assay was published elsewhere [52, 53]. DNA-binding assay was carried out at 25°C for 20 minutes in a buffer containing 10 mM HEPES pH 6.8, 1 mM dithiothreitol, and 7.5 mM magnesium chloride in the presence of 12.5 nM-double stranded DNA substrate (21-mer oligodeoxynucleotide mimicking the U5 viral DNA end, fluorescein-labeled at the 3′-terminal GT) and 100, 150, 200, and 250 nM recombinant IN, respectively. In kinetic study, steady-state fluorescence anisotropy-based 3′-processing activity assay was performed in the presence of 50, 100, 200, and 250 nM recombinant IN proteins and 12.5 nM double stranded fluorescein-labeled DNA substrate, at 37°C for 10, 20, 30, 60, 90, 120 and 180 min.

4.9. IN 3′-Processing and Strand Transfer Activity Assay. In vitro 3′-processing and strand transfer activities assays were carried out using the 21/21-mer or 21/19-mer double

stranded oligodeoxynucleotides marked with [γ-^{32}P] ATP-respectively, as previously described [51]. The duration of the assays was 3 hours, at temperature 37°C, in a buffer containing 10 mM HEPES pH 6.8, 1 mM dithiothreitol, and 7.5 mM magnesium chloride in the presence of 12.5 nM double stranded DNA substrate and 100 nM recombinant IN. The kinetic study was carried out by testing *in vitro* 3′-processing activity in the presence of 50, 100, 150, and 200 nM recombinant IN proteins, at 37°C for 10, 20, 30, 60, 90, 120 and 180 min, respectively.

4.10. Susceptibility to INSTIs. Susceptibility of INs to INSTI was determined by testing in vitro strand transfer activity in the presence of increasing concentration of INSTI in DMSO. Inhibition by the drug was expressed as a fractional product (percentage of the activity of the control without drug). The 50% inhibitory concentration (IC_{50}), defined as the concentration of drug that results in 50% inhibition, was calculated from inhibition curves fitted to experimental data with Prism software, version 5.0 (GraphPad Software, Inc., San Diego, CA, USA).

Abbreviations

HIV-1:	Human immunodeficiency virus
vDNA:	Viral DNA
hDNA:	Host DNA
IN:	Integrase
CRF02_AG:	Circulating recombinant form
LTR:	Long terminal repeat
PFV:	Prototype foamy virus
NTD:	N-terminal domain
CCD:	Catalytic core domain
CTD:	C-terminal domain
ST:	Strand transfer
INSTI:	Integrase strand transfer inhibitor
DKAs:	Diketo acids
RAL:	Raltegravir
ELV:	Elvitegravir
PI:	Protease inhibitors
RMSD:	Root mean square deviation.

Conflict of Interests

The authors have declared no competing interests.

Authors' Contribution

X. Ni, S. Abdel-Azeim, and E. Laine contributed equally in this work. J.-F. Mouscadet and L.Tchertanov conceived and designed the experiments. X. Ni, S. Abdel-Azeim, E. Laine, R. Arora, and O. Osemwota performed the experiments. X. Ni, S. Abdel-Aziem, and E. Laine analysed the data. A.-G. Marcelin and V. Calvez contributed with reagents/materials/analysis tools. E. Laine, J.-F. Mouscadet, and L. Tchertanov wrote the paper.

Funding

This work was funded by the Ecole Normale Supérieure de Cachan, the Centre National de la Recherche Scientifique (CNRS), and SIDACTION.

Acknowledgments

The authors acknowledge Schrödinger for proving licenses.

References

[1] P. O. Brown, "Integration of retroviral DNA," *Current Topics in Microbiology and Immunology*, vol. 157, pp. 19–48, 1990.

[2] S. Y. Rhee, T. F. Liu, M. Kiuchi et al., "Natural variation of HIV-1 group M integrase: implications for a new class of antiretroviral inhibitors," *Retrovirology*, vol. 5, article 74, 2008.

[3] J. Hemelaar, E. Gouws, P. D. Ghys, and S. Osmanov, "Global trends in molecular epidemiology of HIV-1 during 2000–2007," *AIDS*, vol. 25, no. 5, pp. 679–689, 2011.

[4] L. Fischetti, O. Opare-Sem, D. Candotti, F. Sarkodie, H. Lee, and J. P. Allain, "Molecular epidemiology of HIV in Ghana: dominance of CRF02_AG," *Journal of Medical Virology*, vol. 73, no. 2, pp. 158–166, 2004.

[5] L. Fischetti, O. Opare-Sem, D. Candotti, H. Lee, and J. P. Allain, "Higher viral load may explain the dominance of CRF02_AG in the molecular epidemiology of HIV in Ghana," *AIDS*, vol. 18, no. 8, pp. 1208–1210, 2004.

[6] H. F. Njai, Y. Gali, G. Vanham et al., "The predominance of Human Immunodeficiency Virus type I (HIV-1) circulating recombinant form 02 (CRF02_AG) in West Central Africa may be related to its replicative fitness," *Retrovirology*, vol. 3, article 40, 2006.

[7] L. F. A. MacHado, M. O. G. Ishak, A. C. R. Vallinoto et al., "Molecular epidemiology of HIV type 1 in Northern Brazil: identification of subtypes C and D and the introduction of CRF02-AG in the amazon region of Brazil," *AIDS Research and Human Retroviruses*, vol. 25, no. 10, pp. 961–966, 2009.

[8] J. R. Ye, S. Q. Yu, H. Y. Lu, W. S. Wang, R. L. Xin, and Y. Zeng, "Genetic diversity of HIV type 1 isolated from newly diagnosed subjects (2006-2007) in Beijing, China," *AIDS Research and Human Retroviruses*, vol. 28, no. 1, pp. 119–123, 2012.

[9] D. Descamps, M. L. Chaix, B. Montes et al., "Increasing prevalence of transmitted drug resistance mutations and non-B subtype circulation in antiretroviral-naive chronically HIV-infected patients from 2001 to 2006/2007 in France," *Journal of Antimicrobial Chemotherapy*, vol. 65, no. 12, Article ID dkq380, pp. 2620–2627, 2010.

[10] J. L. Martínez-Cajas, N. Pant-Pai, M. B. Klein, and M. A. Wainberg, "Role of genetic diversity amongst HIV-1 non-B subtypes in drug resistance: a systematic review of virologic and biochemical evidence," *AIDS Reviews*, vol. 10, no. 4, pp. 212–223, 2008.

[11] B. S. Taylor, M. E. Sobieszczyk, F. E. McCutchan, and S. M. Hammer, "Medical progress: the challenge of HIV-1 subtype diversity," *New England Journal of Medicine*, vol. 358, no. 15, pp. 1590–1602, 2008.

[12] T. Bar-Magen, R. D. Sloan, V. H. Faltenbacher et al., "Comparative biochemical analysis of HIV-1 subtype B and C integrase enzymes," *Retrovirology*, vol. 6, article 103, 2009.

[13] A. Low, N. Prada, M. Topper et al., "Natural polymorphisms of human immunodeficiency virus type 1 integrase and

inherent susceptibilities to a panel of integrase inhibitors," *Antimicrobial Agents and Chemotherapy*, vol. 53, no. 10, pp. 4275–4282, 2009.

[14] I. Malet, C. Soulie, L. Tchertanov et al., "Structural effects of amino acid variations between B and CRF02-AG HIV-1 integrases," *Journal of Medical Virology*, vol. 80, no. 5, pp. 754–761, 2008.

[15] C. Fenollar-Ferrer, V. Carnevale, S. Raugei, and P. Carloni, "HIV-1 integrase-DNA interactions investigated by molecular modelling," *Computational and Mathematical Methods in Medicine*, vol. 9, no. 3-4, pp. 231–243, 2008.

[16] A. I. Maïga, I. Malet, C. Soulie et al., "Genetic barriers for integrase inhibitor drug resistance in HIV type-1 B and CRF02_AG subtypes," *Antiviral Therapy*, vol. 14, no. 1, pp. 123–129, 2009.

[17] E. Asante-Appiah and A. M. Skalka, "A metal-induced conformational change and activation of HIV-1 integrase," *Journal of Biological Chemistry*, vol. 272, no. 26, pp. 16196–16205, 1997.

[18] J. F. Mouscadet, O. Delelis, A. G. Marcelin, and L. Tchertanov, "Resistance to HIV-1 integrase inhibitors: a structural perspective," *Drug Resistance Updates*, vol. 13, no. 4-5, pp. 139–150, 2010.

[19] S. Hare, A. M. Vos, R. F. Clayton, J. W. Thuring, M. D. Cummings, and P. Cherepanov, "Molecular mechanisms of retroviral integrase inhibition and the evolution of viral resistance," *Proceedings of the National Academy of Sciences of the United States of America*, vol. 107, no. 46, pp. 20057–20062, 2010.

[20] S. Hare, S. S. Gupta, E. Valkov, A. Engelman, and P. Cherepanov, "Retroviral intasome assembly and inhibition of DNA strand transfer," *Nature*, vol. 464, no. 7286, pp. 232–236, 2010.

[21] Z. Yin and R. Craigie, "Modeling the HIV-1 intasome: a prototype view of the target of integrase inhibitors," *Viruses*, vol. 2, no. 12, pp. 2777–2781, 2010.

[22] E. Guiot, K. Carayon, O. Delelis et al., "Relationship between the oligomeric status of HIV-1 integrase on DNA and enzymatic activity," *Journal of Biological Chemistry*, vol. 281, no. 32, pp. 22707–22719, 2006.

[23] O. Delelis, I. Malet, L. Na et al., "The G140S mutation in HIV integrases from raltegravir-resistant patients rescues catalytic defect due to the resistance Q148H mutation," *Nucleic Acids Research*, vol. 37, no. 4, pp. 1193–1201, 2009.

[24] C. Maurin, F. Bailly, E. Buisine et al., "Spectroscopic studies of diketoacids-metal interactions. A probing tool for the pharmacophoric intermetallic distance in the HIV-1 integrase active site," *Journal of Medicinal Chemistry*, vol. 47, no. 22, pp. 5583–5586, 2004.

[25] A. S. Espeseth, P. Felock, A. Wolfe et al., "HIV-1 integrase inhibitors that compete with the target DNA substrate define a unique strand transfer conformation for integrase," *Proceedings of the National Academy of Sciences of the United States of America*, vol. 97, no. 21, pp. 11244–11249, 2000.

[26] T. Kawasuji, T. Yoshinaga, A. Sato, M. Yodo, T. Fujiwara, and R. Kiyama, "A platform for designing HIV integrase inhibitors. Part 1: 2-Hydroxy-3-heteroaryl acrylic acid derivatives as novel HIV integrase inhibitor and modeling of hydrophilic and hydrophobic pharmacophores," *Bioorganic and Medicinal Chemistry*, vol. 14, no. 24, pp. 8430–8445, 2006.

[27] E. Z. Loizidou, I. Kousiappa, C. D. Zeinalipour-Yazdi, D. A. M. C. Van De Vijver, and L. G. Kostrikis, "Implications of HIV-1 M group polymorphisms on integrase inhibitor efficacy and resistance: genetic and structural in silico analyses," *Biochemistry*, vol. 48, no. 1, pp. 4–6, 2009.

[28] R. Hewer, T. Traut, J. Coates, and B. Williams, "Predicted modes of resistance and hypersensensivity confered by natural polymorphisms of HIV-1 integrase," *Antiviral Research*, vol. 82, no. 2, article A24, 2009.

[29] A. Ali, R. M. Bandaranayake, Y. Cai et al., "Molecular basis for drug resistance in HIV-1 protease," *Viruses*, vol. 2, no. 11, pp. 2509–2535, 2010.

[30] R. M. Bandaranayake, M. Kolli, N. M. King et al., "The effect of clade-specific sequence polymorphisms on HIV-1 protease activity and inhibitor resistance pathways," *Journal of Virology*, vol. 84, no. 19, pp. 9995–10003, 2010.

[31] N. Eswar, B. John, N. Mirkovic et al., "Tools for comparative protein structure modeling and analysis," *Nucleic Acids Research*, vol. 31, no. 13, pp. 3375–3380, 2003.

[32] M. A. Larkin, G. Blackshields, N. P. Brown et al., "Clustal W and Clustal X version 2.0," *Bioinformatics*, vol. 23, no. 21, pp. 2947–2948, 2007.

[33] J. D. Thompson, D. G. Higgins, and T. J. Gibson, "CLUSTAL W: improving the sensitivity of progressive multiple sequence alignment through sequence weighting, position-specific gap penalties and weight matrix choice," *Nucleic Acids Research*, vol. 22, no. 22, pp. 4673–4680, 1994.

[34] R. A. Friesner, J. L. Banks, R. B. Murphy et al., "Glide: a new approach for rapid, accurate docking and scoring. 1. Method and assessment of docking accuracy," *Journal of Medicinal Chemistry*, vol. 47, no. 7, pp. 1739–1749, 2004.

[35] G. M. Morris, H. Ruth, W. Lindstrom et al., "Software news and updates AutoDock4 and AutoDockTools4: automated docking with selective receptor flexibility," *Journal of Computational Chemistry*, vol. 30, no. 16, pp. 2785–2791, 2009.

[36] The PyMOL Molecular Grapics System, 2002.

[37] J. Y. Wang, H. Ling, W. Yang, and R. Craigie, "Structure of a two-domain fragment of HIV-1 integrase: implications for domain organization in the intact protein," *EMBO Journal*, vol. 20, no. 24, pp. 7333–7343, 2002.

[38] J. C. H. Chen, J. Krucinski, L. J. W. Miercke et al., "Crystal structure of the HIV-1 integrase catalytic core and C-terminal domains: a model for viral DNA binding," *Proceedings of the National Academy of Sciences of the United States of America*, vol. 97, no. 15, pp. 8233–8238, 2000.

[39] M. Y. Shen and A. Sali, "Statistical potential for assessment and prediction of protein structures," *Protein Science*, vol. 15, no. 11, pp. 2507–2524, 2006.

[40] J. F. Mouscadet, R. Arora, J. André et al., "HIV-1 IN alternative molecular recognition of DNA induced by raltegravir resistance mutations," *Journal of Molecular Recognition*, vol. 22, no. 6, pp. 480–494, 2009.

[41] S. Maignan, J. P. Guilloteau, Q. Zhou-Liu, C. Clément-Mella, and V. Mikol, "Crystal structures of the catalytic domain of HIV-1 integrase free and complexed with its metal cofactor: high level of similarity of the active site with other viral integrases," *Journal of Molecular Biology*, vol. 282, no. 2, pp. 359–368, 1998.

[42] B. R. Brooks, C. L. Brooks, A. D. Mackerell et al., "CHARMM: the biomolecular simulation program," *Journal of Computational Chemistry*, vol. 30, no. 10, pp. 1545–1614, 2009.

[43] A. Sali and T. L. Blundell, "Comparative protein modelling by satisfaction of spatial restraints," *Journal of Molecular Biology*, vol. 234, no. 3, pp. 779–815, 1993.

[44] S. Hare, F. Di Nunzio, A. Labeja, J. Wang, A. Engelman, and P. Cherepanov, "Structural basis for functional tetramerization of lentiviral integrase," *PLoS Pathogens*, vol. 5, no. 7, Article ID e1000515, 2009.

[45] L. Du, L. Shen, Z. Yu et al., "Hyrtiosal, from the marine sponge Hyrtios erectus, inhibits HIV-1 integrase binding to viral DNA by a new inhibitor binding site," *ChemMedChem*, vol. 3, no. 1, pp. 173–180, 2008.

[46] R. Lu, H. Z. Ghory, and A. Engelman, "Genetic analyses of conserved residues in the carboxyl-terminal domain of human immunodeficiency virus type 1 integrase," *Journal of Virology*, vol. 79, no. 16, pp. 10356–10368, 2005.

[47] R. A. Laskowski, M. W. Macarthur, D. S. Moss, and J. M. Thornton, "Procheck—a program to check the stereochemical quality of protein structures," *Journal of Applied Crystallography*, vol. 26, pp. 283–291, 1993.

[48] S. M. Kerwin, "ChemBioOffice Ultra 2010 suite," *Journal of the American Chemical Society*, vol. 132, no. 7, pp. 2466–2467, 2010.

[49] *Gaussian 03*, Gaussian, Wallingford, UK, 2003.

[50] H. Leh, P. Brodin, J. Bischerour et al., "Determinants of Mg^{2+}-dependent activities of recombinant human immunodeficiency virus type 1 integrase," *Biochemistry*, vol. 39, no. 31, pp. 9285–9294, 2000.

[51] I. Malet, O. Delelis, M. A. Valantin et al., "Mutations associated with failure of raltegravir treatment affect integrase sensitivity to the inhibitor in vitro," *Antimicrobial Agents and Chemotherapy*, vol. 52, no. 4, pp. 1351–1358, 2008.

[52] J. Agapkina, M. Smolov, S. Barbe et al., "Probing of HIV-1 integrase/DNA interactions using novel analogs of viral DNA," *Journal of Biological Chemistry*, vol. 281, no. 17, pp. 11530–11540, 2006.

[53] M. Smolov, M. Gottikh, V. Tashlitskii et al., "Kinetic study of the HIV-1 DNA 3′-end processing: single-turnover property of integrase," *FEBS Journal*, vol. 273, no. 6, pp. 1137–1151, 2006.

Provisional chapter

The HIV-1 Integrase: Modeling and Beyond

Rohit Arora and Luba Tchertanov

Additional information is available at the end of the chapter

http://dx.doi.org/10.5772/52344

1. Introduction

Molecular recognition is a fundamental phenomenon observed in all biological system-sorganisation – proteins, nucleic acidsand their complexes, cells and tissues. Molecular recognition is governed by specific attractive interactions between two or more partner molecules through non-covalent bonding such as hydrogen bonds, metal coordination, electrostatic effects, hydrophobic and van der Waals interactions. The partners – receptor(s) and substrate(s) or ligands – involved in molecular recognition exhibit molecular complementarity that can be adjusted over the recognition process. Competition and co-operation, the two opposite natural effects contributing to selective and specific recognition between participating partners, are the basic principles of substrate/ligand/ inhibitor or protein binding to its targets.

The tertiary structures of biological objects (proteins and nucleic acids) are formed mainly by hydrogen bonds (enthalpic contributions) and by hydrophobic contacts (mostly entropic contributions). With a few exceptions, (e.g. ligand binding to the Ah receptor), the organisation of ligand-protein complexes depends primarily on hydrogen bonding.

In the process of a ligand binding to its target the hydrogen bonds contribute to (i) the orientation of the substrates/ligands/inhibitors by a receptor, frequently associated with a conformational/structural adjustment of the interacting agents; (ii) the specific recognition of substrates/ligands/inhibitors and selectivity between sterically or structurally similar but biochemically different species; (iii) the affinity of ligands/inhibitors – the most decisive factor in drug design.

To describe the pharmacological properties of a given ligand or inhibitor, the knowledge of the site where the inhibitor is to bind in the target and of which interaction(s) control the specific recognition of the inhibitor by its target(s), represents a corner stone factor. Only a limited number of target-ligand molecular complexes have been characterized experimen-

tally at the atomic level (X-ray or NMR analysis) [1]. Part of them describes the binding mode of therapeutically relevant ligands to biologically non-relevant and non-pertinent targets (e.g., the HIV-1 integrase specific inhibitor RAL was published as a ligand fixed to the PFV intasome [2,3]). Consequently, a large quantity of reliable information on target-ligand binding is based on molecular docking methods which generate insights into the interactions of ligands with the amino acid residues in the binding pockets of the targets, and also predict the corresponding binding affinities of ligands [4]. The first step of a docking calculation consists in the choice or generation/construction of the therapeutically appropriate target. Frequently the target modeling is a hard computational task which requires the application of sophisticated theoretical methods and constitutes a fascinating creative process.

Therefore, theoretical studies contributed first, to establishing biologically valid models of the targets; second, through the use of these models, to the understanding of the protein functional properties; and finally to apply these data to rational drug design.

Here we compile and review the data on the molecular structure, properties and interactions of the HIV-1 integrase representing from one side, a characteristic example of a polyfunctional and complex biological object interacting with different viral and cellular partners and from another side, an attractive therapeutical target. We attempt to extract key messages of practical value and complement references with our own research of this viral enzyme. We characterized the structural and conformational features of Raltegravir (RAL), the first integrase specific inhibitor approved for the treatment of HIV/AIDS, and we analyzed the factors contributing to RAL recognition by the viral targets.

2. The HIV-1 integrase and integrase-viral DNA pre-integration complex

2.1. Activities

The HIV-1 integrase (IN) is a key enzyme in the replication mechanism of retroviruses, catalyzing the covalent insertion of the reverse-transcribed DNA into the chromosomes of the infected cells [5].Once integrated, the provirus persists in the host cell and serves as a template for the transcription of viral genes and replication of the viral genome, leading to production of new viruses (Figure 1a). A two-step reaction is required for covalent integration of viral DNA (vDNA) into host DNA (hDNA).First, IN binds to a short sequence located at either end of the long terminal repeat (LTR) of the viral DNA and catalyzes an endo-nucleotide cleavage. This process is known as 3′-processing reaction (3′-P), resulting in the removal of two nucleotides from each of the 3′-ends of the LTR and the delivery of hydroxyl groups for nucleophilic attacks (Figure 1 b).

The cleaved (pre-processed) DNA is then used as a substrate for the strand transfer (ST) reaction, leading to the covalent insertion of the vDNA into genome of the infected cell [5,7].The ST reaction occurs at both ends of the vDNA simultaneously, with an offset of precisely five base pairs between the two distant points of insertion. The integration process is accomplished by the removal of unpaired dinucleotides from the 5′-ends of the vDNA, the

filling in of the single-strand gaps between viral and target DNA molecules and ligation of the 3′-ends of the vDNA to the 5′-ends of the hDNA (Figure 1 b). These two reactions are spatially and temporally separated and energetically independent: the 3′-processing takes place in the cytoplasm of the infected cells, whereas strand transfer occurs in the nuclei. They are catalyzed by the enzyme in different conformational and oligomerisation states: dimerization is required for the 3′-processing step [8,9], while tetrameric IN is believed to be required for strand transfer [10-12].

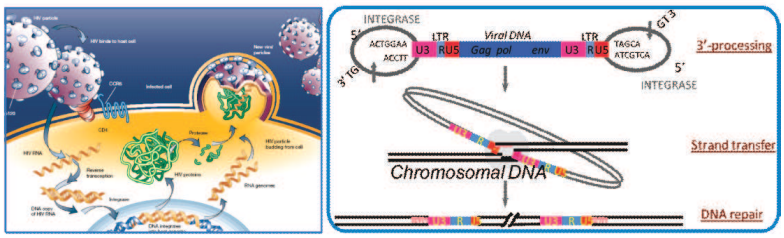

(a) (b)

Figure 1. The HIV-1 replication cycle (a) and catalytic steps involved in the insertion of viral DNA into the human genome (b) [6].

2.2. Structural data

The HIV-1 IN is a 288 amino acids enzyme (32 kDa) that consists in three structurally distinct domains: (i) the N-terminal domain (NTD, $IN^{1–49}$) with a non-conventional HHCC zinc-finger motif, promoting protein multimerization; (ii) the central core domain (CCD, $IN^{50–212}$) containing a canonical D,D,E motif performing catalysis and involved in DNA substrate recognition [35]; (iii) the C-terminal domain (CTD, $IN^{213–288}$), which non-specifically binds DNA and helps to stabilize the IN DNAcomplex [13]. Both integration steps, 3′-P and ST, involve the active site and the active site flexible loop formed by ten residues, $IN^{140-149}$.

Neither the structure of isolated full-length IN from HIV-1 nor that of IN complex with its DNA substrate has been determined. Nevertheless, the structures of the isolated HIV-1 domains or two domains were characterized by X-ray crystallography (34 structures) and NMR analysis (9 structures) [1]. NTD presented by 6 NMR structure solutions (1WJA, 1WJB, 1WJC, 1WJE, and 1WGF) [14-16] was classified by SCOP as the ‘all alpha helix’ structure and consists of four helices stabilized by a Zn^{2+}cation coordinated with the HHCC motif (His12, His16, Cys40 and Cys43); the sequence from 43 to 49 residue are disordered (Figure 2). Structure of CTD was also characterised by NMR (3 deposited solutions (1IHV, 1IHW and 1QMC) [17,18]. According to the SCOP classification it presents the ‘all beta strand’ structure and consists of five anti-parallel β-strands forming a β-barrel and adopting an SH3-like fold (Figure 2).

The human IN CCD characterized by X-ray analysis has been reported as 14 different crystal structures (1HYV, 1HYZ, 1EXQ, 1QS4, 1B92, 1B9D, 1BHL, 1BI4, 1BIS, 1BIU, 1BIZ, 1BL3, 1ITG and 2ITG). The wild-type IN was resolved with a poor precision (1ITG) [19], the other structures represent engineered mutants, either single (F185K/H) [20-23], double (W131E and F185K; G149A and F185K or C56S and F185K) [24-26] or multiple (C56S, W131D, F139D and F185K) [27] mutants which were designed to overcome the poor solubility of the protein. The core domain has a mixed α/β structure, with five β-sheets and six α –helices (Figure 2).

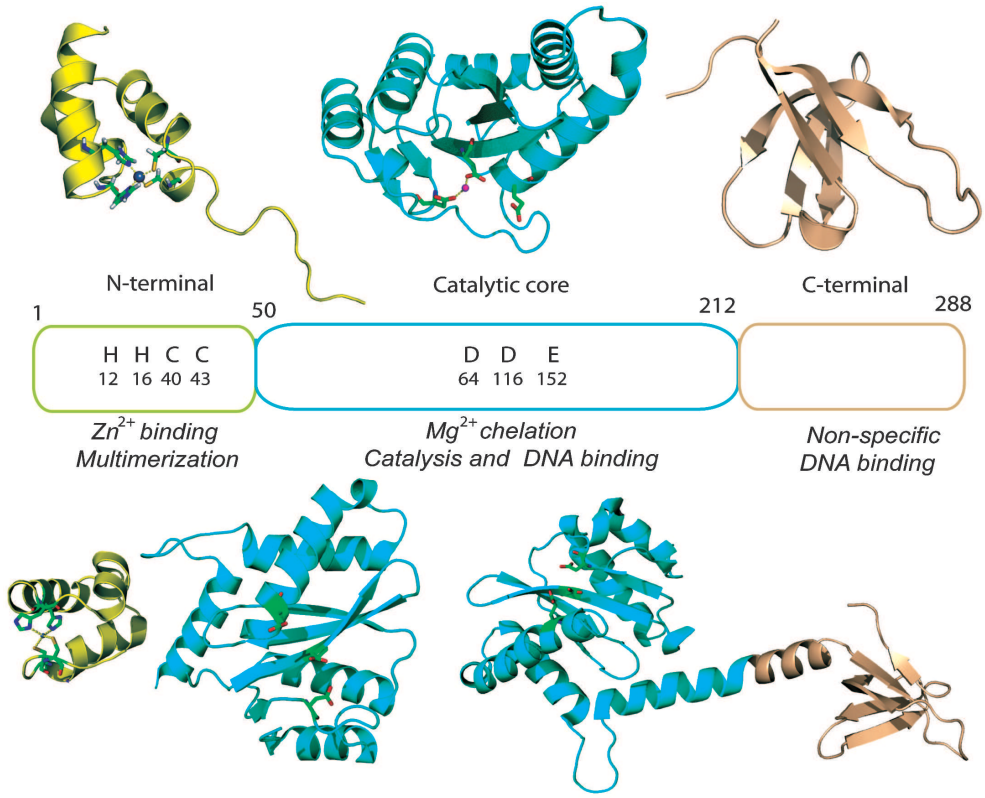

Figure 2. Structural domains of the HIV-1 integrase. (Top) N-terminal (IN^{1-49}, left), catalytic core (IN^{50-212}, middle) and C-terminal ($IN^{219-270}$, right) domains; (bottom) N-terminal with catalytic core domain (IN^{1-212}, left) and catalytic core with C-terminal fragment (IN^{52-288}, right). The structures are shown as cartoon with the side chains of the HHCC and DDE motifs in the N-terminal and catalytic core domains rendered in stick and the Zn^{2+} and Mg^{2+}cations as balls; dashed lines indicate ion coordination [28,29].

The active site residues D64, D116 and E152 are located in different structural elements: β-sheet (β1), coil and helix (α4), respectively. The catalytic core domain also encompasses a

flexible loop comprising residues 140–149, in which conformational changes are required for 3′-P and ST reactions. These activities require the presence of a metallic cofactor(s), the Mg2+ ion(s), which binds to the catalytic residues D64, D116 and E152. The number of Mg2+ cations is different for the distinct enzymatic reactions and consequently, for the different IN states: a single Mg2+ cation in non-processed IN, and two in processed IN. The structures of avian sarcoma virus (ASV) IN [21] and the Tn5 transposase[30] have provided evidence of a two-metal active site structure, which has been used to build metal-containing IN models [31-33].

Crystallographic structures of $IN^{1–212}$ and $IN^{50–288}$ two-domain constructs have also been obtained for W131D/F139D/F185K and C56S/W131D/F139D/F185K/C180S mutants, respectively (Figure 2) [34,35]. In the first one of these structures, there is an asymmetric unit containing four molecules forming pairs of dimers connected by a non-crystallographic two fold axis, in which the catalytic core and N-terminal domains are well resolved, their structures closely matching those found with isolated $IN^{1–45}$ and $IN^{50–212}$ domains, and connected by a highly disordered linking region (47–55 amino acids). The X-ray structure of the other two-domain construct, $IN^{50–288}$, showed there was a two-fold symmetric dimer in the crystal. The catalytic core and C-terminal domains were connected by a perfect helix formed by residues 195–221. The local structure of each domain was similar to the structure of the isolated domains. The dimer core domain interface was found to be similar to the isolated core domain, whereas the dimer C-terminal interface differed from that obtained by NMR.

2.3. Theoretical models

All these structural data characterising the HIV-1 IN single or two-domains allow the generation of biologically relevant models, representing either the unbound dimeric enzyme or IN complexed with the viral or/and host DNA [29].

IN acts as a multimer[36].Dimerization is required for the 3′-processing step, with tetrameric IN catalyzing the ST reaction [37,38]. Dimeric models were built to reproduce the specific contacts between IN and the LTR terminal CA/TG nucleotides identified *in vitro*[39,40]. However, most models include a tetrameric IN alone or IN complex with either vDNA alone or vDNA/hDNA, recapitulating the simultaneous binding of IN to both DNAs required for strand transfer (Figure 3 b–d).

These models were either based on the partial crystal structure of IN [32,44] or constructed by analogy with a synaptic Tn5 transposase complex described in previous studies [42,45,46].

Most models include an Mg^{2+} cationic cofactor and take into account both structural data and biologically significant constraints (Figure 2 b–d). In particular, HIV-1 IN synaptic complexes (IN•vDNA•hDNA) have been constructed taken into account the different enzymatic states occurring during the integration process (Figure 3 d) [41,42]. Such complexes have also been characterized by electron microscopy (EM) and single-particle imaging at a resolution of 27 Å [47]. Recently the X-ray complete structure of the Primate Foamy Virus (PFV)

integrase in complex with the substrate DNA and Raltegravir or Elvitegravir has also recently been reported (Figure 3 e) [2].

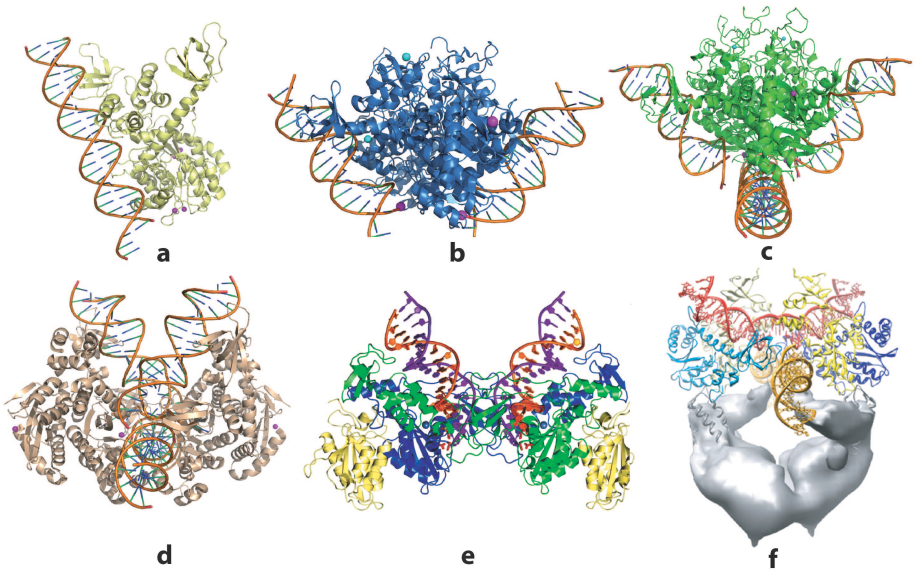

Figure 3. Integrase architecture and organization. Theoretical models: (a) dimeric model of the full-length IN•vDNA-complex[39]; (b) tetramer models of the IN•vDNA[27]; (c and d) synaptic complexes IN4•vDNA•hDNA [41,42]; (e) X-ray structure of the PFV IN•vDNAintasome[2]; and (f) EM maps reconstitution of IN•vDNA•hDNA complex with LEGDF [43]. Protein and DNA structures are presented as cartoon with colour coded nucleotides and Zn^{2+} and Mg^{2+}cations shown as balls. The active site contains two $Mg2^{+}$ cations in (a) and one in (b–d).

In this complex, the retroviral intasome consists of an IN tetramer tightly associated with a pair of viral DNA ends. The overall shape of the complex is consistent with a low-resolution structure obtained by electron microscopy and single-particle reconstruction for HIV-1 IN complex with its cellular cofactor, the lens epithelium-derived growth factor (LEDGF) (Figure 3 d) [43].

2.5. Targets models representing the HIV-1 integrase before and after 3′-processing

Recently new HIV-1 IN models were generated by homology modeling. They represent with a certain level of reliability two different enzymatic states of the HIV-1 IN that can be explored as the biological relevant targets for design of the HIV-1 integrase inhibitors (Figure 4). The generated models are based on the experimental data characterising either the partial structures of IN from HIV-1 or full-length IN from PFV. The models of the separated full-length HIV-1 integrase represent the unbound homodimers of IN (IN1-270) containing either one or two Mg2+ cations in the active site – a plausible enzymatic state before the 3′

processing. The catalytic site loop encompassing ten residues forms the boundary of the active site. This loop shows either a coiled structure [20,22,24] or contains an Ω-shaped hairpin [28,48].

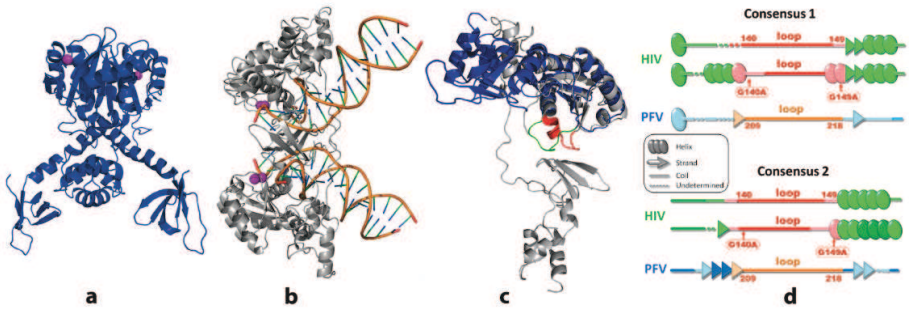

Figure 4. Structural models of the HIV-1 integrase. (a) Model of unbound IN representing the homodimeric enzyme before the 3'-processing; (b) Model of the simplified (dimeric form) IN•DNA pre-integration complex; (c) Superimposition of monomeric subunits from two models in which catalytic site loop residues 140-149 are shown by colours (red and green).The proteins are shown as cartoons, Mg^{2+} ions as spheres (in magenta). (d) Schematic representation of the HIV and PVF active site loop secondary structure prediction, according to consensus 1 and consensus 2.

It will be useful to note that we evidenced a high flexibility of the functional domains in unbound IN by using the Normal Modes Analysis (NMA) [49,50]. Particularly, CTD is characterized by a large scissors-like movement (Figure 5 a). We established that the catalytic site loop in unbound IN with two Mg^{2+}cations in the active site is more rigid due to the stabilising role of the coordination of the Mg^{2+}cations by three active site residues, D64, D116 and E152, whereas the catalytic site loop flexibility increases significantly (Figure 5 b, c).

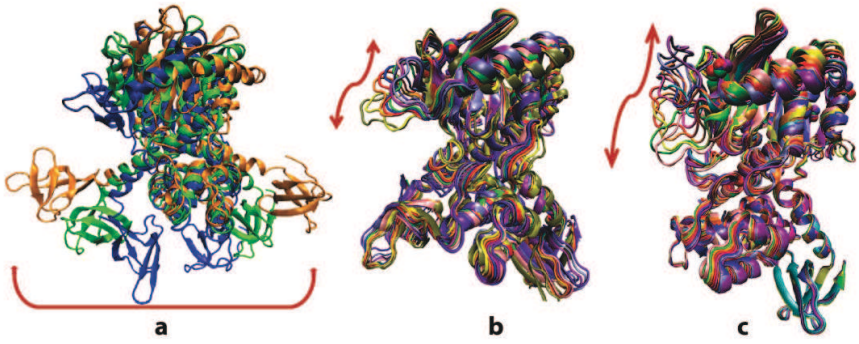

Figure 5. Normal modes illustrating fragments movement in unbound IN. A scissors-like movement in CTD (a); the catalytic site loop displacement in unbound IN with one and two Mg^{2+}cation(s) in the active site (b) and (c) respectively (S. Abdel-Azeim, personal communication).

The simplified model of the HIV-1 IN•vDNA pre-integration complex represents the homodimer of integrase non-covalently attached to the two double strains of the viral DNA with two removed nucleotides GT at each 3′-end (Figure 4 b), and likely depicts the biologically active unit of the IN•vDNA strand transfer intasome. The IN•vDNA model was generated from the X-ray structure of the PFV intasome[2]. Despite the very low sequence identity (22%) between the HIV-1 and PFV INs, the structure-based alignment of the two proteins demonstrates high conservation of key secondary structural elements and the three PFV IN domains shared with HIV-1 IN have essentially the same structure as the isolated IN domains from HIV-1 [51]. Moreover, the structure of the PFV intasome displays a distance between the reactive 3′ ends of vDNA that corresponds to the expected distance between the integration sites of HIV-1 IN target DNA (4 base pairs). Consequently, we suggested that the PFV IN X-ray structure represents an acceptable template for the HIV-1 IN model generation [52].

Two models of different states of the HIV-1 IN show a strong dissimilarity of their structure evidenced by divergent relative spatial positions of their structural domains, NTD, CCD and CTD (Figure 4 c). These tertiary structural modifications altered the contacts between IN domains and the structure and conformation of the linker regions. Particularly, the NTD-CCD interface exhibits substantial changes: in the unbound form the NTD-CCD interface belongs to the same monomer subunit whereas in the vDNA-bound form the interface is composed of residues from the two different subunits.Moreover, IN undergoes important structural transformation leading to structural re-organisation of the catalytic site loop; the coiled portion of the loop reduces from ten residues in the unbound form to five residues in the vDNA-bound form. Such effect may be induced either by the vDNA binding or it can derive as an artefact produced from the use of structural data of the PFV IN as a template for the model generation. Prediction of $IN^{133-155}$ sequence secondary structure elements indicates a more significant predisposition of IN from HIV-1 to be folded as two helices linked by a coiled loop than the IN from PFV (Figure 4 d). Prediction results obtained with high reliability (>75%) correlate perfectly with the X-ray data characterising the WT HIV-1 integrase (1B3L) [22] and its double mutant G140A/G149A (1B9F) [26]. The helix elongation accompanied by loop shortening may be easily induced by the enzyme conformational/structural transition between the two integration steps prompted by substrate binding.

This structure can be used to generate reliable HIV-1 IN models for Integrase Strand Transfer Inhibitors (INSTIs) design. However, the active site loop adopts a five-residue coil structure, rather than the ten-residue extended loop observed in HIV-1IN. This difference may be due to a difference in the sequence of the two enzymes or an effect induced by DNA binding, and caution is therefore required in the use of this structure as a template for modelling biologically relevant conformations of HIV-1 IN [2,45].

2.6. Transition pathway between two IN states and the allosteric binding sites

Two different states of the HIV-1 IN represent the enzyme structures before and after 3′-processing. Under integration process, IN as many other proteins undergo large conformational transitions that are essential for its functions (Figure 6) [53-55]. Tertiary structural

changes precede and accompany these quaternary transitions in the HIV-1 IN as was evidenced by Targeted Molecular Dynamics (TMD) [56] and Meta Dynamics (MD) [57] (Figure 6 c, d).

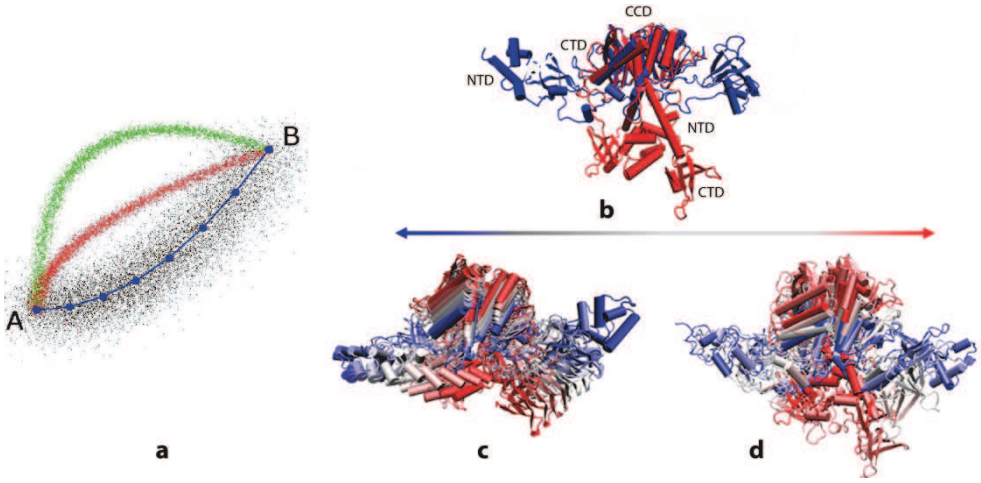

Figure 6. Transition states ensemble between A and B structures (a) (A. Blondel, personal communication). A series of conformations visited by the HIV-1 IN over transition from unbound IN to IN•vDNA complex before (red) and after (blue) 3′-processing (b) obtained by Targeted Molecular Dynamics (TMD) (c) and Meta Dynamics (MD) simulations (d) (S. Abdel-Azeim, personal communication).

Our results, first, provide a description of structure-dynamics-function relationships which in turn supplies a plausible understanding of the IN 3′-processing at the atomic level. Second, the calculated intermediate conformations along the trajectories were scanned for molecular pockets - a means of exploring putative allosteric binding sites, particularly positioned on the IN C-terminal domain (CTD), which is responsible for the vDNA recognition (Figure 7).

3. Raltegravir

The integrase inhibitors were developed to block either the 3′-processing or the strand transfer reaction [58-60]. Raltegravir (RAL), the first IN inhibitor approved for AIDS treatment [61]specifically inhibits the ST activity and was confirmed as an integrase ST inhibitor (INSTI), whereas the 3′-P activity was inhibited only up to a certain concentration [28,62]. The potency of RAL has been described at the level of half-maximal inhibitory concentration (IC50 values) in cellular antiviral and recombinant enzyme assays, kinetic analysis and slow-binding inhibition of IN-catalyzed ST reaction [62-68]. Particularly, it has an IC_{50} of 2 to 7nM for the inhibition of recombinant IN-mediated ST *in vitro* and an IC_{95} of 19 and 31 nM in 10% FBS (fetal bovine serum) and 50 % NHS (normal human serum), respectively. This

drug has been reported to be approximately 100-fold less specific for the inhibition of 3'-processing activity compared to strand transfer.The dissociation rate of RAL with IN•vDNA complex was slow, with k_{off} values of (22 ± 2) × 10^{-6} s^{-1}. The dissociative half-life value measured for RAL with the wild type IN•vDNAcomplex was 7.3 h and 11.0 h obtained at 37°C and at 25°C respectively.

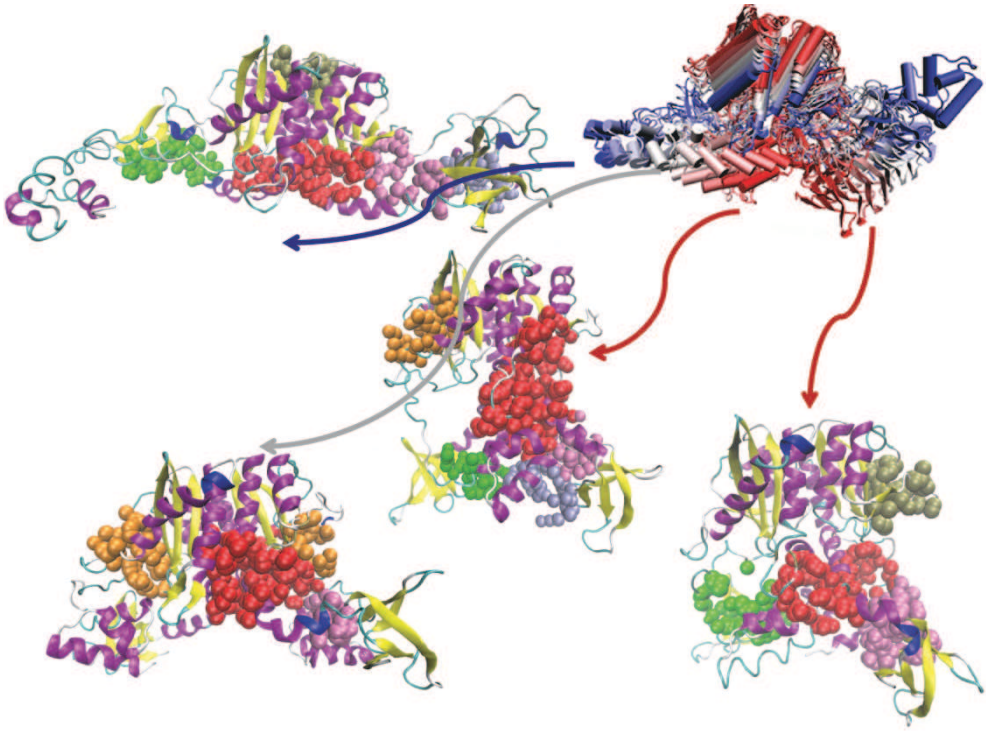

Figure 7. Pockets detected on the surface of the HIV-1 Integrase intermediate conformations obtained by Targeted Molecular Dynamics (TMD) simulations. (S. Abdel-Azeim, personal communication).

Like other antiretroviral inhibitors, RAL develops/induces a resistance effect. Resistance to RAL was associated with amino acids substitutions following three distinct genetic pathways that involve either the N155H, either Q148R/K/H or Y143R primary mutation [69,70]. The last mutation was reported as rarer [71]. It was supposed that the integrase active site mutation N155H causes resistance to raltegravir primarily by perturbing the arrangement of the active site Mg^{2+} ions and not by affecting the affinity of the metals or the direct contacts of the inhibitor with the enzyme [72].

G140S has been shown to enhance the RAL resistance associated with Q148R/K/H [73]. The kinetic gating and/or induced fit effect have been reported as possible mechanisms for RAL

resistance of the G140S/Q148H mutant [74]. A third pathway involving the Y143R/C/H mutation and conferring a large decrease in susceptibility to RAL has been described [75].

3.1. Structure and conformational flexibility

No experimental data characterizing RAL unbound structure or RAL binding mode to the HIV-1 IN has been reported. In this regard, the characterization of RAL conformational preferences and the study of its binding to the HIV-1 IN represent an important task for determining the molecular factors that contribute to the pharmacological action of this drug. Crystallographic data describing the separate domains of the HIV-1 IN and the full-length PFV IN with its cognate DNA deposited in the PDB, provide useful experimental starting guide for the theoretical modeling of the structurally unstudied objects, IN and IN•vDNA complex of HIV-1 as the RAL targets.

RAL, incorporating two pharmacophores, is a multipotent agent capable to hit more than one target in HIV-1, the unbound IN, the viral DNA or IN•vDNA complex. RAL shows the configurational E/Z isomerism and a high conformational flexibility due to eight aliphatic single bonds. Two pharmacophores, (1) 1,3,4-oxadiazole-2-carboxamide and (2) carbonylamino-1-N-alkyl-5-hydroxypyrimidinone, possessing structural versatility through the orientation of carboxamide fragments respective to the aromatic rings, show E-, Z-configuration states characterizing the relative position of the vicinal 1–4 and 1–5 oxygen atoms [48] (Chart 1). The molecule has a set of multiple H-bond donor and acceptor centres. These molecular features together with high structural flexibility provide an abundance of alternative mono- and bi-dentate binding sites in a given RAL conformation.

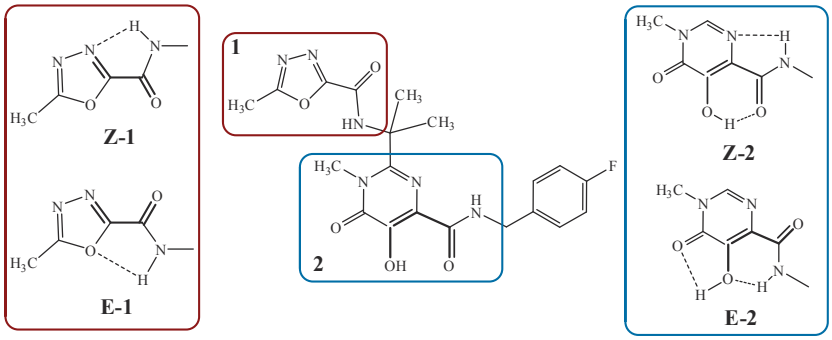

Chart 1. RAL structure. The E- and Z-isomers of 1,3,4-oxadiazole-2-carboxamide (1) and carbonylamino-1-N-alkyl-5-hydroxypyrimidinone (2) pharmacophores are stabilized by intramolecular H-bonds.

The chelating properties of protonated or deprotonated RAL are also determined by the E- or Z- configuration (Chart 2). Consequently, RAL can contribute in the recognition and binding of different partners – H-donor, H-acceptors, charged non-metal atoms and metal cations – in topologically distinct regions of IN by applying the richness of its molecular and

structural properties. For instance, RAL as a bioisoster of adenine can block IN interaction with DNA [48] or sequester metal cofactor ions [76].

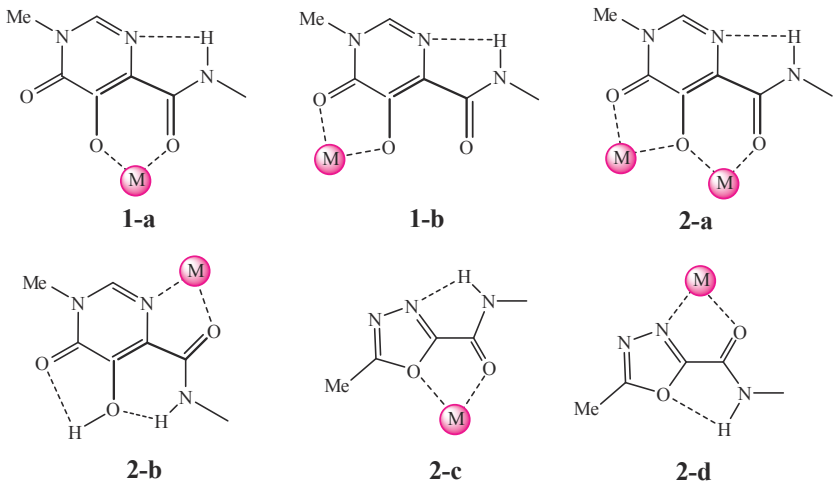

Chart 2. Metal chelating properties of 1, 3, 4-oxadiazole-2-carboxamide (1) and carbonylamino-1-N-alkyl-5-hydroxy-pyrimidinone (2) moieties.

The conformational preferences of RAL were examined in the gas phase (conformational analysis), in water solution (molecular dynamics, MD, in explicit solvent) and in the solid state (the fragment-based analysis using the crystallographic data from Cambridge Structural Database, CSD [77]. Conformational analysis of the different isomeric states of RAL in the gas phase indicates a small difference between the energy profiles of the Z-1/Z-2 and E-1/Z-2 isomers suggesting a relatively low energetical barrier between these two inhibitor states (Figure 8).

A slight preference for the Z-configuration of carbonylamino-hydroxypyrimidinonepharmacophore in the gas phase was observed, in coherence with the established predisposition of β-ketoenols – a principle corner stone of this pharmacophore – to adopt the Z-isomer in the solid state (Figure 9 b) [78-80]. The preference of aliphatic β-ketoenolsto form energetically favourableZ-configuration has been predicted early by*ab initio* studies at the B3LYP/3-G** level of theory [81].

The Cambridge Structural Databank search (CSD) [77] based on molecular fragments mimicking the two RAL pharmacophores statistically demonstrates the preferential E-configuration of oxadiazolecarboxamide–like molecules and the Z-configuration of carbonylamino-hydroxypyrimidinone-like molecules in the solid state (Figure 9 a and b respectively). The halogenated aromatic rings, widely used pharmacophores, show a great level of conformational flexibility (Figure 9, c), allowing to contribute to a better inhibitor affinity in the binding site.

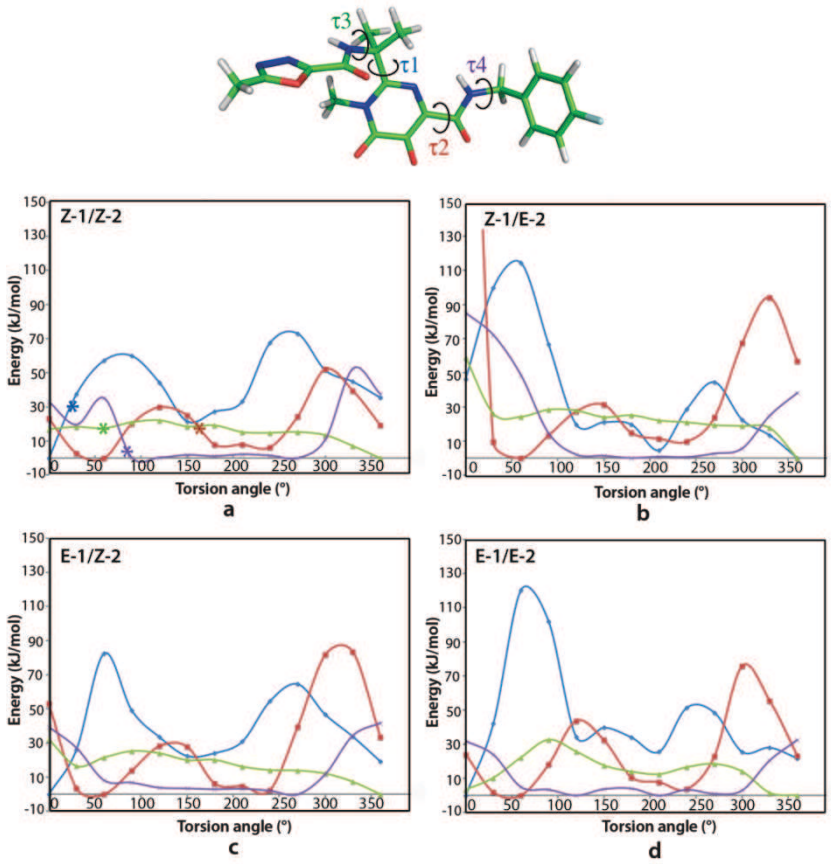

Figure 8. RAL conformations in the gas phase. Free energy profiles obtained by relaxed scans around the single bonds of RAL from 0 to 360º with an increment step of 30º, considering the four RAL isomers: (a) Z-1/Z-2, (b) Z-1/E-2, (c) E-1/Z-2 and (d) E-1/E-2. The curves representing the rotations around torsion angles τ1, τ2, τ3 and τ4 are shown in blue, red, green and violet colours. The values of τ1, τ2, τ3 and τ4 observed in RAL crystal structure 3OYA are indicated by asterisks.

3.2. Raltegravir-metal recognition

Synthesized as a metal cations chelating ligand, RAL can bind the metal by both pharmacophores in the different isomerisation states. Probing the RAL chelating features with the relevant cations, K, Mg and Mn, we evidenced that in the majority of metal complexes, the carbonylaminohydroxypyrimidinone-like fragments are observed in the Z configuration in the solid state (Figure 10).

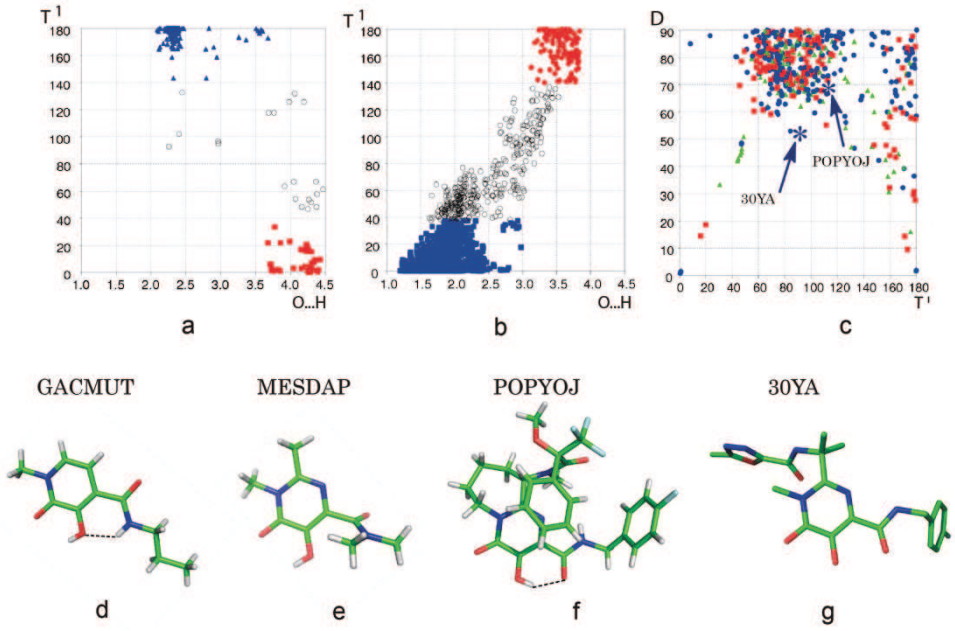

Figure 9. RAL conformations in the solid state. CSD fragment-based analysis of the RAL subunits indicates the E- (blue triangles) and Z- (red squares) conformations of oxadiazolecarboxamide–like molecules (a) and the Z-configuration of carbonylamino-hydroxypyrimidinone-like molecules (b). The halogenated phenyl ring conformation RAL geometry in PFV complex is shown in (c and d respectively). The RAL crystal structure parameters are indicated by asterisks. The alternative configurations of the carbonylamino-hydroxypyrimidinone derivatives are demonstrated by structure of RAL precursor molecules, GACMUT, MEADAP and POPYOJ, and RAL inhibitor (d-g).

The oxadiazolecarboxamide-like pharmacophore is observed in the metal complexes as two isomers and demonstrates a strong selectivity to the metal type: the Z isomer binds K and Mg while the E isomer binds mainly Mn. The higher probability of Mg^{2+}cation coordination by the Z-isomer of both pharmacophores indicates that the presence of two Mg^{2+}cations at the integrase binding site may be a decisive factor for stabilisation of the Z/Z configuration of RAL which is observed in the PFV intasome complex [2,3].

Therapeutically used RAL is in deprotonated state neutralised by K cation. Such drug formula corresponds to the optimal condition allowing efficient cations replacement in cells. The significantly higher affinity of both parmacophores to Mg relatively to K permits a positive competition between these cations, resulting in the change of RAL composition from a pharmaceutically acceptable potassium (K) salt to a biologically relevant Mg complex.

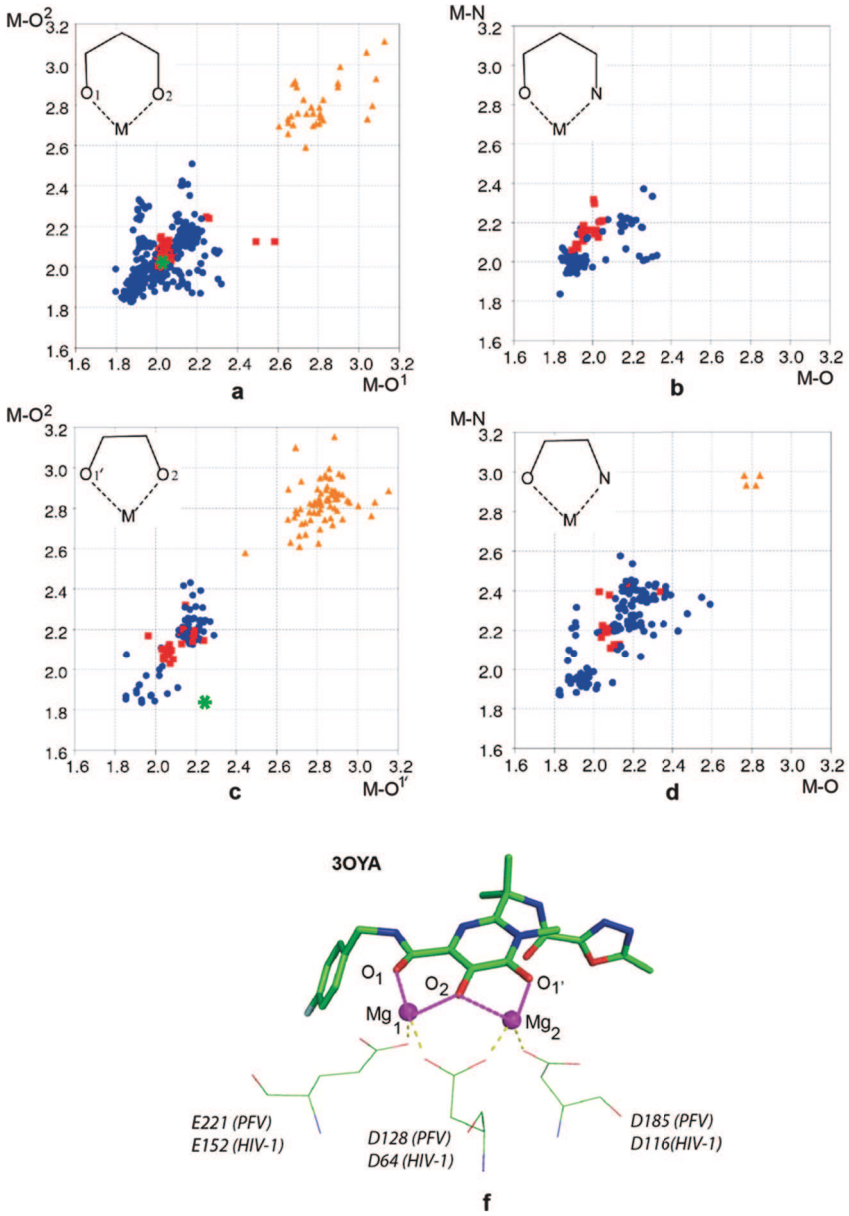

Figure 10. Probing of ligand interactions with Mg, Mn and K by CSD fragment-based search for the metal-ligand complexes (Chart 2, and scatterplots (a-d). Metal complexes are indicated by bull symbols: red squares (Mg), blue circles (Mn) and orange triangles (K). The RAL crystal structure is shown (f) and the RAL parameters are indicated by asterisks in (a and c).

3.3. Raltegravir recognition by the HIV-1 targets

The docking studies reported RAL located within the active site of either unbound IN or IN•vDNA complex. Distinct poses of RAL representing different RAL configuration and modes of Mg^{2+}cations chelation were observed [74,82-84].

Our docking calculations of RAL onto each model evidenced that (i) the large binding pocket delimited by the active site and the extended catalytic site loop in the unbound IN can accommodate RAL in distinct configurational/conformational states showing a lack of interaction specificity between inhibitor and target; (ii) the well defined cavity formed by the active site, vDNA and shortened catalytic site loop provides a more optimised RAL binding site where the inhibitor is stabilised by coordination bonds with Mg2+ cations in the Z/Z-configuration (Figure 11).

Additional stabilisation of RAL is provided by non-covalent interactions with the environing residues of IN and the viral DNA bases. Based on our computing data we suggested earlier the stabilizing role of the vDNA in the inhibitors recognition by IN•vDNA pre-integration complex [51]. It was experimentally evidenced that RAL potently binds only when IN is in a binary complex with vDNA [85], possibly binding to a transient intermediate along the integration pathway [86]. Terminal bases of the viral DNA play a role in both catalytic efficiency [87,88] and inhibitor binding [89-91].

Quite recently it was reported that unprocessed viral DNA could be the primary target of RAL [92]. This study is based on the PFV DNA and several oligonucleotides mimicking the HIV-1 DNA probed by experimental and computing techniques.

To explore the role of the HIV-1 viral DNA in RAL recognition we docked RAL onto the non-cleaved and cleaved DNA (the terminal GT nucleotides were removed) [79]. We found that RAL docked onto the non-cleaved vDNA is positioned in the minor groove of the substrate. No stabilising interactions between the partners, RAL and vDNA, were observed. In contrast, in the processed (cleaved) vDNAthe Z/Z isomer of RAL takes the place of the remote GT based and is stabilised by strong and specific H-bonds with the unpaired cytosine. These H-bonds characterize the high affinity and specific recognition between RAL and the unpaired cytosine similarly to those observed in the DNA bases pair G-C.

Based on the docking results we suggested that the inhibition process may include as a first step the RAL recognition by the processed viral DNA bound to a transient intermediate IN state. RAL coupled to vDNA shows an outside orientation of all oxygen atoms, excellent putative chelating agents of Mg^{2+}cations, which could facilitate the insertion of RAL into the active site. The conformational flexibility of RAL further allows the accommodation/adaptation of the inhibitor in a relatively large binding pocket of IN•vDNA pre-integration complex thus producing various RAL docked conformation. We believe that such variety of the RAL conformations contributing alternatively to the enzyme residue recognition may impact the selection of the clinically observed alternative resistance pathways to the drug [29] and references herein.

http://dx.doi.org/10.5772/52344

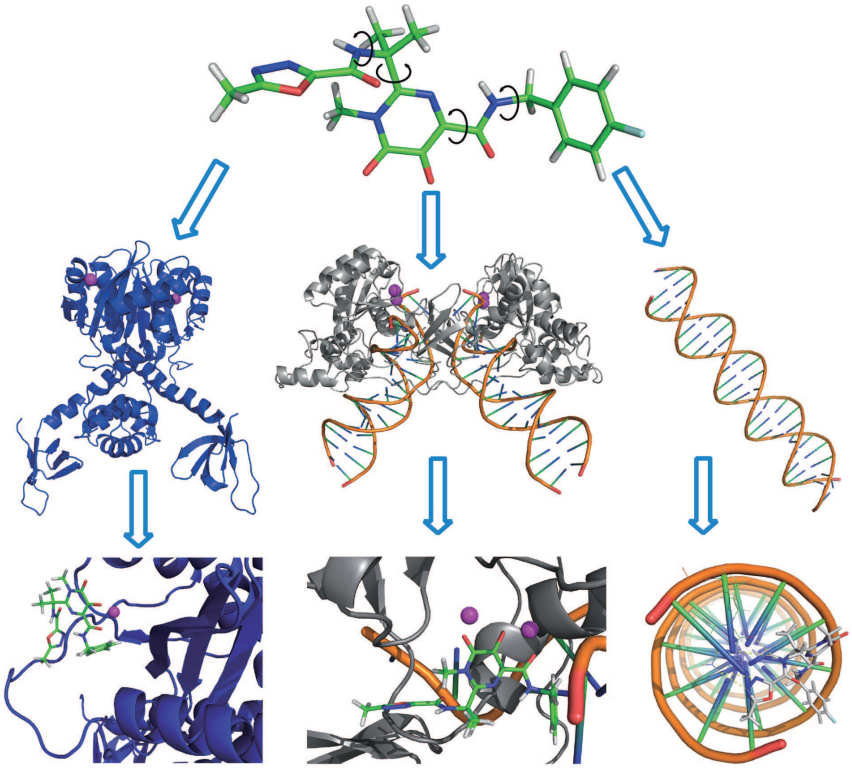

Figure 11. RAL docking onto the active site of unbound IN, IN•vDNA complex and viral DNA. Proteins and DNA are shown as cartoons; inhibitors as sticks and Mg2+ cations as balls.

4. Conclusions and perspectives

The HIV-1 Integrase is an essential retroviral enzyme that covalently binds both ends of linear viral DNA and inserts them into a cellular chromosome. The functions of this enzyme are based on the existence of specific attractive interactions between partner molecules or cofactors – IN, viral DNA and Mg^{2+}cations – in a given case. Structure-based drug development seeks to identify and use such interactions to design and optimize the competitive and specific modulator of such functional interactions. Drug design and optimisation process require knowledge about interaction geometries and binding affinity contributing to molecular recognition that can be gleaned from crystallographic and modeling data.

We have resumed the available structural information related to the retroviral integrase. We used this data to generate biologically relevant HIV-1 targets – the unbound IN, the viral DNA (vDNA) and the IN•vDNA complex – which represent with a certain level of reliability, two different enzymatic states of the HIV-1 over the retroviral integration process.

We have characterised the RAL binding, a very flexible molecule displaying the E/Z isomerism, to the active site of its HIV-1 targets which mimic the integrase states before and after the 3'-processing. The docked conformations represent a spectrum of possible conformational/configurational states. The best docking scores and poses confirm that the generated model representing the IN•vDNA complex is the biologically relevant target of RAL, the strand transfer inhibitor. This finding is consistent with well-documented and commonly accepted inhibition mechanism of RAL, based on integral biological, biochemical and structural data.

RAL docking onto the IN•vDNAcomplex systematically generated the RAL chelated to Mg^{2+}cations at the active site by the pharmacophore oxygen atoms. The identification of IN residues specifically interacting with RAL is likely a very difficult task and the exact modes of binding of this inhibitor remain a matter of debate. Most probably the flexible nature of RAL results in different conformations and the mode of binding may differ in terms of the interacting residues of the target, which trigger the alternative resistance phenomenon.

The identified RAL binding to the processed viral DNA shed light on a putative, even plausible, step of the RAL inhibition mechanism.

We have implemented dynamic properties to the HIV-1 targets characterisation, particularly, the internal protein collective motions and the global conformational transition. Such transitions play an essential role in the function of many proteins, but experiments do not provide the atomic details on the path followed in going from one end structure to the other. For the dimeric IN, the transition pathway between the unbound and bound to vDNA is not known, which limits information of the cooperative mechanism in this typical allosteric system, where both tertiary and quaternary changes are involved. Description of the IN intermediate conformations open a way to localise the allosteric pockets, which in turn can be selected as the putative binding sites for small molecules in a virtual screening protocol.

The novel drugs, targeted the HIV-1 Integrase, outcome primarily due to the rapid emergence of RAL analogues (for example, GS-9137 or elvitegravir, MK-2048 and S/GSK 1349572, currently under clinical trials [93]). The clinical trials of several RAL analogues (BMS-707035, GSK-364735) were suspended. All these molecules specifically suppress the IN ST reaction. We conceive that the future HIV-1 integrase drug development will be mainly oriented to design of inhibitors with a mechanism of action that differs from that of RAL and its analogues. Distinct conceptions are potentially conceivable: (i) Design of the allosteric inhibitors, able to recognize specifically the binding sites that differ from the IN active site. Inhibitor V-165, belonging to such type inhibitors, prevents IN binding with the viral DNA such blocking 3'-processing reaction [94]. (ii) Design of the protein-protein inhibitors (PPIs) acting on interaction interface between either viral components (the IN monomers upon multimerization process or sub-units of the IN•vDNA complex) [95,96], or between viral

and cellular proteins (IN/LEDGF) [97,98]. These alternative strategies represent rational and prospective directions in the HIV-1 integrase drug developement.

Acknowledgement

The authors thank Dr. E. Laine for valuable discussions and for editorial assistance, I. Chauvot de Beauchêne and S. Abdel-Azeim for providing of illustrative materials. This work is funded by the Centre National de la Recherche Scientifique (CNRS), EcoleNormaleSupérieure (ENS) de Cachan and SIDACTION.

Author details

Rohit Arora and Luba Tchertanov

BiMoDyM, LBPA, CNRS -ENS de Cachan, LabEx LERMIT, CEDEX Cachan, France

References

[1] Berman HM, Westbrook J, Feng Z, Gilliland G, Bhat TN, Weissig H, et al. The Protein Data Bank. Nucleic Acids Research 2000 Jan 1;28(1):235-42.

[2] Hare S, Gupta SS, Valkov E, Engelman A, Cherepanov P. Retroviral intasome assembly and inhibition of DNA strand transfer. Nature 2010 Mar 11;464(7286):232-6.

[3] Hare S, Vos AM, Clayton RF, Thuring JW, Cummings MD, Cherepanov P. Molecular mechanisms of retroviral integrase inhibition and the evolution of viral resistance. Proceedings of the National Academy of Sciences of the United States of America 2010 Nov 16;107(46):20057-62.

[4] Krovat EM, Steindl T, Langer T. Recent Advances in Docking and Scoring. Current Computer-Aided Drug Design 2005 Jan;1(1):93-102.

[5] Brown PO. Integration of Retroviral DNA. Current Topics in Microbiology and Immunology 1990;157:19-48.

[6] Weiss RA. Gulliver's travels in HIV land. Nature 2001 Apr 19;410(6831):963-7.

[7] Chiu TK, Davies DR. Structure and function of HIV-1 integrase. Current Topics in Medicinal Chemistry 2004;4(9):965-77.

[8] Hayouka Z, Rosenbluh J, Levin A, Loya S, Lebendiker M, Veprintsev D, et al. Inhibiting HIV-1 integrase by shifting its oligomerization equilibrium. Proceedings of the

National Academy of Sciences of the United States of America 2007 May 15;104(20): 8316-21.

[9] Guiot E, Carayon K, Delelis O, Simon F, Tauc P, Zubin E, et al. Relationship between the oligomeric status of HIV-1 integrase on DNA and enzymatic activity. Journal of Biological Chemistry 2006 Aug 11;281(32):22707-19.

[10] Faure A, Calmels C, Desjobert C, Castroviejo M, Caumont-Sarcos A, Tarrago-Litvak L, et al. HIV-1 integrase crosslinked oligomers are active in vitro. Nucleic Acids Research 2005;33(3):977-86.

[11] Wang Y, Klock H, Yin H, Wolff K, Bieza K, Niswonger K, et al. Homogeneous high-throughput screening assays for HIV-1 integrase 3 '-processing and strand transfer activities. Journal of Biomolecular Screening 2005 Aug;10(5):456-62.

[12] Li M, Mizuuchi M, Burke TR, Craigie R. Retroviral DNA integration: reaction pathway and critical intermediates. Embo Journal 2006 Mar 22;25(6):1295-304.

[13] Asante-Appiah E, Skalka AM. Molecular mechanisms in retrovirus DNA integration. Antiviral Research 1997 Dec;36(3):139-56.

[14] Cai ML, Huang Y, Caffrey M, Zheng RL, Craigie R, Clore GM, et al. Solution structure of the His12 -> Cys mutant of the N-terminal zinc binding domain of HIV-1 integrase complexed to cadmium. Protein Science 1998 Dec;7(12):2669-74.

[15] Cai ML, Zheng RL, Caffrey M, Craigie R, Clore GM, Gronenborn AM. Solution structure of the N-terminal zinc binding domain of HIV-1 integrase. Nature Structural Biology 1997 Jul;4(7):567-77.

[16] Eijkelenboom APAM, vandenEnt FMI, Vos A, Doreleijers JF, Hard K, Tullius TD, et al. The solution structure of the amino-terminal HHCC domain of HIV-2 integrase: a three-helix bundle stabilized by zinc. Current Biology 1997 Oct 1;7(10):739-46.

[17] Eijkelenboom APAM, Sprangers R, Hard K, Lutzke RAP, Plasterk RHA, Boelens R, et al. Refined solution structure of the C-terminal DNA-binding domain of human immunovirus-1 integrase. Proteins-Structure Function and Genetics 1999 Sep 1;36(4): 556-64.

[18] Lodi PJ, Ernst JA, Kuszewski J, Hickman AB, Engelman A, Craigie R, et al. Solution structure of the DNA binding domain of HIV-1 integrase. Biochemistry 1995 Aug 8;34(31):9826-33.

[19] Dyda F, Hickman AB, Jenkins TM, Engelman A, Craigie R, Davies DR. Crystal-Structure of the Catalytic Domain of HIV-1 Integrase - Similarity to Other Polynucleotidyl Transferases. Science 1994 Dec 23;266(5193):1981-6.

[20] Bujacz G, Alexandratos J, ZhouLiu Q, ClementMella C, Wlodawer A. The catalytic domain of human immunodeficiency virus integrase: Ordered active site in the F185H mutant. FEBS Letters 1996 Dec 2;398(2-3):175-8.

[21] Bujacz G, Alexandratos J, Wlodawer A. Binding of different divalent cations to the active site of avian sarcoma virus integrase and their effects on enzymatic activity. Journal of Biological Chemistry 1997 Jul 18;272(29):18161-8.

[22] Maignan S, Guilloteau JP, Zhou-Liu Q, Clement-Mella C, Mikol V. Crystal structures of the catalytic domain of HIV-1 integrase free and complexed with its metal cofactor: High level of similarity of the active site with other viral integrases. Journal of Molecular Biology 1998 Sep 18;282(2):359-68.

[23] Molteni V, Greenwald J, Rhodes D, Hwang Y, Kwiatkowski W, Bushman FD, et al. Identification of a small-molecule binding site at the dimer interface of the HIV integrase catalytic domain. Acta Crystallographica Section D-Biological Crystallography 2001 Apr;57:536-44.

[24] Goldgur Y, Dyda F, Hickman AB, Jenkins TM, Craigie R, Davies DR. Three new structures of the core domain of HIV-1 integrase: An active site that binds magnesium. ProcNatlAcadSci USA 1998 Aug 4;95(16):9150-4.

[25] Goldgur Y, Craigie R, Cohen GH, Fujiwara T, Yoshinaga T, Fujishita T, et al. Structure of the HIV-1 integrase catalytic domain complexed with an inhibitor: A platform for antiviral drug design. Proceedings of the National Academy of Sciences of the United States of America 1999 Nov 9;96(23):13040-3.

[26] Greenwald J, Le V, Butler SL, Bushman FD, Choe S. The mobility of an HIV-1 integrase active site loop is correlated with catalytic activity. Biochemistry 1999 Jul 13;38(28):8892-8.

[27] Chen AP, Weber IT, Harrison RW, Leis J. Identification of amino acids in HIV-1 and avian sarcoma virus integrase subsites required for specific recognition of the long terminal repeat ends. Journal of Biological Chemistry 2006 Feb 17;281(7):4173-82.

[28] Mouscadet JF, Tchertanov L. Raltegravir: molecular basis of its mechanism of action. Eur J Med Res 2009 Nov 24;14 Suppl 3:5-16.

[29] Mouscadet JF, Delelis O, Marcelin AG, Tchertanov L. Resistance to HIV-1 integrase inhibitors: A structural perspective. Drug Resist Updat 2010 Aug;13(4-5):139-50.

[30] Lovell S, Goryshin IY, Reznikoff WR, Rayment I. Two-metal active site binding of a Tn5 transposase synaptic complex. Nature Structural Biology 2002 Apr;9(4):278-81.

[31] Karki R, Tang Y, Nicklaus MC. Model of the HIV-1 integrase-viral DNA complex - A template for structure-based design of HIV in inhibitors. Abstracts of Papers of the American Chemical Society 2002 Aug 18;224:U9-U10.

[32] Karki RG, Tang Y, Burke TR, Nicklaus MC. Model of full-length HIV-1 integrase complexed with viral DNA as template for anti-HIV drug design. Journal of Computer-Aided Molecular Design 2004 Dec;18(12):739-60.

[33] Wang LD, Liu CL, Chen WZ, Wang CX. Constructing HIV-1 integrase tetramer and exploring influences of metal ions on forming integrase-DNA complex. Biochemical and Biophysical Research Communications 2005 Nov 11;337(1):313-9.

[34] Chen ZG, Yan YW, Munshi S, Li Y, Zugay-Murphy J, Xu B, et al. X-ray structure of simian immunodeficiency virus integrase containing the core and C-terminal domain (residues 50-293) - An initial glance of the viral DNA binding platform. Journal of Molecular Biology 2000 Feb 18;296(2):521-33.

[35] Wang JY, Ling H, Yang W, Craigie R. Structure of a two-domain fragment of HIV-1 integrase: implications for domain organization in the intact protein. Embo Journal 2001 Dec 17;20(24):7333-43.

[36] Ellison V, Gerton J, Vincent KA, Brown PO. An Essential Interaction Between Distinct Domains of Hiv-1 Integrase Mediates Assembly of the Active Multimer. Journal of Biological Chemistry 1995 Feb 17;270(7):3320-6.

[37] Faure A, Calmels C, Desjobert C, Castroviejo M, Caumont-Sarcos A, Tarrago-Litvak L, et al. HIV-1 integrase crosslinked oligomers are active in vitro. Nucleic Acids Research 2005;33(3):977-86.

[38] Guiot E, Carayon K, Delelis O, Simon F, Tauc P, Zubin E, et al. Relationship between the oligomeric status of HIV-1 integrase on DNA and enzymatic activity. Journal of Biological Chemistry 2006 Aug 11;281(32):22707-19.

[39] De Luca L, Pedretti A, Vistoli G, Barreca ML, Villa L, Monforte P, et al. Analysis of the full-length integrase - DNA complex by a modified approach for DNA docking. Biochemical and Biophysical Research Communications 2003 Oct 31;310(4):1083-8.

[40] Esposito D, Craigie R. Sequence specificity of viral end DNA binding by HIV-1 integrase reveals critical regions for protein-DNA interaction. EMBO Journal 1998 Oct 1;17(19):5832-43.

[41] Fenollar-Ferrer C, Carnevale V, Raugei S, Carloni P. HIV-1 integrase-DNA interactions investigated by molecular modelling. Computational and Mathematical Methods in Medicine 2008;9(3-4):231-43.

[42] Wielens J, Crosby IT, Chalmers DK. A three-dimensional model of the human immunodeficiency virus type 1 integration complex. Journal of Computer-Aided Molecular Design 2005 May;19(5):301-17.

[43] Michel F, Crucifix C, Granger F, Eiler S, Mouscadet JF, Korolev S, et al. Structural basis for HIV-1 DNA integration in the human genome, role of the LEDGF/P75 cofactor. EMBO J 2009 Apr 8;28(7):980-91.

[44] Gao K, Butler SL, Bushman F. Human immunodeficiency virus type 1 integrase: arrangement of protein domains in active cDNA complexes. Embo Journal 2001 Jul 2;20(13):3565-76.

[45] Davies DR, Goryshin IY, Reznikoff WS, Rayment I. Three-dimensional structure of the Tn5 synaptic complex transposition intermediate. Science 2000 Jul 7;289(5476): 77-85.

[46] Podtelezhnikov AA, Gao K, Bushman FD, McCammon JA. Modeling HIV-1 integrase complexes based on their hydrodynamic properties. Biopolymers 2003 Jan;68(1): 110-20.

[47] Ren G, Gao K, Bushman FD, Yeager M. Single-particle image reconstruction of a tetramer of HIV integrase bound to DNA. Journal of Molecular Biology 2007 Feb 9;366(1):286-94.

[48] Mouscadet JF, Arora R, Andre J, Lambry JC, Delelis O, Malet I, et al. HIV-1 IN alternative molecular recognition of DNA induced by raltegravir resistance mutations. Journal of Molecular Recognition 2009 Nov;22(6):480-94.

[49] Tama F, Gadea FX, Marques O, Sanejouand YH. Building-block approach for determining low-frequency normal modes of macromolecules. Proteins 2000 Oct 1;41(1): 1-7.

[50] Tama F, Sanejouand YH. Conformational change of proteins arising from normal mode calculations. Protein Eng 2001 Jan;14(1):1-6.

[51] Ni X, Abdel-Azeim S, Laine E, Arora R, Osemwota O, Marcelin A-G, et al. In silico and in vitro Comparison of HIV-1 Subtypes B and CRF02_AG Integrases Susceptibility to Integrase Strand Transfer Inhibitors. Advances in Vilology 2012;2012:548657.

[52] Yin ZQ, Craigie R. Modeling the HIV-1 Intasome: A Prototype View of the Target of Integrase Inhibitors. Viruses-Basel 2010 Dec;2(12):2777-81.

[53] Karplus M, Kuriyan J. Molecular dynamics and protein function. Proc Natl Acad Sci U S A 2005 May 10;102(19):6679-85.

[54] Karplus M, Gao YQ, Ma J, van d, V, Yang W. Protein structural transitions and their functional role. Philos Transact A Math Phys Eng Sci 2005 Feb 15;363(1827):331-55.

[55] Gerstein M, Lesk AM, Chothia C. Structural mechanisms for domain movements in proteins. Biochemistry 1994 Jun 7;33(22):6739-49.

[56] Schlitter J, Engels M, Kruger P. Targeted molecular dynamics: a new approach for searching pathways of conformational transitions. J Mol Graph 1994 Jun;12(2):84-9.

[57] Bagley RJ, Farmer JD, Kauffman SA, Packard NH, Perelson AS, Stadnyk IM. Modeling adaptive biological systems. Biosystems 1989;23(2-3):113-37.

[58] Cotelle P. Patented HIV-1 integrase inhibitors (1998-2005). Recent Pat Antiinfect Drug Discov 2006 Jan;1(1):1-15.

[59] Pommier Y, Johnson AA, Marchand C. Integrase inhibitors to treat HIV/AIDS. Nature Reviews Drug Discovery 2005 Mar;4(3):236-48.

[60] Semenova EA, Marchand C, Pommier Y. HIV-1 integrase inhibitors: Update and Perspectives. Adv Pharmacol 2008;56:199-228.

[61] Marchand C, Maddali K, Metifiot M, Pommier Y. HIV-1 IN Inhibitors: 2010 Update and Perspectives. Current Topics in Medicinal Chemistry 2009 Aug;9(11):1016-37.

[62] Hazuda DJ, Felock P, Witmer M, Wolfe A, Stillmock K, Grobler JA, et al. Inhibitors of strand transfer that prevent integration and inhibit HIV-1 replication in cells. Science 2000 Jan 28;287(5453):646-50.

[63] Markowitz M, Morales-Ramirez JO, Nguyen BY, Kovacs CM, Steigbigel RT, Cooper DA, et al. Antiretroviral activity, pharmacokinetics, and tolerability of MK-0518, a novel inhibitor of HIV-1 integrase, dosed as monotherapy for 10 days in treatment-naive HIV-1-infected individuals. J Acquir Immune DeficSyndr. 2006 Dec 15;43(5): 509-15.

[64] Grobler JA, Stillmock K, Hu B, Witmer M, Felock P, Espeseth AS, et al. Diketo acid inhibitor mechanism and HIV-1 integrase: implications for metal binding in the active site of phosphotransferase enzymes.ProcNatlAcadSci USA. 2002 May 14;99(10): 6661-6.

[65] Garvey EP, Schwartz B, Gartland MJ, Lang S, Halsey W, Sathe G, et al. Potent inhibitors of HIV-1 integrase display a two-step, slow-binding inhibition mechanism which is absent in a drug-resistant T66I/M154I mutant.Biochemistry. 2009 Feb 24;48(7):1644-53.

[66] Copeland RA, Pompliano DL, Meek TD. Drug-target residence time and its implications for lead optimization.Nat Rev Drug Discov. 2006 Sep;5(9):730-9.

[67] Dicker IB, Terry B, Lin Z, Li Z, Bollini S, Samanta HK, et al. Biochemical analysis of HIV-1 integrase variants resistant to strand transfer inhibitors. J Biol Chem. 2008 Aug 29;283(35):23599-609.

[68] Hightower KE, Wang R, Deanda F, Johns BA, Weaver K, Shen Y, et al. Dolutegravir (S/GSK1349572) exhibits significantly slower dissociation than raltegravir and elvitegravir from wild-type and integrase inhibitor-resistant HIV-1 integrase-DNA complexes.Antimicrob Agents Chemother. 2011 Oct;55(10):4552-9.

[69] Cooper DA, Steigbigel RT, Gatell JM, Rockstroh JK, Katlama C, Yeni P, et al. Subgroup and resistance analyses of raltegravir for resistant HIV-1 infection. New England Journal of Medicine 2008 Jul 24;359(4):355-65.

[70] Steigbigel RT, Cooper DA, Kumar PN, Eron JE, Schechter M, Markowitz M, et al. Raltegravir with optimized background therapy for resistant HIV-1 infection. New England Journal of Medicine 2008 Jul 24;359(4):339-54.

[71] Sichtig N, Sierra S, Kaiser R, Daumer M, Reuter S, Schulter E, et al. Evolution of raltegravir resistance during therapy. Journal of Antimicrobial Chemotherapy 2009 Jul; 64(1):25-32.

[72] Grobler JA, Stillmock KA, Miller MD, Hazuda DJ. Mechanism by which the HIV integrase active-site mutation N155H confers resistance to raltegravir. Antiviral Therapy 2008;13(4):A41.

[73] Delelis O, Malet I, Na L, Tchertanov L, Calvez V, Marcelin AG, et al. The G140S mutation in HIV integrases from raltegravir-resistant patients rescues catalytic defect due to the resistance Q148H mutation. Nucleic Acids Research 2009 Mar;37(4): 1193-201.

[74] Perryman AL, Forli S, Morris GM, Burt C, Cheng YH, Palmer MJ, et al. A Dynamic Model of HIV Integrase Inhibition and Drug Resistance. Journal of Molecular Biology 2010 Mar 26;397(2):600-15.

[75] Delelis O, Thierry S, Subra F, Simon F, Malet I, Alloui C, et al. Impact of Y143 HIV-1 Integrase Mutations on Resistance to Raltegravir In Vitro and In Vivo. Antimicrobial Agents and Chemotherapy 2010 Jan;54(1):491-501.

[76] Kawasuji T, Fuji M, Yoshinaga T, Sato A, Fujiwara T, Kiyama R. A platform for designing HIV integrase inhibitors. Part 2: A two-metal binding model as a potential mechanism of HIV integrase inhibitors. Bioorganic & Medicinal Chemistry 2006 Dec 15;14(24):8420-9.

[77] Allen FH. The Cambridge Structural Database: a quarter of a million crystal structures and rising. Acta Crystallogr B 2002 Jun;58(Pt 3 Pt 1):380-8.

[78] Tchertanov L, Mouscadet JF. Target recognition by catechols and beta-ketoenols: Potential contribution of hydrogen bonding and Mn/Mg chelation to HIV-1 integrase inhibition. Journal of Medicinal Chemistry 2007 Mar 22;50(6):1133-45.

[79] Arora R, Chauvot de Beauchêne I, Abdel-Azeim S, Polanski J, Laine E, Tchertanov L. Raltegravir flexibility and its impact on recognition by the HIV-1 Integrase targets. Journal of Molecular Recognition 2012. Submitted

[80] Arora R, Tchertanov L. Structural determinants of Raltegravir specific recognition by the HIV-1 Integrase. 2012. Les actes: 57-60. http://jobim2012.inria.fr/jobim_actes_2012_online.pdf

[81] Schiavoni MM, Mack HG, Ulic SE, Della Vedova CO. Tautomers and conformers of malonamide, NH2-C(O)-CH2-C(O)-NH2: vibrational analysis, NMR spectra and ab initio calculations. Spectrochim Acta A Mol Biomol Spectrosc 2000 Jul;56A(8): 1533-41.

[82] Barreca ML, Iraci N, De Luca L, Chimirri A. Induced-Fit Docking Approach Provides Insight into the Binding Mode and Mechanism of Action of HIV-1 Integrase Inhibitors. Chemmedchem 2009 Sep;4(9):1446-56.

[83] Loizidou EZ, Zeinalipour-Yazdi CD, Christofides T, Kostrikis LG. Analysis of binding parameters of HIV-1 integrase inhibitors: Correlates of drug inhibition and resistance. Bioorganic & Medicinal Chemistry 2009 Jul 1;17(13):4806-18.

[84] Serrao E, Odde S, Ramkumar K, Neamati N. Raltegravir, elvitegravir, and metoogravir: the birth of "me-too" HIV-1 integrase inhibitors. Retrovirology 2009;6:25.

[85] Espeseth AS, Felock P, Wolfe A, Witmer M, Grobler, J, Anthony N., et al.HIV-1 integrase inhibitors that compete with the target DNA substrate define a unique strand transfer conformation for integrase. Proc. Natl. Acad. Sci. U.S.A 2000; 97:11244–49.

[86] Pandey KK., Bera S., Zahm J., Vora A, Stillmock K., Hazuda D, et al. Inhibition of human immunodeficiency virus type 1 concerted integration by strand transfer inhibitors which recognize a transient structural intermediate. J. Virol. 2007; 81: 12189–99.

[87] Sherman PA, Dickson ML. and Fyfe JA. Human immunodeficiency virus type 1 integration protein: DNA sequence requirements for cleaving and joining reactions. J. Virol. 1992; 66: 3593–601.

[88] Johnson AA, Santos W, Pais GCG, Marchand C, Amin, R., Burker, T. R., Jr., Verdine, G., and Pommier, Y. Integration requires a specific interaction of the donor DNA terminal 5′-cytosine with glutamine 148 of the HIV-1 integrase flexible loop. J. Biol. Chem. 2006; 281,:461–7.

[89] Johnson AA, Marchand C, Patil SS, Costi R, DiSanto R, Burke, R. R. Jr. et al. Probing HIV-1 integrase inhibitor binding sites with position-specific integrase-DNA crosslinking assays. Mol. Pharmacol. 2007; 71: 893–901.

[90] Dicker IB, Samanta HK, Li A, Hong Y, Tian Y, Banville J et al. Changes to the HIV long terminal repeat and to HIV integrase differentially impact HIV integrase assembly, activity, and the binding of strand transfer inhibitors. J. Biol. Chem. 2008; 282: 31186–96.

[91] Langley D, Samanta HK, Lin Z, Walker MA, Krystal M, and Dicker IB. The Terminal (Catalytic) Adenosine of the HIV LTR Controls the Kinetics of Binding and Dissociation of HIV Integrase Strand Transfer Inhibitors. Biochemistry 2008; 47: 13481–8.

[92] Ammar FF, Abdel-Azeim S, Zargarian L, Hobaika Z, Maroun RG, Fermandjian S Unprocessed Viral DNA Could Be the Primary Target of the HIV-1 Integrase Inhibitor Raltegravir. PLoS One.oS One. 2012;7(7):e40223.

[93] Korolev S, Agapkina Yu, Gottikh M. Clinical Use of Inhibitors of HIV-1 Integration: Problems and Prospects. Acta Naturae 2011;3;3:12-28.

[94] Pannecouque C, Pluymers W, Van Maele B, Tetz V, Cherepanov P, De Clercq E, et al. New class of HIV integrase inhibitors that block viral replication in cell culture. Curr Biol. 2002 Jul 23;12(14):1169-77.

[95] Mazumder A, Wang S, Neamati N, Nicklaus M, Sunder S, Chen J, et al. Antiretroviral agents as inhibitors of both human immunodeficiency virus type 1 integrase and protease.J Med Chem. 1996 Jun 21;39(13):2472-81.

[96] Tsiang M, Jones GS, Hung M, Samuel D, Novikov N, Mukund S, et al. Dithiothreitol causes HIV-1 integrase dimer dissociation while agents interacting with the integrase dimer interface promote dimer formation. Biochemistry. 2011 Mar 15;50(10):1567-81.

[97] De Luca L, Ferro S, Gitto R, Barreca ML, Agnello S, Christ F, et al. Small molecules targeting the interaction between HIV-1 integrase and LEDGF/p75 cofactor. Bioorg Med Chem. 2010 Nov 1;18(21):7515-21.

[98] Tsiang M, Jones GS, Niedziela-Majka A, Kan E, Lansdon EB, Huang W, Hung M, et al. New Class of HIV-1 Integrase (IN) Inhibitors with a Dual Mode of Action.Biol Chem. 2012 Jun 15;287(25):21189-203.

Raltegravir flexibility and its impact on recognition by the HIV-1 IN targets

Rohit ARORA[1], Isaure CHAUVOT de BEAUCHENE[1],

Jaroslaw POLANSKI[2], Elodie LAINE[1] and Luba TCHERTANOV[1]*

[1] BiMoDyM, LBPA, CNRS -ENS de Cachan, LabEx LERMIT, 61 avenue du Président Wilson, Cachan, France

[2] Institute of Chemistry, University of Silesia, PL-40006 Katowice, Poland

* Correspondance to: L. Tchertanov, BiMoDyM, LBPA, CNRS-ENS de Cachan, 61 Avenue du Président Wilson, 94235 Cachan, France; e-mail : Luba.Tchertanov@lbpa.ens-cachan.fr

Abstract

HIV-1 integrase (IN) is a pertinent target for the development of AIDS chemotherapy. The first IN specific inhibitor approved for the treatment of HIV/AIDS, Raltegravir (RAL), was designed to block the strand transfer reaction. To date no experimental data characterising RAL structure or/and RAL binding to its target has been reported. We characterized the structural and conformational features of RAL and its recognition by putative HIV-1 targets – the unbound IN, the viral DNA (vDNA) and the IN•vDNA complex– mimicking the integrase states over the integration process. The obtained data evidenced that (i) a large binding pocket delimited by the active site and an extended loop in the unbound IN accommodates RAL in distinct conformational states all lacking specific interactions with the target; (ii) a well-defined cavity formed by the active site, the vDNA and the shortened loop in the IN•vDNA complex provides a more optimised inhibitor binding site in which RAL chelates Mg^{2+} cations; (iii) a specific recognition between RAL and the unpaired cytosine of the processed DNA is governed by a pair of strong H-bonds similar to those observed in DNA bases pair G-C. The identified RAL pose at the cleaved vDNA shed light on a putative step of the RAL inhibition mechanism. This modeling study indicates that the inhibition process may include as a first step RAL recognition by the processed vDNA bound to a transient intermediate IN state, and thus provides a possible route to the design of IN inhibitors with improved affinity and selectivity.

Keywords: HIV-1 IN, vDNA, IN•vDNA complex, Raltegravir, molecular recognition, Z/E isomerism, modeling, docking

INTRODUCTION

The *pol*-encoded HIV-1 integrase (IN) is a key enzyme in the replication mechanism of retroviruses. It catalyzes the covalent insertion of the viral cDNA into the host DNA (hDNA) of the infected cells (Brown, 1990). A two-step reaction is required for covalent integration of viral DNA. First, IN binds to a short sequence located at each end of the long terminal repeat (LTR) of the viral DNA (vDNA) and catalyzes an endonucleotide cleavage, 3'-processing reaction (3'-P), resulting in the removal of two nucleotides from each of the 3'-ends of LTR and the delivery of hydroxy groups for nucleophilic attacks. The pre-processed DNA is then used as a substrate for the strand transfer (ST) reaction, leading to the covalent insertion of the vDNA into the host genome (hDNA) (Brown, 1990; Chiu and Davies, 2004).

These two reactions are spatially and temporally separated and energetically independent: the 3'-processing takes place in the cytoplasm of the infected cells, whereas the strand transfer occurs in the nuclei. They are catalyzed by the enzyme in different oligomerisation states : dimerization is required for the 3′-processing step (Hayouka *et al.*, 2007) (Guiot *et al.*, 2006), while tetrameric IN is believed to be required for the strand transfer (Faure *et al.*, 2005), (Li *et al.*, 2006; Wang *et al.*, 2005).

The integrase activities require the presence of metallic cofactor(s), the Mg^{2+} or Mn^{2+} ion(s). IN displays non specific nuclease activity in the presence of Mn^{2+} and the Mg^{2+} containing enzyme is much less tolerant of sequence variations at the ends of the LTR than the Mn^{2+} enzyme (Esposito and Craigie, 1998), then the Mg^{2+} cation is considered as the most physiologically relevant of these cations (Gao *et al.*, 2004). The number of Mg^{2+} cations is different for the distinct enzymatic reactions, and consequently for the different IN states: a single Mg^{2+} cation in non-processed IN and two cations in processed one.

Integrase is a 288 amino acids enzyme that consists in three structurally distinct functional domains: (i) the N-terminal domain (NTD, IN^{1-49}) with a non-conventional HHCC Zn-finger motif, promoting protein multimerization; (ii) the central core domain (CCD, IN^{50-212}) with a canonical DDE triad performing catalysis and involved in DNA substrate recognition; (iii) the C-terminal domain (CTD, $IN^{213-288}$) which binds DNA non specifically and contributes in stabilising the IN•vDNA complex (Asante-Appiah and Skalka, 1997). Both integration steps, 3'-P and ST, involve the active site D64-D116-E152 motif, and the active site flexible loop $IN^{140-149}$ formed by 10 residues. Neither the structure of isolated full-length IN nor that of IN complexed with its DNA substrate have been determined. Nevertheless, structures of the

HIV-1 IN single or two-domains allowed the generation of biologically relevant models reviewed in (Mouscadet *et al.*, 2010; Arora and Tchertanov, 2012), representing either the unbound dimeric enzyme or IN complexed with the viral or/and host DNA. The X-ray structure of full-length Prototype Foamy Virus (PFV) IN•DNA complex (or PFV intasome) was reported by Cherepanov group (Hare *et al.*, 2010a; Hare *et al.*, 2010b).

The integrase inhibitors were developed to block either the 3'-P or the ST reaction (Cotelle, 2006; Pommier *et al.*, 2005; Semenova *et al.*, 2008). Raltegravir (RAL), also known as Isentress^{TM}, the first IN inhibitor approved for AIDS treatment (Marchand *et al.*, 2009) specifically inhibits the ST activity and was confirmed as IN ST inhibitor (INSTI), whereas the 3'-P activity was inhibited only up to a certain concentration (Hazuda *et al.*, 2000; Mouscadet and Tchertanov, 2009). The potency of RAL has been described at the level of half-maximal inhibitory concentration (IC_{50} values) in cellular antiviral and recombinant enzyme assays, kinetic analysis and slow-binding inhibition of IN-catalyzed ST reaction (Copeland *et al.*, 2006; Dicker *et al.*, 2008; Garvey *et al.*, 2009; Grobler *et al.*, 2002; Hazuda *et al.*, 2000; Hightower *et al.*, 2011; Markowitz *et al.*, 2006).

Like other antiretroviral inhibitors, RAL induces a resistance effect. Resistance to RAL was associated with amino acids substitutions following three distinct genetic pathways that involve either N155H, either Q148R/K/H or Y143R primary mutation (Cooper *et al.*, 2008; Steigbigel *et al.*, 2008). The last mutation was reported as rarer (Sichtig *et al.*, 2009). G140S has been shown to enhance the RAL resistance associated with Q148R/K/H (Delelis *et al.*, 2009). The kinetic gating and/or induced fit effect has been reported as possible mechanisms for RAL resistance of the G140S/Q148H mutant (Perryman *et al.*, 2010). A third pathway involving the Y143R/C/H mutation and conferring a large decrease in susceptibility to RAL has been described (Delelis *et al.*, 2010).

No experimental data characterizing RAL unbound structure or RAL binding mode to the HIV-1 IN has been reported. In this regard, the characterization of RAL conformational preferences and the study of its binding to the HIV-1 IN represent an important task for determining the molecular factors that contribute to the pharmacological action of this drug.

RAL, incorporating three pharmacophores, is a multipotent agent capable to hit more than one target in HIV-1 – the unbound IN, the viral DNA or IN•vDNA complex. The aromatic cycles of RAL are connected by aliphatic linkers, each of that contains a planar peptide-like

carboxamide moiety connected to pharmacophores by single bonds providing a large conformational flexibility of the inhibitor. Two pharmacophores, (**1**) 1,3,4-oxadiazole-2-carboxamide and (**2**) carbonylamino-1-N-alkyl-5-hydroxypyrimidinone, possessing structural versatility through the orientation of the carboxamide fragments respective to the aromatic rings, show Z- or E- configurational states characterizing the relative position of the vicinal 1–4 &nd 1–5 oxygen atoms (**Chart 1**) (Mouscadet *et al.*, 2009).

Chart 1. RAL structure. The E- and Z-isomers of carbonylamino-1-N-alkyl-5-hydroxypyrimidinone (**1**) and 1,3,4-oxadiazole-2-carboxamide (**2**) pharmacophores are stabilized by intramolecular H-bonds.

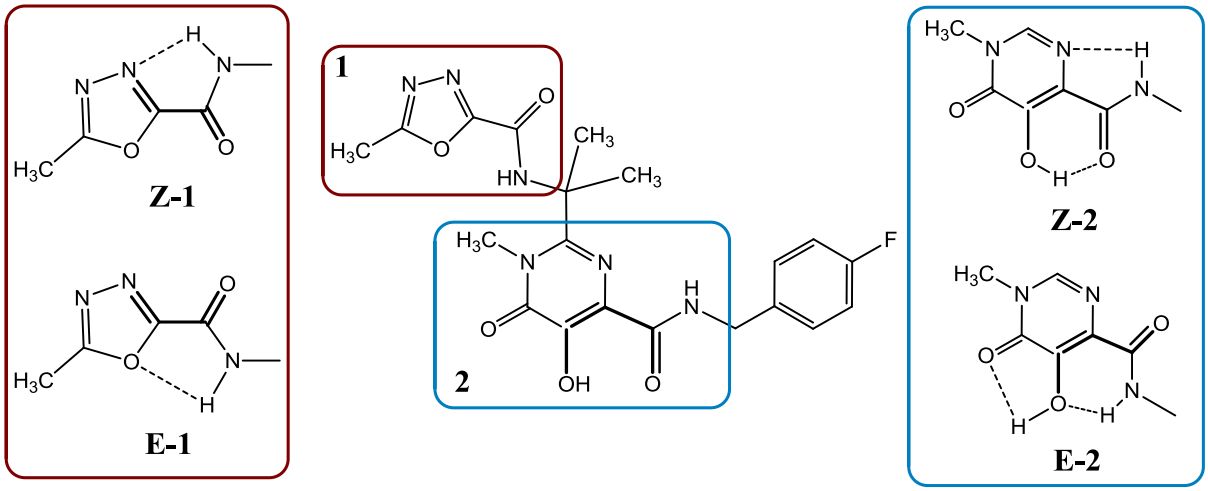

RAL contains a set of multiple H-bond donor (HBD) and H-bond acceptor (HBA) groups, which may affect RAL affinity for its target − 3 HBD and 8 HBA in the protonated state and 2 HBD and 9 HBA in the deprotonated RAL in a pharmaceutically acceptable potassium (K) salt.

These molecular features together with high structural flexibility provide an abundance of alternative mono- and bidentate binding sites in a given RAL conformation. The chelating properties of protonated or deprotonated RAL are also determined by the E- or Z-configuration (**Chart 2**). Consequently, RAL can contribute in the recognition and binding of different partners – H-donor, H-acceptors, charged non-metal atoms and metal cations – in

topologically distinct regions of IN by applying the richness of its molecular and structural properties. For instance, RAL as a bioisoster of adenine can block IN interaction with DNA (Mouscadet *et al*., 2009) or sequester metal cofactor ions (Kawasuji *et al.*, 2006).

Chart 2. Metal chelating properties of 1,3,4-oxadiazole-2-carboxamide (1) and carbonylamino-1-N-alkyl-5-hydroxypyrimidinone (2) moieties.

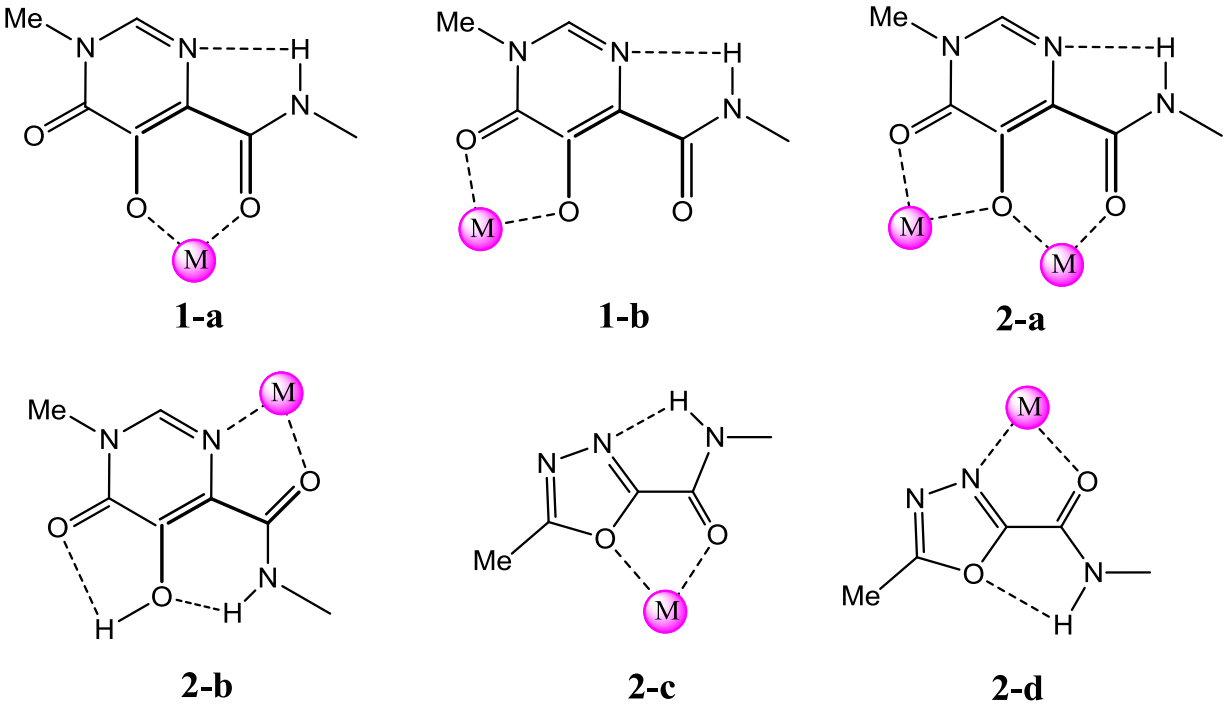

In the first part of this paper we examine the conformational preferences of RAL in the gas phase, in water solution and in the solid state. This analysis was based on three independent methods: (i) conformational analysis of free RAL in the gas phase, (ii) molecular dynamics (MD) in explicit solvent and (iii) fragment-based analysis using the crystallographic data from Cambridge Structural Database (CSD) (Allen, 2002). The second part reports the docking of RAL onto the retroviral targets representing the HIV-1 enzyme and viral DNA before and after 3'-processing. The targets are depicted as the three dimensional (3D) models of the unbound IN, the non-processed and processed vDNA and the IN complexed with vDNA (IN•vDNA), which were constructed as we described previously (Ni *et al.*, 2012). We report also the RAL docking to the viral DNA. This docking study is focused on an understanding of the contribution of IN and vDNA to RAL molecular recognition.

METHODS

All calculations were carried out on a Linux station (4x2 cores) running Centos 5.4. Figures were produced with PyMol (DeLano, 2002) and Chimera (Pettersen *et al.*, 2004). The crystallographic structures were retrieved from Protein Data Base (PDB) (Berman *et al*., 2000) and Cambridge Structural Database (CSD) (Allen, 2002) and reported with their reference codes.

1. RAL structure

Conformational analysis: RAL in Z-1/Z-2 configuration was taken from the X-ray structure of the Prototype Foamy Virus (PFV) integrase co-crystallised with RAL (PDB code: 3OYA, 2.65 Å resolution) (Hare *et al.*, 2010b). Alternative RAL configurations (or isomers) – Z-1/E-2, E-1/Z-2 and E-1/E-2 (Chart 1) – were generated using the SYBYL package (Tripos Inc., 2009) by employing simple carbon-carbon bond rotation to achieve the desired configuration, followed by minimization. Further, the conformational space of each RAL isomer was characterized by relaxed rotation of molecular fragments around four single bonds using the *Jaguar* program of MAESTRO molecular modeling package (Schrödinger, 2007). In each case, rotation was performed from 0 to 360° with an increment step of 30° for each particular single bond while the others were kept fixed. All the rotation scans were performed with 6-31g(d) basis set at the Hartree-Fock (HF) level of theory (Friesner, 1987). Each rotation scan was analyzed and corresponding potential energy plot and the RAL conformations were characterized for each isomer.

Molecular Dynamics simulations : The initial molecular geometry of RAL was taken from the crystallographic coordinates file representing RAL co-crystallized with IN of the PFV (PDB code: 30YA) (Hare *et al*., 2010b). The initial model was prepared with *pdb2gmx* of GROMACS 4.0 (van der Spoel *et al*., 2005); The ligand topology was generated by Acpype using a combination of GAFF and Amber 99sb-ILDN force fields; The charge of the ligand was -1, generated by Acpype; The hydrogen atoms were then added; In-vacuum minimization of RAL for 1000 steps was performed using a Steepest-Descent (SD) integrator. The minimized model of RAL was placed in an octahedral TIP3P water box. The charge of the solvated system was neutralized by adding Na^+ counter ions. The system was then heated up

to 300° K at constant volume using a modified Berendsen thermostat (Berendsen *et al.*, 1984) while restraining the solute atoms by 1 000 kJ/mol/nm^2. The system was then equilibrated for 1 ns under constant volume and temperature conditions (NVT). The pressure coupling was also turned "on" using *Parrinello-Rahman* barostat (Martonak *et al.*, 2003). Thereafter, three replicas of MD simulations were produced for the equilibrated system during 10 ns. The torsion angles τ1-τ4 were monitored over the MD simulations. The average fraction of distribution expressed as a probability of the occurrence of τ1-τ4 is given by (1):

$$f(x) = \frac{1}{\sigma\sqrt{2\pi}} e^{-(x-\mu)^2/2\sigma^2} \qquad (1)$$

where μ is a mean value and σ is a standard deviation.

The H-bonds formed by RAL with water molecules were recovered over the MD simulations. The contacts D-H···A, where D and A = O/N, with D···A distances < 3.4 Å and pseudo valent angles ∠D-H···A > 90° were considered as H-bonds.

CSD structural fragment-based analysis: Relevant structures were retrieved from the CSD (Release 2011, 541,748 entries) (Allen, 2002). Substructural searches, geometry calculations and data analysis were carried out with the CSD programs ConQuest 1.13 (Bruno *et al.*, 1997), Vista v2.1 (CSD, 1994) and Mercury 2.4.5 (Macrae *et al.*, 2006). Structures flagged in the database as being erroneous or disordered were rejected from analysis.

We searched CSD for three groups of molecules based on the 1,3,4-oxadiazole-2-carboxamide (**1**), carbonylamino-1-N-alkyl-5-hydroxypyrimidinone (**2**) and fluorobenzyl carbamoyl (**3**) moieties. No structures included moiety (**1**) and a limited number (3 structures) of molecules based on moiety (**2**) was retrieved, therefore the search was performed using the more general fragments – **F1, F2** and **F3** (**Table 1**). The **F1** and **F2** were investigated to characterise the molecular geometry, intramolecular H-bonding (D-H…A, where D and A = O/N) and coordination geometry in metal complexes (M= Mn, Mg and K) as defined in (Tchertanov and Mouscadet, 2007) and in Table 1. Molecules based on **F3** with halogen atom F, Cl or Br in the *para* position were analysed for the torsion and dihedral angles. Statistical univariate and bivariate analysis was applied to quantify the observations and identify the relationships between the measured parameters. The results obtained for univariate analysis are presented as numerical values, and those for bivariate analyses are presented as scatter plots.

2. Targets modeling

Secondary structure prediction : Secondary structure assignment for the 1BL3 (Maignan *et al.*, 1998), 1B9F (Greenwald *et al.*, 1999) – crystallographic structures of the HIV-1 IN catalytic core domain representing the single F185H mutant and the G140A/G149A/F185K triple mutant respectively, and 3DLR (Valkov *et al.*, 2009a) and 3OYA (Hare *et al.*, 2010b) – the crystallographic structures of PFV IN, either isolated or in complex with DNA, respectively, were achieved with the DSSP (Kabsch and Sander, 1983) and Stride (Frishman and Argos, 1995) algorithms.

The secondary structures of the 23 amino acids (aas) polypeptides $IN^{133-155}$ of the HIV-1 IN and $IN^{202-225}$ of the PFV IN were predicted by combining different methods: GOR4 (Garnier *et al.*, 1996); SIMPA96 (Levin, 1997); PSIpred (McGuffin *et al.*, 2000); APSSP2 (Raghava, 2002); DSC (King *et al.*, 1997); HNN (NPS@ : CLUSTALW ALIGNMENT); PHD (Rost *et al.*, 1994); Jnet (Cuff *et al.*, 1998); MLRC (Guermeur *et al.*, 1999) combining GOR4, SIMPA96 and SOPMA; and SSPRO (Pollastri *et al.*, 2002). A score was assigned to each predicted secondary structures (β-strand, α-helix, coil and turns) per amino acid by each method, to further derive a consensus prediction. Two types of consensus predictions were computed: the first type was derived from the tools that do not perform alignment before computing predictions (DPM, PREDATOR and GOR4), and the second type was derived from the tools that are based on multiple alignments (SIMPA96, PHD, SOPMA, Jnet, DSC, GORV and PSIPRED). The occurrences of each structural element at a given position were summed over all the predictions for each set resulting as consensus 1 and consensus 2. The confidence rate of a consensus prediction at one position was considered as "high" when at least 75% of the predictions of the set converged.

Generation of the models of unbound IN, IN•vDNA complex and vDNA: The IN models were constructed using Modeller package 9V8 (Eswar *et al.*, 2003) as we reported previously (Ni *et al.*, 2012). The sequence alignment was performed using ClustalW server (http://www.ebi.ac.uk/Tools/clustalw2/index.html). Briefly, a 3D model of the full-length IN homo-dimer, IN^{1-270} (unbound state respectively to DNA), was generated by homology modeling from crystallographic structures of isolated pairs of IN domains, IN^{1-210} (PDB code: 1K6Y) (Wang *et al.*, 2001) and IN^{56-270} (PDB code: 1EX4) (Chen *et al.*, 2000). The sequence

of the native HIV-1 IN was aligned to the templates sequences (non wild-type) using ClustalW (Larkin *et al.*, 2007; Thompson *et al.*, 1994). The missing regions, namely the linker from residues 47 to 55 and the catalytic site loop from residues 140 to 148, were constructed by an *ab initio* approach as we reported in (Mouscadet *et al.*, 2009). We shall refer to the model with one Mg^{+2} cation inserted into the active site as reported in structure 1BI4 (Maignan *et al*., 1998) as model **1A**, and to the model with two Mg^{+2} cations inserted as reported in (Mouscadet *et al*., 2009) as model **1B**.

The 3D model of the IN•vDNA pre-integration complex was generated by homology modeling from the crystal structure of the PFV IN•vDNA complex (PDB code: 3OYA, resolution of 2.65 Å) (Hare *et al*., 2010b). Despite the low sequence identity between these two INs (22%), a high conservation of key structural elements in both integrases allowed us to use the PFV IN structure as a template for the HIV-1 IN model generation. We shall refer to the constructed and optimized model as model **2A.** The stereochemical quality of the models was assessed with ProTable Procheck (Laskowski *et al.*, 1993).

A 27 base pair model of the vDNA was constructed using the 3D-DART webserver (van Dijl and Bonvin, 2009) according to the following sequence: TAGTCAGTGTGGAAAATCT CTAGCAGT/complement (Hazuda *et al.*, 2000) in B-form (model **3A)**. A subsequent model was generated by removing *in silico* the two nucleotides GT from the 3'-end of the modelled vDNA, leaving a CA dinucleotide sequence at the terminal end that is required for integration (model **3B**).

3. Procedure of RAL docking onto the targets

Recorded configurational (isomeric) and conformational states of RAL (see **Conformational analysis in METHODS**) were used for the inhibitor docking onto the generated models representing the targets with an extended loop in an open conformation, unbound IN (models **1A** and **1B**), and the target with a shortened loop and a well-delimited binding site, IN•vDNA complex (model **2A**). The docking was performed by using four algorithms: GLIDE (Friesner *et al.*, 2004) incorporated in the Schrödinger suite (Schrödinger Inc.), AutoDock 4.2 (Morris *et al.*, 2009), VINA (Trott and Olson, 2010) and SurFlex (Jain, 2003). The targets were considered as rigid bodies while the inhibitor was treated as wholly flexible. Before the docking, the models were prepared (addition of hydrogen atoms, bond order assignment) according to the given software default requirements.

The conformation of RAL determined by X-ray analysis of PFV IN•DNA complex (PDB code: 3OYA) was optimized and docked onto the vDNA (models **3A** and **3B**) using GLIDE.

AutoDock: AutoDock (Morris *et al.*, 2009) is based on a hybrid search method that applies a Lamarckian genetic algorithm. Exploration of the binding site is based on a global search that uses a Genetic Algorithm (GA) followed by an adaptive local search method derived from the optimization algorithm of Solis and Wets, that has the advantage of not requiring gradient computation while it performs torsional angles space search. The graphical user interface (GUI) of AutoDock 4.2 was used for preparation of ligand and receptor files. Grid maps of interaction energies for various atom types were carried out with a grid box of dimension 25×25×25 $Å^3$ centred on the active site. Calculations were performed with a population size of 150, number of energy evaluations of $5x10^6$, maximum number of generations of 27,000 and crossover rate of 0.02 and 0.8, respectively. The number of runs was set to 100 to explore a large number of poses of the highest affinity, and the Solis and Wets algorithm was used to relax the best 10 % of the obtained conformations. The active site coordinates were explicitly defined in the input file.

GLIDE: GLIDE 4.5 (Grid-based Ligand Docking with Energetics) (Friesner *et al.*, 2004) program uses a hierarchical series of filters to search for possible locations of the ligand in the binding site region of the receptor. The shape and properties of the receptor are represented on a grid by several sets of fields that provide progressively more accurate scoring of the ligand poses. Conformational flexibility of the ligand is handled by an extensive conformational search. Receptor grids were generated by GLIDE within an enclosing box of size 20 Å centred on the active site. The inhibitor was docked flexibly to these pre-computing grids using standard precision (SP) scoring.

VINA: VINA (Trott and Olson, 2010) uses a gradient optimization method in its local optimization procedure. It uses an Iterated Local Search global optimizer algorithm that performs a succession of steps consisting of a mutation in the context of a genetic algorithm, and a local optimization with each step being accepted according to a Metropolis criterion. The general functional form of the conformation-dependent part of the scoring function VINA works with the summation over all the pairs of atoms that can move relative to each other (excluding*1–4 atoms interactions). The binding site for each receptor was explicitly defined. Grid maps were generated on a grid box with dimensions 25 Å centered over the binding site of the receptor. The maximum energy difference between the best and worst binding modes

was set to 4 kcal/mol, while the exhaustiveness and the maximum number of binding modes were set to 80 and 100 respectively.

SURFLEX: SurFlex (Jain, 2003) is a relatively new docking algorithm that combines Hammerhead's empirical scoring function (Welch *et al.*, 1996) with a molecular similarity to generate putative poses of ligand fragments. It implements an incremental construction search approach, as in Hammerhead (Welch *et al*., 1996), associated to a new fragment assembly method that is both faster and more accurate. SurFlex employs an idealized active site ligand (a protomol) as a target to generate putative poses of molecular fragments. These putative poses are scored using the Hammerhead function. The protomol was generated with a threshold value of 0.5 and bloat value of 1 Å. The SurFlex package integrated in SYBYL-X 1.1.1 was used for docking.

The binding affinity of RAL-IN complexes was expressed in terms of docking scores. For each RAL conformation, the lower-scored pose was saved and analyzed.

RESULTS

1. RAL conformations in the gas phase, in water solution and in the solid state

The intrinsic conformational features/preferences of RAL have been investigated in the gas phase, in water solution and the solid state.

Raltegravir conformations in the gas phase: First, the geometry and energy of the protonated RAL were considered in the gas phase. *Ab initio* calculations were performed at the Hartree Fock (HF) level of theory as described in **METHODS**. Full geometry optimization and energy calculations were carried out for each RAL isomer: Z-1/Z-2, Z-1/E-2, E-1/Z-2 and E-1/E-2 (**Chart 1**). Following the geometry optimization, RAL conformations were generated for each isomer by relaxed rotation (scans) around the four aliphatic single bonds of the linkers, characterized by torsion angles τ1-τ4 respectively, with an increment step of 30°.

The energy profiles of the generated RAL conformations differ in terms of energy value, while the local minima and maxima are localized within the approximately same ranges of

torsion angles in all isomeric states (**Figure 1 a-d**). The energy profiles of the free rotation describing the conformational flexibility of RAL substituents relative to the pyrimidine cycle (torsion angles τ1 and τ2, in blue and red colours respectively) show high (~120 kJ/mol) and very high (~500 kJ/mol) energy values at 60° (τ1) and at 20° (τ2) respectively, while the corresponding rotation in the Z-1/Z-2 and E-1/Z-2 isomers manifests a moderate energy barrier, slightly lower in the Z-1/Z-2 isomer. The energy profile describing rotation of the oxadiazole-carboxamide fragment (torsion angle τ3, in green colour) is very similar (Z-1/Z-2 and E-1/Z-2 isomers) or differs only slightly (Z-1/E-2 and E-1/E-2 isomers). All corresponding curves show that the energy values vary weakly within a large torsion angle range from 30 to 330°. The max and min values are observed at 0° and 360° respectively. The energy profile of the fluorobenzyl fragment rotation (torsion angle τ4, in violet colour) is nearly similar in all RAL configurations: its energetical impact is minimal in a wide range from 100 to 300°; two maxima in the ranges 0-70° and 320-360° are observed.

Analysis of RAL conformational flexibility through the free energy estimation for the fragments rotation around four aliphatic single bonds of the linkers evidenced that rotations characterized by torsion angles τ1 and τ2 are indicative and discriminative for selecting the energetically favourable RAL configuration(s). We found that, in the gas phase, the Z-1/E-2 and Z-1/Z-2 configurations display energy profiles characterizing the most unstable and the most energetically favorable RAL conformations, respectively (Figure **1 a, b**).

The energies of E-1/E-2 and E-1/Z-2 configurations display intermediate values with profiles close to those of Z-1/E-2 and Z-1/Z-2, respectively (Figure **1 c**, **d**). The relative stability of the four RAL isomers may be represented as follows for all considered conformers: Z-1/Z-2 ≥ E-1/Z-2 >> E-1/E-2 >> Z-1/E-2. These results indicate that the Z-1/Z-2 configuration of RAL is preferable energetically. The energy profile of the deprotonated species is very similar to that of the neutral molecule (data not shown).

According to the crystallographic data, RAL structure in the PFV IN molecular complex is stabilised as the Z-1/Z-2 isomer, corresponding to the most stable RAL configuration observed in the gas phase. The values of torsion angles τ1 – τ4 observed in the X-ray RAL structure do not exactly correspond to the minimum on the energy profiles charactering the free rotation around the single bonds (Figure **1 a**). Such conformational difference is probably caused by RAL interactions with the PFV IN•vDNA complex.

Molecular dynamics simulations of Raltegravir in water solution: We supposed that the calculated conformer energies of RAL with multiple polar functional groups (dipolar moment of RAL calculated with GAMESS (Fedorov *et al.*, 2003) and CHARMM (http://yuri.harvard.edu/) is 17.0 and 19.5 D respectively) were solvent-dependent and the RAL crystallographic structure was further used as initial template for MD simulations in explicit solvent. Three trajectories of 10 ns of the deprotonated RAL, each following an equilibration of 2 ns, were run to explore the conformational flexibility of the molecule in water. The root mean square deviations (RMSDs) of RAL revealed a high degree of atomic deviations. All three trajectories display comparable conformational drifts with RMSD values of 0.16 ± 0.06 nm (Figure **2 a**). The root mean square fluctuations (RMSFs), measuring the average atomic mobility of RAL atoms during the MD simulations, as it was expected, shows that the most fluctuating non-hydrogen atoms are the fluorophenyl fragment and methyl groups (Figure **2 b**).

The four torsion angles τ1 – τ4 describing RAL flexibility were recorded over the MD simulations. Their occurrences show excellent agreement between the three replicates (**Figure 2 c**). The torsion angles τ1, τ2 and τ3 display Gaussian-like distributions. The torsion angle τ3 mostly displays values in a narrow range, from 10 to 30°. Values for the torsion angles τ1 and τ2 ranged from -190 to -150° and from -25 to 25° respectively. The τ4 values are largely distributed from -130 to 130°.

The RAL H-bonding recorded over the MD trajectories indicates a very high capacity of the deprotonated molecule to bind water molecules (Figure **2 d**). The number of H-bonds formed by RAL varies from 4 to 15 with a mean value of 11. In the majority of conformations the nine acceptor (HBA) and two donor (HBD) groups are exposed to the solvent at the same time, hence each group is capable of forming one or two H-bonds with the water molecules. Most of these H-bonds are strong in terms of their length. The involvement of RAL in multiple H-bonds may strongly affect its molecular conformation in solution compared to those observed in the crystal (PDB code: 3OYA) and in the gas phase (Figure **1 a**).

Fragment-based structural analysis: We analyzed the conformational properties of RAL in the solid state using the structural data available for the building stones or structural blocks of RAL, the 1,3,4-oxadiazole-2-carboxamide (**1**), carbonylamino-1-5-hydroxypyrimidinone (**2**) and 4-fluorobenzylcarbamoyl (**3**) derivatives in crystals. The CSD search for the molecules

based on each pharmacophore produced no hit, only 3 structures and 83 structures for fragments **1**, **2** and **3** respectively (**Table 1**). The absence (for **1**) or limited data (for the **2** and **3**) required the search for the more general fragments – **F1**, **F2** and **F3** ; this search resulted in statistically relevant data (**Table 1**).

The torsion angle T^1 describing the relative position of the O or N vicinal atoms and the intramolecular contact O···H were used to distinguish the **F1** conformations. A scatter plot of the absolute values of the torsion angle and the O···H-N distance (T^1 *vs* O···H) revealed three major clusters and a limited number of randomly distributed observations (**Figure 3**, **a**). Torsion angles within the range from 0 to 25° and from 145 to 180° were considered to meet the criteria for Z- and E-configuration, respectively. Based on this definition, the cluster with $T^1 \sim 0°$ was attributed to the Z- configuration and the two distinct clusters with $T^1 \sim 180°$ to the E-configuration. The randomly distributed points correspond to intermediate conformations and were not considered. The populations of the different clusters were not identical, with most of the **F1** fragments in crystals adopting the E-conformation (~75%). The intramolecular O···H distance was correlated with the **F1** conformation. The O···H distance values in the range from 2.0 to 2.5 Å are indicative of the E-configuration stabilisation by intramolecular H-bonds (IHB). The small cluster with T1 ~180° and O···H distances from 3.35 to 3.65 Å also represents the E-conformation, although with the H-atom of the amino group in an unfavourable position to form IHB.

Retrieved carbonylamino-1-5-hydroxypyrimidinone (**2**) derivatives represent a new class of heterocyclic ligands (Sunderland *et al.*, 2001; Xu *et al.*, 2003). These ligands synthesised by a two step procedure to provide the desired flexibility were characterized by X-ray analysis (CSD codes: GACMUT and MESDAP). GACMUT shows a planar structure stabilized in the E-configuration by N–H···O intramolecular H-bonding with H···O distance of 2.02 Å (**Figure 3 d**). To avoid the H-bond induced stabilization of the E-configuration, the H atom was replaced by methyl group. The produced molecule, MESDAP, conserves its E-conformation but not the planarity : the carbonylamino group is turned at 70° relatively to the hydroxypyrimidinone ring to resolve the steric constrains (**Figure 3 e**). A multistep procedure was applied to synthesized a RAL prototype, the flurobenzyl derivative of carbonylamino-1-5-hydroxypyrimidinone, POPYOJ (Zhong *et al.*, 2009), leading to RAL synthesis, which was finalized by a manufacturing route for the synthesis of RAL potassium salt (Humphrey *et al.*, 2011). Carbonylamino-1-5-hydroxypyrimidinone moiety of POPYOJ is stabilized in a planar Z-configuration by a strong O–H···O intramolecular H-bond with H···O distance of 1.86 Å (**Figure** 3 **f**). Consequently in the solid state carbonylamino-1-5-

hydroxypyrimidinone moiety shows two different configurational isomers, E- and Z (**Chart 1)**.

To retrieve a statistically significant number of structural data for carbonylamino-1-5-hydroxypyrimidinone derivatives, we referenced to a more general fragment, the β-ketoenol moiety, **F2**, a very important pharmacophore and a corner stone of (**1**) besides numerous biologically active molecules. **F2** has been previously characterized in detail (Tchertanov & Mouscadet, 2007). We had shown that the vast majority of β-ketoenols (96%) were stabilized by a very strong intramolecular H-bonding in Z-configuration. In the present work we took into account the last update of the data with a recent version of CSD (version 2011) which enriched considerably the statistical observations (**Figure 3**, **b**).

The halogenated aromatic rings are widely present among drugs. The CSD search was performed for the more generalized fragment **F3** based on benzylcarbamoyl derivatives with a halogen atom (Hal =F/Cl/Br) at the *para* position. The type of the halogen atom was taken into consideration. The rotation of the aromatic ring relatively to the carbamoyl fragment was described with torsion angle T^1 and dihedral angle D formed by two planes P^1 and P^2 defined in **Table 1**. A scatter plot of absolute value of torsion angles T^1 *versus (vs)* D reveals a dense cluster for T^1 ranging from 60° to 120° and D from 65° to 90°. The second and diffused cluster is in the range from 160 to 180° for T1 and from 0° to 90° for D. Such distribution indicates a very large conformational freedom of benzylcarbamoyl derivatives with a halogen atom at the *para* position (blue circles for F, red squares for Cl and green triangles for Br). Conformation of the benzylcarbamoyl fragment from POPYOJ and 20YA is marked by asterisks in **Figure 3 c**. Both structures display T1 values at extremity of the dense cluster.

This structural fragment-based analysis indicates a higher probability of the E-configuration for the oxadiazole-carboxamide–like derivatives than of the Z-one. The stability of such configuration can be attributed to the intramolecular H-bonding or steric and/or other electronic molecular factors. Nevertheless the Z-isomer is observed in ~20% of related structures. The β-ketoenol-based derivatives show a clear preference for the Z-configuration stabilized by a strong or very strong intramolecular O-H···O bond. The molecules stabilised as E-isomer are relatively rare, as evidenced by the dense cluster at T1 ~180° and illustrated with two representative structures GACMUT and MESDAP. The benzylcarbamoyl derivatives with a halogen atom at the *para* position are characterised by a very high flexibility. The structural data does not suffice to distinguish between the F, Cl or Br

derivatives. These data should be considered together with other physicochemical characteristics of such molecules.

Probing the RAL coordination of Mg, Mn and K cations: Both partners, inhibitor and its target, contain metal cations. The pharmaceutically acceptable form of RAL is its potassium (K) salt. The HIV-1 integrase requires Mn^{2+} or Mg^{2+} cations for enzymatic activities *in vitro* (Feng *et al.*, 2004) and *in vivo* (Neamati *et al*., 2002). The active site conformation of the HIV-1 integrase may differ depending on whether it contains Mn^{2+} or Mg^{2+} ions, which in turn influence the mode of interaction between the inhibitor and the ion-loaded active site.

We focused here on the interactions of 1,3,4-oxadiazole-2-carboxamide (**1**) and carbonylamino-1-N-alkyl-5-hydroxypyrimidinone (**2**) moieties with K, Mg and Mn. Each pharmacophore, **1** and **2**, is polydentate, and binds metals either *via* a single atom or through chelation. Chelation gives more stable complexes and is therefore the only mode of coordination considered here. **1** and **2** possess chelating fragment(s) differing by the Z- and E-isomers at the chelating atom types (**Chart 2**). The vicinal 1–4 oxygen atoms of hydroxypyrimidinone and β-ketoenolate can chelate two metal cations simultaneously (**Chart 2, 2-d**).

The 5- and 4-atom based ligands with either two oxygen ligating atoms (L1 and L3) or heteroatoms O/N (L2 and L4) were used for retrieving and analysing the M-L complexes (M = K, Mg and Mn) (**Table 2**). The number of crystal structures containing both a metal atom (K, Mg or Mn) and a ligand with identical ligating atoms (L1 and L3) are trice more common respectively to complexes formed with heteroatomic ligands (L2 and L4). Structures based on ligand L1 are trice as numerous as structures based on ligand L3, while a quantity of structures based on ligands L2 and L4 differ slightly (ratio of 1 : 1.5). The proportion of complexes in which the metal is chelated by ligand L1 or L3 and L2 or L4 is approximately the same. The metals occurrences show K:Mg:Mn ratio of 8:1:5 for all analysed crystal structures while the ratio of metals chelated with all ligands L1 – L4 is K:Mg:Mn of 1.5:1:6. L1 and L4 appears to display preferential binding to Mn, while L4 chelates better K.

The scatter plot of M–O coordination bond distances in M-L1 complexes shows four clusters (**Figure 4 a**). Three dense clusters correspond to MnIII/MnIV (MnIII and MnIV complexes considered together), MgII and MnII complexes. Mn/Mg···O bond distances were characterized in detail and correlation between their geometrical parameters and the metal

type, oxidation state and size were established (Tchertanov and Mouscadet, 2007). Update of these data with a recent version of CSD (2011) confirmed the earliest finding. Taken into consideration the potassium complexes, we identified on the scatter plot a diffuse cluster composed of K complexes. K···O bond distances range from 2.6 to 3.6 Å, indicating weak or very weak ionic interactions.

The distribution of the M–O coordination distances in M–L3 is generally similar to that observed in M–L1 complexes (**Figure 4 a** and **c**). However, some difference is manifested : (i) M–O distances distribution is more symmetric in M–L3 complexes, (ii) clusters formed with different metals are not identical, Mn–L1 and K–L3 showing a higher population density, (iii) Mg–L3 displays two separated clusters corresponding to six- and seven-coordinated complexes with Mg–O bond distance of 2.065 and 2.170 Å, respectively.

M–O *vs* M–N scatter plot characterising M–L2 complexes contains only two clusters composed with MnIII/MnIV and MnII separated by a cluster containing the Mg-based complexes (**Figure 4 b**). In M–L4 complexes, M–O *vs* M–N scatter plot is similar to that in M–L3, but the density of clusters is higher for Mn and lower for Mg cations (**Figure 4 d**). A very limited number of points with M–O/M–N bond distances of 2.80/2.90 Å correspond to K–L4 complexes.

In RAL co-crystallized with the PFV IN•vDNA complex (PDB code: 30YA), the length of coordination bonds M–O correspond very well to statistical observations for M-L1 complexes, whereas these distances are different from the corresponding statistical data for M–L3 complexes and shows a strong asymmetry (**Figure 4 a**, **c**). The Mg^{2+} cations in the IN active site are fixed as a two-atoms cluster by means of the D64 residue establishing a bridge between two Mg^{2+} cations (**Figure 4 f**). Steric constrains in the active site and conjugated electronic effect in RAL may be the major factors for such distorted coordination geometry.

2. Targets models, representing the HIV-1 integrase before and after 3'-processing

Four integrase models were generated by homology modeling (**Figure 5**). Models **1A** and **1B** (**Figure 5a**) represent the unbound homodimer of the full-length integrase (IN^{1-270}), which plausibly depicts the conformational state of the enzyme before the 3'-processing of vDNA (unbound state of IN). The models differ by the number of Mg^{2+} atoms localized in the active site (one and two cations in model **1** and 2 respectively). Model **2A** (**Figure 5b**) represents the

IN homodimer in complex with two double-strand vDNA, which likely depicts the active unit of the IN•vDNA strand transfer intasome; models **2B** (not shown) was derived from model **2A** by removing vDNA.

The models **1A** and **1B** did not show any significant structural change induced by the different number of Mg^{2+} cations in the active site. This finding is coherent with our early published results for the catalytic core domain (CCD) where we reported that a second Mg^{2+} ion would likely enter the active site upon movement of the E152 side chain toward the active site conserving the overall structure of CCD (Mouscadet *et al*., 2009). Therefore only the model **1A** is presented on **Figure 5 a**. It is useful to note that the Normal Modes Analysis (NMA) shows that in unbound IN with two Mg^{2+} cations the active site is more rigid, due to the stabilising role of the coordination of the Mg^{2+} cations by three active site residues –D64, D116 and E152 –, whereas the catalytic site loop flexibility increases significantly (Arora & Tchertanov, 2012).

Model **2A** was generated from the X-ray structure of the PFV intasome (Hare *et al*., 2010a). As we reported, despite a very low sequence identity (22%) between the HIV-1 and PFV INs, the structure-based alignment of the two proteins demonstrates high conservation of key secondary structural elements, and the three PFV IN domains shared with HIV-1 IN have essentially the same structure as the isolated IN domains from HIV-1 (Ni *et al*., 2012). Moreover, the structure of the PFV intasome displays a distance between the reactive 3' ends of vDNA that corresponds to the expected distance between the integration sites of HIV-1 IN target DNA (4 base pairs) (Yin and Craigie, 2010). Consequently, we suggested that the PFV IN X-ray structure represents an acceptable template for the HIV-1 IN model generation. We considered that a simplified dimer model of the IN•vDNA complex (**Figure 5 b)** is appropriate for the modeling procedure.

It is worth noting large structural and conformational changes between the unbound (model **1A**) and vDNA-bound (model **2A**) integrase states regarding the relative positions of the IN domains (RMSD of 31 Å, based on C_α) (**Figure 5 c**). These structural modifications result in different contacts between the IN domains. As such, in the model **1A** no interaction was detected between CTD and CCD whereas the two domains interact tightly in model **2A**. The NTD-CCD interface also exhibits substantial changes: in the unbound form the NTD-CCD interface belongs to the same monomer subunit whereas in the vDNA-bound form it is composed of residues from the two different subunits.

Moreover, in the homology modelled IN•vDNA complex, IN undergoes important structural transformation leading to structural re-organisation of the catalytic site loop; the coiled portion of the loop reduces from 10 residues (140 -149 aas) in the unbound form to 5 residues (140-144 aas) in the vDNA-bound form. Two hypotheses we proposed: (i) such effect may be induced by the vDNA binding, or (ii) it is an artefact derived from homology modeling with the structural data of the PFV IN in which the shorter loop may be a natural fold of the PFV IN sequence.

To explore the influence of the sequence on the loop folding we used a large range of algorithms designed to predict secondary structure elements. Efficiency of secondary structure prediction tools has been recently improved by the use of evolutionary information from multiple alignments: the query sequence is aligned with homologous sequences taken from a protein structures database (PDB), and the experimental structures of the homologous sequences are considered in the prediction. Such method can produce biased results, particularly if an existing structure shows high sequence similarity but its structure is influenced by the ligand binding. This case correspond to that studied here. To avoid this discrepancy, we separated the prediction tools based on either multiple alignements or not for computation of consensus predictions (see **METHODS**).

Three amino acid sequences $IN^{133-155}$ of the wild-type (WT) and the double mutant G140A/G149A IN from HIV-1 and the WT IN from PFV were considered. According to the secondary structure predictions, the sequence segment $IN^{150-155}$, a part of the α-helix $IN^{150-166}$ is preceded by a random coil composed of 10 residues, $IN^{140-149}$, in the HIV-1 WT, while in the double mutant G140A/G149A a reduced coil formed by only 7 amino acids, $IN^{141-147}$, and an increased α-helix $IN^{148-166}$ are observed (**Figure 5 d**). Mutation G140A also influences the secondary structure of the $IN^{133-139}$ sequence segment, favouring a β-sheet structure. Prediction results obtained with high reliability (>75%) correlate perfectly with the X-ray data characterising the WT HIV-1 integrase (PDB code: 1B3L) (Maignan *et al*., 1998) and its double mutant G140A/G149A (PDB code: 1B9F) (Greenwald *et al*., 1999).

Prediction for the PFV IN indicates a high probability of a two β-strands organisation of sequence segments $IN^{204-208}$ and $IN^{220-222}$ (corresponding to $IN^{135-139}$ and $IN^{151-153}$ in the HIV-1), linked by a random coil including 10 residues, $IN^{209-219}$, ($IN^{140-152}$ in the HIV-1) (**Figure 5 d**). Consequently, the WT $IN^{133-155}$ segment from HIV-1 and corresponding $IN^{202-224}$ segment from PFV should naturally fold in different and unlike structural elements. Crystallographic

data characterising the unbound PFV IN reports that $IN^{210-220}$ residues were not identified (PDB code: 3DLR) (Valkov *et al.*, 2009b). Apparently this sequence represents a strongly flexible coiled structure as we observed in our prediction. In contrast, the X-ray structure of the PFV IN bound to the vDNA shows a shortened coil and a long well-organized α-helix in $IN^{214-234}$ sequence (PDB code: 3L2U) (Hare *et al.*, 2010a). This partial folding of the catalytic site loop is stabilized through intra-IN domain-domain interactions and interactions with vDNA that probably contribute to stabilisation and elongation of the α4-helix.

To complete the RAL targets definition, structural models representing the non-cleaved and cleaved HIV-1 viral DNA (model **3A** and **3B** respectively) were constructed as described in **METHODS** section and represent the double strands helix which is slightly distorted at 3'-end in **3A** model.

RAL-targets recognition

Characterization of RAL recognition by its viral targets was performed as follows. First, RAL in each conformation generated from the crystallographic structure representing the Z-1/Z-2 isomer (PDB ID: 3OYA) was docked onto the active site of three targets – unbound IN with one and two Mg^{2+} cations at the catalytic site (models **1A** and **1B**) and IN•vDNA pre-integration complex (model **2A**). RAL was considered in its deprotonated form, corresponding to its pharmaceutically acceptable form. Four different programs, AutoDock, GLIDE, VINA and SurFlex, were used for the docking procedure. Such routine allows (i) to optimize the algorithm choice to dock the flexible inhibitor and (ii) to evaluate RAL binding with different types of targets, flexible (unbound IN with one Mg^{2+} cations in the catalytic site), semi-flexible (unbound IN with two Mg^{2+} cations in the catalytic site) and rather rigid (IN•vDNA complex).

To distinguish between the RAL conformations we will refer to the crystallographic structure of RAL as the "crystallographic conformation", the conformations generated by relaxed rotation scan from crystallographic structure of RAL as the "generated conformations" and RAL conformations produced by docking to targets as the "docked conformations".

The docked conformations of RAL produced by docking the generated conformations onto the unbound IN with a single Mg^{2+} cation within the catalytic site are positioned mainly at the area delimited by the catalytic site loop in an extended (open) conformation (**Figure 6,** top panel, snapshots on the left and on the right). They differ strongly from the generated conformations and their isomeric state is frequently not coincident with the initial Z-1/Z-2 isomer. The binding energy values obtained by all applied scoring functions range from -8.8 to -5.1 kcal/mol (**Figure 6**, top panel, central graph).

Docking of the same RAL conformations onto the unbound IN with two Mg^{2+} cations within the catalytic site shows that the molecule is re-positioned from the loop towards the active site (**Figure 6,** middle panel, snapshots on the left and on the right). The binding energies are slightly lower ranging from -9.5 to -5.6 kcal/mol (**Figure 6**, middle panel, central graph). Similarly to the docking of RAL onto the unbound IN with a single Mg^{2+} cation, a large variety of sampled isomers/conformers are realized. The RAL is oriented rather randomly respectively to the active site and the active site loop.

Docking of the RAL generated conformations onto the IN•vDNA model resulted in binding modes with significantly lower scores (from -11.9 to -6.2 kcal/mol) than those found for the unbound IN (**Figure 6,** bottom panel, central graph). In all cases, RAL is positioned in the catalytic site of the pre-integration complex and chelates the Mg^{2+} cations by the oxygen atoms of carbonylamino-1-5-hydroxypyrimidinone pharmacophore (**Figure 6,** bottom panel, snapshots on the left and on the right). The oxadiazole-2-carboxamide pharmacophore demonstrates alternative docking configurational/conformation states and occupies an either axial or equatorial position relatively to the plane of the carbonylamino-1-5-hydroxypyrimidinone pharmacophore. In contrast, the fluorobenzyl moiety is favourably oriented to form a π-staking with Cyt16 of the vDNA in nearly all docked conformations obtained with the different programs.

The docking calculations with four different docking algorithms evidenced that the lowest scores and most adequate docking poses were obtained for RAL docked onto the IN•vDNA model. Nevertheless, the docked conformations of RAL differ from the generated conformations and some of them represent alternative isomers different from the initial one (Z/Z).

We analysed the docking results individually for each docking method and compared the efficiency of docking algorithms relatively to the chosen target. The score profiles obtained

for RAL docking onto the same target by the different programs are significantly altered (Figure **6,** central column). For RAL docked onto the unbound IN with a single Mg^{2+} cation, the lowest score values were obtained with VINA and AutoDock (**Figure 6,** top panel, central column). Binding energies for all RAL conformations are very similar, with values ranging from -8.8 to -7.0 kcal/mol. Binding energies obtained with SurFlex and GLIDE are characterized by more important fluctuations and higher values, from -8.0 to - 5.2 kcal/mol. The RAL docking onto the unbound IN with two Mg^{2+} cations with VINA and AutoDock show very small difference in predicted binding energies (**Figure 6,** middle panel, central column). The score profiles superimposed perfectly within the range from -9.5 to -7.4 kcal/mol. Binding energies obtained with GLIDE and SurFlex fluctuate more significantly and show slightly decreased values ranging from -9.1 to -5.6 kcal/mol.

RMSDs between generated, docked and crystallographic conformations of RAL complexed to unbound IN with either a single Mg^{2+} cation or two Mg^{2+} cations and IN•vDNA complex revealed a very high degree of RAL average atomic fluctuations between the different targets for all applied programs, with the exception of few docked conformations obtained with GLIDE.

As was mentioned above, the RAL docking onto the IN•vDNA model produced the lowest binding scores with all applied scoring functions. Particularly the best scores were obtained with AutoDock (from -11.0 to -8.8 kcal/mol) and GLIDE (from -11.3 to -6.2 kcal/mol) as compared to the other two docking algorithms, VINA (from -10.4 to -9.1 kcal/mol) and SurFlex (from -8.7 to -5.6 kcal/mol). Regarding the RAL docking poses together with the scores, we concluded that GLIDE is the most appropriate software to dock the flexible ligand onto the relevant target.

We generated the others RAL isomers, E-1/Z-2, Z-1/E-2 and E-1/E-2. The RAL conformations were derived for each isomer similarly to the procedure applied to the Z-1/Z-2 isomer. We used GLIDE to dock the RAL generated conformation onto the IN targets applying the same strategy as previously. The obtained results show a general similarity with the docking data observed for Z-1/Z-2 isomer, nevertheless the predicted scores are significantly lower in the majority of cases and the RAL binding poses rarely show chelation of the Mg^{2+} ion(s) in the active site of the IN targets (data not shown).

To provide further information concerning RAL recognition by the viral targets, we docked the inhibitor onto the non-cleaved and cleaved viral DNA (the terminal GT

nucleotides at 3'-end were removed) by using Glide. RAL docked onto the non-cleaved vDNA is positioned in the minor groove of the substrate (**Figure 7 a**). The chelating centre of the molecule are oriented towards the helix centre; no stabilizing interactions between the partners, RAL and vDNA, were observed. In contrast, RAL docked onto the cleaved vDNA is located in the area of the removed dinucleotides GT. The best score corresponds to the Z-1/Z-2 isomer of RAL with all chelating centres oriented outside the vDNA helix (**Figure 7 b**). Such RAL orientation is stabilized by H-bonds with the unpaired cytosine. The nitrogen atom of RAL oxadiazole cycle interacts with amino group of cytosine forming a strong H-bond (N-H···N distance of 2.85 Å). The NH group from the adjacent (neighbouring) carbonylamine group interacts with the oxygen atom of cytosine (N-H···O distance of 2.43 Å). These two strong H-bonds first are indicative of a high affinity and specific recognition between RAL and the unpaired cytosine, and second are of the same interaction type as those that stabilize the bases pair G-C. Consequently, RAL plays the role of the removed guanidine and completes the vacant position at the viral DNA 3'-end. The additional pair of N-H···N contacts with distances of 3.29 and 3.50 Å contributes to the stability of RAL···Cytosine interactions.

Finally, to further explore the role of vDNA in RAL recognition prosess, the substrate was removed from the IN•vDNA complex and RAL was docked again on unbound IN with a fold corresponding to vDNA-bound, model **2B**. The binding energies of RAL are depreciated significantly upon vDNA removal and range from -8.9 to 8.9 kcal/mol. Consequently, unbound IN in the conformations representing either IN before 3'-processing or an isolated component of the IN•vDNA complex does not appear as a suitable RAL target.

DISCUSSION

In the context of drug design, the conformation adopted by an inhibitor when unbound and bound to a target is of fundamental importance. The variety of inhibitor conformations observed in different conditions may arise from interactions with a local environment and frequently differ from the bioactive conformation. Systematic differences may occur between the solid state conformation and those observed in solution or gas phase.

Our conformational analysis of the different isomeric states of RAL in the gas phase indicates a small difference between the energy profiles of the Z-1/Z-2 and E-1/Z-2 isomers suggesting a relatively low energetical barrier between these two inhibitor states. A slight preference for the Z-configuration of carbonylamino-hydroxypyrimidinone pharmacophore in the gas phase was observed, in coherence with the established predisposition of β-ketoenols – a principle corner stone of this pharmacophore – to adopt the Z-isomer in the solid state (Tchertanov & Mouscadet, 2007). The predisposition of aliphatic β-ketoenols to form energetically favourable Z-configuration has been predicted early by *ab initio* studies at the B3LYP/3-G** level of theory (Schiavoni *et al*, 2001).

Our structural databank search based on molecular fragments mimicking the RAL pharmacophores statistically demonstrates the preferential Z-configuration of carbonylamino-hydroxypyrimidinone-like molecules and the E-configuration of oxadiazole carboxamide–like molecules in the solid state.

Synthesized as a metal cations chelating ligand, RAL can bind the metal by two pharmacophores in different isomerisation states. Probing the RAL chelating features with relevant cations, K, Mg and Mn, we evidenced that, in the majority of metal complexes, the carbonylamino hydroxypyrimidinone-like fragments are observed in the Z configuration in the solid state. The oxadiazole carboxamide-like pharmacophore is observed in the metal complexes as two isomers and demonstrates a strong selectivity to the metal type: the Z isomer binds K and Mg while the E isomer binds mainly Mn. The higher probability of Mg^{2+} cation coordination by the Z-isomer of both pharmacophores indicates that the presence of two Mg^{2+} cations at the integrase binding site may be a decisive factor for stabilisation of the Z/Z configuration of RAL, which is observed in the PFV intasome complex (Hare *et al*., 2010a; Hare *et al*., 2010b). The significantly higher affinity of both pharmacophores to Mg relatively to K permits a positive competition between these cations, resulting in the change of RAL composition from a pharmaceutically acceptable potassium (K) salt to a biologically relevant Mg complex.

The experimental data describing inhibitors binding at the atomic level (X-ray or NMR analysis) is presented in only a limited number of target-ligand molecular complexes. Part of them characterize the binding of therapeutically relevant ligands to biologically non-relevant and non-pertinent targets. For example, the HIV-1 integrase specific inhibitor RAL was published as a ligand fixed to the PFV intasome (Hare *et al*., 2010a; Hare *et al*., 2010b).

Consequently, a large quantity of reliable information on target-ligand binding is based on molecular docking methods, which generate insights into the interactions of ligands with the amino acid residues in the binding pockets of the targets and predict the corresponding binding affinities (Krovat *et al.*, 2005). The first step of a docking calculation consists in the choice or generation of the therapeutically appropriate target.

The structural models reported here were generated by homology modeling based on the experimental data characterising either the partial structures of IN from HIV-1 or full-length IN from PFV. All generated models represent, with a certain level of reliability, different enzymatic states of the HIV-1 IN that can be explored as RAL biologically relevant targets. The models of the separated full-length HIV-1 integrase represent the unbound homodimers of IN (IN^{1-270}) containing either one or two Mg^{2+} cations in the active site – a plausible enzymatic state before the 3'-processing. Our simplified model of the HIV-1 IN•vDNA pre-integration complex represents the homodimer of integrase attached non-covalently to the two double strains of the viral DNA with two removed nucleotides GT at each 3'-end.

Two models of different states of the HIV-1 IN show a strong dissimilarity of their structure evidenced by divergent relative spatial positions of their structural domains, NTD, CCD and CTD. These tertiary structural modifications altere the contacts between IN domains and the structure and conformation of the linker regions. Moreover, IN undergoes important structural transformations leading to structural re-organisation of the catalytic site loop; the coiled portion of the loop reduces from 10 residues in the unbound form to 5 residues in the vDNA-bound form. Prediction of $IN^{133-155}$ sequence secondary structure elements indicates a more significant predisposition of IN from HIV-1 to be folded as two helices linked by a coiled loop than the IN from PFV. The helix elongation accompanied by loop shortening may be easily induced over the enzyme conformational/structural transition between the two integration steps prompted by substrate binding.

The docking calculations of RAL onto each model evidenced that (i) the large binding pocket delimited by the active site and the extended catalytic site loop in the unbound IN can accommodate RAL in distinct configurational/conformational states showing a lack of interaction specificity between inhibitor and target; (ii) the well defined cavity formed by the active site, vDNA and shortened catalytic site loop provides a more optimised RAL binding site where the inhibitor is stabilised by coordination bonds with Mg^{2+} cations in the Z/Z-configuration. Such binding is in agreement with the generally accepted mechanism of action

of the integrase strand transfer inhibitors. Additional stabilisation of RAL is provided by non-covalent interactions with the environmental residues of IN and the viral DNA bases.

Based on our computing data we suggested earlier the stabilizing role of the vDNA in the inhibitors recognition by IN•vDNA pre-integration complex (Ni *et al*., 2012). It was experimentally evidenced that RAL potently binds only when IN is in a binary complex with vDNA (Espeseth *et al.*, 2000), possibly binding to a transient intermediate along the integration pathway (Pandey *et al.*, 2007). Terminal bases of the viral DNA play a role in both catalytic efficiency (Johnson *et al.*, 2006; Sherman *et al.*, 1992) and inhibitor binding (Dicker *et al.*, 2007; Johnson *et al.*, 2007; Langley *et al.*, 2008). It was reported recently that unprocessed viral DNA could be the primary target of RAL (Ammar *et al.*, 2012). This study is based on the PFV DNA and several oligonucleotides mimicking the HIV-1 DNA probed by experimental and computing techniques.

Our docking study shows that RAL is positioned in the minor groove of the HIV-1 non-cleaved vDNA. No stabilising interactions between partners, RAL and vDNA, were observed. In contrast, in the processed (cleaved) vDNA the Z/Z isomer of RAL takes the place of the remote GT bases and is stabilised by strong and specific H-bonds with the unpaired cytosine. These H-bonds characterize the high affinity and specific recognition between RAL and the unpaired cytosine similarly to those observed in the DNA bases pair G-C. Based on our docking results, we suggested that the inhibition process may include as a first step the RAL recognition by the processed viral DNA bound to a transient intermediate IN state. RAL coupled to vDNA shows an outside orientation of all oxygen atoms, excellent putative chelating agents of Mg^{2+} cations, which could facilitate the insertion of RAL into the active site. The conformational flexibility of RAL further allows the accommodation/adaptation of the inhibitor in a relatively large binding pocket of the IN•vDNA pre-integration complex illustrated by various RAL docked conformation. We believe that such variety of RAL conformations contributing to the alternative enzyme residues recognition may impact the selection of the clinically observed alternative resistance pathways to the drug.

The other question considered in our work relates to the choice of the most adapted molecular docking method to study a very flexible inhibitor with flexible or relatively rigid targets represented here by the HIV-1 IN unbound or bound to the viral DNA respectively.

Although the docking problem seems intuitively easy, searching the space of all possible 3-dimensional protein–ligand conformations and determining the energetically most favorable solution is a hard computational problem. In case where both the protein and ligand are kept rigid, (wherein only the translational and rotational degrees of freedom are considered), the docking problem is six-dimensional (Thomsen, 2003). However, if flexibility in either the ligand or the receptor or both, is allowed during the search process, the dimensionality of the problem increases with the number of "rotatable" bonds. This generates an enormous search space attributed to the possible conformations of the flexible ligand.

The published docking studies report RAL located within the active site of either unbound IN or IN•vDNA complex. Distinct poses of RAL representing different RAL configuration and modes of Mg^{2+} cations chelation were observed (Barreca *et al.*, 2009, Loizidou *et al.*, 2009, Perryman *et al*., 2010, Serrao *et al.*, 2009).

Our trials to dock the generated RAL conformations demonstrate that the four used programs produce different results which depend more on the targets choice than on the initial configurational/conformational state of the flexible inhibitor. Docking of the flexible RAL onto a flexible target (the unbound IN) with an extended and poor-defined (deleterious) binding pocket produced contradictory results with all used algorithms. The programs were not capable to discriminate between the docked conformations using the scoring functions.

The binding of strand-transfer inhibitors displaces the reactive vDNA end from the active site, disarming the viral nucleoprotein complex. The early reported data and our results indicate as "interacting" with the strand-transfer inhibitors a large number of the IN residues forming the cavity defined as the active site for the strand-transfer reaction (Agapkina *et al.*, 2006; Dolan *et al.*, 2009; Dhaked *et al.*, 2009; Ni *et al*., 2012). The identification of IN residues specifically interacting with RAL by docking algorithms is a very difficult task and the exact binding modes of this inhibitor remain a matter of debate. Most probably the flexible nature of RAL results in different conformations and the mode of binding may differ in terms of the interacting residues of the target, which trigger the alternative resistance phenomenon.

Conformational flexibility in protein-ligand interactions is a general event in biological systems; numerous cases have been reported, for example the oestrogen and tyrosine kinases receptors (Barnett, 2012; Nebel, 2012; Johnson, 2009). Using the model systems presented

here, we studied the extent of conformational variability and related this to the RAL-IN interaction. Clearly, many aspects such a solvation/desolvation or entropic/ethalpic contributions remain open questions. Further studies of the energetic and dynamics of theses process will give us a better understanding of what makes a target attractive for an inhibitor, which in turn may assist the search for novel candidate drugs related with raltegravir for the AIDS treatment.

Novel drugs, targeting the HIV-1 Integrase, outcome mainly due to the rapid emergence of RAL analogues (for example, GS-9137 or elvitegravir, MK-2048 and S/GSK 1349572, currently under clinical trials (Korolev *et al*., 2011). All these molecules specifically suppress the IN ST reaction. We conceive that the future HIV-1 integrase drug development will be mainly oriented to the design of inhibitors with a mechanism of action that differs from that of RAL and its analogues. Distinct conceptions are potentially conceivable: (i) Design of allosteric inhibitors able to recognize specifically binding sites that differ from the IN active site. Inhibitor V-165, belonging to such type inhibitors, prevents IN binding with the viral DNA such blocking 3'-processing reaction (Pannecouque *et al*., 2002). (ii) Design of protein-protein inhibitors (PPIs) acting on interaction interface between either viral components (the IN monomers upon multimerization or sub-units of the IN•vDNA complex) (Mazumer *et al*., 1996; Tsiang *et al*., 2011), or between viral and cellular proteins (IN/LEDGF) (De Luca *et al*., 2010; Tsiang *et al*., 2012).

CONCLUSIONS

In the current paper, we report the first detailed characterisation of RAL and its putative HIV-1 targets – the unbound IN, the viral DNA (vDNA) and IN•vDNA complex – mimicking the integrase states before and after the 3'-processing. The structural features of RAL in three different states evidenced the most probable inhibitor configuration/conformation in the gas phase, in water solution and in the solid state.

The generated structural models of the HIV-1 integrase evidence considerable differences between unbound and vDNA-bound integrases that indicate a global structural and conformational transformation of enzyme upon substrate binding. The modifications consist in changes first in the positions of the N- and C-terminal domains relatively to the catalytic

core domain, and second in the secondary structures of the inter-domains linkers and of the catalytic site loop.

The RAL docking onto its putative HIV-1 IN targets shows a large spectrum of RAL conformational/configurational states, which evidences the complexity inherent in deriving affinity data of very flexible inhibitor. The docking onto the unbound IN evidenced that RAL adopts different conformations/configurations within a large binding cavity formed by the catalytic active site and the adjacent loop RAL. All observed RAL poses show an absence of specific interactions with the target. The docking onto the IN•vDNA complex systematically produced the RAL chelated to Mg^{2+} cations at the active site by the pharmacophores oxygen atoms. The low docking scores, RAL poses and observed inhibitor-target interactions confirm that the generated structure of the IN•vDNA complex is the biologically relevant target of the inhibitor. This finding is consistent with well-documented and commonly accepted inhibition mechanism of RAL, based on biological, biochemical and structural data. The identified RAL pose at the cleaved vDNA shed light on a putative even plausible step of RAL inhibition mechanism. We suggest that the inhibition process may include as a first step RAL recognition by the processed viral DNA bound to a transient intermediate IN state. Such statement provides a possible route to the design of IN inhibitors with improved affinity and selectivity.

LIST OF ABBREVIATION USED: HIV-1, Human Immunodeficiency Virus; vDNA, viral DNA; hDNA, host DNA; LTR, Long Terminal Repeat; IN, integrase; PFV, prototype foamy virus; NTD, N-terminal domain; CCD, catalytic core domain; CTD, C-terminal domain; ST, strand transfer; INSTI, integrase strand transfer inhibitor; G, T, C, A – DNA bases; RAL, raltegravir; RMSD, root mean square deviation; PDB, Protein Data Base; CSD, Cambridge Structural Database

COMPETING INTERESTS: The authors have declared no competing interests.

AUTHORS' CONTRIBUTIONS: Conceived and designed the experiments: LT. Performed the experiments: RA, ICB. Analysed data: RA, ICB, EL, JP. Wrote the paper: RA, LT.

Acknowledgements

The authors thank Tripos, Schrödinger and CSD for providing licences. This work is funded by the Centre National de la Recherche Scientifique (CNRS) and Ecole Normale Supérieure (ENS) de Cachan.

REFERENCES

Agapkina, J., Smolov, M., Barbe, S., Zubin, E., Zatsepin, T., Deprez, E., Le Bret, M., Mouscadet, J. F., & Gottikh, M. 2006. Probing of HIV-1 integrase/DNA interactions using novel analogs of viral DNA. *Journal of Biological Chemistry* ***281***, 11530-11540, doi:DOI 10.1074/jbc.M512271200.

Allen, F. H. 2002. The Cambridge Structural Database: a quarter of a million crystal structures and rising. *Acta Crystallogr. B* ***58***, 380-388.

Ammar, F. F., Abdel-Azeim, S., Zargarian, L., Hobaika, Z., Maroun, R. G., & Fermandjian, S. 2012. Unprocessed Viral DNA Could Be the Primary Target of the HIV-1 Integrase Inhibitor Raltegravir. *Plos One 7*, e40223, doi:10.1371/journal.pone.0040223 [doi];PONE-D-12-11847 [pii].

Arora R., Tchertanov L. 2012. The HIV-1 Integrase: Modeling and Beyond. In *An Integrated View of the Molecular Recognition and Toxinology - From Analytical Procedures to Biomedical Applications*. Dejan Grgur (Ed.). INTECH. ISBN 980-953-307-586-5. *In press*

Asante-Appiah, E. & Skalka, A. M. 1997. Molecular mechanisms in retrovirus DNA integration. *Antiviral Research* ***36***, 139-156.

Barnett, C. M. 2012. Everolimus: targeted therapy on the horizon for the treatment of breast cancer. *Pharmacotherapy* ***32***, 383-396, doi:10.1002/j.1875-9114.2012.01084.x [doi].

Barreca, M. L., Iraci, N., De Luca, L., & Chimirri, A. 2009. Induced-Fit Docking Approach Provides Insight into the Binding Mode and Mechanism of Action of HIV-1 Integrase Inhibitors. *ChemMedChem* ***4***, 1446-1456, doi:DOI 10.1002/cmdc.200900166.

Berendsen, H. J. C., Postma, J. P. M., Vangunsteren, W. F., Dinola, A., & Haak, J. R. 1984. Molecular-Dynamics with Coupling to An External Bath. *Journal of Chemical Physics* ***81***, 3684-3690.

Berman, H. M., Westbrook, J., Feng, Z., Gilliland, G., Bhat, T. N., Weissig, H., Shindyalov, I. N., & Bourne, P. E. 2000. The Protein Data Bank. *Nucleic Acids Research* ***28***, 235-242.

Brown, P. O. 1990. Integration of Retroviral DNA. *Current Topics in Microbiology and Immunology*. **15**, 19-48.

Bruno, I. J., Cole, J. C., Lommerse, J. P. M., Rowland, R. S., Taylor, R., & Verdonk, M. L. 1997. IsoStar: A library of information about nonbonded interactions. *Journal of Computer-Aided Molecular Design* ***11***, 525-537.

Chen, J. C. H., Krucinski, J., Miercke, L. J. W., Finer-Moore, J. S., Tang, A. H., Leavitt, A. D., & Stroud, R. M. 2000. Crystal structure of the HIV-1 integrase catalytic core and C-terminal domains: A model for viral DNA binding. *Proceedings of the National Academy of Sciences of the United States of America* ***97***, 8233-8238.

Chiu, T. K. & Davies, D. R. 2004. Structure and function of HIV-1 integrase. *Current Topics in Medicinal Chemistry* ***4***, 965-977.

Cooper, D. A., Steigbigel, R. T., Gatell, J. M., Rockstroh, J. K., Katlama, C., Yeni, P., Lazzarin, A., Clotet, B., Kumar, P. N., Eron, J. E., Schechter, M., Markowitz, M., Loutfy, M. R., Lennox, J. L., Zhao, J., Chen, J., Ryan, D. M., Rhodes, R. R., Killar, J. A., Gilde, L. R., Strohmaier, K. M., Meibohm, A. R., Miller, M. D., Hazuda, D. J., Nessly, M. L., DiNubile, M. J., Isaacs, R. D., Teppler, H., & Nguyen, B. Y. 2008. Subgroup and resistance analyses of raltegravir for resistant HIV-1 infection. *New England Journal of Medicine* ***359***, 355-365.

Copeland, R. A., Pompliano, D. L., & Meek, T. D. 2006. Drug-target residence time and its implications for lead optimization. *Nat. Rev. Drug Discov.* ***5***, 730-739, doi:nrd2082 [pii];10.1038/nrd2082 [doi].

Cotelle, P. 2006. Patented HIV-1 integrase inhibitors (1998-2005). *Recent Pat Antiinfect. Drug Discov.* ***1***, 1-15.

CSD. 1994. Vista - A Program for the Analysis and Display of Data Retrieved from the CSD. Cambridge Crystallographic Data Centre, 12 Union Road, Cambridge, England.

Cuff, J. A., Clamp, M. E., Siddiqui, A. S., Finlay, M., & Barton, G. J. 1998. JPred: a consensus secondary structure prediction server. *Bioinformatics* ***14***, 892-893.

Delano, W. L. 2002. The PYMOL molecular graphics system.

Delelis, O., Malet, I., Na, L., Tchertanov, L., Calvez, V., Marcelin, A. G., Subra, F., Deprez, E., & Mouscadet, J. F. 2009. The G140S mutation in HIV integrases from raltegravir-resistant patients rescues catalytic defect due to the resistance Q148H mutation. *Nucleic Acids Research* ***37***, 1193-1201, doi:DOI 10.1093/nar/gkn1050.

Delelis, O., Thierry, S., Subra, F., Simon, F., Malet, I., Alloui, C., Sayon, S., Calvez, V., Deprez, E., Marcelin, A. G., Tchertanov, L., & Mouscadet, J. F. 2010. Impact of Y143 HIV-1 Integrase Mutations on Resistance to Raltegravir In Vitro and In Vivo. *Antimicrobial Agents and Chemotherapy* ***54***, 491-501, doi:DOI 10.1128/AAC.01075-09.

De Luca, L., Ferro, S, Gitto, R., Barreca, M. L., Agnello, S., Christ, F., Debyser, Z., Chimirri, A. 2010. Small molecules targeting the interaction between HIV-1 integrase and LEDGF/p75 cofactor. *Bioorg. Med. Chem*. **18**(21), 7515-7521.

Dhaked, D. K., Verma, J., Saran, A., & Coutinho, E. C. 2009. Exploring the binding of HIV-1 integrase inhibitors by comparative residue interaction analysis (CoRIA). *Journal of Molecular Modeling* ***15***, 233-245, doi:DOI 10.1007/s00894-008-0399-4.

Dicker, I. B., Samanta, H. K., Li, Z. F., Hong, Y., Tian, Y., Banville, J., Remillard, R. R., Walker, M. A., Langley, D. R., & Krystal, M. 2007. Changes to the HIV long terminal repeat and to HIV integrase differentially impact HIV integrase assembly, activity, and the binding of strand transfer inhibitors. *Journal of Biological Chemistry* ***282***, 31186-31196, doi:DOI 10.1074/jbc.M704935200.

Dicker, I. B., Terry, B., Lin, Z., Li, Z., Bollini, S., Samanta, H. K., Gali, V., Walker, M. A., & Krystal, M. R. 2008. Biochemical analysis of HIV-1 integrase variants resistant to strand transfer inhibitors. *J. Biol. Chem.* ***283***, 23599-23609, doi:M804213200 [pii];10.1074/jbc.M804213200 [doi].

Dolan, J., Chen, A. P., Weber, I. T., Harrison, R. W., & Leis, J. 2009. Defining the DNA Substrate Binding Sites on HIV-1 Integrase. *Journal of Molecular Biology 385*, 568-579, doi:DOI 10.1016/j.jmb.2008.10.083.

Espeseth, A. S., Felock, P., Wolfe, A., Witmer, M., Grobler, J., Anthony, N., Egbertson, M., Melamed, J. Y., Young, S., Hamill, T., Cole, J. L., & Hazuda, D. J. 2000. HIV-1 integrase inhibitors that compete with the target DNA substrate define a unique strand transfer conformation for integrase. *Proceedings of the National Academy of Sciences of the United States of America* ***97***, 11244-11249.

Esposito, D. & Craigie, R. 1998. Sequence specificity of viral end DNA binding by HIV-1 integrase reveals critical regions for protein-DNA interaction. *EMBO Journal* ***17***, 5832-5843.

Eswar, N., John, B., Mirkovic, N., Fiser, A., Ilyin, V. A., Pieper, U., Stuart, A. C., Marti-Renom, M. A., Madhusudhan, M. S., Yerkovich, B., & Sali, A. 2003. Tools for comparative protein structure modeling and analysis. *Nucleic Acids Research* ***31***, 3375-3380, doi:DOI 10.1093/nar/gkg543.

Faure, A., Calmels, C., Desjobert, C., Castroviejo, M., Caumont-Sarcos, A., Tarrago-Litvak, L., Litvak, S., & Parissi, V. 2005. HIV-1 integrase crosslinked oligomers are active in vitro. *Nucleic Acids Research* ***33***, 977-986, doi:DOI 10.1093/nar/gki241.

Fedorov, D. G., Koseki, S., Schmidt M. W., Gordon, M.S. 2003. Spin-orbit coupling in molecules: chemistry beyond the adiabatic approximation. *Int. Rev. Phys. Chem.* **22**, 551-592.

Feng, M., Patel, D., Dervan, J. J., Ceska, T., Suck, D., Haq, I., & Sayers, J. R. 2004. Roles of divalent metal ions in flap endonuclease-substrate interactions. *Nature Structural & Molecular Biology* ***11***, 450-456, doi:10.1038/nsmb754.

Friesner, R.A. 1987. Solution of the Hartree-Fock equations for polyatomic molecules by a pseudospectral method. *Journal of Chemical Physics* ***86***, 3522-3531.

Friesner, R. A., Banks, J. L., Murphy, R. B., Halgren, T. A., Klicic, J. J., Mainz, D. T., Repasky, M. P., Knoll, E. H., Shelley, M., Perry, J. K., Shaw, D. E., Francis, P., & Shenkin, P. S. 2004. Glide: A new approach for rapid, accurate docking and scoring. 1. Method and assessment of docking accuracy. *Journal of Medicinal Chemistry* ***47***, 1739-1749, doi:DOI 10.1021/jm0306430.

Frishman, D. & Argos, P. 1995. Knowledge-based protein secondary structure assignment. *Proteins-Structure Function and Genetics* ***23***, 566-579.

Gao, K., Wong, S., & Bushman, F. 2004. Metal binding by the D,DX35E motif of human immunodeficiency virus type I integrase: Selective rescue of Cys substitutions by Mn-2 in vitro. *Journal of Virology* ***78***, 6715-6722, doi:DOI 10.1128/JVI.78.13.6715-6722.2004.

Garnier, J., Gibrat, J. F., & Robson, B. 1996. GOR method for predicting protein secondary structure from amino acid sequence. *Computer Methods for Macromolecular Sequence Analysis* ***266***, 540-553.

Garvey, E. P., Schwartz, B., Gartland, M. J., Lang, S., Halsey, W., Sathe, G., Carter, H. L., III, & Weaver, K. L. 2009. Potent inhibitors of HIV-1 integrase display a two-step, slow-binding inhibition mechanism which is absent in a drug-resistant T66I/M154I mutant. *Biochemistry* ***48***, 1644-1653, doi:10.1021/bi802141y [doi];10.1021/bi802141y [pii].

Greenwald, J., Le, V., Butler, S. L., Bushman, F. D., & Choe, S. 1999. The mobility of an HIV-1 integrase active site loop is correlated with catalytic activity. *Biochemistry* ***38***, 8892-8898.

Grobler, J. A., Stillmock, K., Hu, B., Witmer, M., Felock, P., Espeseth, A. S., Wolfe, A., Egbertson, M., Bourgeois, M., Melamed, J., Wai, J. S., Young, S., Vacca, J., & Hazuda, D. J. 2002. Diketo acid inhibitor mechanism and HIV-1 integrase: implications for metal binding in the active site of phosphotransferase enzymes. *Proc. Natl. Acad. Sci. U. S A* ***99***, 6661-6666, doi:10.1073/pnas.092056199 [doi];092056199 [pii].

Guermeur, Y., Geourjon, C., Gallinari, P., & Deleage, G. 1999. Improved performance in protein secondary structure prediction by inhomogeneous score combination. *Bioinformatics* ***15***, 413-421.

Guiot, E., Carayon, K., Delelis, O., Simon, F., Tauc, P., Zubin, E., Gottikh, M., Mouscadet, J. F., Brochon, J. C., & Deprez, E. 2006. Relationship between the oligomeric status of HIV-1 integrase on DNA and enzymatic activity. *Journal of Biological Chemistry* ***281***, 22707-22719, doi:DOI 10.1074/jbc.M602198200.

Hare, S., Gupta, S. S., Valkov, E., Engelman, A., & Cherepanov, P. 2010a. Retroviral intasome assembly and inhibition of DNA strand transfer. *Nature* ***464***, 232-236, doi:DOI 10.1038/nature08784.

Hare, S., Vos, A. M., Clayton, R. F., Thuring, J. W., Cummings, M. D., & Cherepanov, P. 2010b. Molecular mechanisms of retroviral integrase inhibition and the evolution of viral resistance. *Proceedings of the National Academy of Sciences of the United States of America* ***107***, 20057-20062, doi:DOI 10.1073/pnas.1010246107.

Hayouka, Z., Rosenbluh, J., Levin, A., Loya, S., Lebendiker, M., Veprintsev, D., Kotler, M., Hizi, A., Loyter, A., & Friedler, A. 2007. Inhibiting HIV-1 integrase by shifting its oligomerization equilibrium. *Proceedings of the National Academy of Sciences of the United States of America* ***104***, 8316-8321, doi:DOI 10.1073/pnas.0700781104.

Hazuda, D. J., Felock, P., Witmer, M., Wolfe, A., Stillmock, K., Grobler, J. A., Espeseth, A., Gabryelski, L., Schleif, W., Blau, C., & Miller, M. D. 2000. Inhibitors of strand transfer that prevent integration and inhibit HIV-1 replication in cells. *Science* ***287***, 646-650.

Hightower, K. E., Wang, R., Deanda, F., Johns, B. A., Weaver, K., Shen, Y., Tomberlin, G. H., Carter, H. L., III, Broderick, T., Sigethy, S., Seki, T., Kobayashi, M., & Underwood, M. R. 2011. Dolutegravir (S/GSK1349572) exhibits significantly slower dissociation than raltegravir and elvitegravir from wild-type and integrase inhibitor-resistant HIV-1 integrase-DNA complexes. *Antimicrob. Agents Chemother.* ***55***, 4552-4559, doi:AAC.00157-11 [pii];10.1128/AAC.00157-11 [doi].

Humphrey, G. R., Pye, P. J., Zhong, Y. L., Angelaud, R., Askin, D., Belyk, K. M., Maligres, P. E., Mancheno, D. E., Miller, R. A., Reamer, R. A., & Weissman, S. A. 2011. Development of a Second-Generation, Highly Efficient Manufacturing Route for the HIV Integrase Inhibitor Raltegravir Potassium. *Organic Process Research & Development* ***15***, 73-83, doi:10.1021/op100257r.

Jain, A. N. 2003. Surflex: Fully automatic flexible molecular docking using a molecular similarity-based search engine. *Journal of Medicinal Chemistry 46*, 499-511, doi:DOI 10.1021/jm.020406h.

Johnson, A. A., Marchand, C., Patil, S. S., Costi, R., Di Santo, R., Burke, T. R., & Pommier, Y. 2007. Probing HIV-1 integrase inhibitor binding sites with position-specific integrase-DNA cross-linking assays. *Molecular Pharmacology* ***71***, 893-901, doi:DOI 10.1124/mol.106.030817.

Johnson, A. A., Santos, W., Pais, G. C. G., Marchand, C., Amin, R., Burke, T. R., Verdine, G., & Pommier, Y. 2006. Integration requires a specific interaction of the donor DNA terminal 5 '-cytosine with glutamine 148 of the HIV-1 integrase flexible loop. *Journal of Biological Chemistry* ***281***, 461-467.

Johnson, L. N. 2009. Protein kinase inhibitors: contributions from structure to clinical compounds. *Q. Rev. Biophys.* ***42***, 1-40, doi:S0033583508004745.

Kabsch, W. & Sander, C. 1983. Dictionary of Protein Secondary Structure - Pattern-Recognition of Hydrogen-Bonded and Geometrical Features. *Biopolymers* ***22***, 2577-2637.

Kawasuji, T., Fuji, M., Yoshinaga, T., Sato, A., Fujiwara, T., & Kiyama, R. 2006. A platform for designing HIV integrase inhibitors. Part 2: A two-metal binding model as a potential mechanism of HIV integrase inhibitors. *Bioorganic & Medicinal Chemistry* ***14***, 8420-8429, doi:DOI 10.1016/j.bmc.2006.08.043.

King, R. D., Saqi, M., Sayle, R., & Sternberg, M. J. E. 1997. DSC: public domain protein secondary structure prediction. *Computer Applications in the Biosciences 13*, 473-474.

Krovat, E. M., Steindl, T., & Langer, T. 2005. Recent Advances in Docking and Scoring. *Current Computer-Aided Drug Design* ***1***, 93-102.

Korolev S, Agapkina Yu, Gottikh M. 2011. Clinical Use of Inhibitors of HIV-1 Integration: Problems and Prospects. *Acta Naturae*, **3**,12-28.

Langley, D. R., Samanta, H. K., Lin, Z., Walker, M. A., Krystal, M. R., & Dicker, I. B. 2008. The terminal (catalytic) adenosine of the HIV LTR controls the kinetics of binding and dissociation of HIV integrase strand transfer inhibitors. *Biochemistry* ***47***, 13481-13488, doi:10.1021/bi801372d [doi].

Larkin, M. A., Blackshields, G., Brown, N. P., Chenna, R., McGettigan, P. A., McWilliam, H., Valentin, F., Wallace, I. M., Wilm, A., Lopez, R., Thompson, J. D., Gibson, T. J., &

Higgins, D. G. 2007. Clustal W and clustal X version 2.0. *Bioinformatics* ***23***, 2947-2948, doi:DOI 10.1093/bioinformatics/btm404.

Laskowski, R. A., Macarthur, M. W., Moss, D. S., & Thornton, J. M. (1993). Procheck - A Program to Check the Stereochemical Quality of Protein Structures. *Journal of Applied Crystallography* ***26***, 283-291.

Levin, J. M. 1997. Exploring the limits of nearest neighbour secondary structure prediction. *Protein Engineering 10*, 771-776.

Li, M., Mizuuchi, M., Burke, T. R., & Craigie, R. 2006. Retroviral DNA integration: reaction pathway and critical intermediates. *Embo Journal* ***25***, 1295-1304, doi:DOI 10.1038/sj.emboj.7601005.

Loizidou, E. Z., Zeinalipour-Yazdi, C. D., Christofides, T., & Kostrikis, L. G. 2009. Analysis of binding parameters of HIV-1 integrase inhibitors: Correlates of drug inhibition and resistance. *Bioorganic & Medicinal Chemistry* ***17***, 4806-4818, doi:DOI 10.1016/j.bmc.2009.04.058.

Macrae, C. F., Edgington, P. R., McCabe, P., Pidcock, E., Shields, G. P., Taylor, R., Towler, M., & van de Streek, J. 2006. Mercury: visualization and analysis of crystal structures. *Journal of Applied Crystallography* ***39***, 453-457, doi:10.1107/S002188980600731X.

Maignan, S., Guilloteau, J. P., Zhou-Liu, Q., Clement-Mella, C., & Mikol, V. 1998. Crystal structures of the catalytic domain of HIV-1 integrase free and complexed with its metal cofactor: High level of similarity of the active site with other viral integrases. *Journal of Molecular Biology* ***282***, 359-368.

Marchand, C., Maddali, K., Metifiot, M., & Pommier, Y. 2009. HIV-1 IN Inhibitors: 2010 Update and Perspectives. *Current Topics in Medicinal Chemistry* ***9***, 1016-1037.

Markowitz, M., Morales-Ramirez, J. O., Nguyen, B. Y., Kovacs, C. M., Steigbigel, R. T., Cooper, D. A., Liporace, R., Schwartz, R., Isaacs, R., Gilde, L. R., Wenning, L., Zhao, J., & Teppler, H. 2006. Antiretroviral activity, pharmacokinetics, and tolerability of MK-0518, a novel inhibitor of HIV-1 integrase, dosed as monotherapy for 10 days in treatment-naive HIV-1-infected individuals. *J. Acquir. Immune Defic. Syndr.* ***43***, 509-515, doi:10.1097/QAI.0b013e31802b4956 [doi];00126334-200612150-00002 [pii].

Martonak, R., Laio, A., & Parrinello, M. 2003. Predicting crystal structures: the Parrinello-Rahman method revisited. *Phys. Rev. Lett.* ***90***, 075503.

Mazumder, A., Wang, S., Neamati, N., Nicklaus, M., Sunder, S., Chen, J., Milne, G. W., Rice, W. G., Burke, T. R. Jr, Pommier, Y. 1996. Antiretroviral agents as inhibitors of both human immunodeficiency virus type 1 integrase and protease. *J. Med. Chem*. **39**(13), 2472-2481.

McGuffin, L. J., Bryson, K., & Jones, D. T. 2000. The PSIPRED protein structure prediction server. *Bioinformatics* ***16***, 404-405.

Morris, G. M., Huey, R., Lindstrom, W., Sanner, M. F., Belew, R. K., Goodsell, D. S., & Olson, A. J. 2009. AutoDock4 and AutoDockTools4: Automated Docking with Selective Receptor Flexibility. *Journal of Computational Chemistry* ***30***, 2785-2791, doi:DOI 10.1002/jcc.21256.

Mouscadet, J. F., Arora, R., Andre, J., Lambry, J. C., Delelis, O., Malet, I., Marcelin, A. G., Calvez, V., & Tchertanov, L. 2009. HIV-1 IN alternative molecular recognition of DNA induced by raltegravir resistance mutations. *Journal of Molecular Recognition* ***22***, 480-494, doi:DOI 10.1002/jmr.970.

Mouscadet, J. F., Delelis, O., Marcelin, A. G., & Tchertanov, L. 2010. Resistance to HIV-1 integrase inhibitors: A structural perspective. *Drug Resist. Updat.* ***13***, 139-150, doi:S1368-7646(10)00021-X [pii];10.1016/j.drup.2010.05.001 [doi].

Mouscadet, J. F. & Tchertanov, L. 2009. Raltegravir: molecular basis of its mechanism of action. *Eur. J. Med. Res.* ***14*** *Suppl 3*, 5-16.

Neamati, N., Lin, Z. W., Karki, R. G., Orr, A., Cowansage, M., Strumberg, D., Pais, G. C. G., Voigt, J. H., Nicklaus, M. C., Winslow, H. E., Zhao, H., Turpin, J. A., Yi, J. Z., Skalka, A. M., Burke, T. R., & Pommier, Y. 2002. Metal-dependent inhibition of HIV-1 integrase. *Journal of Medicinal Chemistry* ***45***, 5661-5670, doi:10.1021/jm0201417.

Nebel, D. 2012. Functional importance of estrogen receptors in the periodontium. *Swed. Dent. J. Suppl* 11-66.

Ni, X., Abdel-Azeim, S., Laine, E., Arora, R., Osemwota, O., Marcelin, A.-G., Calvez, V., Mouscadet, J.-F., & Tchertanov, L. 2012. *In silico* and *in vitro* Comparison of HIV-1 Subtypes B and CRF02_AG Integrases Susceptibility to Integrase Strand Transfer Inhibitors. *Advances in Virology*. Volume 2012, Article ID 548657, 13 pages ; doi:10.1155/2012/548657

Pandey, K. K., Bera, S., Zahm, J., Vora, A., Stillmock, K., Hazuda, D., & Grandgenett, D. P. 2007. Inhibition of human immunodeficiency virus type I concerted integration by strand transfer inhibitors which recognize a transient structural intermediate. *Journal of Virology* ***81***, 12189-12199, doi:DOI 10.1128/JVI.02863-06.

Pannecouque, C., Pluymers, W., Van Maele, B., Tetz, V., Cherepanov, P., De Clercq, E., Witvrouw, M. and Debyser, Z. 2002. New class of HIV integrase inhibitors that block viral replication in cell culture. *Curr. Biol*. **12**(14), 1169-1177.

Perryman, A. L., Forli, S., Morris, G. M., Burt, C., Cheng, Y. H., Palmer, M. J., Whitby, K., McCammon, J. A., Phillips, C., & Olson, A. J. 2010. A Dynamic Model of HIV Integrase Inhibition and Drug Resistance. *Journal of Molecular Biology* ***397***, 600-615, doi:10.1016/j.jmb.2010.01.033.

Pettersen, E. F., Goddard, T. D., Huang, C. C., Couch, G. S., Greenblatt, D. M., Meng, E. C., & Ferrin, T. E. 2004. UCSF Chimera – a visualization system for exploratory research and analysis. *J. Comput. Chem.* ***25***, 1605-1612, doi:10.1002/jcc.20084 [doi].

Pollastri, G., Przybylski, D., Rost, B., & Baldi, P. 2002. Improving the prediction of protein secondary structure in three and eight classes using recurrent neural networks and profiles. *Proteins-Structure Function and Genetics* ***47***, 228-235, doi:10.1002/prot.10082.

Pommier, Y., Johnson, A. A., & Marchand, C. 2005. Integrase inhibitors to treat HIV/AIDS. *Nature Reviews Drug Discovery* ***4***, 236-248, doi:DOI 10.1038/nrd1660.

Raghava, G. P. S. 2002. APSSP2 : A combination method for protein secondary structure prediction based on neural network and example based learning. CASP5. A-132.

Rost, B., Sander, C., & Schneider, R. 1994. Phd - An Automatic Mail Server for Protein Secondary Structure Prediction. *Computer Applications in the Biosciences* ***10***, 53-60.

Schiavoni, M. M., Di Loreto, H. E., Hermann, A., Mack, H. G., Ulic, S. E., Della Vedova, C. O. 2001. Keto-enol tautomerism in beta-ketoesters: CH3C(O)CHXC(O)OY (X = H, Cl; Y =CH3, C2H5). Vibrational analyses, NMR spectra and quantum chemical calculations. *J. Raman Sp*., ***32(***5), 319-329.

Schrödinger, L. 2007. Jagaur, Version 7.0.

Semenova, E. A., Marchand, C., & Pommier, Y. 2008. HIV-1 integrase inhibitors: update and perspectives. *Adv. Pharmacol.* ***56***, 199-228, doi:S1054-3589(07)56007-2 [pii];10.1016/S1054-3589(07)56007-2 [doi].

Serrao, E., Odde, S., Ramkumar, K., & Neamati, N. 2009. Raltegravir, elvitegravir, and metoogravir: the birth of "me-too" HIV-1 integrase inhibitors. *Retrovirology* ***6***, 25, doi:1742-4690-6-25 [pii];10.1186/1742-4690-6-25 [doi].

Sherman, P. A., Dickson, M. L., & Fyfe, J. A. 1992. Human immunodeficiency virus type 1 integration protein: DNA sequence requirements for cleaving and joining reactions. *J. Virol. 66*, 3593-3601.

Sichtig, N., Sierra, S., Kaiser, R., Daumer, M., Reuter, S., Schulter, E., Altmann, A., Fatkenheuer, G., Dittmer, U., Pfister, H., & Esser, S. 2009. Evolution of raltegravir resistance during therapy. *Journal of Antimicrobial Chemotherapy* ***64***, 25-32, doi:DOI 10.1093/jac/dkp153.

Steigbigel, R. T., Cooper, D. A., Kumar, P. N., Eron, J. E., Schechter, M., Markowitz, M., Loutfy, M. R., Lennox, J. L., Gatell, J. M., Rockstroh, J. K., Katlama, C., Yeni, P., Lazzarin, A., Clotet, B., Zhao, J., Chen, J., Ryan, D. M., Rhodes, R. R., Killar, J. A., Gilde, L. R., Strohmaier, K. M., Meibohm, A. R., Miller, M. D., Hazuda, D. J., Nessly, M. L., DiNubile, M. J., Isaacs, R. D., Nguyen, B., & Teppler, H. 2008. Raltegravir with optimized background therapy for resistant HIV-1 infection. *New England Journal of Medicine* ***359***, 339-354.

Sunderland, C. J., Botta, M., Aime, S., & Raymond, K. N. 2001. 6-carboxamido-5,4-hydroxypyrimidinones: A new class of heterocyclic ligands and their evaluation as gadolinium chelating agents. *Inorganic Chemistry* ***40***, 6746-6756, doi:10.1021/ic010313a.

Tchertanov, L. & Mouscadet, J. F. 2007. Target recognition by catechols and beta-ketoenols: Potential contribution of hydrogen bonding and Mn/Mg chelation to HIV-1 integrase inhibition. *Journal of Medicinal Chemistry* ***50***, 1133-1145, doi:DOI 10.1021/jm061375j.

Thompson, J. D., Higgins, D. G., & Gibson, T. J. 1994. Clustal-W - Improving the Sensitivity of Progressive Multiple Sequence Alignment Through Sequence Weighting, Position-Specific Gap Penalties and Weight Matrix Choice. *Nucleic Acids Research* ***22***, 4673-4680.

Thomsen, R. 2003. Flexible ligand docking using evolutionary algorithms: investigating the effects of variation operators and local search hybrids. *Biosystems* ***72***, 57-73, doi:DOI 10.1016/S0303-2647(03)00135-7.

Tripos Inc. 2009. SYBYL-X 1.1.1.

Trott, O. & Olson, A. J. 2010. Software News and Update AutoDock Vina: Improving the Speed and Accuracy of Docking with a New Scoring Function, Efficient Optimization, and Multithreading. *Journal of Computational Chemistry* ***31***, 455-461, doi:DOI 10.1002/jcc.21334.

Tsiang, M., Jones, G. S., Hung, M., Samuel, D., Novikov, N., Mukund, S., Brendza, K. M., Niedziela-Majka, A., Jin, D., Liu, X., Mitchell, M., Sakowicz, R., Geleziunas, R. 2011. Dithiothreitol causes HIV-1 integrase dimer dissociation while agents interacting with the integrase dimer interface promote dimer formation. *Biochemistry.* **50**(10), 1567-1681.

Tsiang, M., Jones, G. S., Niedziela-Majka, A., Kan, E., Lansdon, E. B., Huang, W., Hung, M., Samuel, D., Novikov, N., Xu, Y., Mitchell, M., Guo, H., Babaoglu, K., Liu, X., Geleziunas, R., Sakowicz, R. 2012. New Class of HIV-1 Integrase (IN) Inhibitors with a Dual Mode of Action. *Biol Chem.* **287**(25), 21189-11203.

Valkov, E., Gupta, S. S., Hare, S., Helander, A., Roversi, P., McClure, M., & Cherepanov, P. 2009. Functional and structural characterization of the integrase from the prototype foamy virus. *Nucleic Acids Res.* ***37***, 243-255, doi:gkn938 [pii];10.1093/nar/gkn938 [doi].

van der Spoel, D., Lindahl, E., Hess, B., Groenhof, G., Mark, A. E., & Berendsen, H. J. 2005. GROMACS: fast, flexible, and free. *J. Comput. Chem.* ***26***, 1701-1718, doi:10.1002/jcc.20291 [doi].

Van Dijk, D. M., Bonvin, A. M. 2009. 3D-DART: a DNA structure modelling server. *Nucleic Acids Res.* ***37***, W235-W239, doi:gkp287 [pii];10.1093/nar/gkp287 [doi].

Wang, J. Y., Ling, H., Yang, W., & Craigie, R. 2001. Structure of a two-domain fragment of HIV-1 integrase: implications for domain organization in the intact protein. *EMBO Journal* ***20***, 7333-7343.

Wang, Y., Klock, H., Yin, H., Wolff, K., Bieza, K., Niswonger, K., Matzen, J., Gunderson, D., Hale, J., Lesley, S., Kuhen, K., Caldwell, J., & Brinker, A. 2005. Homogeneous high-throughput screening assays for HIV-1 integrase 3 '-processing and strand transfer activities. *Journal of Biomolecular Screening* ***10***, 456-462, doi:DOI 10.1177/108705710275212.

Welch, W., Ruppert, J., & Jain, A. N. 1996. Hammerhead: Fast, fully automated docking of flexible ligands to protein binding sites. *Chemistry & Biology* ***3***, 449-462.

Xu, J. D., Whisenhunt, D. W., Veeck, A. C., Uhlir, L. C., & Raymond, K. N. 2003. Thorium(IV) complexes of bidentate hydroxypyridinonates. *Inorganic Chemistry 42*, 2665-2674, doi:10.1021/ic0259888.

Yin, Z. Q. & Craigie, R. 2010. Modeling the HIV-1 Intasome: A Prototype View of the Target of Integrase Inhibitors. *Viruses-Basel* ***2***, 2777-2781, doi:10.3390/v2122777.

Zhong, Y. L., Krska, S. W., Zhou, H., Reamer, R. A., Lee, J., Sun, Y. K., & Askin, D. 2009. Catalytic Asymmetric Synthesis of an HIV Integrase Inhibitor. *Organic Letters* ***11***, 369-372, doi:10.1021/ol802604v.

Table 1. RAL conformations in the solid state: CSD fragment-based search for the RAL pharmacophore subunits

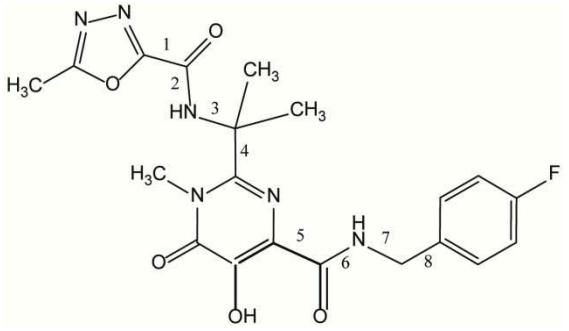

Pharmacophore	1,3,4-oxadiazole-2-carboxamide 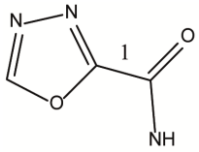	carbonylamino-1-5-hydroxypyrimidinone 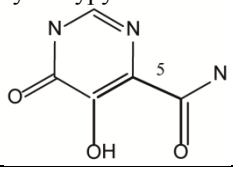	4-fluorobenzylcarbamoyl 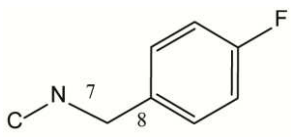
N Hits/Fragments	non	3/3	83/239
	F1	F2	F3
Fragment	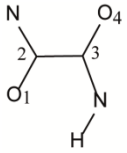	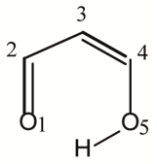	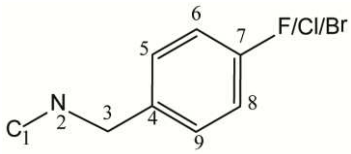
N Hits/Fragments	194/310	1785/2336	200/521
Parameters	$T^1[O_1C_2C_3O_4]$,° D^1 $[O_1...H]$, Å	T^1 $[O_1C_2C_3C_4]$,° T^2 $[C_2C_3C_4O_5]$,° D^1 $[O_1…H]$, Å	T^1 $[C_1N_2C_3C_4]$,° D = P^1/P^2, °; P^1 $[C_1N_2C_3C_4]$ P^2 $[C^4\text{-}C^9]$
Conformation	E ~75%, Z ~20%	E~ 2%, Z ~ 95%	T^1 : 60°-120°, 160°-180° D : 65°-90°, 0°-90°

Table 2. Probing of the RAL coordination to Mg, Mn and K cations: CSD fragment-based search. $N_{Total}/N_{Fragments}$ represent the total number of crystal structures (hits) where the both metal cation and ligand are present (N_{Total}) and the number of fragments corresponding to the metal-ligand complexes ($N_{Fragments}$) ; metal-ligating atom distance (M – O/N, Å).

	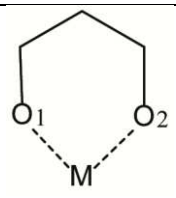	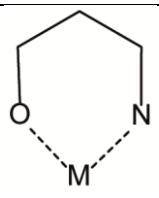	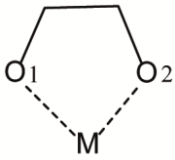	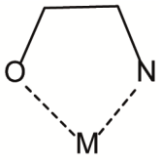
M/L	L1	L2	L3	L4
K	3504/36 M – O1 = 2.808 M – O2 = 2.802	452/0	2126/181 M – O1 = 2.830 M – O2 = 2.826	1338/4 M – O = 2.799 M – N = 2.957
Mg	649/74 M – O1= 2.055 M – O2= 2.063	162/26 M – O = 1.958 M – N = 2.136	80/29 M – O1 = 2.129 M – O2 = 2.104	143/14 M – O = 2.099 M – N = 2.240
Mn	2918/469 M – O1 = 2.043 M – O2 = 2.054	753/149 M – O = 1.963 M – N = 2.027	331/82 M – O1 = 2.138 M – O2 = 2.130	543/149 M – O = 2.116 M – N = 2.190

Legends to Figures

Figure 1. RAL conformations in the gas phase. Free energy profiles obtained by relaxed scans around the single bonds of RAL from 0° to 360° with an increment step of 30°, considering the four RAL isomers: (**a**) Z-1/Z-2, (**b**) Z-1/E-2, (**c**) E-1/Z-2 and (**d**) E-1/E-2. The curves representing the rotations around torsion angles τ1, τ2, τ3 and τ4 are shown in blue, red, green and violet colours. The values of τ1, τ2, τ3 and τ4 observed in RAL crystal structure are indicated by asterisks.

Figure 2. MD simulations of the Z-1/Z-2 isomer of RAL. (**a**) The root mean square deviations (RMSDs in nm), (**b**) the root mean square fluctuations (RMSFs in nm) and (**c**) the normalized probability distributions of the torsion angles were calculated from MD simulations of RAL. The 10-ns simulations replicas **1**, **2** and **3** are shown by red, green and black colours. (**d**) The RAL H-bonding with the solvent water molecules recorded during the MD simulations over the 2 ns equilibration step (in black), common for all of the three trajectories, is shown by green, blue and brown colours. The representative RAL conformations forming the maximum and the minimum number of H-bonds are shown as the inserts.

Figure 3. RAL conformations in the solid state. CSD fragment-based analysis of the RAL subunits as defined in **Table 1**. (**a**) **F1**: Scatter plots of the absolute value of torsion angle T^1 *vs* intermolecular distance O···H. The E- (blue triangles) and Z- (red squares) conformations are indicated by closed symbols. Intermediate conformations are shown as hollow symbols. (**b**) **F2**: Absolute value of torsion angle T^1 *vs* intermolecular distance O···H. The E- (red circles) and Z- (blue squares) conformations are indicated by closed symbols. Intermediate conformations are shown as hollow symbols. (**c**) **F3**: Absolute value of torsion angles T^1 *vs* T^2. The data represent F (blue circles), Cl (red squares) and Br (green triangles) substituent at the phenyl ring. The RAL and POPYOJ crystal structure parameters are indicated by asterisks.

Figure 4. Probing of ligand interactions with Mg, Mn and K: CSD fragment-based search as defined in **Table 2**. Scatter plots of M – O^1 *vs* M – O^2 distances in M–L1 (**a**), M–L2 (**c**) and M – O *vs* M – N distances in M–L3 (**b**) and M-L4 (**d**) complexes. Metal complexes are

indicated by bull symbols: red squares (Mg), blue circles (Mn) and orange triangles (K). The RAL crystal structure parameters are indicated by asterisks.

Figure 5. Structural models of the HIV-1 integrase. (**a**) Model **1A**, representing the homodimeric enzyme before the 3'-processing; (**b**) Model **3A**, representing the simplified IN-DNA pre-integration complex (dimeric form); (**c**) Superimposition of monomeric subunits from models **1A** and **2A**. The proteins are shown as cartoons, Mg^{2+} ions as spheres (in magenta). (**d**) Schematic representation of the HIV and PVF active site loop secondary structure prediction, according to consensus 1 and consensus 2.

Figure 6. RAL – Integrase binding predicted by docking. The docking of RAL generated conformations for the Z-1/Z-2 isomer onto the unbound IN with a single Mg^{2+} cation within active site (model **1A**), with two Mg^{2+} cations within the active site (model **1B**), and the IN•vDNA complex (model **3A)** are presented at the top, middle and bottom panels, respectively. The graphs in the middle column shows the score profiles obtained by docking with four algorithms – GLIDE (in red, line **1**), SurFlex (in violet, line **2**), AutoDock (in blue, line **3**), and VINA (in green, line **4**). Snapshots on the right and on the left show the representative poses of RAL obtained by docking onto the targets **1A**, **1B** and **3A** by using the four different programs. Numeration of the scores curves and snapshots showed on the top panel is valid for other panels. The proteins are shown as cartoons with a colour coding the used docking program, Mg^{2+} ions as spheres (in yellow) and RAL as sticks.

Figure 7. RAL – viral DNA recognition. The inhibitor docked onto the viral non-cleaved (**a**) and cleaved DNA (**b**). The vDNA is shown as cartoons; the guanine and RAL are shown as thin lines and sticks respectively.

Figure 1

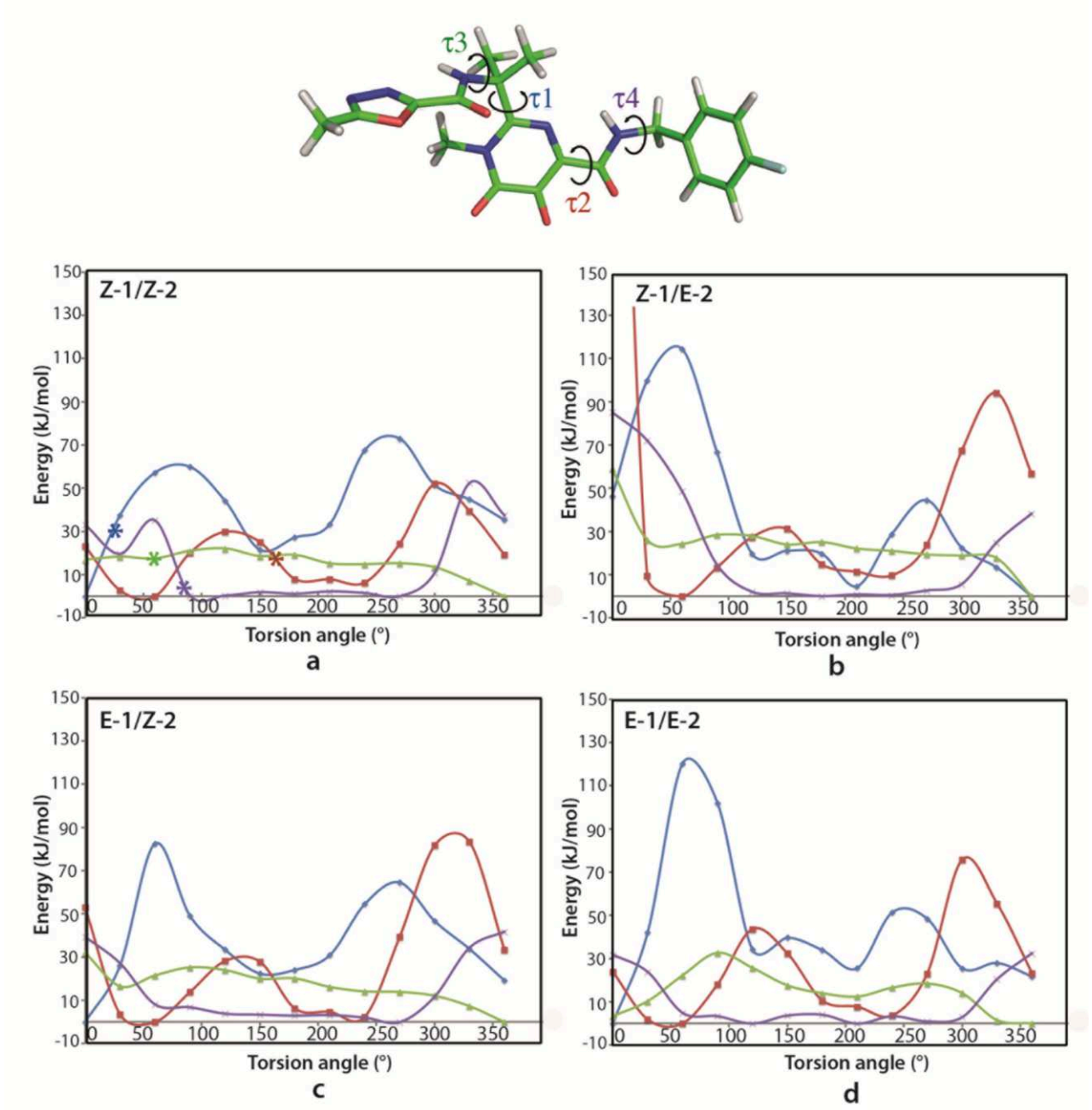
τ3
τ1
τ4
τ2
Z-1/Z-2
Z-1/E-2
E-1/Z-2
E-1/E-2
Energy (kJ/mol)
Torsion angle (°)
a
b
c
d

Figure 2

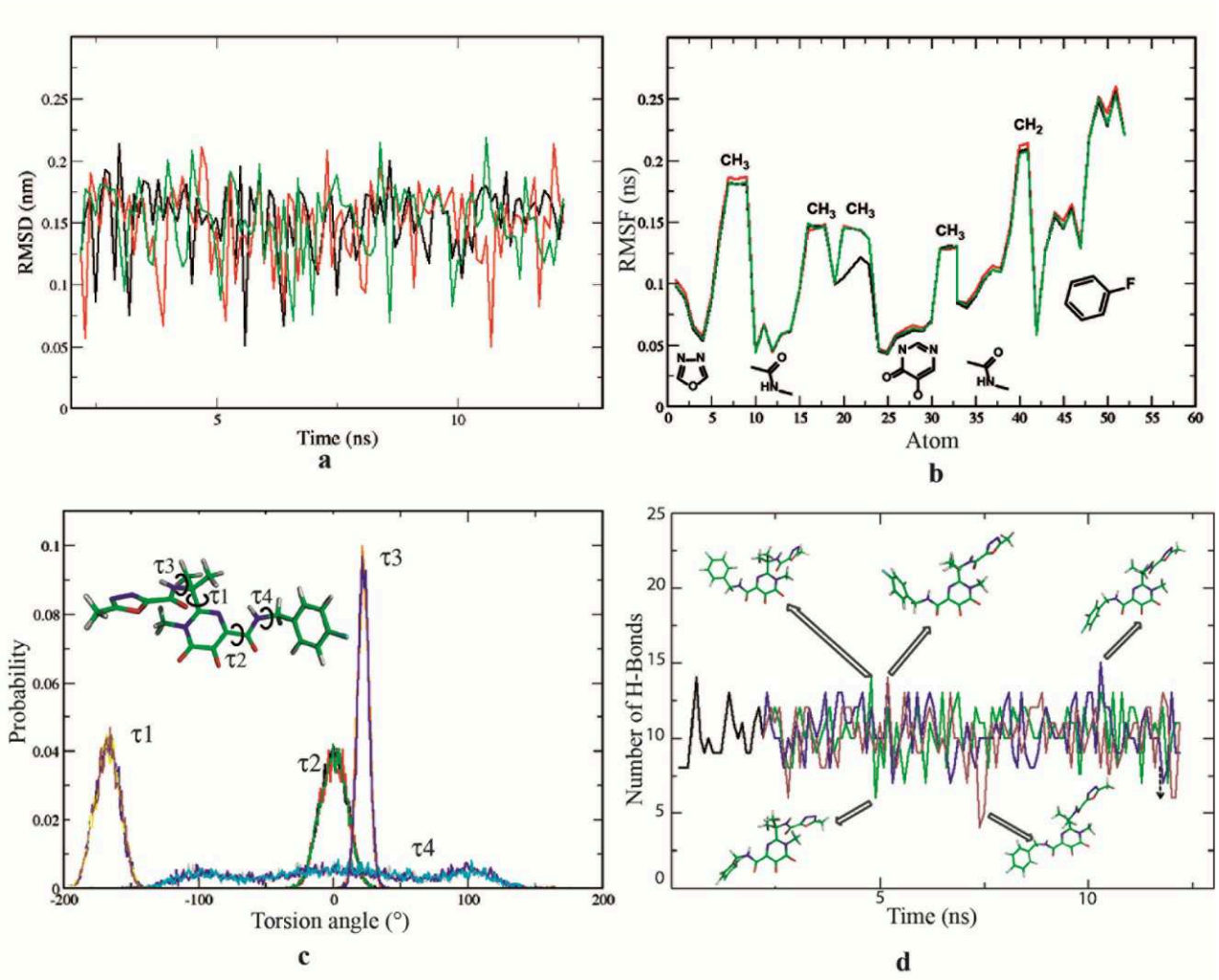
RMSD (nm)
Time (ns)
a
RMSF (ns)
Atom
b
Probability
Torsion angle (°)
τ1
τ2
τ3
τ4
c
Number of H-Bonds
Time (ns)
d

Figure 3

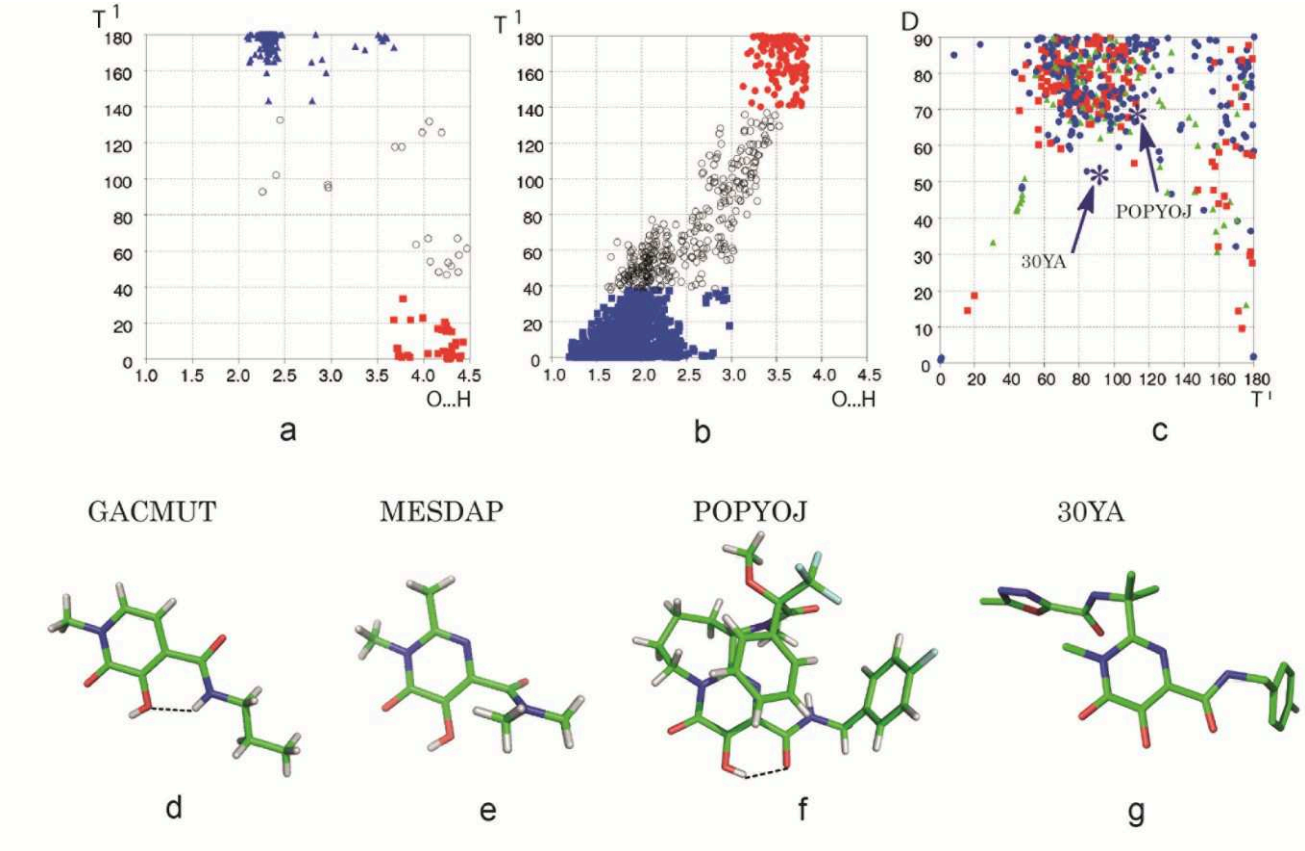
T 1
180
160
140
120
100
80
60
40
20
0
1.0 1.5 2.0 2.5 3.0 3.5 4.0 4.5
O...H
a
T 1
180
160
140
120
100
80
60
40
20
0
1.0 1.5 2.0 2.5 3.0 3.5 4.0 4.5
O...H
b
D
90
80
70
60
50
40
30
20
10
0
0 20 40 60 80 100 120 140 160 180
T 1
POPYOJ
30YA
c
GACMUT
MESDAP
POPYOJ
30YA
d
e
f
g

Figure 4

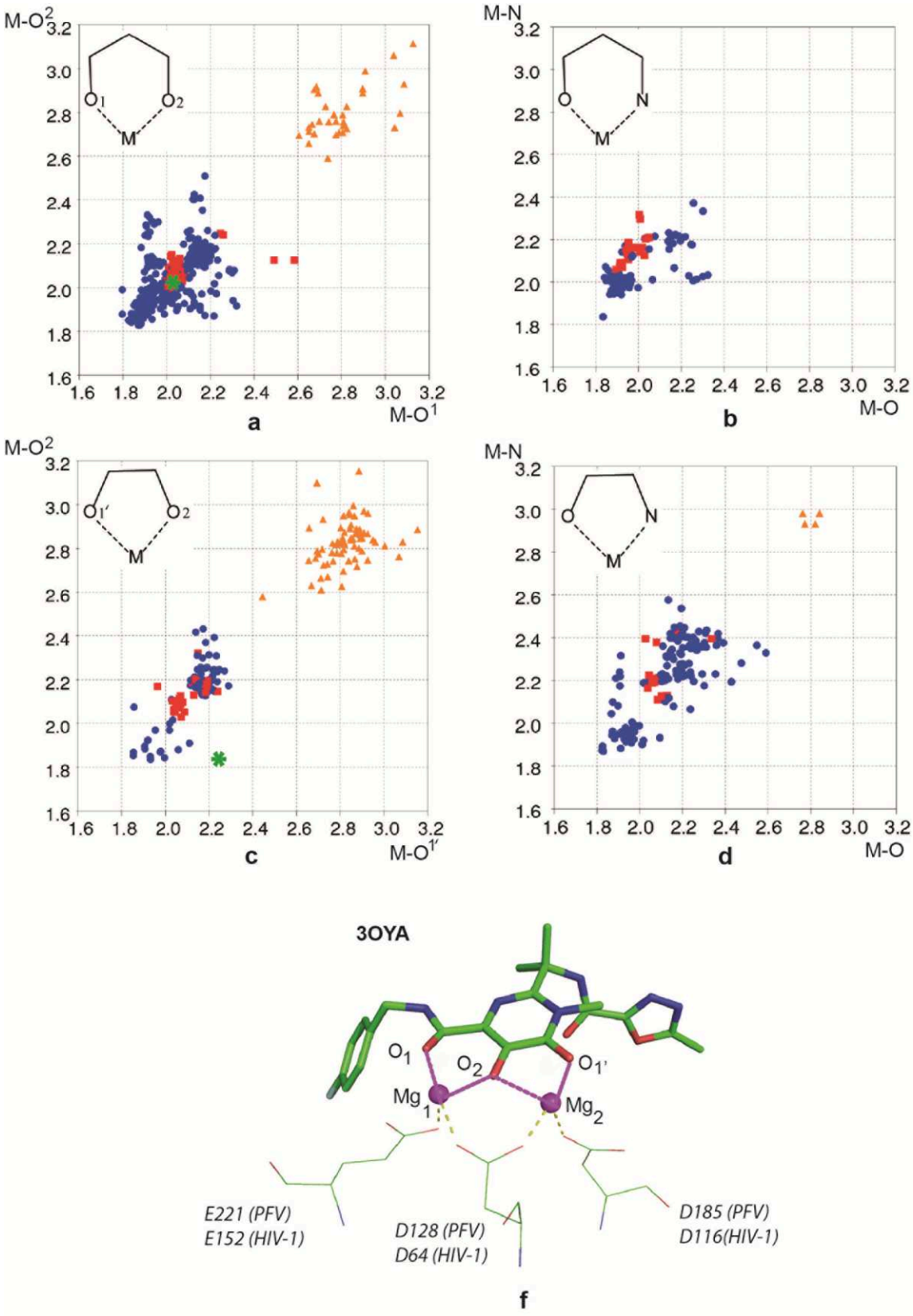
M-O2
M-O1
a
M-N
M-O
b
M-O2
M-O1'
c
M-N
M-O
d
3OYA
O1
O2
O1'
Mg1
Mg2
E221 (PFV)
E152 (HIV-1)
D128 (PFV)
D64 (HIV-1)
D185 (PFV)
D116(HIV-1)
f

Figure 5

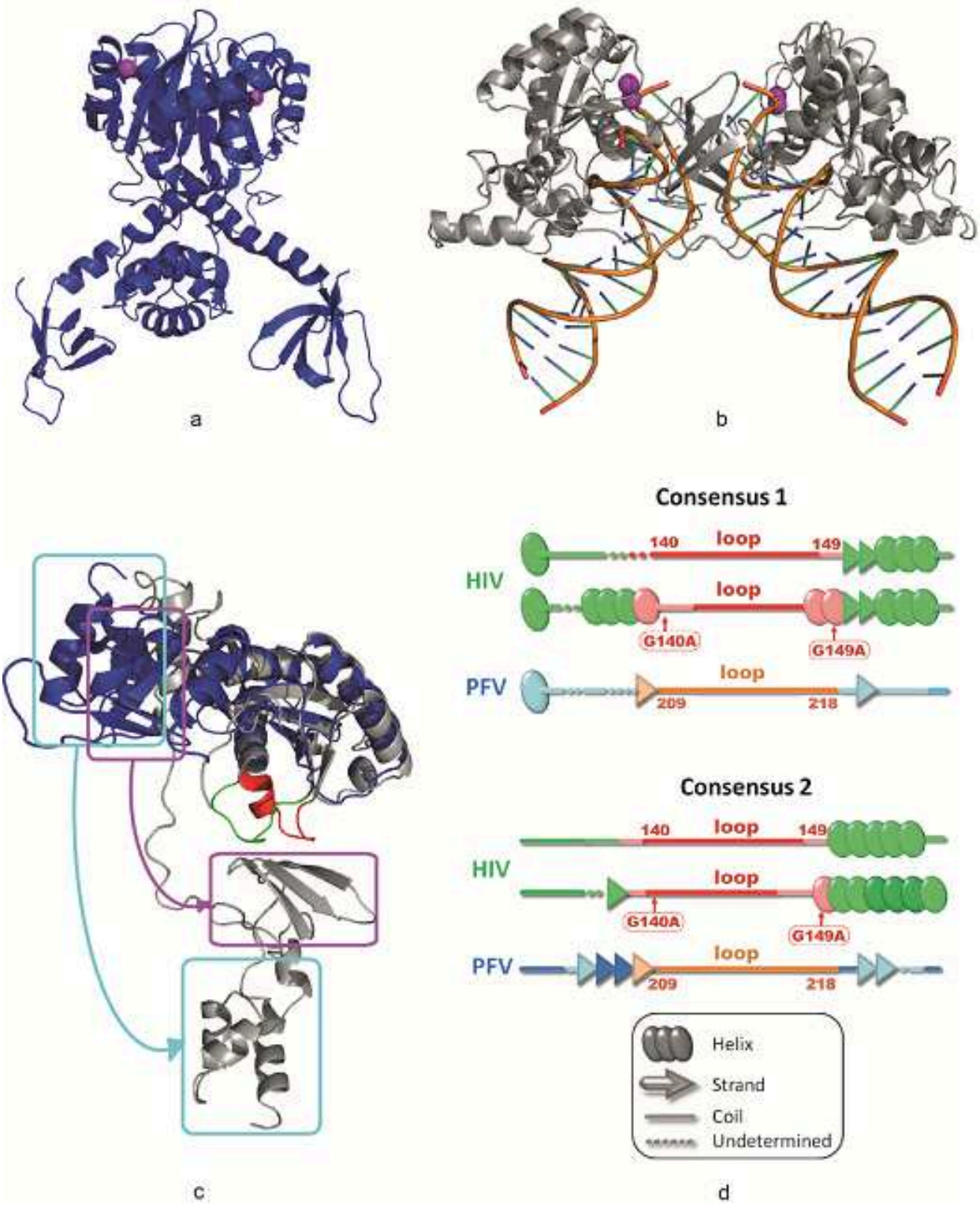
a
b
c
Consensus 1
HIV
140
loop
149
loop
G140A
G149A
PFV
loop
209
218
Consensus 2
HIV
140
loop
149
loop
G140A
G149A
PFV
loop
209
218
Helix
Strand
Coil
Undetermined
d

Figure 6

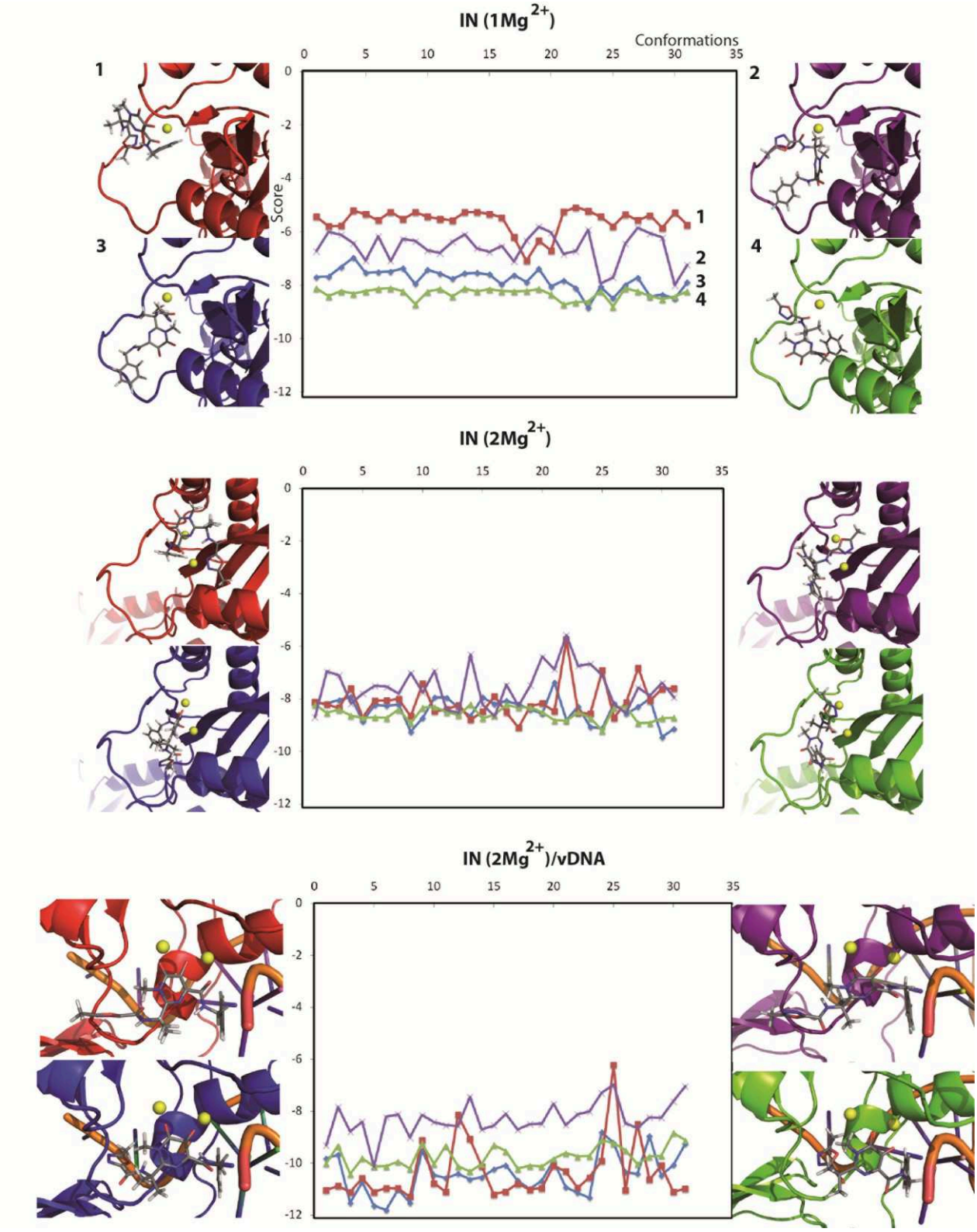
IN (1Mg2+)
Conformations
0 5 10 15 20 25 30 35
Score
0 -2 -4 -6 -8 -10 -12
1
2
3
4
IN (2Mg2+)
IN (2Mg2+)/vDNA

Figure 7

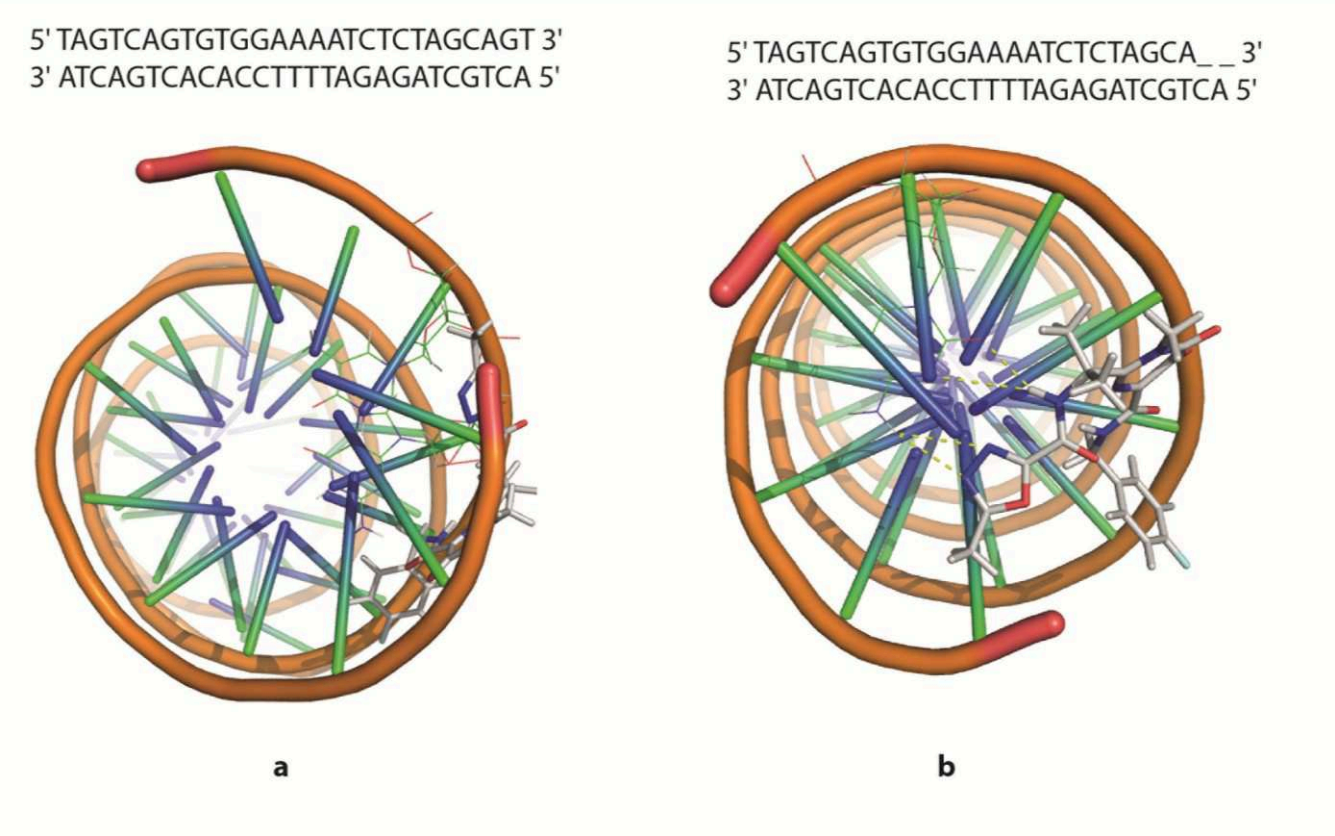
5' TAGTCAGTGTGGAAAATCTCTAGCAGT 3'
3' ATCAGTCACACCTTTTAGAGATCGTCA 5'
a
5' TAGTCAGTGTGGAAAATCTCTAGCA_ _ 3'
3' ATCAGTCACACCTTTTAGAGATCGTCA 5'
b